

Report No. K-TRAN: KU-05-3  
FINAL REPORT

## **SOIL CHARACTERIZATION AND P-Y CURVE DEVELOPMENT FOR LOESS**

Rebecca Johnson  
Robert L. Parsons  
The University of Kansas

Steven Dapp  
Dan Brown  
Dan Brown and Associates



FEBRUARY 2007

### **K-TRAN**

A COOPERATIVE TRANSPORTATION RESEARCH PROGRAM  
BETWEEN:  
KANSAS DEPARTMENT OF TRANSPORTATION  
KANSAS STATE UNIVERSITY  
THE UNIVERSITY OF KANSAS

<b>1 Report No.</b> K-TRAN: KU-05-3	<b>2 Government Accession No.</b>	<b>3 Recipient Catalog No.</b>	
<b>4 Title and Subtitle</b> SOIL CHARACTERIZATION AND P-Y CURVE DEVELOPMENT FOR LOESS		<b>5 Report Date</b> February 2007	<b>6 Performing Organization Code</b>
		<b>8 Performing Organization Report No.</b>	
<b>7 Author(s)</b> Rebecca Johnson & Robert L. Parsons, both with University of Kansas, and Steven Dapp and Dan Brown, both with Dan Brown and Associates		<b>10 Work Unit No. (TRAIS)</b>	
<b>9 Performing Organization Name and Address</b> University of Kansas Civil, Environmental & Architectural Engineering Department 1530 West 15 <sup>th</sup> Street Lawrence, Kansas 66045-7609		<b>11 Contract or Grant No.</b> C1483	
		<b>13 Type of Report and Period Covered</b> Final Report July 2004 – July 2006	
<b>12 Sponsoring Agency Name and Address</b> Kansas Department of Transportation Bureau of Materials and Research 700 SW Harrison Street Topeka, Kansas 66603-3754		<b>14 Sponsoring Agency Code</b> RE-0376-01	
		<b>15 Supplementary Notes</b> For more information write to address in block 9.	
<b>16 Abstract</b> <p>Lateral loads on drilled shafts are often the controlling factor in their design. These lateral loads are transferred to the surrounding soil or rock, and estimation of the capacity of the shaft to resist lateral loads is a critical part of the design. The lateral load-deformation relationship of a drilled shaft and its supporting soil is commonly modeled using the p-y curve method. P-y curves vary with soil type, deposition characteristics and depth, but general curves have been developed to represent common soils. Unfortunately, no p-y curves have been developed to represent the behavior of loess, cemented silt that is common throughout much of Kansas. This lack of available p-y relationships has meant that less applicable curves, normally those for sandy soils, must be used.</p> <p>The purpose of this research was to define the significant engineering properties of Kansas' loessal soils through a literature review, laboratory tests, and in situ tests and to determine the soil-structure response by performing full scale lateral load tests on six drilled shafts.</p> <p>Laboratory testing included saturated and unsaturated triaxial, direct shear, consolidation and collapse testing. Field tests included SPT, CPT, vane shear, and pressuremeter testing. Two pairs of shafts with diameters of 30 and 42 inches were tested under static loading. A third pair of 30 inch shafts was tested under repeated loading. Shaft deflections were measured using inclinometer soundings and correlated with the CPT cone tip resistance (<math>q_c</math>). A hyperbolic model was developed to correlate ultimate soil resistance (<math>P_{uo}</math>) to the CPT cone tip resistance (<math>q_c</math>) for both static and repeated loading at any given depth and was used to develop a family of p-y curves unique to loess.</p> <p>This model may be entered into the commercially available software package LPILE for design of laterally loaded drilled shafts constructed in loess.</p>			
<b>17 Key Words</b> Drilled Shafts, In Situ Testing, Loess, P-Y Curves, Soil and Triaxial Testing.		<b>18 Distribution Statement</b> No restrictions. This document is available to the public through the National Technical Information Service, Springfield, Virginia 22161	
<b>19 Security Classification (of this report)</b> Unclassified	<b>20 Security Classification (of this page)</b> Unclassified	<b>21 No. of pages</b> 199	<b>22 Price</b>

# SOIL CHARACTERIZATION AND P-Y CURVE DEVELOPMENT FOR LOESS

Final Report

Prepared by

Rebecca Johnson  
Robert L. Parsons  
The University of Kansas

Steven Dapp  
Dan Brown  
Dan Brown and Associates

A Report on Research Sponsored By

THE KANSAS DEPARTMENT OF TRANSPORTATION  
TOPEKA, KANSAS

and

UNIVERSITY OF KANSAS CENTER FOR RESEARCH, INC.  
LAWRENCE, KANSAS

February 2007

© Copyright 2007, Kansas Department of Transportation

## **PREFACE**

The Kansas Department of Transportation's (KDOT) Kansas Transportation Research and New-Developments (K-TRAN) Research Program funded this research project. It is an ongoing, cooperative and comprehensive research program addressing transportation needs of the state of Kansas utilizing academic and research resources from KDOT, Kansas State University and the University of Kansas. Transportation professionals in KDOT and the universities jointly develop the projects included in the research program.

## **NOTICE**

The authors and the state of Kansas do not endorse products or manufacturers. Trade and manufacturers names appear herein solely because they are considered essential to the object of this report.

This information is available in alternative accessible formats. To obtain an alternative format, contact the Office of Transportation Information, Kansas Department of Transportation, 700 SW Harrison, Topeka, Kansas 66603-3754 or phone (785) 296-3585 (Voice) (TDD).

## **DISCLAIMER**

The contents of this report reflect the views of the authors who are responsible for the facts and accuracy of the data presented herein. The contents do not necessarily reflect the views or the policies of the state of Kansas. This report does not constitute a standard, specification or regulation.

## Abstract

Lateral loads on drilled shafts are often the controlling factor in their design. These lateral loads are transferred to the surrounding soil or rock, and estimation of the capacity of the shaft to resist lateral loads is a critical part of the design. The lateral load-deformation relationship of a drilled shaft and its supporting soil is commonly modeled using the p-y curve method. P-y curves vary with soil type, deposition characteristics and depth, but general curves have been developed to represent common soils. Unfortunately, no p-y curves have been developed to represent the behavior of loess, cemented silt that is common throughout much of Kansas. This lack of available p-y relationships has meant that less applicable curves, normally those for sandy soils, must be used.

The purpose of this research was to define the significant engineering properties of Kansas' loessal soils through a literature review, laboratory tests, and in situ tests and to determine the soil-structure response by performing full scale lateral load tests on six drilled shafts.

Laboratory testing included saturated and unsaturated triaxial, direct shear, consolidation and collapse testing. Field tests included SPT, CPT, vane shear, and pressuremeter testing. Two pairs of shafts with diameters of 30 and 42 inches were tested under static loading. A third pair of 30 inch shafts was tested under repeated loading. Shaft deflections were measured using inclinometer soundings and correlated with the CPT cone tip resistance ( $q_c$ ). A hyperbolic model was developed to correlate ultimate soil resistance ( $P_{uo}$ ) to the CPT cone tip resistance ( $q_c$ ) for both static and

repeated loading at any given depth and was used to develop a family of p-y curves unique to loess.

This model may be entered into the commercially available software package LPILE for design of laterally loaded drilled shafts constructed in loess.

## **Acknowledgements**

The authors wish to acknowledge the financial and logistical support of the Kansas Department of Transportation and James Brennan and the people of the Materials and Research Geotechnical Unit in particular. Their assistance in drilling, sampling, testing and data processing were essential for the preparation of this report. The authors also wish to acknowledge the substantial contributions of Mike Hayes, Luke Schuler, and the people of Hayes Drilling, who volunteered to construct the shafts for the benefit of this research. The contributions of all involved are greatly appreciated.

# Table of Contents

<b>ABSTRACT</b> .....	<b>III</b>
<b>ACKNOWLEDGEMENTS</b> .....	<b>IV</b>
<b>TABLE OF CONTENTS</b> .....	<b>V</b>
<b>CHAPTER 1</b> .....	<b>1</b>
<b>INTRODUCTION</b> .....	<b>1</b>
<b>CHAPTER 2</b> .....	<b>4</b>
<b>LITERATURE REVIEW</b> .....	<b>4</b>
2.1 LOESS .....	4
2.1.1 <i>Origin</i> .....	4
2.1.2 <i>Geotechnical Characteristics</i> .....	7
2.2 LATERAL LOADS .....	16
2.3 BEAM THEORY .....	19
<b>CHAPTER 3</b> .....	<b>24</b>
<b>SCOPE OF RESEARCH</b> .....	<b>24</b>
3.1 SITE INVESTIGATION .....	24
3.2 TEST SHAFTS .....	28
3.2.1 <i>Configuration and Construction</i> .....	28
3.2.2 <i>Instrumentation</i> .....	33
3.2.3 <i>Static Tests</i> .....	35
3.2.4 <i>Cyclic Test</i> .....	36
<b>CHAPTER 4</b> .....	<b>38</b>
<b>TEST RESULTS</b> .....	<b>38</b>
4.1 LABORATORY RESULTS .....	38
4.1.1 <i>Index Properties</i> .....	39
4.1.2 <i>Triaxial Compression Testing</i> .....	41
4.1.3 <i>Unconfined Compression Testing</i> .....	43
4.1.4 <i>Direct Shear</i> .....	43
4.1.5 <i>Consolidation and Collapse</i> .....	44
4.2 IN-SITU TESTING .....	46
4.2.1 <i>Pressuremeter Test</i> .....	46
4.2.2 <i>Cone Penetration Test</i> .....	48
4.2.3 <i>Standard Penetration Test</i> .....	49
<b>CHAPTER 5</b> .....	<b>53</b>

<b>ANALYSIS AND COMPARISON OF LABORATORY AND IN-SITU TESTING</b>	<b>53</b>
5.1 SOIL CLASSIFICATION .....	53
5.2 DIRECT SHEAR .....	54
5.3 <i>Triaxial Compression</i> .....	57
5.4 COHESION AND FRICTION ANGLE.....	63
5.5 ANISOTROPIC STRENGTH CHARACTERISTICS.....	67
5.6 ELASTIC MODULUS .....	72
<b>CHAPTER 6.....</b>	<b>75</b>
<b>P-Y ANALYSIS.....</b>	<b>75</b>
<b>CHAPTER 7 .....</b>	<b>78</b>
<b>CONCLUSION AND RECOMMENDATIONS.....</b>	<b>78</b>
7.1 SOIL CLASSIFICATION .....	78
7.2 COLLAPSE .....	79
7.3 ANISOTROPY .....	80
7.4 SOIL MODULUS VALUES .....	80
7.5 STRENGTH PARAMETERS .....	81
7.6 IN-SITU MOISTURE CONDITIONS .....	81
7.7 CORRELATION FOR P-Y CURVES .....	82
7.8 ADDITIONAL RESEARCH.....	82
<b>REFERENCES: .....</b>	<b>83</b>
<b>APPENDIX A .....</b>	<b>86</b>
<b>AS BUILT TEST CONDITIONS.....</b>	<b>86</b>
<b>APPENDIX B .....</b>	<b>91</b>
<b>BORING LOGS .....</b>	<b>91</b>
<b>APPENDIX C.....</b>	<b>104</b>
<b>LABORATORY TESTING .....</b>	<b>104</b>
<b>APPENDIX D .....</b>	<b>143</b>
<b>P-Y MODEL DERIVED FROM LATERAL LOAD TESTING .....</b>	<b>143</b>
D.1 INTRODUCTION .....	143
D.2 TESTING SEQUENCE .....	143
D.3 IDEALIZED MODEL PROFILE FROM CPT TESTING.....	145
D.4 INSTRUMENTATION AND TEST DATA REDUCTION PROCEDURES.....	147
D.4.1 <i>Introduction</i> .....	147
D.4.2 <i>Load Cell Readings and Hydraulic Pressure Transducer to Provide Load</i> .....	148
D.4.3 <i>LVDT Readings to Provide Boundary Condition at Top of Shaft</i> .....	148



D.4.4	<i>Inclinometer Readings to Provide Deflected Pile Shape</i> .....	149
D.5	FORMULATION OF P-Y MODEL PARAMETERS .....	150
D.5.1	<i>Introduction</i> .....	150
D.5.2	<i>Ultimate Soil Resistance Parameter (<math>P_{uo}</math> and <math>P_u</math>) from CPT Testing, and Cyclic Degradation with Cycle Number (<math>N</math>)</i> .....	153
D.5.3	<i>Reference Displacement Parameter (<math>Y_i</math>)</i> .....	154
D.5.4	<i>Initial Modulus Parameter (<math>E_i</math>) and Hyperbolic Model of Secant Modulus (<math>E_s</math>)</i> 155	
D.5.5	<i>Generation of the P-Y Curve from Secant Modulus Relationship with Displacement</i> .....	158
D.5.6	<i>Summary: Step-by-Step Procedure for Generating P-Y Curves</i> .....	160
D.6	COMPARISONS OF MEASURED RESULTS WITH LPILE COMPUTER RUNS... 163	
D.6.1	<i>Introduction</i> .....	163
D.6.2	<i>Pile Displacement Profile with Static Lateral Load</i> .....	164
D.6.3	<i>Depth to Maximum Moment in Pile with Static Lateral Load</i> .....	166
D.6.4	<i>Pile Head Displacement with Static Lateral Load</i> .....	167
D.6.5	<i>Cyclic Results</i> .....	170
	<b>APPENDIX E</b> .....	<b>176</b>
	<b>INCLINOMETER DATA</b> .....	<b>176</b>

## List of Tables

Table 2.1 Pleistocene Stratigraphy in Kansas.....	7
Table 2.2: Range in Values of Engineering Properties of Loess in the U.S.....	12
Table 3.1: In-Situ Testing .....	27
Table 3.2: Laboratory Tests .....	27
Table 3.3: Load Increments for the 30-inch Diameter Cyclic Test.....	37
Table 4.1: Index Properties and Classification .....	41
Table 4.2: Triaxial Compression Results, 2004.....	42
Table 4.3: Triaxial Compression Results, 2005.....	43
Table 4.4: Unconfined Compressive Strength Results, 2004.....	43
Table 4.5: Direct Shear Results, 2004.....	44
Table 4.6: Preconsolidation Pressure.....	45
Table 4.7: Collapse Index.....	45
Table 4.8: Pressuremeter Results.....	47
Table 4.9: CPT 1 in 2004 .....	49
Table 4.10: CPT in 2005 .....	49
Table 4.11: Average SPT N Values .....	50
Table 4.12: SPT Correlations for sand .....	51
Table 4.13: Average SPT Correlated Values .....	51

## List of Figures

Figure 2.1: Outline of major loess deposits in the United States [7].	5
Figure 2.2: Vertical cut loess bluff along Highway 210 in North Kansas City, Missouri	8
Figure 2.3: Vertical cuts formed by erosion in bluff along Highway 210 in North Kansas City, Missouri.	16
Figure 2.4: Representation of a Laterally Loaded Foundation Element [18]:	18
Figure 2.5: Laterally Loaded Pile Failure.	19
Figure 2.6: a) Typical p-y curve, b) Family of p-y curves.	20
Figure 3.1: a) Site location [25]; b) Topographic map of site [26]; c) Aerial photo of test site [26].	26
Figure 3.2: Drilled shaft loading layout	30
Figure 3.3: Reinforcement cage with spacers and inclinometer casing attached	31
Figure 3.4: Drilled Shaft Layout	32
Figure 3.5: a) Side photo of test shafts 5 and 6; b) Plan view of load test set up; c) load cell.	34
Figure 3.6: a) Side view photo of test shaft 6; b) Side view schematic of test shaft	35
Figure 3.7: shaft 1: a) 6" top of shaft displacement; b) soil gap at the end of cyclic load test	36
Figure 4.1: Typical Boring Log	40
Figure 4.2: 2004 and 2005 PMT	47
Figure 4.3: Average SPT Correlated Values	52
Figure 5.1a to 5.1c: Mohr-Coulomb Failure Envelopes for Direct Shear Tests Subjected to Horizontal Shearing	57
Figure 5.2: Orientation of Direct Shear Samples with DSH Notation	57
Figure 5.3: Stress paths (p-q plots) for consolidated-undrained tests on loess samples from 3 feet below ground surface	59
Figure 5.4: Stress paths for consolidated-undrained test on loess samples from 7 feet below ground surface	60
Figure 5.5: Stress path for consolidated-undrained test on loess samples from 25 feet below ground surface	60
Figure 5.6: Unconsolidated-undrained tests performed in 2004 and 2005	61

Figure 5.7: Mohr-Coulomb failure envelopes for triaxial compression tests .....	62
Figure 5.8: Laboratory strength tests for samples obtained at 1 and 3 feet.....	63
Figure 5.9: Laboratory strength tests for samples obtained at 5 and 7 feet.....	64
Figure 5.10: Laboratory strength tests for samples obtained at 15 and 25 feet.....	65
Figure 5.11: Laboratory cohesion results for the soil profile. ....	66
Figure 5.12: Laboratory friction angle results for the soil profile. ....	67
Figure 5.13: Anisotropic sample orientation for direct shear testing .....	68
Figure 5.14: Direct shear test results for specimens sampled at 1 foot.....	69
Figure 5.15: Direct shear test results for specimens sampled at 3 feet.....	69
Figure 5.16: Direct shear test results for specimens sampled at 5 feet.....	70
Figure 5.17: Direct shear test results for specimens sampled at 7 feet.....	70
Figure 5.18: Direct shear test results for specimens sampled at 15 feet.....	71
Figure 5.19: Direct shear test results for specimens sampled at 25 feet.....	71
Figure 5.20: Comparison of moduli for CPT and PMT soundings .....	72
Figure 5.21: Elastic modulus determined from in-situ and laboratory results .....	73

# Chapter 1

## Introduction

Drilled shafts are a common type of deep foundation used when upper soils are weak or subject to scour. They are capable of bearing large compressive or uplift forces as well as large lateral loads. They are most commonly constructed by inserting a reinforcing steel cage into a drilled hole and filling it with concrete. They are often used for bridge foundations, retaining structures, and large highway signs on transportation projects.

Depending on the function, deep foundations must support axial loads, lateral loads, and react against moments. Axial loads are transferred to the soil through side friction and toe bearing resistance. Lateral loads can be static, such as water pressures on piers or earth pressures on retaining walls, or dynamic, such as wave action through soil due to earthquakes. Lateral loads produce lateral deflections through shear and moment reactions and are transferred to adjacent soil through lateral bearing.

The lateral load-deformation relationship of a shaft and its interaction with supporting soil must be evaluated when developing a safe and economical structural design. Drilled shaft deflection depends on the soil response and the soil response is a function of the shaft deflection. This soil-structure reaction is modeled as a p-y curve, where p is the lateral soil resistance per unit length of the foundation and y is the lateral deflection. Therefore, the p-y curve behavior is a function of both soil and foundation properties. The p-y curve for a particular point on a foundation depends on soil type, type of loading, foundation diameter and cross-sectional shape, coefficient of friction between the foundation and the soil, and how the foundation was constructed [1].

The soil-structure interaction is modeled using a beam on elastic foundation analysis, also known as the Winkler method. Through this method the soil is represented by a series of independent nonlinear springs. Deformations of these springs are the p-y curves. Thus, the foundation is represented using beam theory and the soil resistance is represented by the p-y curves. The solution to the nonlinear p-y curve takes the form of a fourth order differential equation that can easily be solved using a computer program. Com624P and LPILE are two popular programs that model lateral loads on foundations using a two-dimensional finite difference approach. Com624P was the first widely used p-y analysis software [1], however LPILE is now widely used and is the analysis tool used by the Kansas Department of Transportation (KDOT). The p-y curves for this project were generated using LPILE.

Reese and others performed a majority of the load tests in the 1970's [2]. They correlated field and laboratory tests to derive a family of p-y curves for the lateral load response in each of the following soils: soft clay, stiff clay, and sand above and below the water table [2]. No family of p-y curves has been published from load tests in loessial soils although Clowers and Frantzen conducted a full-scale lateral load test in loessial soil on piles in the early 1990's [3]. They concluded the soil-structure interaction of loess was similar to sandy soils and the family of sandy soil p-y curves could, therefore, be used in foundation design and analysis. However, loess has many unique properties that set it apart from sandy soil. Much of the soil structure strength is gained from clay and calcite cementation which can be lost due to a rise in moisture content; the soil may also be susceptible to large settlements when saturated.

The purpose of this research was to define the significant engineering properties of Kansas' loessial soils through a literature review, laboratory tests, and in situ tests and to determine the soil-structure response by constructing and testing a set of full-scale drilled shafts. Laboratory tests were conducted in conjunction with KDOT on soil specimens obtained from a total of eleven borings and two continuous soil samplings. Laboratory testing consisted of: one dimensional consolidation, collapse, unconfined compressive strength, unconsolidated-undrained triaxial, consolidated-undrained triaxial, repeated loading triaxial, direct shear, and routine index testing. Field tests included standard penetration tests (SPT), cone penetration tests (CPT), and pressuremeter tests (PMT). Selected field tests were conducted in 2004 and during the week of testing in 2005. The full scale load test included monitoring the behavior of six laterally loaded drilled shafts. Shafts were subjected to static and repeated loads. The soil-structure response of drilled shafts in loessial soils was analyzed to develop a family of p-y curves.

## Chapter 2

### Literature Review

#### 2.1 Loess

##### 2.1.1 Origin

Multiple competing theories concerning the origin of loess have been proposed. There are five different theories discussed in *Loess, Lithology and Genesis* [4]; however, nearly all authors accept and discuss the theory of an eolian origin in textbooks and journal articles alike. Terzaghi, Peck, and Mesri define loess in general as uniform, cohesive, wind-blown sediment [5]. Loess is a clastic soil mostly made of silt-sized quartz particles and loosely arranged grains of sand, silt, and clay. Cohesion is due to clay or calcite bonding between particles which are significantly weakened upon saturation. When dry, loess has the unique ability to stand and support loads on nearly vertical slopes.

Loess was formed during arid to semi-arid periods following the Pleistocene continental glaciation. As the glaciers retreated, strong winds swept up sediments from the outwash. Larger particles were sorted and deposited near the original riverbeds while silt-size particles were transported downwind. The glacial till continued to be swept up and reworked throughout the arid times, creating a loosely arranged soil mass. Loess is present in central parts of the United States, Europe, the former Soviet Union, Siberia, and in large parts of China and New Zealand [6]. Within the United States, major loess deposits are found in Nebraska, Kansas, Iowa, Wisconsin, Illinois, Tennessee, Mississippi, southern Idaho, and Washington, as mapped on figure 2.1 [7].



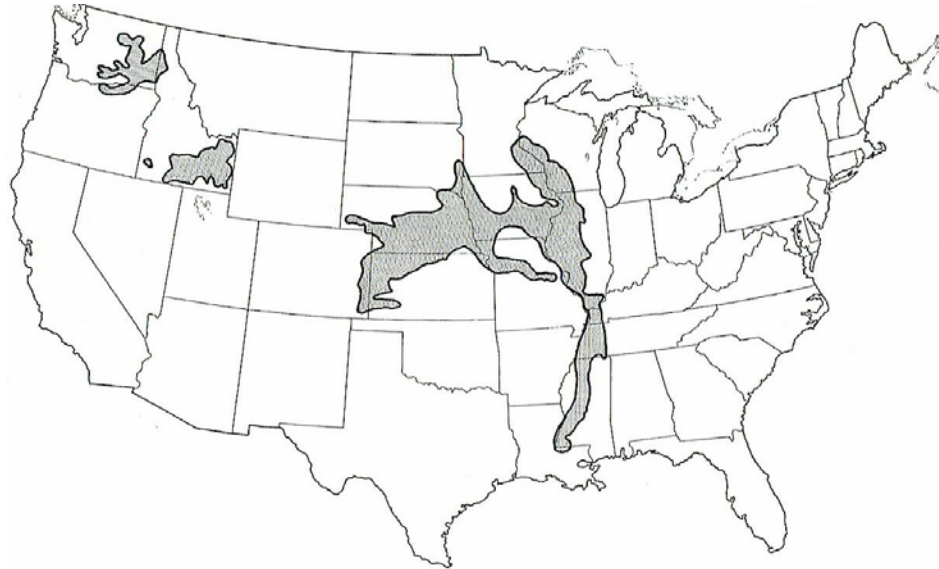


**Figure 2.1: Outline of major loess deposits in the United States [7].**

Four stages of continental glaciation and interglacial periods are identified during the Pleistocene epoch, about 1.8 million to 8000 years ago. The two glacial stages of concern in the Great Plains region are the Illinoian and Wisconsinian. Wind-eroded deposits of silt, sand, and clay minerals were swept up across glacial outwash toward the end of each stage. The alluvium particles were transported, sorted, and redeposited along bordering uplands, forming loess. There are three members found in loess formations throughout Kansas. They are the Loveland, Peoria, and Bignell members.

The Loveland member is the oldest and was deposited during the Illinoian stage. The maximum depth is about 20 feet (6 meters) along the Missouri River valley. Its wind-born particles were derived from alluvial deposits, dune sand, and older Pleistocene and Pliocene deposits [8]. The Peoria member is a nearly continuous, silty, alluvium deposit formed during the early Wisconsinian Stage. This member can reach depths of 100 feet (30 meters) along the Missouri River valley and is the most extensive of loess units in the Great Plains region. The Bignell member, youngest of all loess

members, was deposited during the late Wisconsinan Stage. It is largely made of reworked Peoria loess. The member is generally discontinuous and can reach depths of 35 feet (10.6 meters) along the Missouri River valley. A layer of soil identified as the Brady soil separates the Peoria and Bignell members. It was established during a brief pause in loess formation and is widespread but discontinuous. Sangamon soils formed between the Illinosian and Wisconsinian periods and are found above beds of Loveland loess [6 - 14]. These soils formed during interglacial periods differ from loess in that they were products of worldwide climatic factors, not local erosion or deposition. In Table 2.1, Bandyopadhyay presents a pictorial representation of the Pleistocene stratigraphy layers in Kansas [6].

The major drainageways that produced Kansas' loess members were the Republican River valley in the north, the Smoky Hill River valley in north-central and western Kansas, and the Missouri River valley for the extreme northeastern border of Kansas. During the dry, warm weather following glacial retreat, northeastern Kansas was predominantly mixed woodland and prairie while western Kansas was dominated by short grasses and subject to strong winds. Due to the woodland wind barriers, loess deposits in northeastern Kansas are thicker than western Kansas deposits and not as uniform. Here, open terrains allowed the wind to deposit, pick-up, and rework silt particles. This secondary source of deposition produced thinner, well-sorted, uniform loess members [9].

**Table 2.1 Pleistocene Stratigraphy in Kansas [6]**

Youngest ↑ Oldest	Time – Stratigraphy 1.8 million to 8000 years ago	Rock - Stratigraphy	
		Recent Stage	Low Terraces and Alluvium
	Wisconsinan Stage	Bignell Loess Fluvial Deposits Brady Soils Peoria Loess Fluvial Deposits	
		Sangamonian Stage	Sangamon Soils
		Illinoisan Stage	Loveland Loess Fluvial Deposits
	Yarmouthian Stage	Yarmouth Soils	
	Kansan Stage	Pearlette Ash Bed Fluvial and Eolian Deposits Till	
	Aftonian Stage	Afton Soils	
	Nebraskan Stage	Fluvial and Eolian Deposits Till	

**2.1.2 Geotechnical Characteristics**

Several characteristics are used to separate loess from other silty soils. In its natural state, loess has an open, cohesive particle structure with low density and high dry strength. Non-cohesive silty or clayey soils similar to loess in particle size, deposition, and open particle arrangement are not considered loess. They are considered wind-deposited silts, fine sands, or clays. Loess has a metastable structure due to the high degree of settlement and large loss of strength that may occur upon saturation. Gibbs and Holland clearly express the importance of understanding the geotechnical aspects of loess [7]. They state:

Because of the unstable properties of loess which may cause settlement of foundations of structures, such knowledge of the limitations of loess for engineering purposes is important not only to the geologist and soil

mechanics engineer but also to design and construction engineers who are required to build structures on loessial soils [7].

One well known unique characteristic of loess is its considerable stability and strength when dry which enables the near vertical road cut slopes commonly seen along roadways to remain stable, as shown in Figure 2.2. Because the vertical permeability of loess is much greater than the horizontal permeability [6], strength and stability decrease for intermediate slope angles. Loess is subject to large consolidation, poor stability, seepage, erosion, and leaching of carbonates under various moisture and load combinations. Other defining characteristics include grain structure, color, major elements, and engineering properties.



**Figure 2.2: Vertical cut loess bluff along Highway 210 in North Kansas City, Missouri**

Eolian soil particles are often loosely arranged with numerous voids and root-like channels. The coarser particles settle out near the source and finer particles are

deposited progressively further away. Therefore, local differences occur in the type and quantity of mineral content. In general, the fabric of loess consists of fine, loosely arranged angular grains of silt, fine sand, calcite, and clay. Most of the grains are coated with thin films of clay and some with a mixture of calcite and clay. It is often classified as a silty clay loam or a silt loam [6]. For Peoria loess, Swineford and Frye noted a strong relationship between particle size and the degree of sorting. Coarser samples are generally better sorted than the finer ones [9].

The granular components of loess are quartz, feldspars, volcanic ash shards, carbonates, and micas. The percent of composition varied with each site sampled, but in general quartz makes up around half the total volume of the deposit. [7, 15]

Color and particle size are strong identifiers of loess. It is commonly a buff, medium to coarse-grained silt with fine to very fine grains of sand. In general, the median grain size ranges from 0.00083-0.002 in. (0.02-0.05 mm) [9]. Thus, the average grain size is smaller than the upper limit of silt, 0.0029 in. (0.074 mm). The Loveland member is dark brown at the bottom and a very distinctive reddish brown at the top. The greatest amount of sand is near the bottom of the member. Peoria and Bignell members are light yellowish brown or buff. They are well sorted near the river bluffs and the range of particle size varies with distance [9, 13, 14, 16].

Calcite is believed to be a major cementing material in loess. It can be leached into the soil from above or can be brought into the soil by evaporation of capillary water from the groundwater below. However, clay is more commonly the bonding agent that gives loess its cohesive nature. Bandyopadhyay found montmorillonite clay to be the major cementing material in Kansas loess, while calcite “usually occurs in distinct silt-

sized grains throughout the loess in a finely dispersed state rather than as a cementing material [6].” Gibbs and Holland found that, in general, intergranular supports were composed mostly of montmorillonite clay with small amounts of illite [7]. They contend that carbonates and clays react differently in water; therefore, if calcite was the main cementing material, loess would not subside, consolidate, or lose strength as rapidly as it does. Most often, calcite serves as a secondary support structure and clay as the primary soil matrix [7].

Montmorillonite, kaolinite, and illite have all been identified in samples in Kansas [8] along with calcite, quartz, and feldspars [15]. Crumpton and Badgley studied the clay content in Kansas [8]. They found the clay content generally decreased with increasing depth and decreased from east to west. With regard to the general loess formation, there is an increase in clay content with increasing depth. The Loveland member contains more clay than the Peoria and Bignell members. Loveland and Peoria members are separated by the Sangamon soil, which also shows increasing percent clay with increasing depth. The mineral types discussed are consistent for all three members [8, 9, 15].

Montmorillonite and mixed layers of montmorillonite and illite are the cementing material for the soil. These clay particles coat the host silt grains and the walls of various holes forming the inter-granular support structure and serve as the matrix. These supports give dry loess its impressive strength, stability, and ability to withstand large loads with little settlement in the arid regions of the Midwest. As moisture content increases, clay particles swell and bond strength is greatly reduced. There is a potential for the soil matrix to collapse and extensive settlement to occur. With high vertical

permeability due to large voids and vertical root holes, moisture quickly dissipates and loess remains dry. If it overlies less permeable materials such as clayey shale and retains water, the bond strength and soil structure will weaken upon saturation.

Sheeler researched quantitative properties of loess, including specific gravity, Atterberg limits, permeability, density, shear strength, and natural moisture content as shown in Table 2.2 [16].

Specific gravity is influenced by local variations in the type and quantity of mineral content. Values range from 2.57 to 2.78, as shown in Table 2.2. The average value is 2.66 [6, 7, 16], which is similar to the typical value of clean, light colored quartz sand.

The Plasticity Indices for loess range from 5 to 37 and the Liquid Limits range from 25 to 60 depending on the amount of clay present [7, 8, 16]. High Plasticity Index values correspond to high percentages of montmorillonite in the soil [6].

Permeability is influenced by soil properties such as particle size and shape, gradation, void ratio and continuity, and soil structure [14]. It is a widely varied local feature with in-place vertical permeabilities of loess ranging from 10 to over 1000 ft/yr ( $1 \times 10^{-5}$  to  $1 \times 10^{-3}$  cm/s), determined after consolidation was complete under a given load [16]. Bandyopadhyay states the vertical permeability of Peoria loess in Kansas is on the order of 900 ft/yr ( $9 \times 10^{-4}$  cm/s) and is much larger than the horizontal permeability. “[The higher vertical permeability] is partly due to the existence of vertical tubules and shrinkage joints within the soil mass [6].” Terzaghi viewed permeability in loess as an elusive property because the structure changes when it is saturated. It breaks down, becomes denser, and its permeability is decreased [16].

Shear strength of a soil depends on the frictional and cohesive strength between individual particles [17]. The initial density, moisture content, and clay content of the loess controls the two strength parameters. The angle of internal friction ranges from 28-36 degrees for samples tested with a moisture content below saturation [16]. The cohesive strength varies from 0-70 psi (0-483 kPa) with the high values of cohesion resulting from high densities. Also, cohesive strength increases with increasing clay content [16]. There is a distinct difference in the shear strength between wet and dry loess. Dry loess has greater shearing resistance under an applied load and greater cohesion than when saturated.

**Table 2.2: Range in Values of Engineering Properties of Loess in the U.S.**

Property	Location							
	Iowa	Nebraska	Tennessee	Mississippi	Illinois	Alaska	Washington	Colorado
<b>Specific Gravity:</b>	2.58 - 2.72	2.57 - 2.69	2.65 - 2.70	2.66 - 2.73		2.57 - 2.79		
<b>Mechanical Analysis</b>								
Sand, %	0 - 27	0 - 41	1 - 12	0 - 8	1 - 4	2 - 21	2 - 10	30
Silt, %	56 - 85	30 - 71	68 - 94	75 - 85	48 - 54	65 - 93	60 - 90	50
Clay, %	12 - 42	11 - 49	4 - 30	0 - 25	35 - 49	3 - 20	8 - 20	20
<b>Atterberg limits</b>								
LL, percent	24 - 53	24 - 52	27 - 39	23 - 43	39 - 58	22 - 32	16 - 30	37
PL, percent	17 - 29	17 - 28	23 - 26	17 - 29	18 - 22	19 - 26		20
PI	3 - 34	1 - 24	1 - 15	2 - 20	17 - 37	NP - 8	<8	17



**Table 2.2: Range in Values of Engineering Properties of Loess in the U.S.**  
(continued)

Property	Location							
	Iowa	Nebraska	Tennessee	Mississippi	Illinois	Alaska	Washington	Colorado
<b>Classification</b>								
Textural	SL, SCL, SC	SL, SCL, SC	SL, SCL, SC	SL, SCL	SC, C	SL, SCL		SL
AASHO	A-4(8), A-7-6(19)	A-4, A-6	A-4(8), A-6(10)	A-4(8), A-6(9)	A-6(11), A-7-6(20)	A-4(8)		A-6(10)
Unified	ML, CL, CH	ML, CL	ML, CL	ML, CL	CL, CH	ML, CL-ML		CL
<b>water content, %</b>	4 - 31		12 - 25	19 - 38		11 - 49		8 - 10
<b>Shear strength</b>								
UU triaxial shear								
c, psi		0 - 67		2 - 10				
Ø		31 - 36		0 - 28				
Direct shear								
c, psi	.3 - 1.8			0				
Ø	24 - 25			32 - 33				

Adapted from "Summarization and Comparison of Engineering Properties of Loess in the United States" by J.B. Sheeler [16]

Loess is often associated with terms such as “collapse,” “hydroconsolidation,” or “hydrocompaction [6].” Consolidation may be the most outstanding physical and structural property of loess. Its susceptibility to settlement makes it a potentially unstable foundation material. Because of the reaction between montmorillonite and moisture, slight variations in clay content and moisture content may cause collapse and consolidation. An increase in moisture content may cause clay bonds to weaken, reducing the original soil strength. Saturated loess consolidates under lower stress conditions than when dry. Therefore, an increase in moisture content is often a more important contributor to collapse and consolidation than loading [7, 21].

Bandyopadhyay found that:

Soils susceptible to hydroconsolidation can be identified by a density criterion – that is, if density is sufficiently low to give a space larger than needed to hold the liquid-limit water content, collapse problems on saturation are likely [6].

In general, settlement will be large for loess with dry unit weights below 80 pounds per cubic foot (pcf) and small for those exceeding 90 pcf (1.28 g/cm<sup>3</sup> and 1.44 g/cm<sup>3</sup>, respectively) [6, 7]. Therefore, loessial soils with low field densities and clay cementation can be expected to have a high consolidation and collapse potential [6].

Observed dry unit weights of loessial soils vary from 66-104 pcf (1.06-1.67 g/cm<sup>3</sup>) [16]. For the Bignell loess member, unit weight varies from 75-90 pcf (1.20-1.44 g/cm<sup>3</sup>). Peoria members typically have unit weights around 85 pcf (1.36 g/cm<sup>3</sup>) or less. Therefore, as previously discussed, Peoria loess can suffer great settlement. Loveland loess generally has a denser fabric, unit weights from 90-104 pcf (1.44-1.67 g/cm<sup>3</sup>) because of increased clay content and is less susceptible to large settlements [6].

The ultimate bearing capacity of a soil is the bearing pressure required such that shear stresses induced by a footing just exceed shear strength of the soil [14]. For dry loess, bearing capacity may exceed 10,000 pounds per square foot (psf) (480 kPa) but may drop to 500 psf (24 kPa) upon saturation.

In-situ moisture contents of loess range from 4 to 49%. There is a strong correlation between regional average annual rainfall and the natural moisture content. Because the structure of loess is loosely arranged and filled with voids, rainfall quickly infiltrates and loess may remain dry within a few feet of the surface, unless there is a water table near the surface. Gibbs and Holland concluded that maximum dry strength occurs at moisture contents below 10%, and high resistance to settlement should be expected. Soils with moisture contents between 10 to 15% have moderately high strength, with strength declining as moisture approaches 20%. Moisture contents above 20% are considered high and will permit full consolidation to occur under load. Saturation occurs at about 35% moisture [7].

Loess has very little resistance to erosion by flowing water because of the softening of clay bonds. Therefore, erosion is the main force in creating naturally occurring vertical cuts in loess, shown in Figure 2.3.



**Figure 2.3: Vertical cuts formed by erosion in bluff along Highway 210 in North Kansas City, Missouri**

In summary, Sheeler states the following conclusions: loess is an open and porous silt-sized soil with small amounts of sand; the physical characteristics are very uniform; host grains are bonded together primarily with thin clay coatings; in-place unit weights range from 66-104 pcf ( $1.06-1.67 \text{ g/cm}^3$ ) with large settlements occurring at densities under 80 pcf ( $1.28 \text{ g/cm}^3$ ); natural moisture contents are generally well below saturation; field unit weight is the main determinant of bearing capacity; large consolidation occurs in saturated loaded loess; and shearing strength depends on moisture content [16].

## **2.2 Lateral Loads**

In general, piles and drilled shafts respond to axial and lateral loads in the same manner, although there are some differences resulting from the method of construction. Because piles are driven or vibrated into place, cohesive soils are prone to consolidation and non-cohesive soils are subject to densification. Piles and drilled shafts in clay will still have similar responses; piles may have a stiffer response when

placed in sandy soils [18]. Additionally, cement will migrate into the adjacent soil during construction of drilled shafts, causing an increase in stiffness of the surrounding soil. The stiffness increase is small and the estimated response of the soil is considered to be equivalent for both drilled shafts and piles [3, 18].

Careful consideration should be given to the nature of lateral loads on piles and drilled shafts. Potential types of loading include short-term, repeated, sustained, and seismic or dynamic. Short-term, or static, loading is often used in field tests to correlate the soil response with its engineering properties. Sustained loads come from retaining walls or bridge abutments. Traffic on a curved bridge, currents or waves, and ice are examples of repeated loads. Dynamic loads can come from machinery vibrations and earthquakes [2].

Foundation deflection due to lateral loading is a function of both the foundation properties and the soil response. Likewise, the soil response depends on soil properties and the foundation reaction. This soil-structure interaction is modeled as a nonlinear beam on elastic foundation. The model assumes the soil is a continuous, isotropic, and elastic medium. The drilled shaft or pile is divided into equally spaced sections and the soil response is modeled by a series of closely spaced discrete springs called Winkler's springs, shown in Figure 2.4 [18].

Because the foundation is divided into sections, the soil response at a point is independent of pile deflection elsewhere and a continuum is not perfectly modeled. This discrepancy is minor and a means for correction is included in COM624P [2]. While horizontal beams-on-foundation use conventional bearing capacity for shallow foundations to determine the ultimate resistance of the soil,  $p_u$ , laterally loaded

foundations must consider both surface and toe failures. Near the surface, the soil fails as a passive wedge being pushed up and out and at the toe, it fails by flowing around the shaft, shown in Figure 2.5 a and b respectively. Effective unit weight, soil shear strength, and the diameter of the shaft determine the point of change from surface to toe failure. Welch and Reese present equations to determine  $p_u$  for horizontal loading [19].

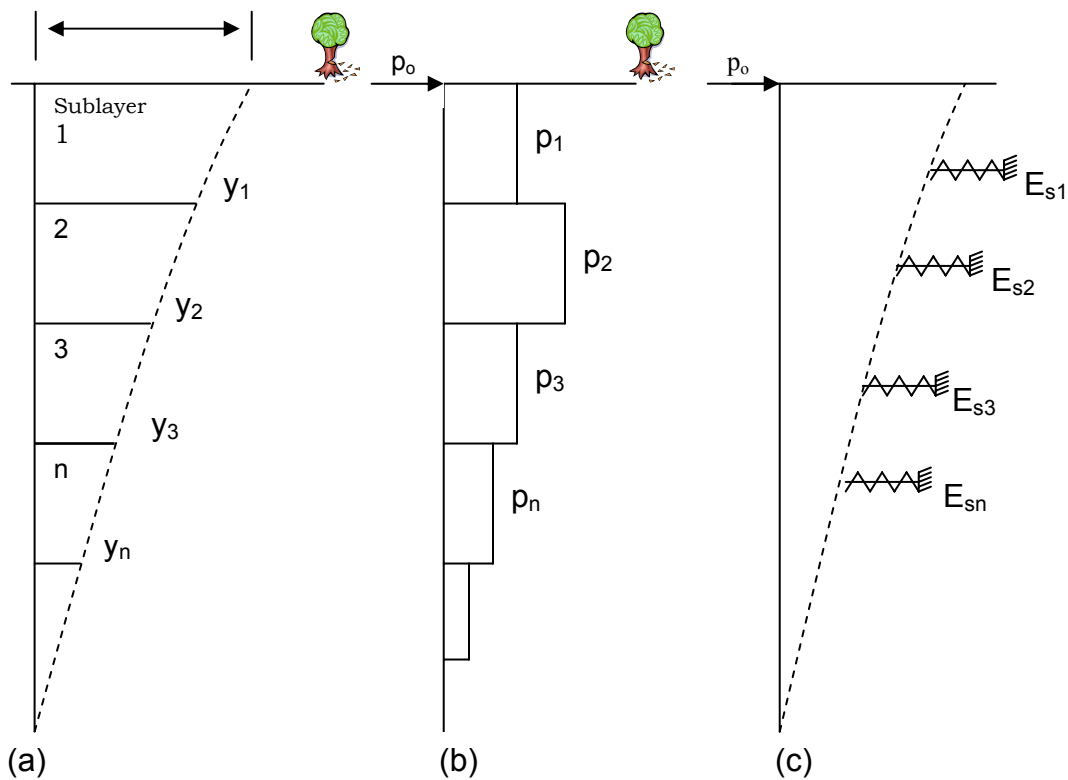


**Figure 2.4: Representation of a Laterally Loaded Foundation Element [18]:**  
**a) pile deflection;**  
**b) soil reaction;**  
**c) soil-pile interaction**

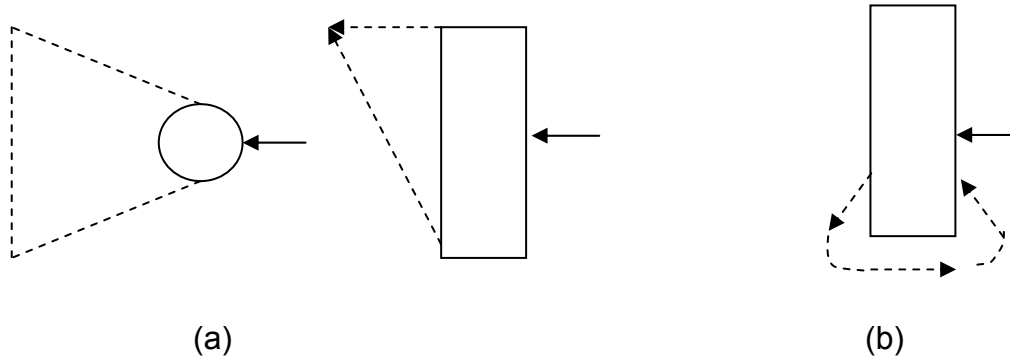


**Figure 2.5: Laterally Loaded Pile Failure [19]:  
a) Surface Failure;  
b) Toe Failure**

### 2.3 Beam Theory

For beam theory, a fourth order differential equation, based on the basic beam slope equation, is used to derive a mathematical expression for the soil resistance,  $p$ , against foundation deflection,  $y$ . This is described below [18, 19]:

$$\theta = dy/dx \dots\dots\dots (2.1)$$

$$M = EI d\theta/dx = EI d^2y/dx^2 \dots\dots\dots (2.2)$$

Where  $M/EI = d^2y/dx^2$  is the basic equation for curvature of a bent beam.

$$V = dM/dx = EI d^3y/dx^3 \dots\dots\dots (2.3)$$

$$p = dV/dx = EI d^4y/dx^4 \dots\dots\dots (2.4)$$

The notation is as follows:

$\theta$  = slope of the beam (radians)

$M$  = moment in the beam (in-lb.)

$V$  = shear in the beam (lb.)

$p$  = soil reaction against the beam (lb. /in.)

$x$  = distance along the axis of the beam (in.)

$y$  = deflection of the beam perpendicular to the axis (in.)

The slope, moment, shear, soil reaction, and deflection are determined for all sections along the drilled shaft or pile. As stated and shown, laterally loaded foundation deflection and soil reaction are interconnected. This is known as the p-y relationship and is described by p-y curves. Figure 2.6 a and b show typical p-y curves.

Soil response,  $p$ , will increase with increasing foundation deflection,  $y$ , as loading begins. However, at some deflection  $p$  will reach a limit and remain constant or possibly decrease with further deflection. Thus,  $p$  and  $y$  have a nonlinear relationship [20]. A family of p-y curves is formed from curves created for different depths along the drilled shaft or pile. Each p-y curve represents only a single depth. They mirror in form and significance the familiar stress-strain curves, determined from laboratory testing, and shift upward with increasing depth in a consistent manner [21]. Three factors influence p-y curves. They are soil properties, foundation geometry, and the nature of loading.

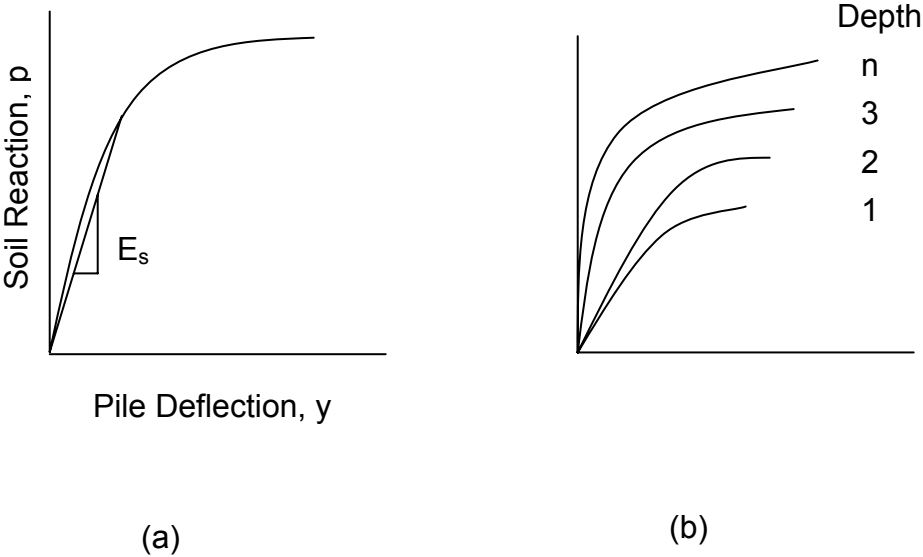


**Figure 2.6: a) Typical p-y curve, b) Family of p-y curves**



There are many equations relating soil resistance,  $p$ , and deflection,  $y$ , with the soil stress-strain properties determined in a lab or measured in the field. The general formula is [19]:

$$p/p_u = 0.5 (y/y_{50})^n \dots\dots\dots(2.5)$$

where  $n$  depends on the soil. For stiff clay above the water table,  $n$  equals  $1/4$ . For soft clay below the water table,  $n$  equals  $1/3$  [19]. Duncan and others developed  $p$ - $y$  curves for partly saturated silts and clays. They presented “the general form of the cubic parabola relationship” [20] as:

$$p = 0.5 p_u [y/(A\varepsilon_{50}D)]^n \dots\dots\dots[2.6]$$

where  $n$  equals  $1/3$ ,  $A$  is a coefficient that controls the magnitude of deflections,  $D$  is the diameter or width of the pile or drilled shaft, and  $\varepsilon_{50}$  is the strain required to mobilize 50% of the soil strength. Reese and Matlock recommend using triaxial compression tests, with confining pressure equal to the overburden pressure, for determining the shear strength of sand above and below the water table. “Values obtained from the triaxial tests might be somewhat conservative but would represent more realistic strength values than other tests [19].” Matlock recommended in-situ vane-shear tests and unconsolidated-undrained triaxial compression tests for soft clays below the water table. The values of shear strength,  $c$ , and strain should be taken at one-half the maximum total principal stress difference.

The ratio of  $p$  to  $y$  is expressed as the soil modulus of the pile reaction,  $E_s$  (lb/in<sup>3</sup>).

$$E_s = - p/y \dots\dots\dots(2.7)$$

$$p = - E_s y \dots\dots\dots(2.8)$$

Mathematically, it is the slope of the p-y curve and will usually increase with depth. At a given depth it will become smaller as pile deflection increases because of the nonlinear relationship of p and y.  $E_s$  represents the stiffness of the Winkler springs, shown in figure 2.6 d and e.

Axial loads are usually the primary form of loading on foundations, and will affect the response to horizontal loading on drilled shafts and piles. Welch and Reese clearly explain that “the application of a horizontal load or a moment reduces the axial stiffness of the element. The flexural stiffness is reduced by axial compression and increased by axial tension [18].” Therefore, the new fourth order differential equation to consider includes a constant axial force, P. The equation is:

$$EI \frac{d^4 y}{dx^4} + P \frac{d^2 y}{dx^2} + E_s y = 0 \dots\dots\dots(2.9)$$

The derivation of equation 2.9 is given in the Com624P manual along with the solutions for soft and stiff clay, sand, and layered systems [19].

Initial p-y analyses came from full-scale load tests. Lateral load tests were performed by the following people in the indicated soils: soft clay by Matlock in 1970; stiff clay by Welch, Reese and others in 1972 and 1975; sand by Cox, Reese, and Grubbs in 1974; vuggy limestone by Reese and Nyman in 1978 [19]. This type of analysis is expensive and most accurate for the exact soil it was performed in. However, using experienced engineering judgment, the p-y curves generated can be extrapolated to fit other soil types.

Com624P uses soil parameters and incremental structural loads to find a condition of static equilibrium and compute the shear, moment, and lateral deflection at each interval [1]. For all soil types, the basic input parameters include the soil effective

unit weights,  $\gamma'$ , and the horizontal subgrade modulus,  $k$ . For cohesive soils, the parameters include the cohesion,  $c_u$ , and the measured strain and 50% of the maximum principal stress. For cohesionless soils and cohesive soils under drained conditions, the parameter includes the internal friction angle,  $\phi$ . The soil parameters are obtained for laboratory tests or correlations using the results from field tests. Anderson, Townsend, and Grajales concluded that the standard penetration test (SPT) correlation based predictions were conservative while the cone penetration tests (CPT) best-predicted field behavior. The DMT derived p-y curves predicted performance well at low loads and the pressuremeter test (PMT) derived p-y curve predicted performance well for sands and clays [22].

Another method of analysis often used begins with assuming a point of zero deflection on the drilled shaft or pile. This is called the point-of-fixity. Slope, moment, and deflection can be determined through superposition for different points along the pile or drilled shaft. However, it is nearly impossible to accurately assume the point-of-fixity. Therefore, a conservative estimation of its location must be made.

## Chapter 3

### Scope of Research

The strength of loess and its resistance to lateral forces depends primarily on its clay content, moisture content, and dry unit weight. Even though these are highly regional properties, Swineford and Frye found that:

[P]roperties of the loess, especially those of the Nebraska and Kansas area, are sufficiently similar to establish certain important generalized findings for resolving soil mechanics and foundation problems [12].

Therefore, by relating a full scale load test with soil parameters obtained from in-situ and laboratory tests, a pertinent soil-structure relationship can be established. Multiple load tests were conducted as a part of this research under the conditions described in this chapter.

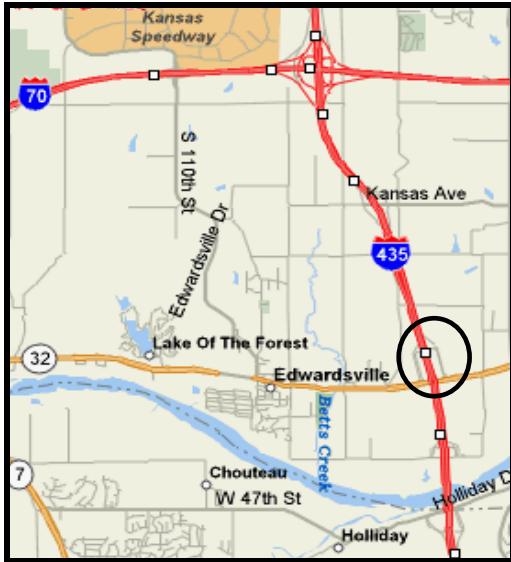
#### 3.1 Site Investigation

A uniform deposit of loess located on the northwest corner of I-435 and highway 32 in Wyandotte County, Kansas was selected by the University of Kansas (KU) and KDOT for the full scale lateral load test. Figure 3.1 shows the location of the test. In the early 1990's, Frantzen and Clowers [3] performed a full scale load test on cast-in-place piles on the north bound side of I-435, shown in the northeast corner of Figure 3.2, opposite the current test site. The site, which is part of the Loveland member, was chosen for its deep, uniform deposit of loess and deep groundwater table.

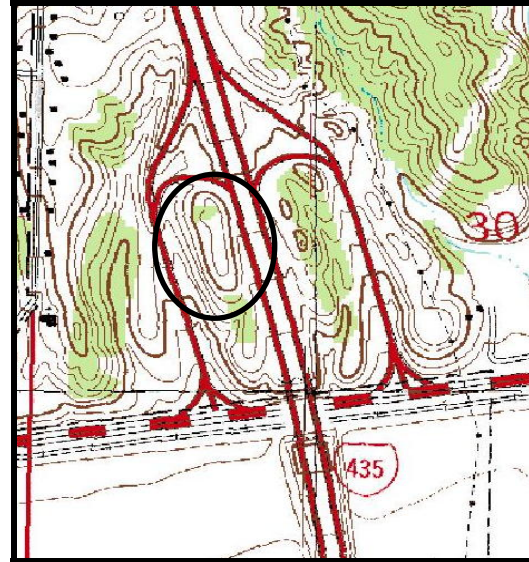
The soil profile consisted of tan to brown, silty, sandy clay to clayey and sandy silt. Water contents decreased after 12 feet below the surface; the soil was dry and stiff

below 16 feet boring termination. Ten borings were drilled by KDOT using a CME-45 truck. Nine were drilled during June of 2004 and one was drilled June of 2005 during the week of load testing. KDOT located the borings in the field and provided relative location information.

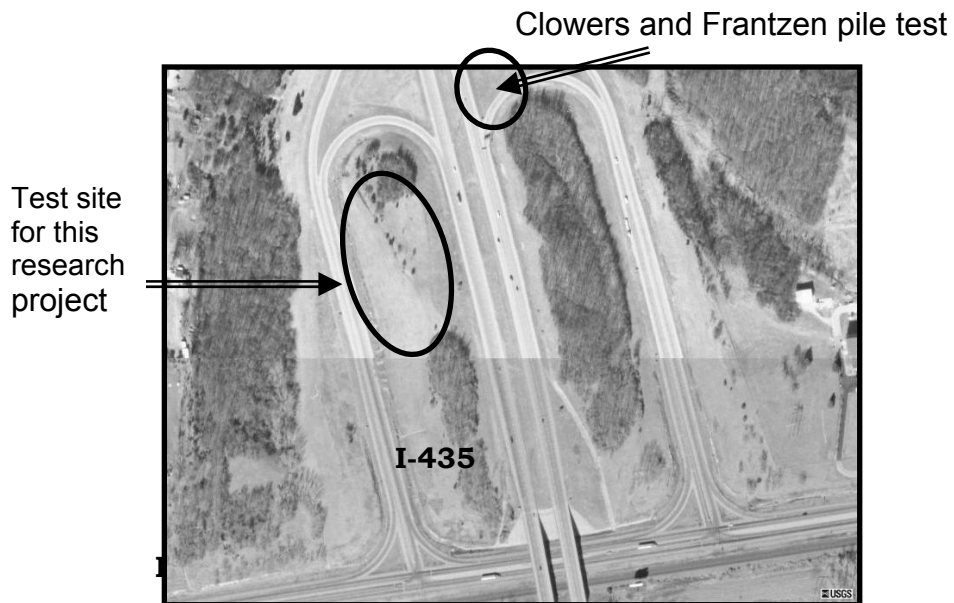
Field tests included standard penetration tests (SPT) in Borings A-D using an automatic hammer, a total of three cone penetration tests (CPT), two pressuremeter tests (PMT), and two continuous soil profiles obtained using a bull probe sampler, shown in Table 3.3. The PMT tests were performed using a Rocktest pressuremeter, model G-AM, at depths of 2, 5, and 10 feet. All in-situ tests performed in 2005 were conducted within two days of the final lateral load test to provide the most accurate soil profile possible when determining the soil's response to loading. Undisturbed soil was sampled using 3.5 inch diameter, thin-walled shelly tubes. The tubes were hydraulically advanced to depths of 1, 5, 7, 15, 23, and 25 feet on average. Boring logs are presented in Appendix B detailing at what depths each test was performed and shelly tubes were taken for each of the ten borings.



[a]



[b]



[c]

Figure 3.1: a) Site location [25]; b) Topographic map of site [26]; c) Aerial photo of test site [26]

**Table 3.1: In-Situ Testing**

2004	2005
Shelby Tubes	Shelby Tubes
SPT	CPT (2)
CPT	PMT
PMT	Bull Probe
Bull Probe	

**Table 3.2: Laboratory Tests**

Test	ASTM
Specific Gravity	D854
Moisture Content	D2216
Atterberg Limits	D4318
Grain-Size Distribution	D422
Unconfined Compression	D2166
Unconsolidated Undrained Triaxial Compression	D2850
Consolidated Undrained Triaxial Compression	D4767
Direct Shear	D3080
Consolidation	D2435
Collapse	D5333
Classification	D2487

Laboratory testing was performed in accordance with American Standard of Testing Materials (ASTM) procedures, as shown in Table 3.4. This included index property testing, consolidation, triaxial compression tests, direct shear, collapse, and repeated loading tests [25].

KDOT performed laboratory tests on undisturbed 2.8 inch diameter samples trimmed from 3.5 inch shelly tubes. KU performed laboratory tests on 1.4 inch diameter samples. Testing smaller samples caused more variations in the test results; however, it conserved enough sample to test for anisotropy within each shelly tube. The 1.4 inch sample sets were carved for unconsolidated undrained triaxial compression and direct shear so the long axis was in the vertical and horizontal direction. Comparisons were made at 1, 5, and 24 feet below the surface.

## **3.2 Test Shafts**

### **3.2.1 Configuration and Construction**

Drilled shaft dimensions and test configurations were based on the recommendations of Dan Brown and Associates. The expected soil response was estimated using laboratory results to determine the amount of concrete reinforcement required. Test shafts 1 and 2 were 42 inches in diameter; shafts 3, 4, 5, and 6 were 30 inches in diameter. The total design length of 27 feet was determined so the shafts were longer than the estimated point-of-fixity. Approximately 3.15 feet of the total length was cased above ground to facilitate application of the lateral load. Shafts were spaced 12 feet on center in all directions. Table A.1 in Appendix A lists as-built dimensions and details of all test shafts. Shafts were designed to react against each other under static and repeated loading as shown in Figure 3.2. Inclinometer casings were installed the full length of all six test shafts. Table A.2 in Appendix A shows as-built dimensions of the inclinometer casings.

Drilled shafts were constructed in a typical dry excavation manner. The 30-inch holes were drilled first. Spacers were added to the outside of each rebar cage to

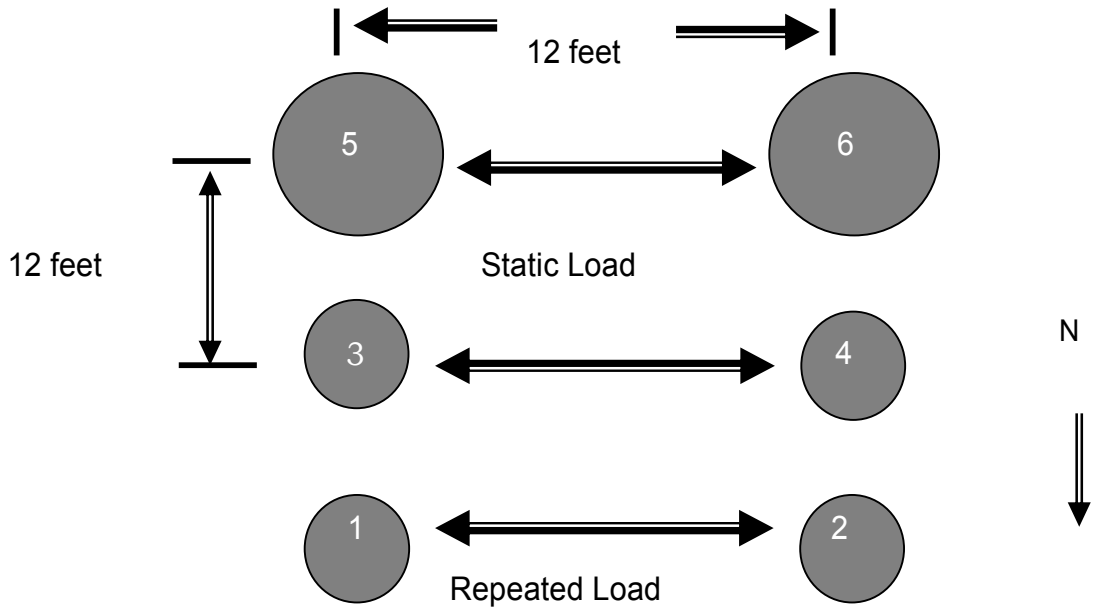


ensure the cages were centered upon installation. Inclinator casings were attached to the inside of each cage, shown in Figure 3.3. The reinforcement was then lowered into place and concrete was poured. Concrete specifications and strengths are shown in Appendix A, Table A3 and Figure A4, respectively. After construction, the shafts were allowed to cure for 70 days prior to loading.

Figure 3.4 relates the six drilled shafts to the location of in-situ tests performed and borings drilled. Locations were plotted approximately to scale. Borings A through I were drilled in 2004 and boring J was drilled in 2005, one day after the final load test was completed.



[a]



[b]

Figure 3.2: Drilled shaft loading layout



**Figure 3.3: Reinforcement cage with spacers and inclinometer casing attached**

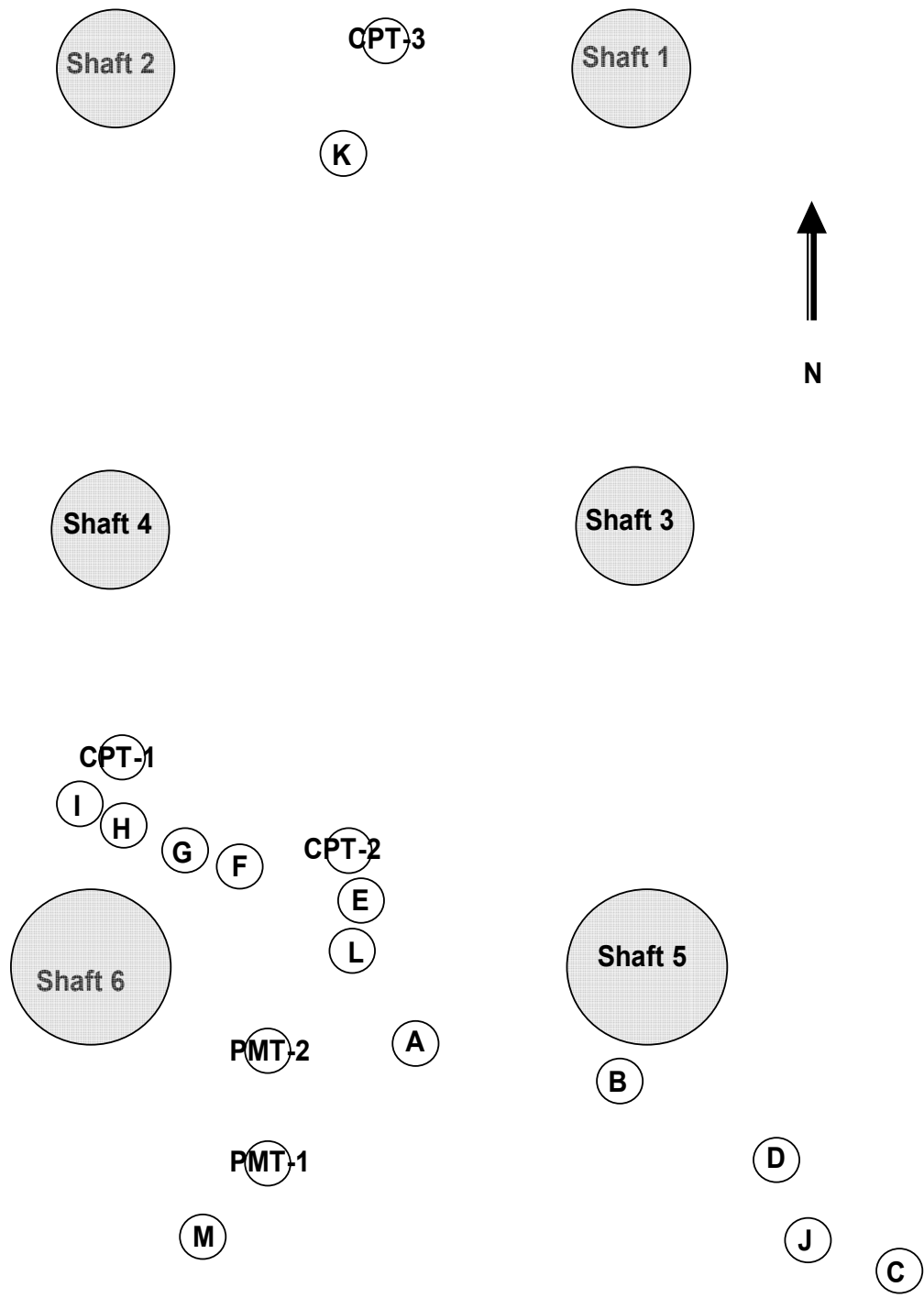


**Figure 3.4: Drilled Shaft Layout**

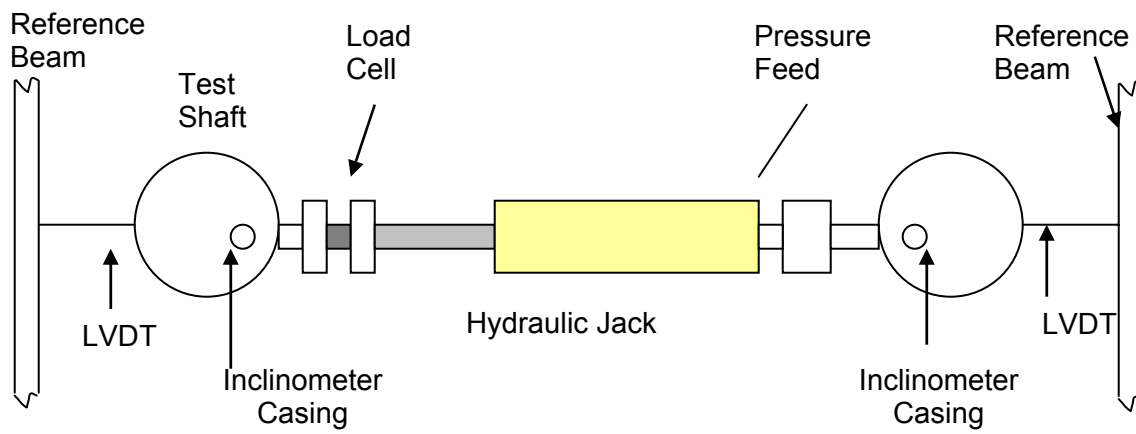
### **3.2.2 Instrumentation**

A load cell, used to apply the compressive lateral force, and a hydraulic jack were mounted inline between each pair of drilled shafts as shown in Figure 3.5 a and b. The applied load was measured using a calibrated load cell that was attached to the shaft by a steel collar as shown in Figure 3.5c. Two linear variable displacement transducers, LVDTs, were mounted on each collar to measure the top of shaft displacement. One LVDT was approximately 6 inches above and one was approximately 6 inches below the point of load application, shown in Figure 3.6.

Shaft deflections were measured using inclinometer soundings. The first set of inclinometer soundings were measured at ½ inch top of shaft displacement. At this time, the inclinometer was oriented along the north – south groove inside the casing and lowered into the drilled shaft. Readings were taken at two foot intervals for the length of the shaft. The inclinometer was brought back to the surface, realigned along the east – west groove inside the casing and again lowered into the drilled shaft. Readings were taken at two foot intervals for the length of the shaft. This ended the first inclinometer sounding.



[a]



[b]



[c]

Figure 3.5: a) Side photo of test shafts 5 and 6; b) Plan view of load test set up; c) load cell

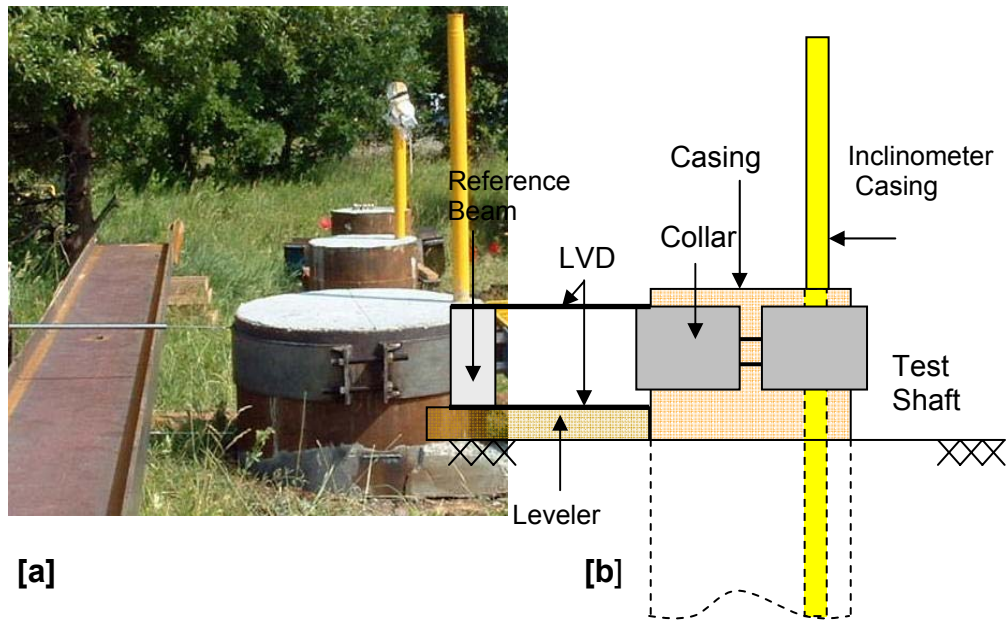


**Figure 3.6: a) Side view photo of test shaft 6; b) Side view schematic of test shaft**

### **3.2.3 Static Tests**

Static loads on the 30-inch diameter shafts (shafts 3 and 4) were applied and released in approximately 10 kip increments and 14 kip decrements, respectively. Three additional decrements, ranging from 30 to 44 kips, were applied. Inclinator soundings were performed at the beginning and ending of each test and at loads 51, 79, 99, and 127 kips. Load increments for the 30-inch diameter static test are presented in Table A.7 of Appendix A. Static loads were applied and released to the 42-inch diameter shafts (shafts 5 and 6) in approximately 15 kip increments and decrements ranging from 52 to 60 kip, respectively. Inclinator soundings were performed at the beginning and ending of each test and at loads 107, 150, 193, and 219 kips. Load increments for the 42-inch diameter static test are presented in Table A.8 of Appendix A.

Load increments and decrements without inclinator soundings were sustained approximately 5 minutes. Inclinator soundings took approximately 10 minutes per

shaft to perform; the total load duration was 20 minutes. Lateral pressures were maintained for load increments without inclinometer soundings. The hydraulic pressure was locked off during each sounding to better maintain deflected pile shape with depth.

### **3.2.4 Cyclic Test**

A cyclic load test was performed on two 30-inch diameter shafts (shafts 1 and 2). The shafts were subjected to four load increments (labeled “A” through “D”) with ten load cycles per increment. Load increments were performed at approximate top of shaft displacements of ½, 1, 2 ½, and 5-inches. Figure 3.7a shows drilled shaft 1 with a 5-inch top of shaft displacement and Figure 3.7b shows the soil gap at the conclusion of the test. Table 3.3 presents load increments A through D with respective approximate applied loads for shaft deflection and return and the inclinometer soundings performed. For each increment, shaft displacements were greater than the previous load increment. By doing this, the effects of plastic soil deformation from the previous load were negated.



[a]



[b]

**Figure 3.7: shaft 1: a) 6” top of shaft displacement; b) soil gap at the end of cyclic load test**



For each cycle, loads were sustained for only a few seconds and increment durations (A through D) are presented in Table 3.11. Inclinometer soundings were performed on the first and last cycles for each load increment (cycles 1 and 10); therefore, loads were held for approximately 20 minutes. As with each static load test, the hydraulic pressure was locked off during each inclinometer sounding to help maintain deflected pile shape with depth.

**Table 3.3: Load Increments for the 30-inch Diameter Cyclic Test**

Load Increment	Increment Duration (min)	Load Cycles	Approximate Load (kips)		Inclinometer Soundings Performed
			Deflect	Return	
N/A	N/A	None	0	0	Prior to Loading
A	1	1 through 10	50	-15	at Load Cycles 1 and 10 for each Load Increment
B	2	1 through 10	79	-25	
C	3.5	1 through 10	99	-30	
D	6.5	1 through 10	127	-30	

## **Chapter 4**

### **Test Results**

Laboratory and field testing was performed to estimate engineering and index properties of loess. Analytical results are presented in this chapter. Results of laboratory tests are presented on boring logs in Appendix B. Laboratory and field test results are presented in Appendix C.

#### **4.1 Laboratory Results**

KDOT conducted consolidated-undrained triaxial compression tests, unconsolidated-undrained triaxial compression tests, and unconfined compressive strength tests on samples 2.8 inches in diameter with a height to diameter ratio of approximately 2.2:1. Direct shear, consolidation, and index property tests were also performed. Testing was conducted on samples obtained in June 2004.

KU conducted unconsolidated-undrained triaxial compression tests on 1.4 inch diameter samples with a 2:1 height to diameter ratio. KDOT and KU both performed direct shear tests on 2.5 inch diameter samples. Pairs of samples tested in direct shear, from the same depth, were trimmed such that shear planes of the samples were parallel and perpendicular to the vertical effective field stress, respectively. This was done to analyze anisotropic strength characteristics. Consolidation, collapse, and index property testing were also conducted. Testing was conducted on samples collected in 2004 and 2005. Soil samples collected in 2005 were obtained during the week of load testing.

Figure 4.1 shows a subsurface profile of the test site along with representative soil parameters. The lithology and soil parameters presented are representative of all 13 borings. The SPT blow counts have been averaged within each sample from three to four SPT tests at the same depths.  $N$ ,  $N_{60}$ , and  $N_{1(60)}$  correlations are discussed in section 4.2.3. Natural moisture content, Atterberg limits, and shear strength values are from the 2004 Shelby tube samples.

#### **4.1.1 Index Properties**

Standard characterization tests were conducted on the soil samples. These included specific gravity, Atterberg limits, grain size distribution, and classification according to the ASTMs listed in Table 3.2. Table 4.1 presents the results; grain size distribution curves are shown in Appendix C.

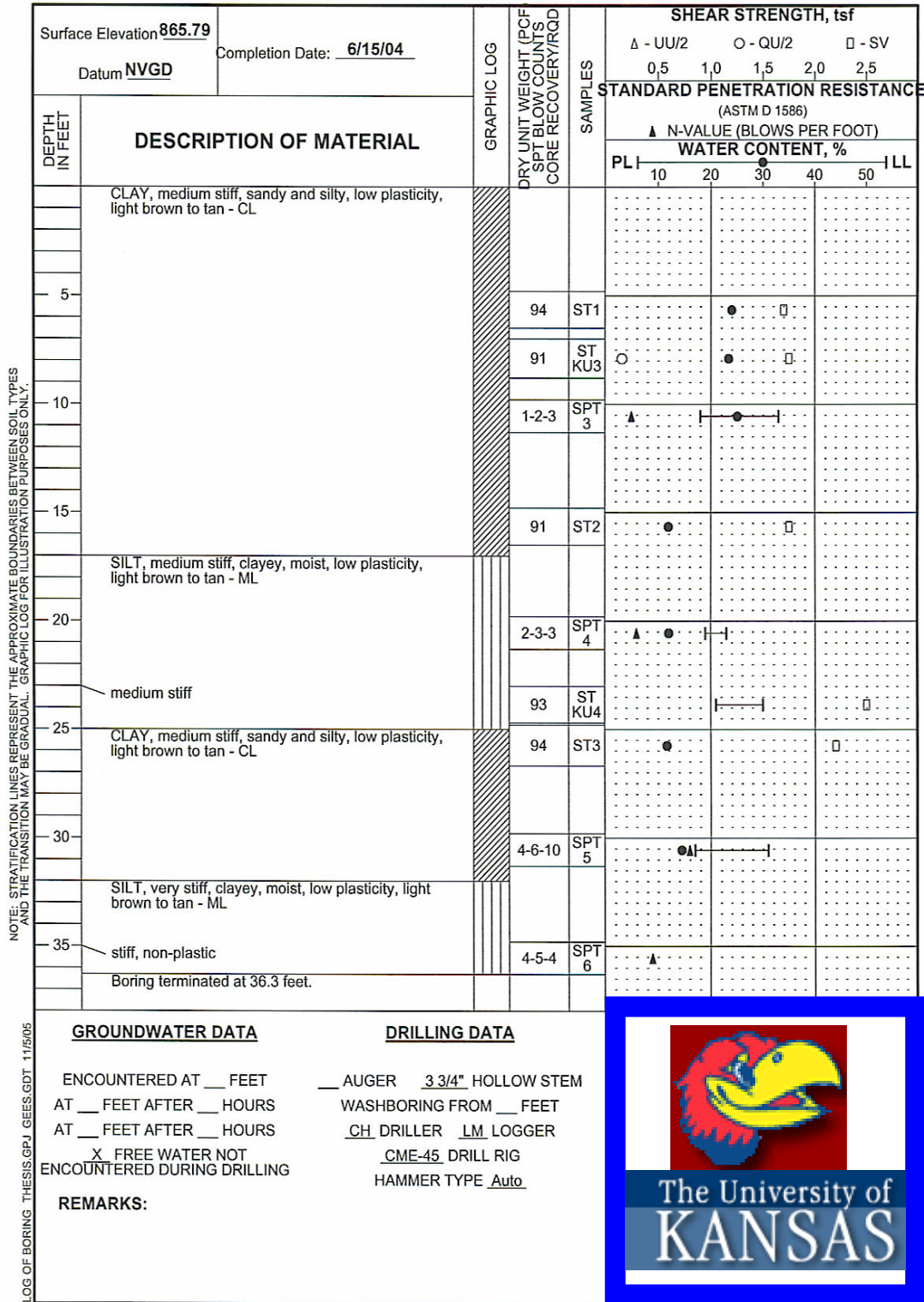


Figure 4.1: Typical Boring Log

**Table 4.1: Index Properties and Classification**

Depth (ft)	Atterberg Limits				Classification
	Gs	LL	PL	PI	
0 - 4	2.63	31	18	13	CL
4 - 8	2.68	36	17	19	CL
8 - 12	2.62	36	16	22	CL
12 - 16	2.62	33	18	15	CL
16 - 20	2.61		np		ML
20 - 24	2.61		np		ML
24 - 28	2.63		np		ML
28 - 32	2.63	38	17	21	CL

**4.1.2 Triaxial Compression Testing**

Consolidated-undrained (CU) and unconsolidated-undrained (UU) triaxial compression tests were performed according to ASTM D4767 and D2850, respectively, on undisturbed samples of loess to determine the cohesion, friction angle, and elastic modulus. The failure stress was taken as the maximum deviator stress the sample experienced. When the stress-strain curve showed a pronounced peak, the failure stress corresponding to the peak was chosen at the point of plastic yield.

Because the groundwater table in the field was at a great depth below the loess deposit tested, the probability of field saturation during the life of a structure was low. Therefore, total stress UU tests were performed under field conditions (partially saturated). The failure envelopes were nearly linear over the range of stresses tested. Deviations from the linear failure envelope were attributed to differences in the natural water content of the three UU samples tested [26]. Failure envelopes were drawn to

best represent behavior for in-situ stress conditions, where practical. Values of cohesion,  $c$ , and friction angle,  $\phi$ , were selected accordingly.

Samples sheared under consolidated-undrained conditions were saturated. Pore pressure was measured during all CU tests to obtain effective stress parameters. The values of effective cohesion ( $c'$ ) and effective friction angle ( $\phi'$ ) were based on the effective stress corresponding to the maximum deviator stress or peak stress. Results for the tests performed in 2004 are shown in Table 4.3 and those performed in 2005 are shown in Table 4.4. Normalized stress-strain curves and p-q plots for UU and CU tests are shown in Appendix C, listed in order by depth below ground surface.

Young's elastic modulus was computed as the slope of the elastic region for the normalized stress-strain curve. The point of plastic yield was chosen as either the failure stress corresponding to a pronounced peak or one-half the maximum deviator stress the sample experienced. Tables 4.2 and 4.3 contain the elastic moduli determined from the test data.

**Table 4.2: Triaxial Compression Results, 2004**

Depth (ft)	$c$ (psi)	$\phi$ (degrees)	$E_m$ (ksf)	Test	Lab
<b>1</b>	<b>5</b>	<b>18</b>	<b>202</b>	<b>UU</b>	<b>KU</b>
3	3	20	271	CU	KDOT
<b>5</b>	<b>4.5</b>	<b>25</b>	<b>124</b>	<b>UU</b>	<b>KU</b>
7	1.75	26	615	CU	KDOT
<b>15</b>	<b>3.5</b>	<b>30</b>	<b>163</b>	<b>UU</b>	<b>KU</b>
25	1.5	30	170	CU	KDOT

**Table 4.3: Triaxial Compression Results, 2005**

Depth (ft)	c (psi)	$\phi$ (degrees)	Em (ksf)	Test	Lab
1	4	22	152	UU	KU
5	1.5	23	150	UU	KU
15	0	32	228	UU	KU

**4.1.3 Unconfined Compression Testing**

Unconfined compression tests were performed according to ASTM D2166 on four samples at depths of 2.6, 5.3, 10.7, and 17.4 feet below the surface. The soil's elastic modulus was determined in the same manner as for the triaxial tests. Table 4.4 shows the results of the unconfined compressive strength tests. Stress-strain curves are presented in Appendix C.

**Table 4.4: Unconfined Compressive Strength Results, 2004**

Depth (ft)	Em (ksf)	Qu (tsf)	Qu (psf)	Consistency	Lab
2.6	101	1.36	2715	very stiff	KDOT
5.3	38	0.31	627	medium stiff	KDOT
10.7	17	0.25	501	medium stiff	KDOT
17.4	21	0.29	585	medium stiff	KDOT

**4.1.4 Direct Shear**

Direct shear tests were performed according to ASTM D3080 on submerged samples and those at in-situ moisture conditions. As with the triaxial compression tests, shear failure was considered to occur at the maximum shear stress. Shear stress versus strain curves and the normal stress versus shear stress curves are presented in Appendix C. Table 4.5 lists the values determined.

**Table 4.5: Direct Shear Results, 2004**

Depth	c (psi)		$\phi$ (degrees)		submerged	lab
	vertical shear	horizontal shear	vertical shear	horizontal shear		
<b>1</b>	<b>6.5</b>	<b>5</b>	<b>27</b>	<b>21</b>	<b>no</b>	<b>KU</b>
3	1.5	4	25	24	yes	KDOT
<b>5</b>	<b>1</b>	<b>1</b>	<b>23</b>	<b>24</b>	<b>no</b>	<b>KU</b>
7	0	1.5	27	27	yes	KDOT
15	5.5	2	28	25	yes	KDOT
<b>25</b>	<b>2</b>	<b>0</b>	<b>22</b>	<b>21</b>	<b>no</b>	<b>KU</b>

**4.1.5 Consolidation and Collapse**

Consolidation testing was performed at 3, 7, 15, and 24 feet below the surface. Conventional fixed ring odometers were used with the Geocomp automated soil testing system. Readings were automatically taken after consolidation was completed in accordance with ASTM D2435 and loads were automatically applied when 100% consolidation was achieved. The initial load increment was 1/8 tsf and loads were doubled with each application up to 16 tsf. One rebound curve was plotted for each test where the load was taken from 16 tsf to ¼ tsf, dropping by 4 tsf per increment. Table 4.6 presents the consolidation parameters determined and Appendix C has the void ratio verses the log of pressure curves.



**Table 4.6: Preconsolidation Pressure**

Depth (ft)	$p_c$ (psf)	OCR
7	2160	3.1
15	5040	3.4
25	3168	1.3

Collapse tests were conducted on relatively undisturbed shelly tube samples in accordance with ASTM D5333 at 1 foot and 25 feet below the surface. In general, the soil at these depths had the largest void ratios and, therefore, will have the largest degree of collapsibility. The collapse index ( $I_e$ ) is a basic index property of the soil and was determined in both tests. According to ASTM D5333, “[ $I_e$ ] is used to describe the degree of collapse that a particular soil will exhibit under specified conditions [25].”

Testing conditions for ASTM D5333 are not intended to replicate in-situ conditions. This preserves test repeatability and enables correlations between field and lab behavior to be drawn. Collapse tests were conducted in a manner similar to the one dimensional consolidation tests; however, the sample was kept unsaturated until the 2 tsf load increment and was then inundated with water. The change in void ratio after the sample was saturated was evaluated to determine collapsibility. Loess at the test sight was found to be slightly collapsible as presented in Table 4.7.

**Table 4.7: Collapse Index**

Depth (ft)	$I_e$ (%)	Degree of Collapse
1	0.5	slight
25	0.4	slight

## 4.2 In-Situ Testing

Field testing included PMT, CPT, Shelby tubes, and a continuous soil profile taken from a bull sampler as presented in Table 3.1. The continuous soil profile was presented in the representative boring log on Figure 4.1. Parameters needed for p-y curves are not directly obtained from the tests but can be estimated using correlated parameters presented in this section.

### 4.2.1 Pressuremeter Test

Three pressuremeter tests were conducted by KDOT, two in 2004 and one during the week of the full scale load test in 2005. Tests were performed at depths of 2, 5, and 10 feet below the ground surface. Table 4.8 lists the values recorded and Figure 4.2 shows the difference between the 2004 and 2005 tests. Figures of each test are shown individually in Appendix C. The following two equations were used to determine the elastic modulus ( $E_m$ ) and the at-rest earth pressure coefficient [5]:

$$E_{pm} = 2(1+\nu)(V_0+v_m)(\Delta p/\Delta v) \dots\dots\dots 4.1$$

Where  $v_m = (v_o + v_f) / 2$

$E_{pm}$  = pressuremeter elastic modulus

$\nu$  = Poisson's ratio = 0.33

$V_0$  = initial volume of pressuremeter cell

$\Delta p$  = change in pressure corresponding to  $\alpha v$

$\Delta v$  = change in volume corresponding to  $\alpha p$

$$E_m = E_{pm} / \alpha \dots\dots\dots 4.2$$

Where  $\alpha = 0.5$

The at rest earth pressure coefficient was calculated as the horizontal stress divided by the vertical overburden stress.

**Table 4.8: Pressuremeter Results**

depth (ft)	Em (ksf)		K <sub>o</sub>	
	2004	2005	2004	2005
2	276	208	2.6	3.1
5	159	446	1.3	1.5
10	225	240	0.7	1

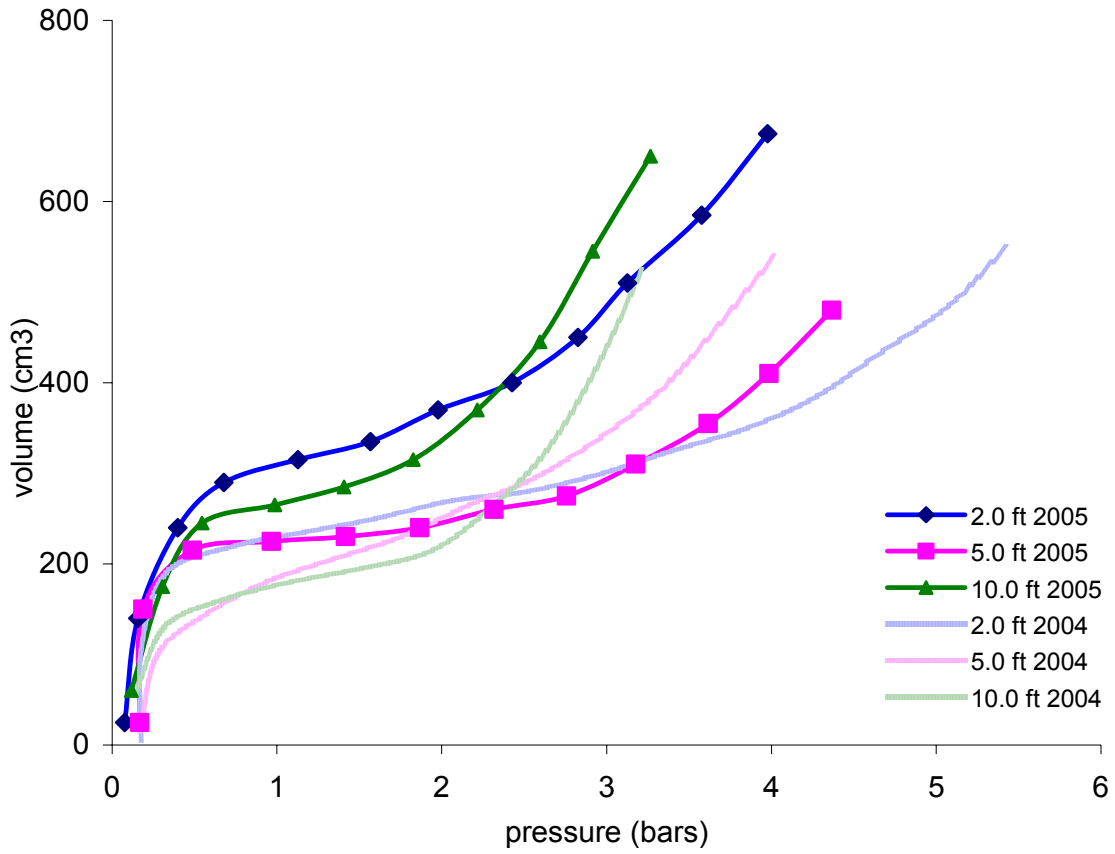


**Figure 4.2: 2004 and 2005 PMT**

### **4.2.2 Cone Penetration Test**

KDOT performed three CPT tests; one in 2004 and two during the week of the lateral load test. The software used to collect and analyze the field data was CPT-LOG Ver. 2.15a and CPT-pro Ver. 5.22, respectively. Figure 3.6 shows the location of the CPT tests in relation to the testing shafts. CPT logs are presented in Appendix C.

There are two soil profiles; one was computerized and the other was conducted manually by KU. The computer generated profile contains several layers of gravelly sand. However, the soil profiles obtained from the continuous bull sampler and from laboratory testing indicated the soil was silt to sandy silt with no gravel present.

Therefore, KU performed a CPT profile analysis using correlations derived from Robertson & Campanella[28]. These figures are presented in Appendix C.

The correlation by Schmertmann [30] was used to determine the elastic modulus and the correlation by Kulhawy and Mayne [32] was used to determine the effective friction angle of the soil. The equations are as follows:

$$E_m = 2 * q_c \text{ (ksf)} \dots\dots\dots 4.3$$

$$\Phi' = \tan^{-1} (0.1 + 0.38 * \log (q_c / \sigma_z')) \dots\dots\dots 4.4$$

Table 4.9 and 4.10 show the results from the KU CPT analysis for 2004 and 2005 respectively.

**Table 4.9: CPT 1 in 2004**

4.3	100	42
15.7	180	38
23.6	320	39
27.3	320	38
31.6	280	36
36.4	350	37
40.8	400	37
42.4	720	40

**Table 4.10: CPT in 2005**

**[a] CPT 2**

Depth (ft)	Em (ksf)	$\phi'$ (degrees)
1.4	50	44
5.8	40	34
9.6	80	36
13.1	120	36
17.4	190	37
20.3	180	36
22.6	190	36
25.1	200	35
27.5	250	36
31.5	238	35

**[b] CPT 3**

Depth (ft)	Em (ksf)	$\phi'$ (degrees)
1.8	50	43
8.0	40	32
13.1	56	31
13.9	90	34
14.6	124	36
22.9	210	36
31.4	260	36
33.3	220	34

### **4.2.3 Standard Penetration Test**

KDOT performed 14 SPT tests in 2004 using a 7-¾ inch hollow-stem auger, an automatic hammer, a sampler without a liner, a 7-¾ inch borehole, and a rod length that

varied from 20 to 40 feet depending on what depth the test was performed. Several correlations were considered for the effective friction angle using SPT blow counts (reported in Appendix C).

The correlations were derived for sandy soil by Peck [27], Schmertmann [30], and Wolff [31]. The equations were used since the loess sampled was sandy. Table 4.12 shows the average  $N$ ,  $N_{60}$ , and  $(N_1)_{60}$  values determined from equations presented in Appendix C with the appropriate corrections. The corrections for the  $N_{60}$  value are as follows: the energy ratio,  $C_E$ , was 0.90, the borehole correction,  $C_B$ , was 1.15, the sampling method correction,  $C_S$ , was 1.2, and the rod length correction,  $C_R$ , varied from 0.85 at 10 feet to 1.0 at 30 feet and deeper.

**Table 4.11: Average SPT N Values**

Depth	$N$	$N_{60}$	$(N_1)_{60}$
10	5	9	13
20	6	12	12
30	14	29	25
35	10	21	16

Table 4.12 and Figure 4.3 show the correlated values and equations for the total friction angle (shown in Appendix C, Table C7.2), the effective friction angle (from Schmertmann, Wolff, and Peck), and the elastic modulus (from Kulhawy and Mayne). A discussion of the results is presented in Chapter 6.

**Table 4.12: SPT Correlations for sand**

Author	Equation
Schmertmann [30]	$\phi' = \tan^{-1} \left[ \frac{N_{60}}{12.2 + 20.3(\sigma_z' / p_a)} \right]^{0.34}$
Wolff [31]	$\phi' = 27.1 + 0.3(N_1)_{60} - 0.00054(N_1)_{60}^2$
Peck [27]	$\phi' = 53.881 - 27.6034 * e^{-0.0147N}$
Kulhawy and Mayne [32]	$E_m = (5 N_{60}) * 100 \text{ kPa}$

**Table 4.13: Average SPT Correlated Values**

Depth	$\phi'$			Em (ksf)
	Schmertmann	Wolff	Peck	Sands with fines
10	37	31	28	94
20	36	31	29	116
30	42	34	31	255
35	38	32	30	172

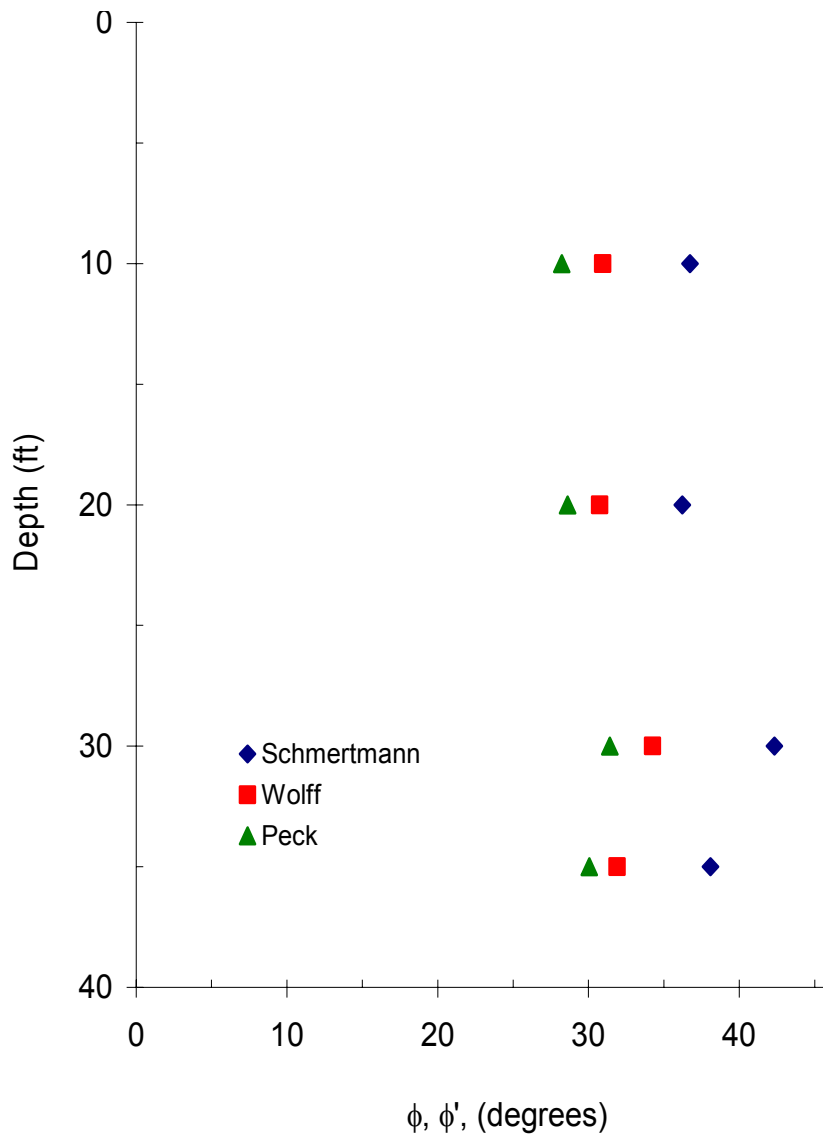


**Figure 4.3: Average SPT Correlated Values**



## Chapter 5

### Analysis and Comparison of Laboratory and In-Situ Testing

The use of accurate, and even elaborate, methods of testing requires no justification in the research laboratory. The extent to which these methods should be adopted in routine testing depends largely on whether or not they reduce the margin of uncertainty in design sufficiently to justify their cost. [25]

Most empirical geotechnical correlations are for soils categorized as sand or clay. Loess has some of the characteristics of both sand and clay. In this chapter, field and laboratory results are compared along with empirical correlations to determine which correlations best suit loess.

#### 5.1 Soil Classification

Soil from the site was classified by laboratory and in-situ methods. A visual classification, based on split spoon samples, Atterberg limits, and shear strength testing, is presented on boring logs in Appendix B.

The soil was classified based on laboratory testing as low plasticity clay (CL) from the ground surface to a depth of 16 feet. The soil was classified as non-plastic to low plasticity silt (ML) from 16 to 28 feet below the surface. The soil was again classified as low plasticity clay (CL) from 28 to 32 feet below the surface.

The soil was classified in-situ using a computer generated CPT profile. Three different CPT tests were performed. CPT analyses 1 and 3 indicated a clay layer approximately 9 to 12 feet thick just below the ground surface. This CPT method does

not distinguish between high and low plasticity clay. Below the clay layer, the computerized CPT analysis indicates alternating layers of silty sand, sandy silt, and clayey silt. CPT analysis 2 presents a soil profile consisting of alternating layers of sand, clayey sand, gravely sand, and no silt. CPT 1 was located on the south side of the test site, between drilled shafts 4 and 6. CPT 2 was also located on the south side, between shafts 5 and 6. CPT 3 was located on the north side of the test site, between shafts 1 and 2. Test 1 and 3 were on opposite sides of the test site and had similar computer generated soil profiles. Test 1 and 2 were around the same test shaft, shaft 6, but had a large discrepancy in the computer generated soil profile (see Figures C6.1, 6.3, and 6.4 in Appendix C).

A CPT analysis was performed manually using correlations from Robertson and Campanella [28]. These profiles consisted of alternating layers of sand, silty sand, and sandy silt, see Figures C6.1, 6.3, and 6.4 in Appendix C. The soil profile produced is more consistent with the laboratory classification but still differs significantly from actual soil samples. It was concluded that samples are required to obtain the most reliable soil classification information for loessial soils.

These results suggest that soil classification in loess deposits based on CPT correlations can vary significantly based on the correlation used and confirmation of soil type through borings is recommended.

## **5.2 Direct Shear**

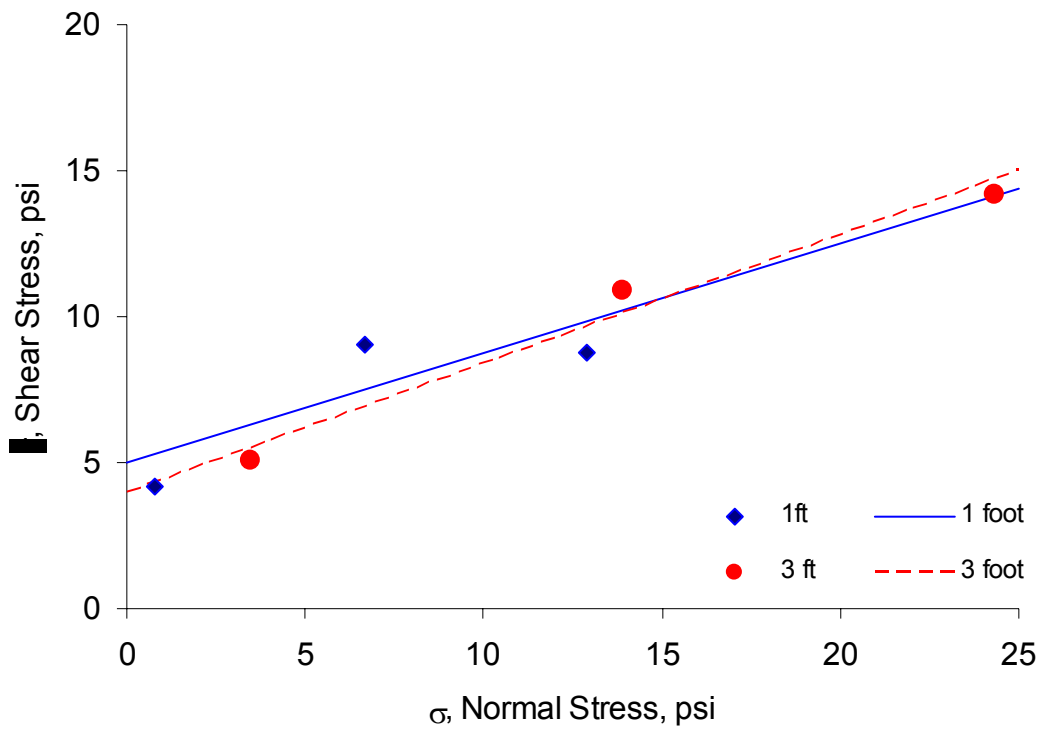
The direct shear test is the oldest method for investigating the shearing strength of soils [5]. Samples were tested under submerged and in-situ conditions to analyze the effect of increasing moisture on strength and cohesion. All samples quickly consolidated

before testing began and submerged samples were sheared at a rate to achieve drained conditions. Using Coulomb's strength equation,

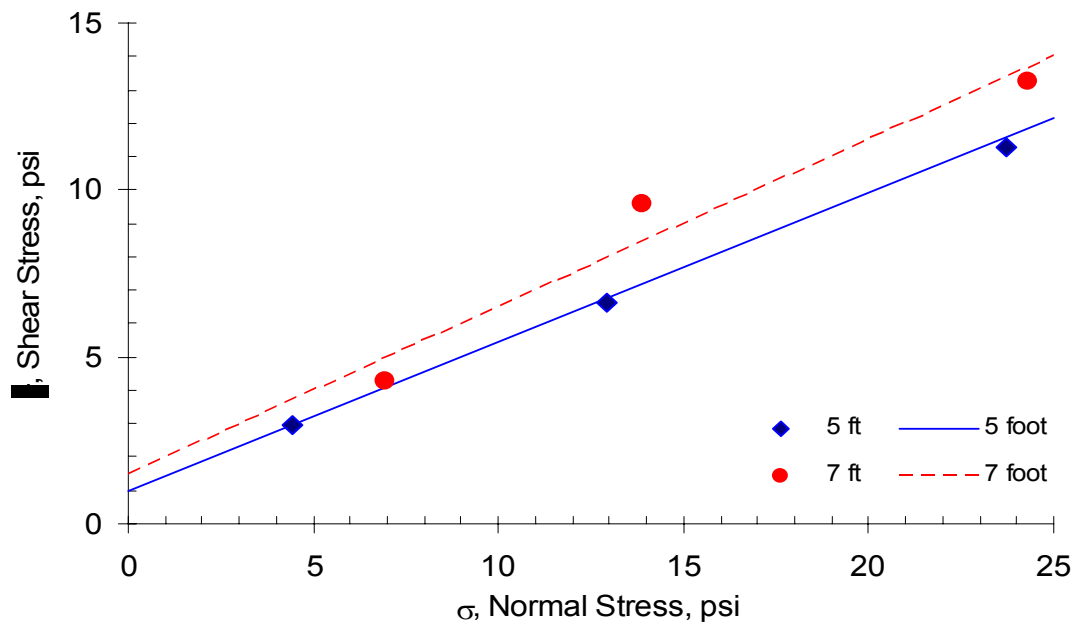
$$s = c + \sigma' \tan \Phi' \dots\dots\dots 5.1$$

critical combinations of shearing and normal stresses were plotted to create Mohr-Coulomb failure envelopes for selected depths. True failure envelopes that extend over a wide range of normal stresses are often curved under a given set of conditions; however it is common practice to approximate the overall failure with a linear relationship by assuming the soil parameters ( $c$ ,  $\Phi$ ) are constant. Shear strengths were plotted in Figure 5.1 up to the maximum overburden stress of the samples tested using equation 5.1.

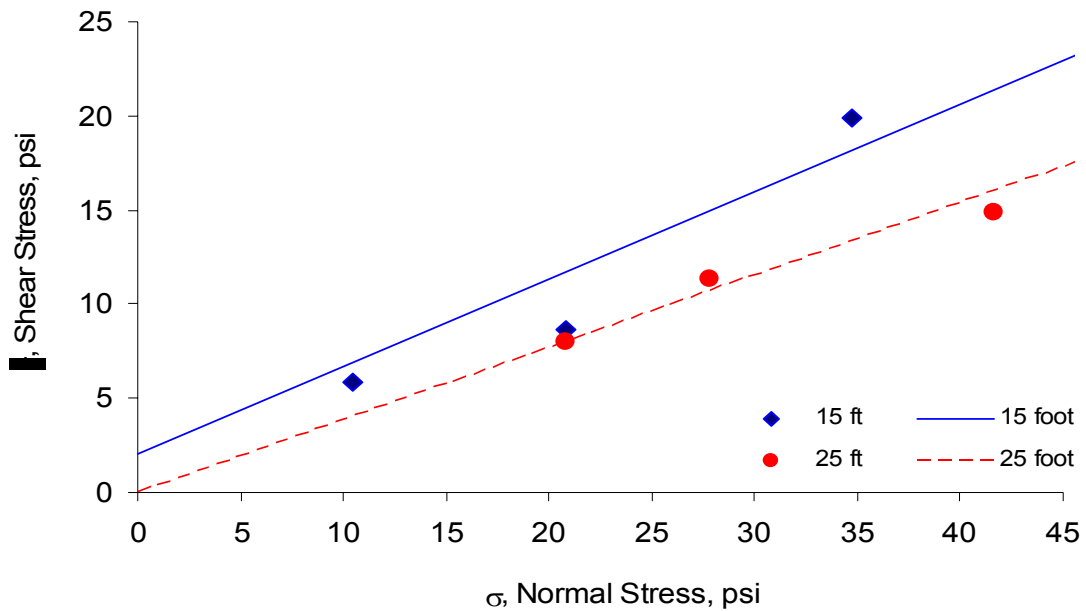
In-situ sample orientation for direct shear laboratory tests is shown in Figure 5.2. Samples were tested to replicate in-situ shear where the shearing plane is parallel to the vertical stress in the field are denoted DSV. Submerged tests, performed by KDOT, were conducted on samples obtained from shelby tubes taken at depths of 3, 7, and 15 feet. Submerged tests are noted by (s) in the following figures. Samples taken at 1, 5, and 25 feet below the ground surface were tested at in-situ conditions by KU.



(a) Mohr-Coulomb failure envelop for 1 and 3 feet below the surface



(b) Mohr-Coulomb failure envelop for 5 and 7 feet below the surface



(c) Mohr-Coulomb failure envelop for 15 and 25 feet below the surface

Figure 5.1a to 5.1c: Mohr-Coulomb Failure Envelopes for Direct Shear Tests Subjected to Horizontal Shearing

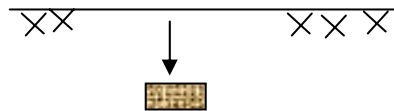


Figure 5.2: Orientation of Direct Shear Samples with DSH Notation

Cohesion generally decreased with depth. However, submerged samples from depths of 7 and 15 feet were less cohesive than soils sampled at a depth of 25 feet and tested at in-situ moisture conditions. Shear strength tended to decrease with depth for samples tested under both submerged and in-situ moisture conditions.

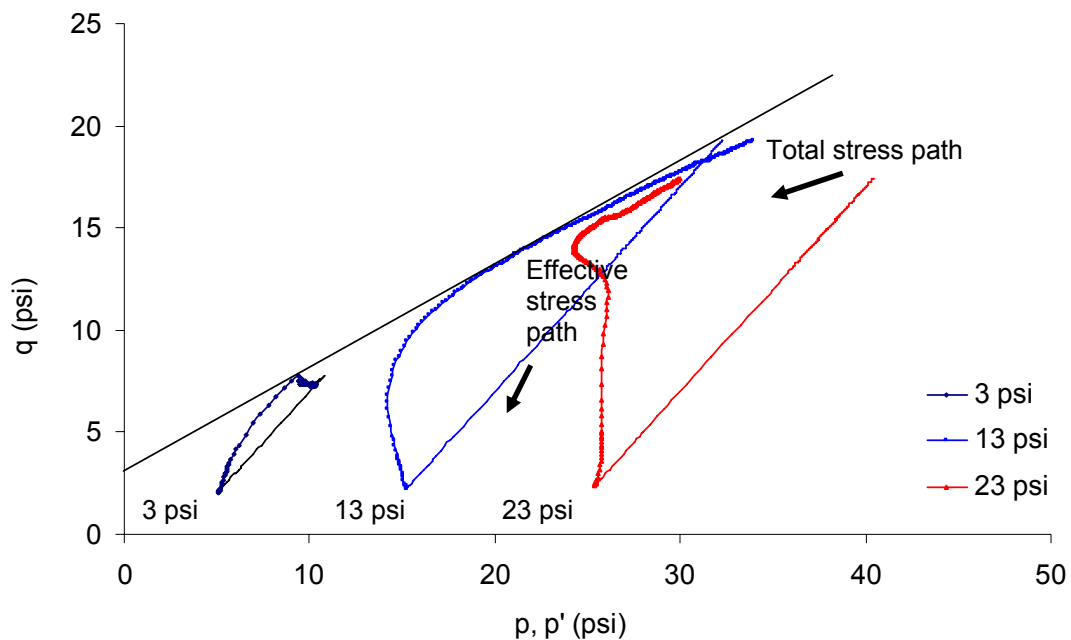
### 5.3 Triaxial Compression

Stress-strain curves developed under unconsolidated-undrained and consolidated-undrained triaxial compression testing conditions were similar to stress-

strain curves of sandy material with sufficient normal stress to not induce sample expansion. Terzaghi states:

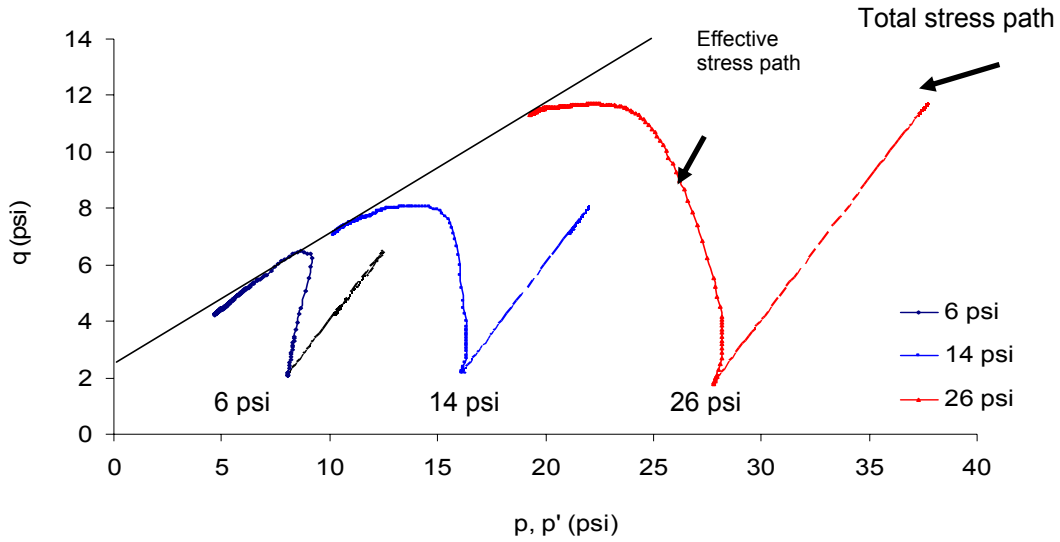
(that) to interpret laboratory or field strength tests and to select strength parameters for stability analysis, it is useful to examine the manner in which the effective normal stress and the shear stress change during mobilization of the shearing resistance [5].

Stress paths were plotted for all triaxial compression tests performed. Figures 5.3, 5.4, and 5.5 contain the stress paths of the three consolidated-undrained tests performed on samples taken from 3, 7, and 25 feet below the ground surface, respectively. All samples were consolidated under isotropic pressure conditions. Pore water pressure was measured and total and effective stress paths were plotted, p-q and p'-q, respectively. P and p' were determined from consolidated-undrained triaxial compression tests performed by KDOT in 2004. Triaxial test results are presented in Appendix C. p and q were calculated from  $(\sigma_1 + \sigma_3) / 2$  and  $(\sigma_1 - \sigma_3) / 2$ , respectively. p' and q' include effects from pore water pressure, calculated as  $(\sigma_1' + \sigma_3') / 2$  and  $q = q'$ , respectively.



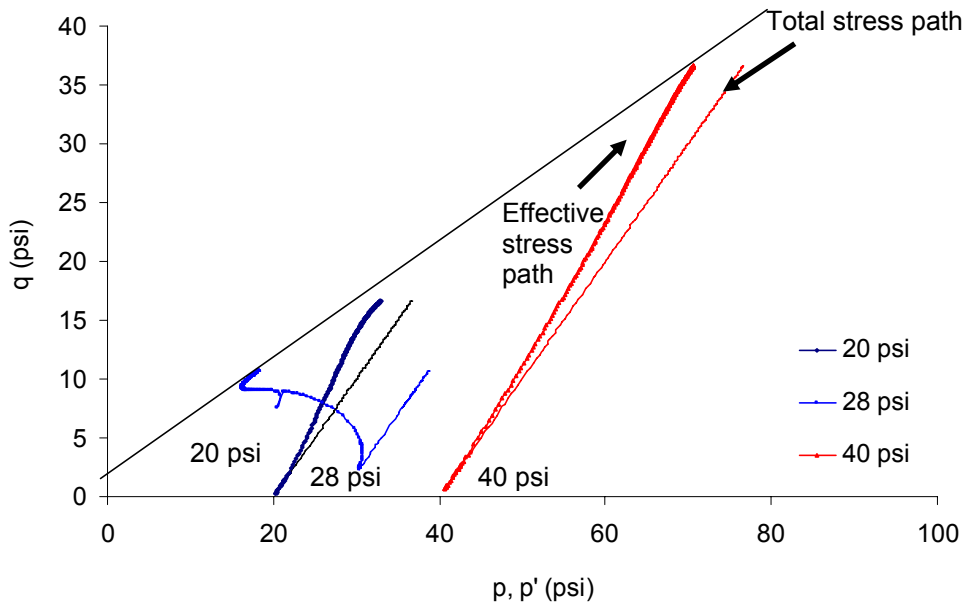
**Figure 5.3: Stress paths (p-q plots) for consolidated-undrained tests on loess samples from 3 feet below ground surface**

Figure 5.3 shows the total and effective stress paths (p-q, p'-q) of loess at a depth of 3 feet. At a low confining pressure of 3 psi, effective stresses, p', continued to increase, on average, even after the sample reached the maximum shearing stress, q. There was a small decrease during shear in p' on the samples tested under the 13 and 23 psi confining pressures before a sharp increase occurred as the sample neared failure. The decrease in effective normal stress from total stress indicates an increase in pore water pressure. The increase in pore water pressure comes from the sample contracting during shearing.



**Figure 5.4: Stress paths for consolidated-undrained test on loess samples from 7 feet below ground surface**

At a depth of 7 feet below the surface, Figure 5.4 shows a decrease in  $p'$  by the time the maximum shear stress,  $q$ , was achieved. The soil sampled behaves similar to that of a contractive material.

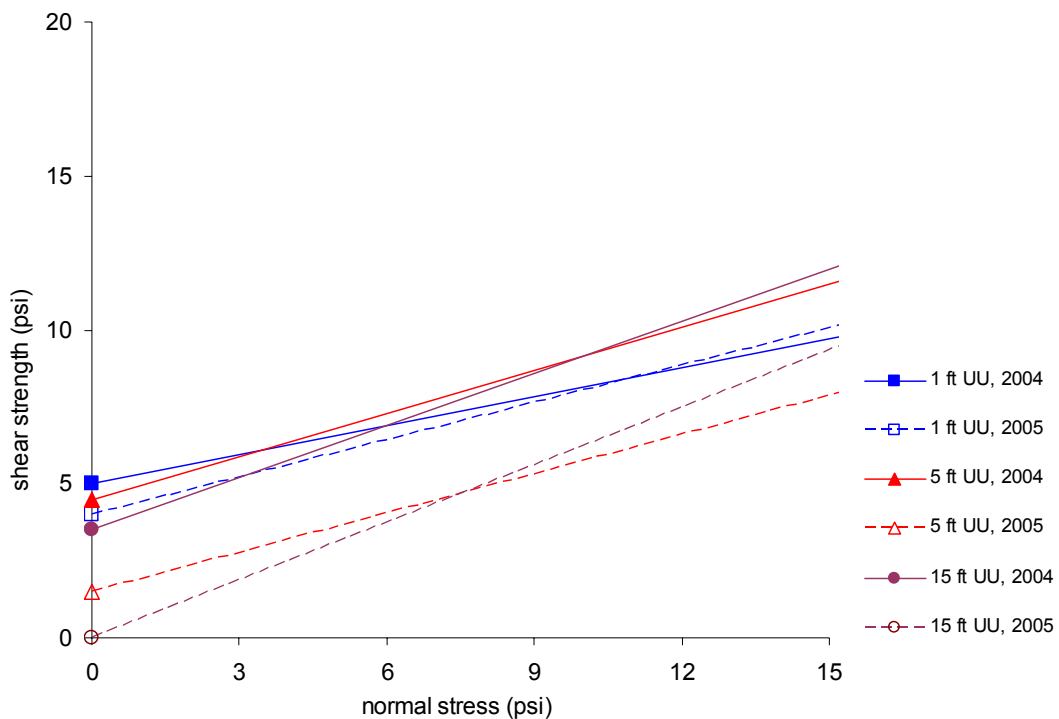


**Figure 5.5: Stress path for consolidated-undrained test on loess samples from 25 feet below ground surface**



Figure 5.5 is similar to Figure 5.1 in that  $p'$  continued to increase as the shear strength increases (20 and 40 psi samples), but the gap between  $p$  and  $p'$  increased for each case, indicating increased pore pressure for all samples. For the sample tested at a confining pressure of 28 psi,  $p'$  decreased as the sample began to shear. This indicates the sample contracted as it sheared, similar to a loose sand. Therefore, the soil profile, from depths of 3-25 feet, is contractive.

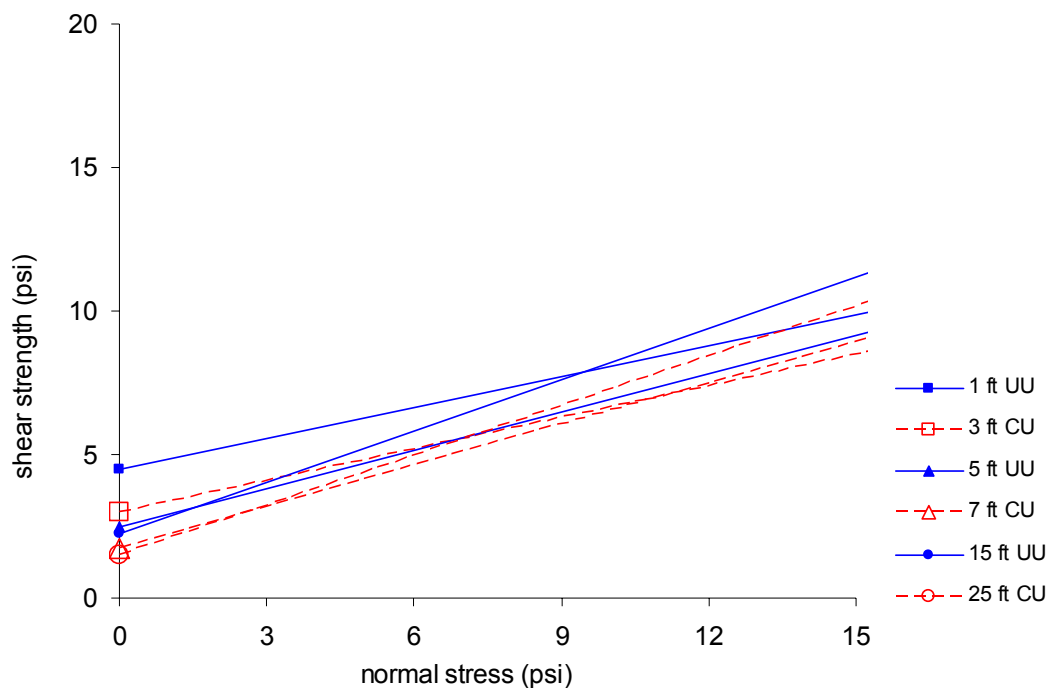
Soils sampled at 1, 5, and 15 feet below the ground surface were sheared under unconsolidated, undrained conditions. Tests at each depth were conducted on samples obtained in 2004 and during the week of the load test in 2005. Figure 5.6 shows the difference in cohesion and friction angles between the two tests at each depth.



**Figure 5.6: Unconsolidated-undrained tests performed in 2004 and 2005**

Cohesion decreased and friction angle increased with depth in 2004 and 2005. Overall, cohesion was lower in 2005 and friction angles were similar for each year. Unconsolidated-undrained parameters analyzed and discussed from here on are an average of 2004 and 2005.

Figure 5.7 shows all Mohr-Coulomb failure envelopes developed from samples sheared in the triaxial compression tests. Samples developed similar failure envelopes with common  $c'$  and  $\Phi'$  values. Friction angles  $\Phi$  and  $\Phi'$  were similar through out the soil profile for both in-situ moisture and saturated conditions.



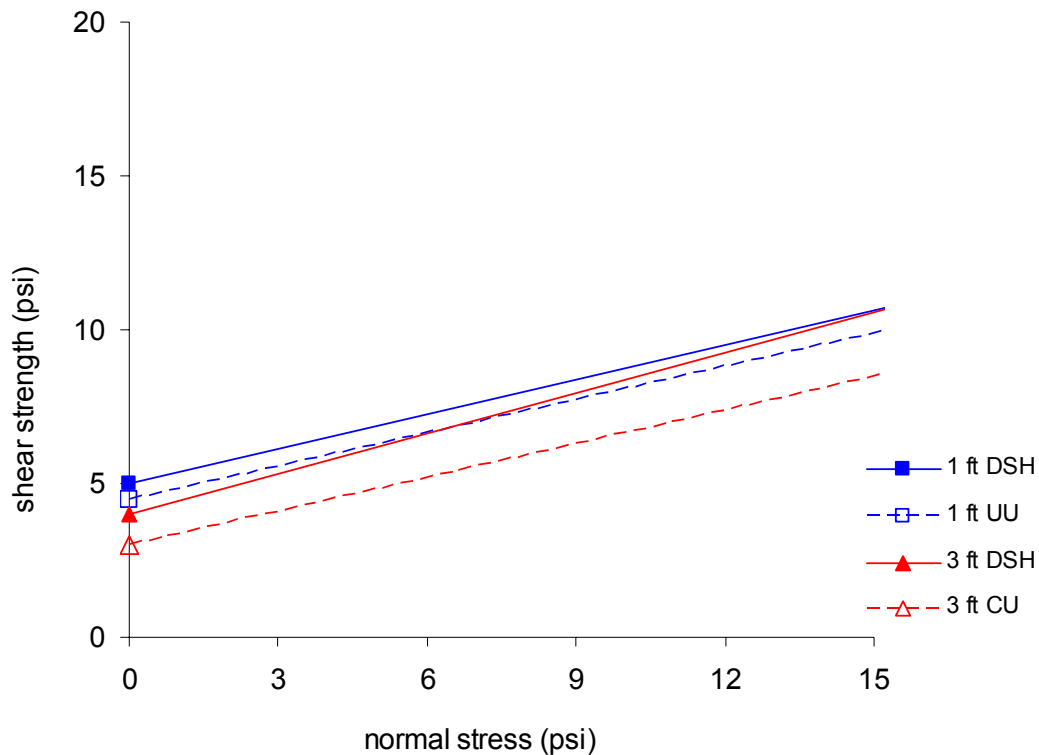
**Figure 5.7: Mohr-Coulomb failure envelopes for triaxial compression tests**

Figure 5.7 shows the cohesive and frictional nature of loess. This figure also confirms that, in general, cohesion decreases with depth. The soil profile was described in section 5.1 as a cohesive-sandy material at the surface that becomes sandier with

depth. Results from the laboratory testing and visual classification confirm that loess at the test site behaves as slightly cohesive loose sand.

#### 5.4 Cohesion and Friction Angle

Figures 5.8, 5.9, and 5.10 compare the Mohr-Coulomb failure envelopes of samples tested under direct shear and triaxial compression. Direct shear failure envelopes are the same as those presented in Figure 5.1 a, b, and c. Triaxial compression failure envelopes are the same as those presented in Figure 5.7. All test data is presented in Appendix C.

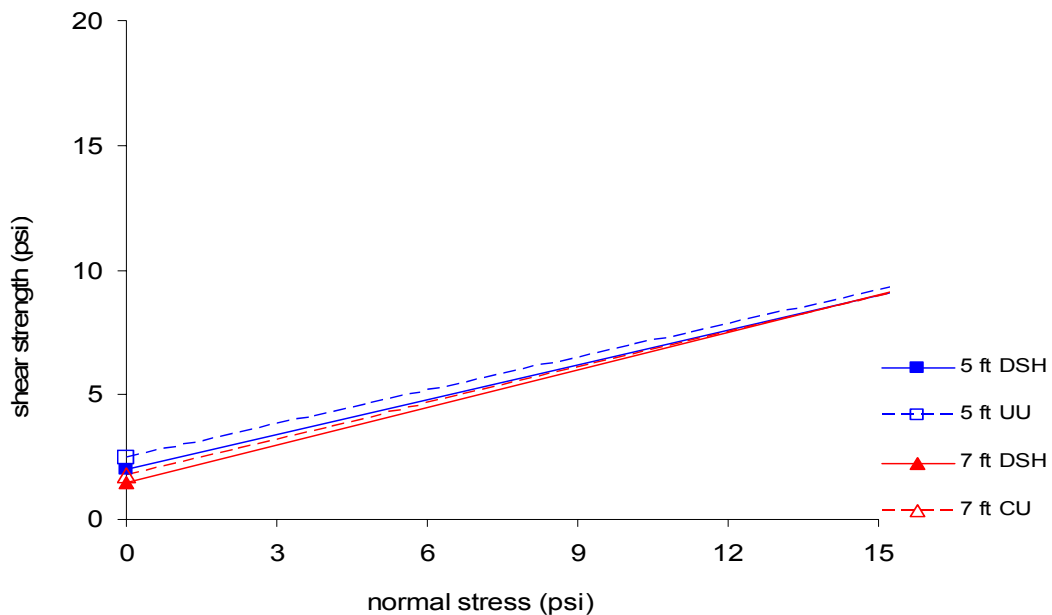


**Figure 5.8: Laboratory strength tests for samples obtained at 1 and 3 feet.**

Samples collected at 1 foot below the ground surface were tested at in-situ moisture conditions in triaxial compression and direct shear. The consolidated-undrained triaxial and submerged direct shear tests were performed on samples

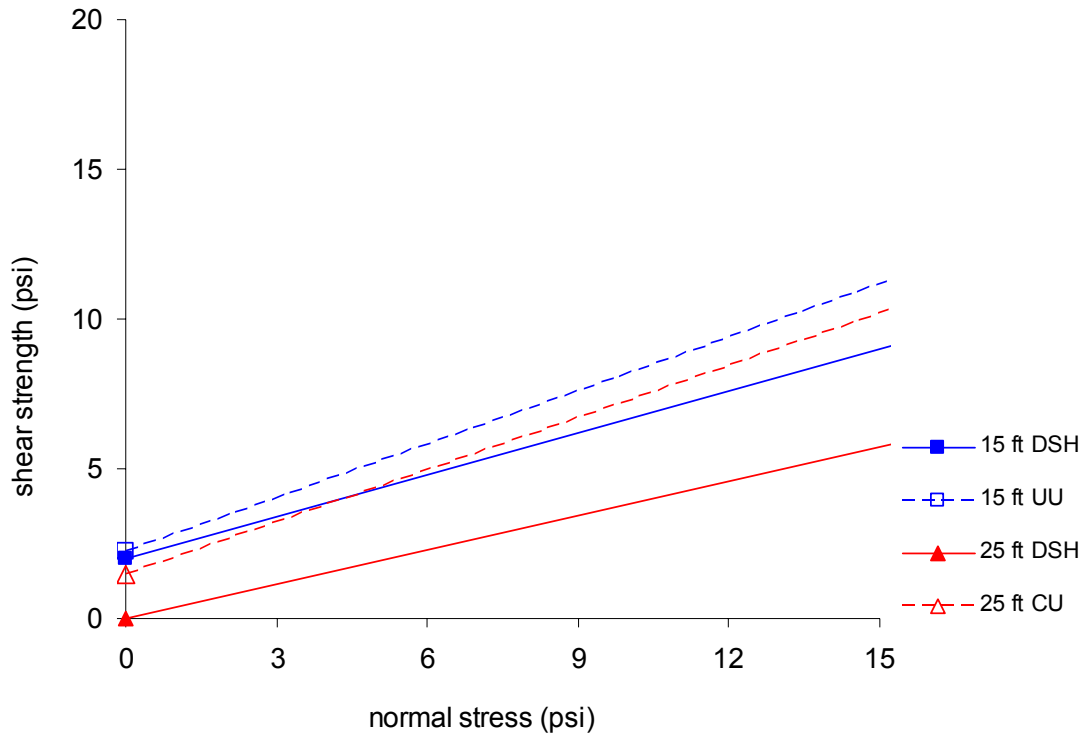
collected at a 3 ft depth. Direct shear test results were similar to the triaxial compression test results.

Soils sampled at 5 feet below the ground surface were tested at in-situ moisture conditions. Soils sampled at 7 feet below the ground surface were subjected to submerged direct shear and consolidated-undrained triaxial compression tests. Results for all four tests were similar and consistent with previous results.



**Figure 5.9: Laboratory strength tests for samples obtained at 5 and 7 feet.**

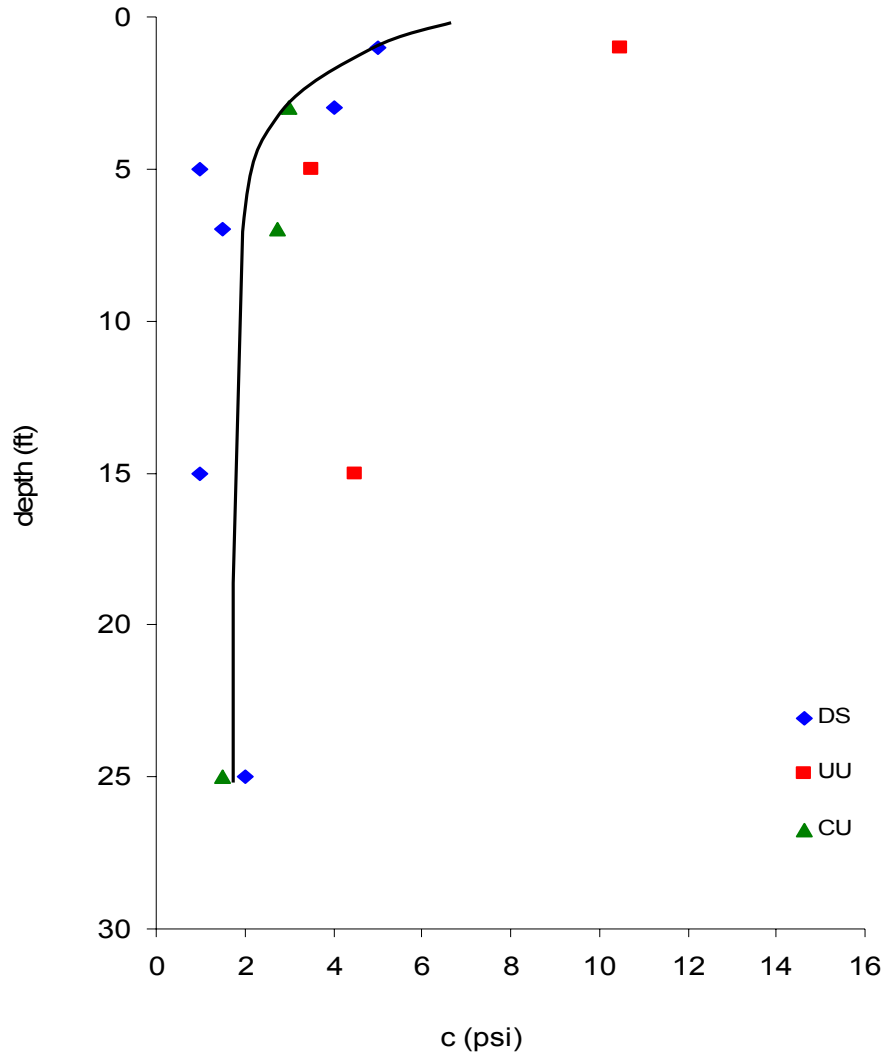
Soils sampled at 15 feet below the ground surface were tested at in-situ moisture conditions for both test types. Soils sampled at 25 feet below the ground surface were tested in direct shear at in-situ moisture conditions and consolidated-undrained triaxial compression. Samples from 25 feet had similar cohesive values. The friction angle derived from the direct shear test was higher than from the triaxial test.



**Figure 5.10: Laboratory strength tests for samples obtained at 15 and 25 feet**

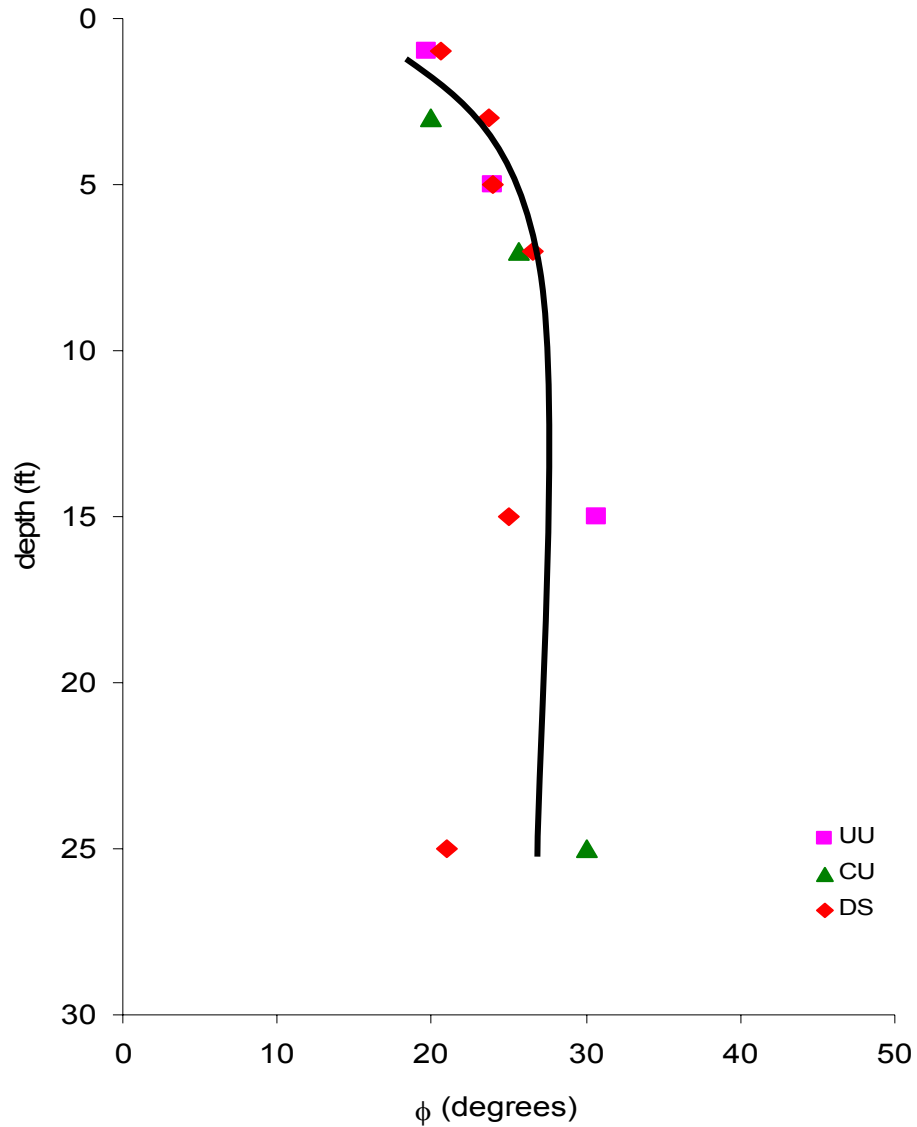
Overall, friction angles derived from triaxial compression tests were slightly lower than the direct shear results. Samples failed through direct shear are not failed along the weakest plane and, therefore, will have a higher friction angle than those failed in triaxial compression. Comparisons of varying moisture conditions on test samples indicate moisture levels have little impact on the shear strength.

Figure 5.11 presents all the cohesive values obtained from the unconsolidated-undrained triaxial test (UU), the consolidated-undrained triaxial test (CU), and the direct shear test (DS). Cohesion varied from 5 to 0 psi, decreasing with depth.



**Figure 5.11: Laboratory cohesion results for the soil profile.**

As stated in Chapter 2, the angle of internal friction ranges from 28-36 degrees for samples tested with moisture content below saturation [16]. Friction angles averaged from the 2004 and 2005 triaxial compression tests ranged from 20.0 degrees at a depth of 1 foot to 31 degrees at depths ranging from 15 to 25 feet below the surface. Friction angles determined from direct shear tests ranged from 21 degrees at a depth of 1 foot to 27 degrees at depth of 7 feet below the surface.



**Figure 5.12: Laboratory friction angle results for the soil profile.**

### 5.5 Anisotropic Strength Characteristics

Pairs of samples from the same depth were trimmed such that shear planes of the samples were parallel and perpendicular to the vertical effective field stress, respectively. Shearing planes of samples marked DSH were perpendicular to the vertical effective stress and shearing planes of samples marked DSV were parallel to the vertical effective stress, shown in figure 5.13.

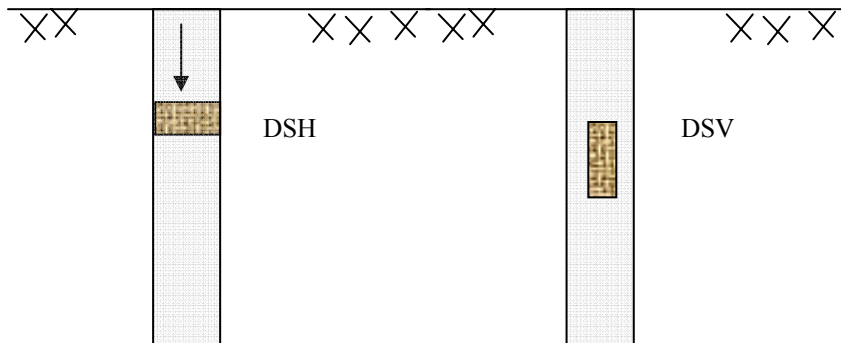


**Figure 5.13: Anisotropic sample orientation for direct shear testing**

Figures 5.14 to 5.19 contain direct shear and unconsolidated-undrained triaxial compression results to compare anisotropic strength characteristics. Samples tested in direct shear at depths of 1, 5, and 25 feet below the surface were sheared under in-situ moisture conditions. Samples tested in direct shear at depths of 3, 7, and 15 feet below the surface were submerged.



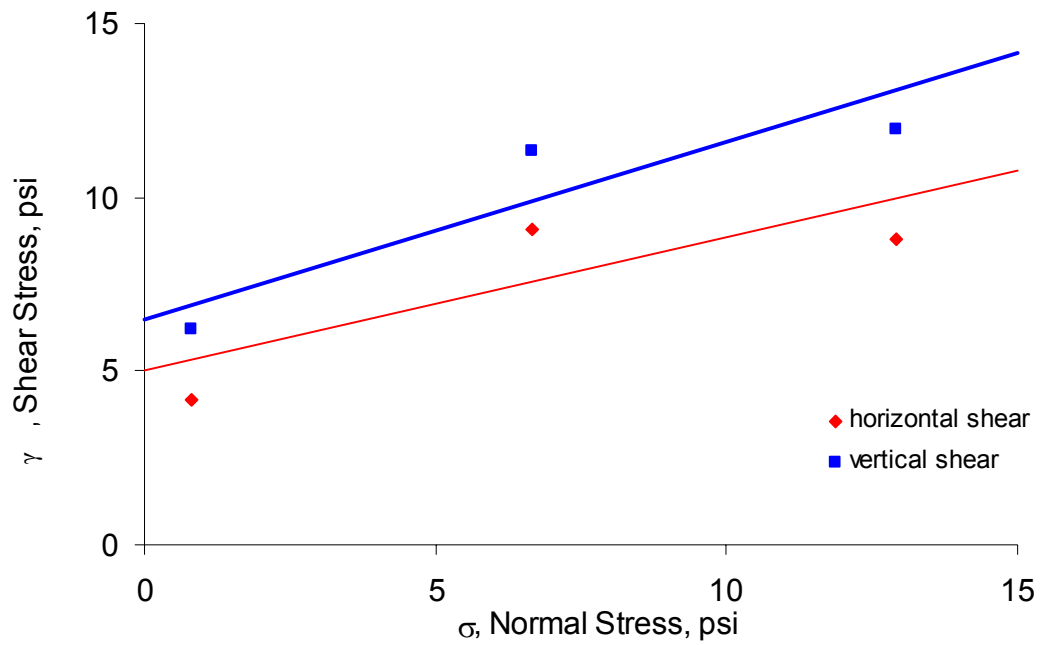


**Figure 5.14: Direct shear test results for specimens sampled at 1 foot**

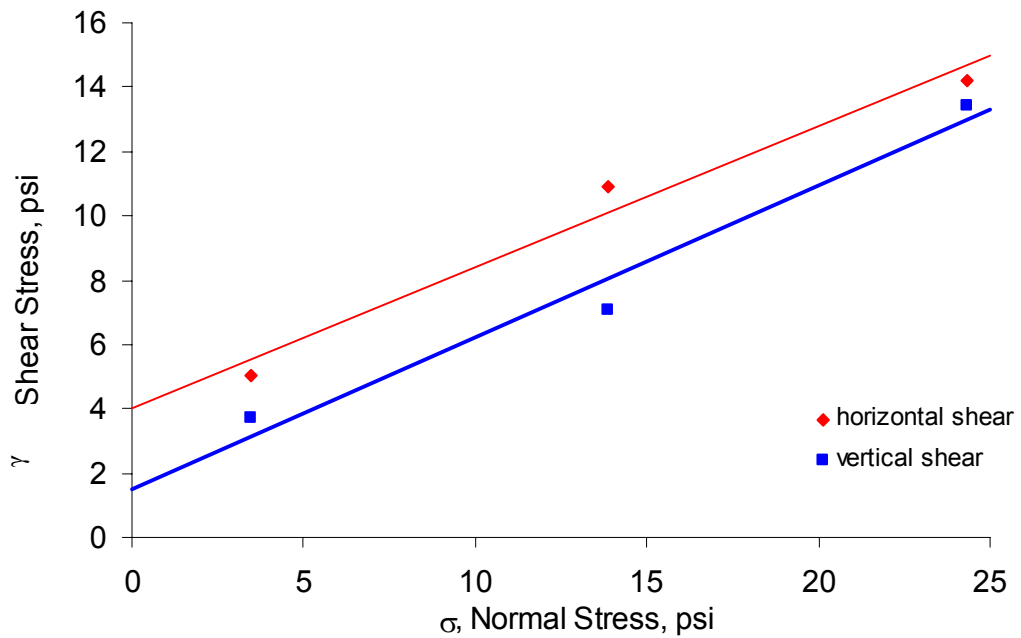


**Figure 5.15: Direct shear test results for specimens sampled at 3 feet**

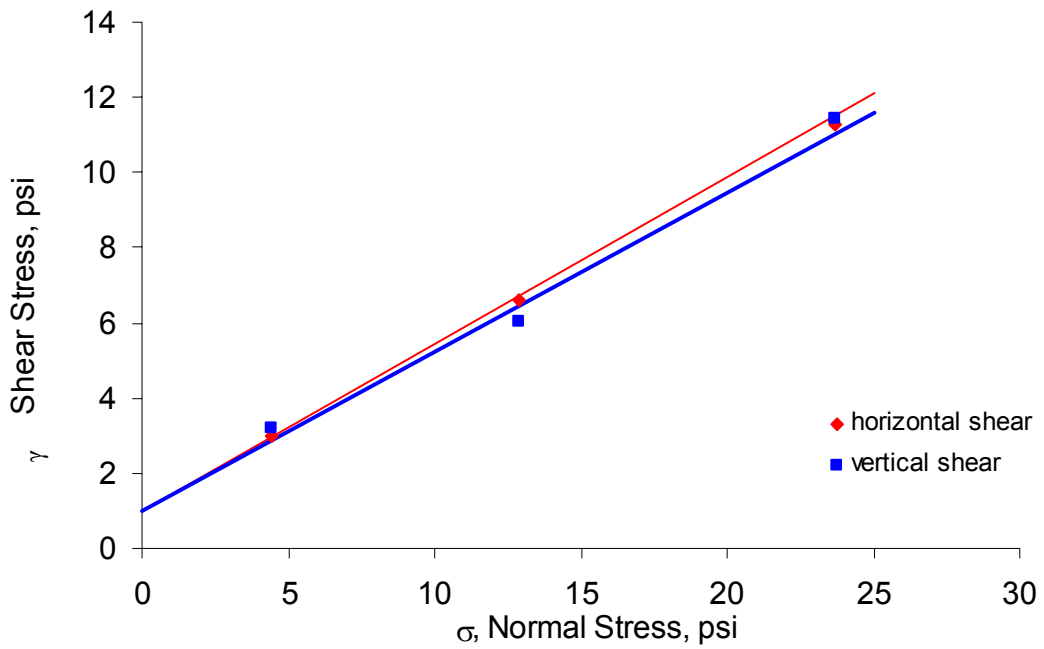


**Figure 5.16: Direct shear test results for specimens sampled at 5 feet**

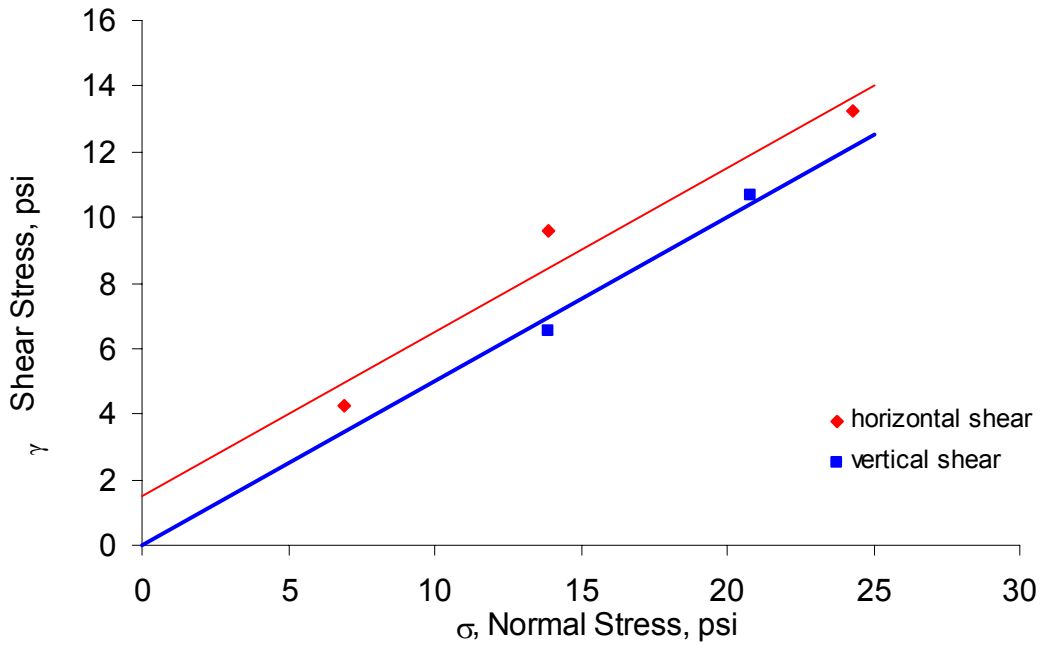


**Figure 5.17: Direct shear test results for specimens sampled at 7 feet**

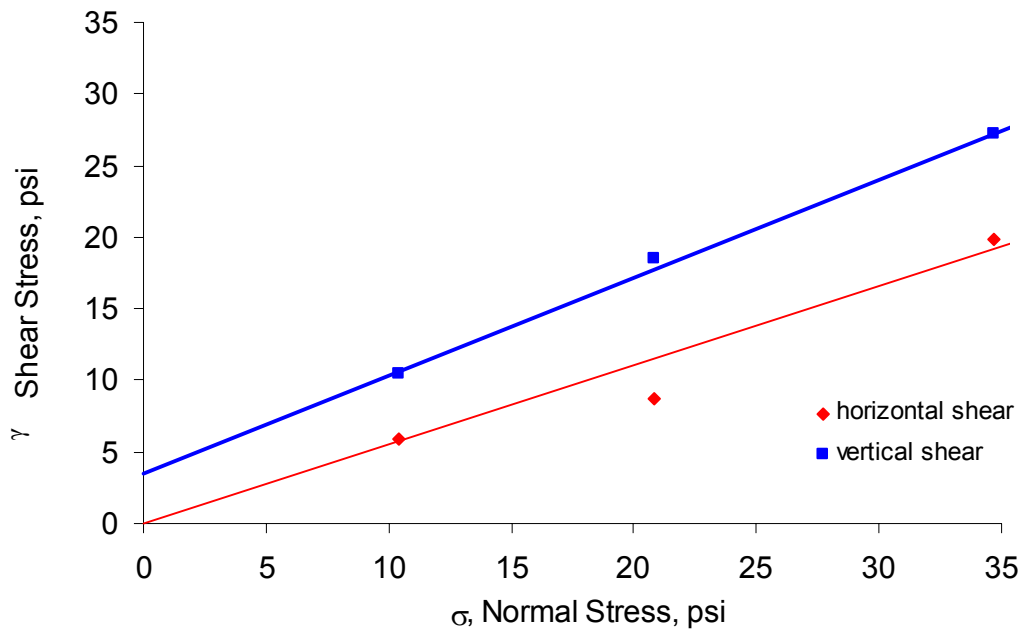


**Figure 5.18: Direct shear test results for specimens sampled at 15 feet**

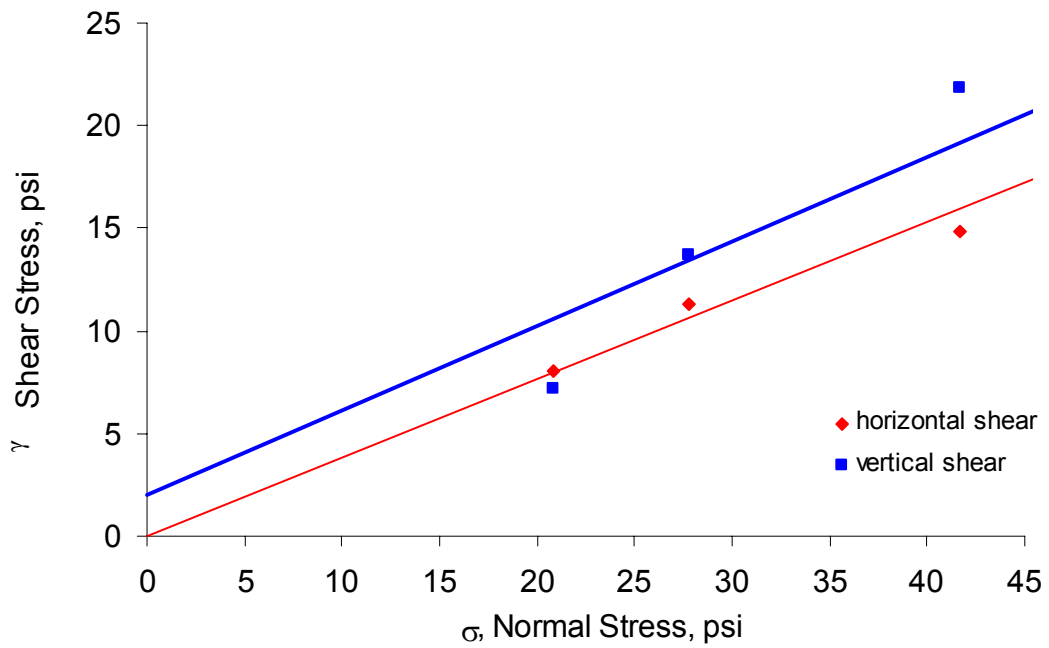


**Figure 5.19: Direct shear test results for specimens sampled at 25 feet**

Overall, no significant difference was found in soil properties due to orientation. Cohesion varied with depth but friction angles averaging 26 degrees were consistently measured for both orientations. This was true for samples submerged and in-situ moisture conditions.

### 5.6 Elastic Modulus

Figure 5.20 and 5.21 present comparisons of in-situ and laboratory elastic modulus values. The values from the consolidated-undrained triaxial test were relatively high when compared with the other tests. Elastic moduli from the unconfined compression tests were consistently low. Elastic moduli computed from CPT test results test had limited variability and reflected an intermediate value between laboratory and SPT correlated values.

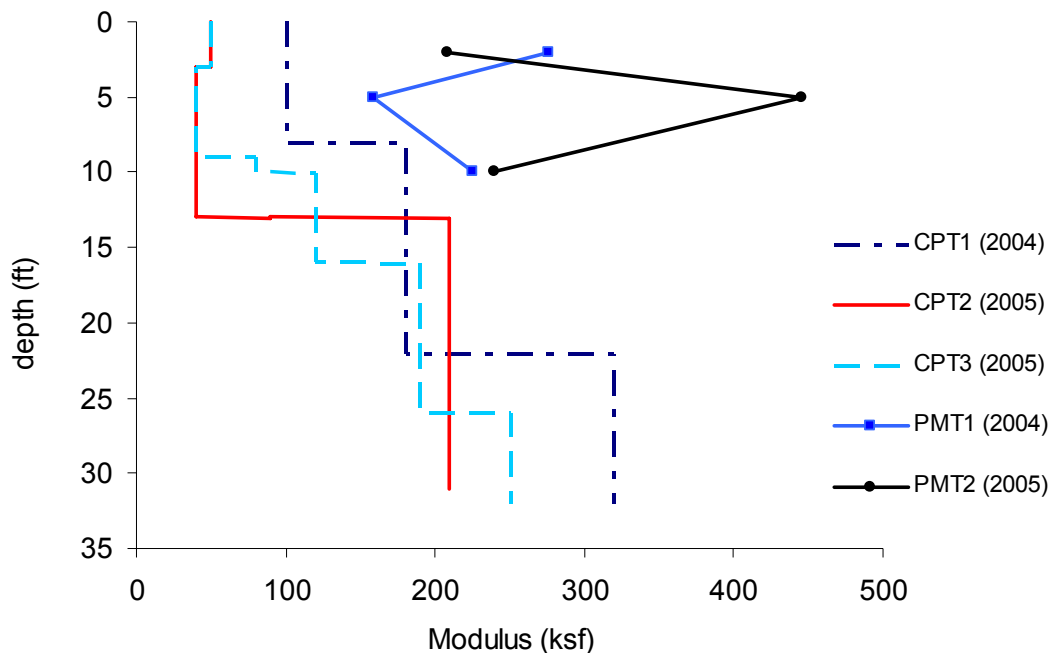


**Figure 5.20: Comparison of moduli for CPT and PMT soundings**

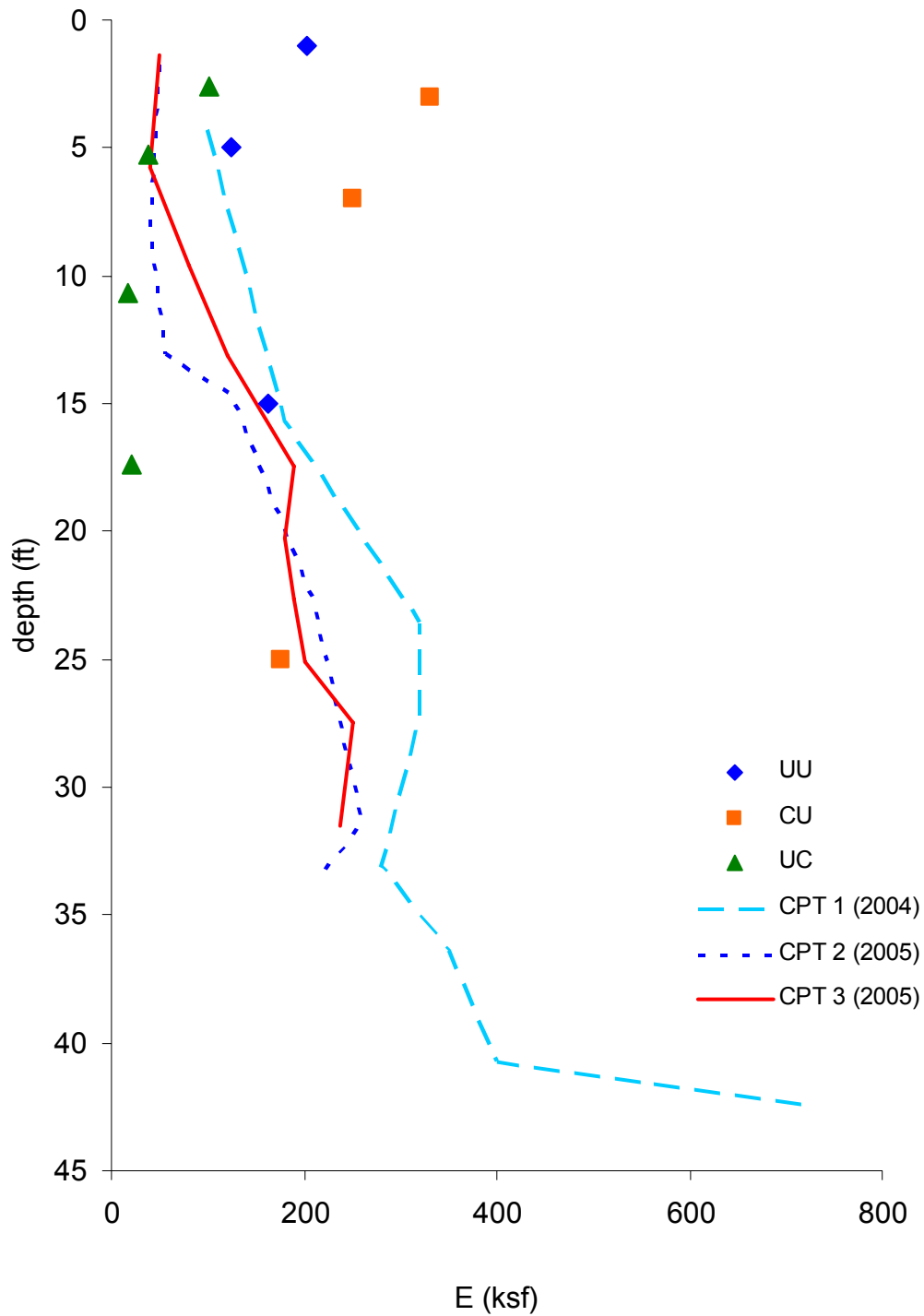


**Figure 5.21: Elastic modulus determined from in-situ and laboratory results**

In general, the friction angle varied from approximately 17 degrees near the surface to approximately 30 degrees near 25 feet below the surface. Soil cohesion was

at a maximum near the surface and decreased with depth to approximately 2 psi at 5 feet below the surface. The soil's elastic modulus increased with depth and is approximated best by CPT results. Moisture conditions and sample orientation had little effect on the soil's shear strength. All test results and soil properties analyzed indicate loess at the test site behaved as a frictional soil with some cohesion.

## Chapter 6

### P-Y Analysis

KU did not have the capability to conduct full scale lateral load testing at the time of this project. Therefore load testing and subsequent analysis was subcontracted to Dan Brown and Associates. Dr. Steve Dapp conducted the testing and analysis with the assistance of Dr. Brown. This chapter presents the equations developed by Drs. Dapp and Brown to derive p-y curves specific to loess. A more detailed discussion by Drs. Dapp and Brown is provided in Appendix D.

A hyperbolic model was developed to correlate ultimate soil resistance ( $P_{uo}$ ) to the CPT cone tip resistance ( $q_c$ ) at any given depth below the surface. Cone values were determined using an acoustic cone meeting the requirements of ASTM D 5778 and manufactured by Geotech AB of Sweeden. The ultimate soil resistance is proportional to  $q_c$  by a dimensionless correlation constant,  $N_{po} = 0.409$ .

$$P_{uo} = 0.409 \cdot q_c \dots\dots\dots 6.1$$

Where:  $P_{uo}$ , and  $q_c$  are in any consistent units of (force / length<sup>2</sup>)

The ultimate soil resistance is dependant only on the soil's strength. It can be made specific to a given pile ( $P_u$ ) by multiplying by the diameter (b). Ultimate soil resistance is now expressed as a unit length of the pile. This parameter is degraded for a given load cycle (N) with the correlation constant of 0.24. The cyclic degradation term in the denominator reduces to 1 for the initial cycle where N=1. In the case of a static load, N=1.

$$P_u = \frac{P_{uo} \cdot b}{1 + 0.24 \cdot \log(N)} \dots\dots\dots 6.2A$$

or

$$P_u = \frac{0.409 \cdot qc}{1 + 0.24 \cdot \log(N)} \dots\dots\dots 6.2B$$

Where: b is in any consistent unit of (length),

N is dimensionless

P<sub>u</sub> is in any consistent units of (force / length).

The second parameter needed is the reference displacement (Y<sub>i</sub>). The reference displacement is the displacement at which the tangent to the p-y curve at zero displacement (E<sub>i</sub>) intersects the ultimate soil resistance asymptote (P<sub>u</sub>). For lateral displacement of the pile, this reference displacement (Y<sub>i</sub>) may be considered as analogous to axial quake of a perfectly elastic-plastic bi-linear curve. It was determined that the best fit to the load test data was obtained with the following reference displacement (Y<sub>i</sub>).

$$Y_i = 0.117 \text{ inches}$$

Where Y<sub>i</sub> should be the displacement cited, and expressed in any consistent unit of (length) corresponding to the other model parameters used.

The third parameter needed is the initial modulus (E<sub>i</sub>), and is thus a simple definitive expression of the ultimate soil resistance expressed on a per length of pile basis (P<sub>u</sub>), and the reference displacement (Y<sub>i</sub>).

$$E_i = \frac{P_u}{Y_i} \dots\dots\dots 6.3$$

Where: P<sub>u</sub> is in any consistent units of (force / length).

Y<sub>i</sub> is in any consistent units of (length), and thus

E<sub>i</sub> results in any consistent units of (force / length<sup>2</sup>).



The Secant Modulus ( $E_s$ ) may be determined for any given displacement ( $Y$ ) by the following hyperbolic relationship involving the Initial Modulus expressed on a per unit length of pile basis ( $E_i$ ) and a hyperbolic term ( $Y'_h$ ) which is in turn a function of the given displacement ( $Y$ ), the reference displacement ( $Y_i$ ), and a dimensionless correlation constant ( $a$ ).

$$E_s = \frac{E_{si}}{1 + Y'_h} \dots\dots\dots 6.4$$

$$Y'_h = \left( \frac{Y}{Y_i} \right) \cdot \left[ 1 + a \cdot e^{-\left( \frac{Y}{Y_i} \right)} \right] \dots\dots\dots 6.5$$

Where:  $E_s$  and  $E_i$  are in any consistent units of (force / length<sup>2</sup>), and  $a$  and  $Y'_h$  are dimensionless.

It was determined that the best fit to the load test data was obtained with the following correlation constants:

$$a = 0.10$$

The ratio of Secant Modulus to Initial Modulus ( $E_s/E_i$ ) vs. displacement ( $Y$ ) used for development of the P-Y curves is shown in Appendix D in Figure D.3. Note that the modulus ratio ( $E_s/E_i$ ) is only a function of the hyperbolic parameters of the correlation constant ( $a$ ) and the reference displacement ( $Y_i$ ), thus the curve presented is valid for all pile diameters and CPT tip bearing values ( $q_c$ ) tested.

## Chapter 7

### Conclusion and Recommendations

#### 7.1 Soil Classification

Soil classification parameters were determined from laboratory and in-situ methods. Laboratory analyses included all index property testing and in-situ classification was determined by three CPT analyses. Laboratory index property results are presented on grain-size distribution curves in Appendix C, section 4. The soil was classified as low plasticity clay from the surface to a depth of 16 feet, low plasticity silt from depths of 16-28 feet, and low plasticity clay from depths of 28-32 feet, where borings were terminated.

Three computerized CPT profiles were generated and are presented in Appendix C, section 6. In general, the profiles consisted of alternating layers of clay, sand, silty sand, and sandy silt. As shown in Figure 3.7, CPT 1 and CPT 2 were located near drilled shaft 6 in 2004 and 2005, respectively. CPT 3 was located between shaft 1 and 2 in 2005. Computerized results from CPT 1 and 3 were similar, while results for CPT 2 included five layers of gravely sand. The results were inconsistent. Therefore, computerized CPT results in loess are not reliable and should be viewed with caution.

Correlations derived from Robertson & Campanella [28] generally classify the soil as sand, silty sand, and sandy silt. It did not account for the cohesive nature of the loess. From the literature review, the greatest amount of clay should be found near the surface and the largest amount of sand should be located near the bottom of Loveland

members. Therefore, the most accurate soil classification was derived from laboratory index property tests.

## **7.2 Collapse**

As stated in the literature review, loess is well known for its collapsibility. Large settlements associated with collapse are an important physical and structural property of loess. Soils with montmorillonite as the cementing material tend to swell with an increase in moisture and create a potential for the soil matrix to collapse. Plasticity indices are an indication of the amount of clay present in the soil. A high value corresponds to high percentages of montmorillonite in the soil. Dry unit weight is also an indicator of the soil's collapsibility. With an increase in moisture, settlement will be small for soils with dry unit weights exceeding 90 pcf. Soils with moisture contents between 10 to 15 percent have moderately high strength and a small amount of settlement [7]. Therefore, soils with high field densities, low moisture contents, and clay cementation can be expected to have a low collapse potential.

Soil at the test sight was subjected to collapse tests at 1 and 25 feet below the surface. At these depths, the soil had the highest void ratio and would suffer the largest settlement due to an increase in moisture. Loess samples tested had an average dry unit weight of 90 pcf, a plastic index and moisture content of 13 and 20% at 1 foot and were non-plastic with a moisture content of 10% at 25 feet. At both depths, the test sight had low plastic index values, moderate to low moisture contents, and high dry unit weights. As expected, the test sight was found to be slightly collapsible. If a soil is not tested directly for its collapse potential, a combination of dry unit weight, moisture

content, and the plastic index are good parameters for approximating collapse susceptibility.

### **7.3 Anisotropy**

Strength parameters were used to determine soil anisotropy. As presented in Figure 5.12, pairs of samples from the same depth were trimmed such that shear planes of the samples were parallel and perpendicular to the vertical effective field stress, respectively. There was some variability in cohesion due to varying moisture conditions. For each depth friction angles were consistent regardless of test orientation. Overall, no significant difference was found in soil properties due to orientation.

### **7.4 Soil Modulus Values**

Soil modulus of elasticity ( $E_m$ ) is a measure of the stiffness of the soil and can be calculated from laboratory and in-situ test data. Figure 5.17 presents a comparison of the soil's elastic modulus derived from unconsolidated-undrained, consolidated-undrained, unconfined compression, and CPT tests. The average values for the modulus of elasticity were consistent among the tests. However, laboratory tests calculated higher  $E_m$  values near the surface and decreased with depth. The three CPT tests developed lower  $E_m$  values near the surface and continued to increase with depth. When compared to all the tests, unconfined compression results developed into the lowest values of  $E_m$  and consolidated-undrained test results were the highest values. Overall, the three CPT tests provided a representative and continuous profile of  $E_m$  results and the test is recommended for estimation of elastic modulus. The CPT results were used as the basis for the p-y curve analysis.

## **7.5 Strength Parameters**

Total and effective shear strength parameters were determined from direct shear and triaxial compression tests. Overall, friction angles derived from triaxial compression tests were slightly lower than the direct shear results. Reese and Matlock recommend using triaxial compression tests, with confining pressure equal to the overburden pressure, for determining the shear strength of sand above and below the water table. They state the strength values may be conservative but would be more representative than other tests [19]. Matlock recommended in-situ vane-shear tests and unconsolidated-undrained triaxial compression tests for soft clays below the water table. For the loess at the test site (which was far above the groundwater table), unconsolidated-undrained total strength parameters and consolidated-undrained effective strength parameters were similar and more conservative than the direct shear results. As determined in Chapter 5, loess behaves more like loose sand than a cohesive material. Therefore, triaxial compression testing is recommended to determine strength parameters, with test conditions dependent on soil profile.

## **7.6 In-Situ Moisture Conditions**

Moisture conditions in 2004 and 2005 are plotted on boring logs L and M, respectively, in Appendix B. From the surface to an approximate depth of 12 feet, moisture contents ranged from 20-25 %. From an approximate depth of 12-26 feet below the surface, moisture contents decreased with depth from 20-10 % in 2004. Moisture conditions in 2005 were similar. From the surface to an approximate depth of 10 feet, moisture contents ranged from 20-23 %. From an approximate depth of 10-32 feet below the surface, moisture contents decreased with depth from 20-10 %.

A comparable amount of rainfall occurred during sampling in 2004 and the day before sampling in 2005. In-situ moisture conditions in 2005 were slightly drier than 2004; however, no substantial difference occurred in any test result due to the small moisture difference.

### **7.7 Correlation for P-Y Curves**

As discussed in Chapter 5 and sections 7.1 to 7.6, the Loveland loess tested and analyzed behaved as loose sand with slight cohesion. This confirms Frantzen and Clowers statement that “in the case of static loading, p-y curves developed for sand may be used to predict lateral load response of piles embedded in dry loess [3].”

Dan Brown and Associates developed a hyperbolic model specific to p-y curves in loess. The equations were presented in Chapter 6 and detailed in Appendix D. The hyperbolic model was developed to provide the secant modulus of the p-y curve at any given displacement.

### **7.8 Additional Research**

Future laboratory testing could include analyzing results from consolidated-drained and consolidated-undrained triaxial compression tests on loess samples that are more susceptible to collapse.

## References:

- [1] Coduto, Donald P., Foundation design, Prentice-Hall, Inc., Upper Saddle River, New Jersey, 1999.
- [2] COM624P (1993), "Laterally Loaded Pile Analysis Program for the Microcomputer," FHWA-SA-91-048, computer program documentation by Wang, S.T. and Reese, L.C. 487 pp 487.
- [3] Clowers, Karen A. and Frantzen, Jeffrey A., "Response of Piles in Loess to Lateral Loads," Research Report No. FHWA-KS-92-4, Kansas Department of Transportation, Division of Operations Bureau of Materials and Research, November, 1992.
- [4] Marosi, Paul, "A Review of the Evolution of Theories on the Origin of Loess," Loess, Lithology and Genesis, Ian J. Smalley; Ed., Dowden, Hutchinson, & Ross, Inc., Distributed by Halsted Press, 1975, pp. 402-414.
- [5] Terzaghi, Karl, Peck, Ralph B., and Mesri, Gholamreza, Soil Mechanics in Engineering Practice, third ed., John Wiley & Sons, Inc., New York, NY, 1996.
- [6] Bandyopadhyay, S.S., "Geotechnical Evaluation of Loessial Soils in Kansas," Transportation Research Record 945.
- [7] Gibbs, H.J. and Holland, W.Y., "Petrographic and Engineering Properties of Loess", Engineer Monograph No. 28, U.S. Bureau of Reclamation, Denver, CO, 1960.
- [8] Crumpton, Carl F. and Badgley, William S., "A Study of the Clay Mineralogy of Loess in Kansas in Relation to its Engineering Properties," U.S. Department of Commerce Bureau of Public Roads, 1965.
- [9] Swineford, A. and Frye, J.C., "Petrography of the Peoria Loess in Kansas," Journal of Geology, Vol. 59, No. 4, 1951, pp. 306-322.
- [10] Beavers, A.H., "Source and Deposition of Clay Minerals in Peorian Loess," Loess, Lithology and Genesis; Ian J. Smalley; Ed., Dowden, Hutchinson, & Ross, Inc., Distributed by Halsted Press; 1975, pp. 149.
- [11] Smalley, Ian J., "Introduction," Loess, Lithology and Genesis; Ian J. Smalley; Ed., Dowden, Hutchinson, & Ross, Inc., Distributed by Halsted Press; 1975, pp. 1-9.

- [12] Swinford, Ada and Frye, John C., "Petrographic Comparison of Some Loess Samples from Western Europe with Kansas Loess," Loess, Lithology and Genesis, Ian J. Smalley; Ed., Dowden, Hutchinson, & Ross, Inc., Distributed by Halsted Press, 1975, pp.183.
- [13] Zeller, Doris E., The Stratigraphic Succession in Kansas, State Geological Survey of Kansas, Bulletin 189.
- [14] Howe, Wallace B., The Stratigraphic Succession in Missouri, John W. Koenig; Ed., State Geological Survey of Missouri, Vol. XL, second series, September 1961.
- [15] Paliwal, K.V., Hobbs, J.A., Bidwell, O.H., and R. Ellis, Jr., "Mineralogical and Chemical Characteristics of Four Western Kansas Soils," Transactions of the Kansas Academy of Science, Vol. 67, Issue 4, 1965, pp. 617-629.
- [16] Sheeler, J.B., "Summarization and Comparison of Engineering Properties of Loess in the United States," Record No. 212, Highway Research Board, Washington, DC 1968, pp 1-9.
- [17] Coduto, Donald P., Geotechnical Engineering, Principles and Practices, Prentice-Hall, Inc., Upper Saddle River, New Jersey, 1999.
- [18] Ashour, Mohamed and Norris, G., "Modeling Lateral Soil-Pile Response Based on Soil-Pile Interaction," Journal of Geotechnical and Geoenvironmental Engineering, Vol. 126, No. 5, May 2000.
- [19] Welch, Robert C. and Reese, Lymon C., "Lateral Load Behavior of Drilled Shafts," Research Report 89-10, Project 3-5-65-89, Center for Highway Research, the University of Texas at Austin, May 1972.
- [20] Mokwa, Robert L., Duncan, Michael, and Helmers, Matthew J., "Development of p-y Curves for Partly Saturated Silts and Clays," Geotechnical Special Publication, ASCE, NO. 100, 2000, pp 224-239.
- [21] McClelland, Bramlette and Focht, John A., Jr., "Soil Modulus for Laterally Loaded Piles," Journal of the Proceedings of the American Society of Civil Engineers, Soil Mechanics and Foundations Division, Proceeding Paper 1081.



- [22] Anderson, J.B., Townsend, F.C., and Grajales, B., "Case History Evaluation of Laterally Loaded Piles," Journal of Geotechnical and Geoenvironmental Engineering, ASCE, March 2003, #187.
- [23] Duncan, Michael J., Evans, Leonard T. Jr., and Ooi, Phillip S. K., "Lateral Load Analysis of Single Piles and Drilled Shafts," Journal of Geotechnical Engineering, Copyright ASCE, vol. 120 NO. 6, 1994, pp 1018.
- [24] Lamb, R.O., "Geotechnical Aspects of Leaching of Carbonates from Loessial Soils," Physico-Chemical Aspects of Soil and Related Materials, ASTM STP 1095, "K.B. Hodinott and R.O. Lamb, Eds., American Society for Testing and Materials, Philadelphia, 1990, pp. 29-43.
- [25] ASTM International, West Conshohocken, PA.
- [26] Bishop and Henkel, The Measurement of Soil Properties in the Triaxial Test, 2nd ed, Edward Arnold (Publishers) Ltd., London W1X 8LL.
- [27] Peck, R.B., Hanson, W.E., and Thornburn, T.H., Foundation Engineering, Wiley, New York, 1974.
- [28] Robertson, P.K. and Campanella, R.G., Interpretation of cone penetration tests - Part I: Sand. Can. Geotech. Journ., 20:718-733.
- [29] Robertson, P.K., Campanella, R.G., and Wightman, A., SPT-CPT correlations. Technical report, Soil Mech. Series No. 62, Dept. of Civil Engrng., Univ. of British Columbia.
- [30] Schmertmann, J.H., "Measurement of In-situ Shear Strength," Journal of the Proceedings of the American Society of Civil Engineers, June 1-4, 1975, vol. II.
- [31] Wolff, Thomas F, "Geotechnical Judgment in Foundation Design." Foundation Engineering: Current Principles and Practice, Vol. 2, ASCE Evanston, IL, June 25-29, 1989, ASCE, New York, NY, pp 903-917.
- [32] Kulhawy, F.H., Mayne, P.W., "Relative density, SPT and CPT interrelationships," Proc Int Symp Calibration Chamber Test, 1992.

## Appendix A

### As Built Test Conditions

**Table A1: Drilled shaft detail**

Shaft	Inclinometer casing #	Diameter	Total Depth	Casing Length	Rebar Cage Length	#10 Rebar	#4 Rebar Hoops	Truck #
		in	ft	ft	ft	used	used	
1	5	42	26.80	3.30	26.7	16	29	2,3
2	6	42	27.20	3.18	27.3	16	31	3,4
3	3	30	27.15	3.09	27.1	12	28	2
4	4	30	27.00	3.10	27.1	12	28	1,2
5	1	30	26.90	3.10	27.1	12	28	1
6	2	30	27.15	3.10	27.0	12	29	1

**Table A2: Inclinometer Detail**

shaft	Inclinometer Casings (in.)			direction
	A	B	C	
1	8.0	2.2	OC	
2	10.3	1.3	OC	
3	9.6	2.3	0.3	left
4	9.0	3.2	OC	
5	13.9	6.7	7.2	right
6	16.1	1.9	1.9	right

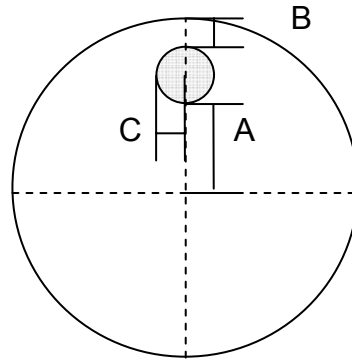


**Table A3: Concrete Specifications**

Truck	Slump in.	Air %	Temperature °F	Cylinder Strength on Test Day psi	Unit Weight pcf
1	2.5	3.2	70	7144	147
2	6.25	n/a	70	6614	n/a
3	3.5	n/a	70	6225	n/a
4	5	n/a	70	5464	n/a

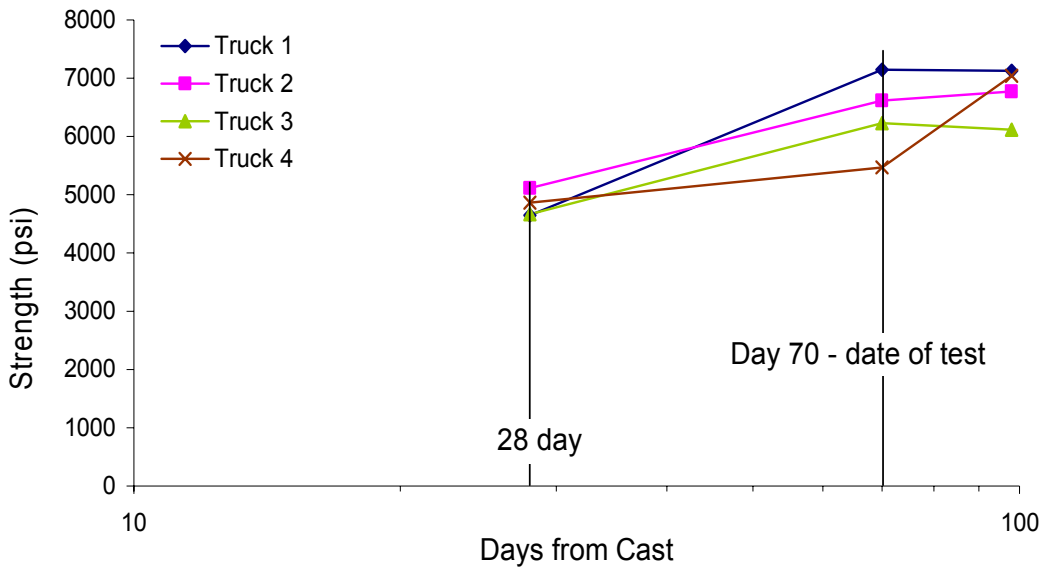


**Figure A4: Concrete Cylinder Strength**

**Table A5: LVDT Detail**

Shaft	LVDT	distance (in.)		
		A	B	C
1	2	43	39.6	NA
	4	17.3	NA	27.6
2	1	68.8	36.66	NA
	3	68.8	NA	21.41
3	2	53	36.58	NA
	4	27.3	NA	24.58
4	1	50.1	37.2	NA
	3	50.1	NA	19.2
5	2	42	37.2	NA
	4	16.3	NA	21.7
6	1	51	35.7	NA
	3	51	NA	19.7

A = distance from shaft to reference beam connection

B = distance from ground surface to top LVDT

C = distance from ground surface to bottom LVDT

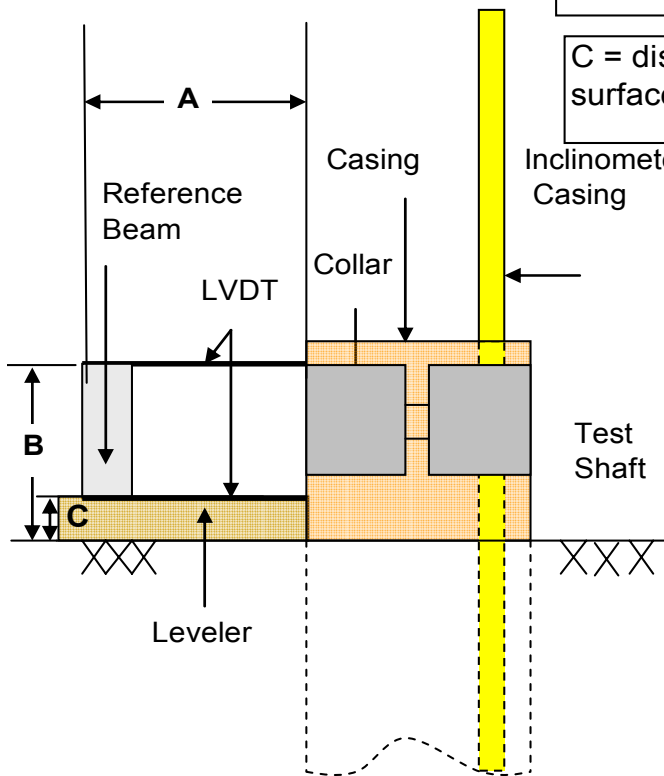


**Table A.6: Test Shaft Set-up**

Test Shaft Number East Side	Diameter (in)	Test Type	Test Shaft Number West Side
1	30	Cyclic	2
3	30	Static	4
5	42	Static	6

**Table A.7: Load Increments for 30-inch Diameter Static Test**

Load Number	Load (kips)	Inclinometer Soundings Performed
0	0	Yes
1	10	
2	21	
3	30	
4	39	
5	51	Yes
6	59	
7	70	
8	79	Yes
9	90	
10	99	Yes
11	110	
12	120	
13	127	Yes
14	113	
15	83	
16	44	
17	0	Yes

**Table A.8: Load Increments for the 42-inch Diameter Static Test**

Load Number	Load (kips)	Inclinometer Soundings Performed
0	0	Yes
1	18	
2	33	
3	49	
4	62	
5	78	
6	92	
7	107	Yes
8	123	
9	137	
10	150	Yes
11	168	
12	183	
13	193	Yes
14	214	
15	219	Yes
16	165	
17	113	
18	60	
19	0	Yes

**Table A.9: Load Increments for the 30-inch Diameter Cyclic Test**

Load Increment	Load Cycles	Approximate Load (kips)		Inclinometer Soundings
		Deflect	Return	
N/A	None	0	0	Prior to Loading
A	1 through 10	50	-15	at Load Cycles 1 and 10 for each Load Increment
B	1 through 10	79	-25	
C	1 through 10	99	-30	
D	1 through 10	127	-30	

# Appendix B

## Boring Logs

Surface Elevation <b>865.61</b>		Completion Date: <u>6/14/04</u>		
Datum <b>NVGD</b>		GRAPHIC LOG		
DEPTH IN FEET	<b>DESCRIPTION OF MATERIAL</b>	DRY UNIT WEIGHT (PCF) SPT BLOW COUNTS CORE RECOVERY/RQD	SAMPLES	<b>SHEAR STRENGTH, tsf</b> Δ - UU/2    ○ - QU/2    □ - SV 0,5   1,0   1,5   2,0   2,5
				<b>STANDARD PENETRATION RESISTANCE</b> (ASTM D 1586) ▲ N-VALUE (BLOWS PER FOOT) WATER CONTENT, % PLI 10   20   30   40   50   LL
5	SILT, medium stiff, clayey, moist, low plasticity, light brown to tan - ML           soft           non-plastic           Boring terminated at 29.0 feet.	96	ST1	Δ    ○    □  -----
10		86	ST KU1	Δ    ○    □  -----
15		2-2-3	SPT 1	▲    ●     -----
20		87	ST2	○    ●    □  -----
25		2-3-3	SPT 2	▲    ●     -----
30		93	ST3	○    ●    □  -----
35				

**GROUNDWATER DATA**

ENCOUNTERED AT \_\_\_ FEET  
 AT \_\_\_ FEET AFTER \_\_\_ HOURS  
 AT \_\_\_ FEET AFTER \_\_\_ HOURS  
 FREE WATER NOT ENCOUNTERED DURING DRILLING

**REMARKS:**

**DRILLING DATA**

\_\_\_ AUGER    3 3/4" HOLLOW STEM  
 WASHBORING FROM \_\_\_ FEET  
 \_\_\_ CH DRILLER    LM LOGGER  
CME-45 DRILL RIG  
 HAMMER TYPE Auto

**Lateral Load Research  
Wyandotte County, Kansas**

---

**LOG OF BORING: A**


---

Project No. \_\_\_\_\_

NOTE: STRATIFICATION LINES REPRESENT THE APPROXIMATE BOUNDARIES BETWEEN SOIL TYPES AND THE TRANSITION MAY BE GRADUAL. GRAPHIC LOG FOR ILLUSTRATION PURPOSES ONLY.

Surface Elevation <b>865.79</b>		Completion Date: <b>6/15/04</b>		GRAPHIC LOG		<b>SHEAR STRENGTH, tsf</b> Δ - UU/2    ○ - QU/2    □ - SV 0,5    1,0    1,5    2,0    2,5		
Datum <b>NVGD</b>						<b>STANDARD PENETRATION RESISTANCE</b> (ASTM D 1586) ▲ N-VALUE (BLOWS PER FOOT)		
						<b>WATER CONTENT, %</b> PL   10 20 30 40 50   LL		
DEPTH IN FEET	DESCRIPTION OF MATERIAL	DRY UNIT WEIGHT (PCF)	SPT BLOW COUNTS	CORE RECOVERY/RQD	SAMPLES			
0	CLAY, medium stiff, sandy and silty, low plasticity, light brown to tan - CL							
5								
			94		ST1			
			91		ST KU3			
10			1-2-3		SPT 3			
15								
			91		ST2			
20	SILT, medium stiff, clayey, moist, low plasticity, light brown to tan - ML							
	medium stiff		2-3-3		SPT 4			
			93		ST KU4			
25	CLAY, medium stiff, sandy and silty, low plasticity, light brown to tan - CL							
			94		ST3			
30			4-6-10		SPT 5			
	SILT, very stiff, clayey, moist, low plasticity, light brown to tan - ML							
35	stiff, non-plastic		4-5-4		SPT 6			
	Boring terminated at 36.3 feet.							

<b>GROUNDWATER DATA</b>  ENCOUNTERED AT ___ FEET AT ___ FEET AFTER ___ HOURS AT ___ FEET AFTER ___ HOURS <input type="checkbox"/> FREE WATER NOT ENCOUNTERED DURING DRILLING  <b>REMARKS:</b>	<b>DRILLING DATA</b>  ___ AUGER <u>3 3/4"</u> HOLLOW STEM WASHBORING FROM ___ FEET <u>CH</u> DRILLER <u>LM</u> LOGGER <u>CME-45</u> DRILL RIG HAMMER TYPE <u>Auto</u>
--	---



**The University of KANSAS**


**Lateral Load Research  
Wyandotte County, Kansas**

**LOG OF BORING: B**

Project No. \_\_\_\_\_



LOG OF BORING: THESIS.GPJ, GEEES.GDT, 11/5/05

Surface Elevation <b>866.01</b>		Completion Date: <b>6/15/04</b>		SHEAR STRENGTH, tsf Δ - UU/2    ○ - QU/2    □ - SV 0,5   1,0   1,5   2,0   2,5			
Datum <b>NVGD</b>		GRAPHIC LOG				STANDARD PENETRATION RESISTANCE (ASTM D 1586)	
DEPTH IN FEET		DESCRIPTION OF MATERIAL				▲ N-VALUE (BLOWS PER FOOT)	
				WATER CONTENT, %			
				PL   10   20   30   40   50   LL			
5		CLAY, soft to medium stiff, sandy and silty, low plasticity, light brown to tan - CL		92	ST1		
				94	ST KU5		
10				2-2-3	SPT 7		
15							
					4.35		
20		SILT, medium stiff, clayey, moist, low plasticity, light brown to tan - ML					
		non-plastic		3-3-4	SPT 8		
					ST KU6		
25		CLAY, stiff, sandy and silty, low plasticity, light brown to tan - CL		99	ST3		
30				4-4-5	SPT 9		
		SAND, stiff, silty, non-plastic, orange-brown - SM					
35				4-6-8	SPT 10		
		Boring terminated at 36.5 feet.					
<b>GROUNDWATER DATA</b> ENCOUNTERED AT ___ FEET AT ___ FEET AFTER ___ HOURS AT ___ FEET AFTER ___ HOURS <input checked="" type="checkbox"/> FREE WATER NOT ENCOUNTERED DURING DRILLING <b>REMARKS:</b>		<b>DRILLING DATA</b> ___ AUGER    3 3/4" HOLLOW STEM WASHBORING FROM ___ FEET ___ CH DRILLER    LM LOGGER CME-45 DRILL RIG HAMMER TYPE <u>Auto</u>		 <b>Lateral Load Research</b> <b>Wyandotte County, Kansas</b> <b>LOG OF BORING: C</b> Project No.			

NOTE: STRATIFICATION LINES REPRESENT THE APPROXIMATE BOUNDARIES BETWEEN SOIL TYPES AND THE TRANSITION MAY BE GRADUAL. GRAPHIC LOG FOR ILLUSTRATION PURPOSES ONLY.

Surface Elevation <u>865.61</u>		Completion Date: <u>6/16/04</u>		SHEAR STRENGTH, tsf Δ - UU/2    ○ - QU/2    □ - SV 0,5   1,0   1,5   2,0   2,5	
Datum <u>NVGD</u>					
DEPTH IN FEET	DESCRIPTION OF MATERIAL	GRAPHIC LOG	DRY UNIT WEIGHT (PCF) SPT BLOW COUNTS CORE RECOVERY/RGD	SAMPLES	STANDARD PENETRATION RESISTANCE (ASTM D 1586)
					▲ N-VALUE (BLOWS PER FOOT)
					PLI
					10   20   30   40   50   LL
5	CLAY, soft to medium stiff, sandy and silty, low plasticity, light brown to tan - CL	[Hatched pattern]			
			93	ST1	
10					
			2-2-4	SPT 11	▲
15					
			95	ST2	●
20	SILT, medium stiff, clayey, moist, low plasticity, light brown to tan - ML	[Vertical lines]			
			3-3-4	SPT 12	▲
25	CLAY, soft to medium stiff, sandy and silty, low plasticity, light brown to tan - CL	[Hatched pattern]			
			96	ST3	●
30	SAND, stiff, silty, non-plastic, orange-brown - SM	[Dotted pattern]			
			5-8-10	SPT 13	▲
35	Boring terminated at 36.5 feet.				
			3-3-3	SPT 14	▲


**GROUNDWATER DATA**

ENCOUNTERED AT \_\_\_ FEET  
 AT \_\_\_ FEET AFTER \_\_\_ HOURS  
 AT \_\_\_ FEET AFTER \_\_\_ HOURS  
 FREE WATER NOT ENCOUNTERED DURING DRILLING

**DRILLING DATA**

\_\_\_ AUGER    3 3/4" HOLLOW STEM  
 WASHBORING FROM \_\_\_ FEET  
 \_\_\_ CH. DRILLER    LM LOGGER  
CME-45 DRILL RIG  
 HAMMER TYPE Auto

REMARKS:



The University of  
**KANSAS**

**Lateral Load Research  
Wyandotte County, Kansas**


---

**LOG OF BORING: D**

---

Project No. \_\_\_\_\_

NOTE: STRATIFICATION LINES REPRESENT THE APPROXIMATE BOUNDARIES BETWEEN SOIL TYPES AND THE TRANSITION MAY BE GRADUAL. GRAPHIC LOG FOR ILLUSTRATION PURPOSES ONLY.

Surface Elevation <b>864.95</b>		Completion Date: <u>8/12/04</u>		GRAPHIC LOG	<b>SHEAR STRENGTH, tsf</b>			
Datum <b>NVGD</b>		DRY UNIT WEIGHT (PCF) SPT BLOW COUNTS CORE RECOVERY/RQD			Δ - UU/2    ○ - QU/2    □ - SV 0,5    1,0    1,5    2,0    2,5			
DEPTH IN FEET	<b>DESCRIPTION OF MATERIAL</b>				SAMPLES	<b>STANDARD PENETRATION RESISTANCE</b> (ASTM D 1586)		
	SILT, medium stiff, clayey, moist, low plasticity, light brown to tan - ML				▲ N-VALUE (BLOWS PER FOOT)			
					<b>WATER CONTENT, %</b>			
5				99	ST1	PLI 10 20 30 40 50 ILL		
10				95	ST2	●		
15						●		
20						●		
25						●		
26.6	Boring terminated at 26.6 feet.			99	ST3	○ ●		
30						●		
35						●		
<b>GROUNDWATER DATA</b>		<b>DRILLING DATA</b>			 <b>Lateral Load Research</b> <b>Wyandotte County, Kansas</b>  <b>LOG OF BORING: E</b>  Project No.			
ENCOUNTERED AT ___ FEET		___ AUGER <u>3 3/4"</u> HOLLOW STEM						
AT ___ FEET AFTER ___ HOURS		WASHBORING FROM ___ FEET						
AT ___ FEET AFTER ___ HOURS		<u>DE</u> DRILLER <u>RF</u> LOGGER						
<input checked="" type="checkbox"/> FREE WATER NOT ENCOUNTERED DURING DRILLING		<u>CME-45</u> DRILL RIG						
<b>REMARKS:</b>		HAMMER TYPE <u>Auto</u>						

Surface Elevation <b>864.9</b>		Completion Date: <u>8/12/04</u>								
Datum <b>NVGD</b>										
DEPTH IN FEET	<b>DESCRIPTION OF MATERIAL</b>	GRAPHIC LOG	DRY UNIT WEIGHT (PCF)	SAMPLES	SHEAR STRENGTH, tsf					
			SPT BLOW COUNTS		▲ - UU/2    ○ - QU/2    □ - SV 0,5   1,0   1,5   2,0   2,5					
STANDARD PENETRATION RESISTANCE (ASTM D 1586)										
▲ N-VALUE (BLOWS PER FOOT)										
PLI    WATER CONTENT, %    LL										
10					10	20	30	40	50	LL
5	CLAY, soft to medium stiff, sandy and silty, low plasticity, light brown to tan - CL	101	ST1	ST2	●	●	●	●	●	●
5	Boring terminated at 4.8 feet.									
10										
15										
20										
25										
30										
35										

<b>GROUNDWATER DATA</b>  ENCOUNTERED AT ___ FEET AT ___ FEET AFTER ___ HOURS AT ___ FEET AFTER ___ HOURS <input checked="" type="checkbox"/> FREE WATER NOT ENCOUNTERED DURING DRILLING  <b>REMARKS:</b>	<b>DRILLING DATA</b>  ___ AUGER <u>3 3/4"</u> HOLLOW STEM WASHBORING FROM ___ FEET <u>DE</u> DRILLER <u>RF</u> LOGGER <u>CME-45</u> DRILL RIG HAMMER TYPE <u>Auto</u>
---	---

The University of  
**KANSAS**

Lateral Load Research  
Wyandotte County, Kansas

LOG OF BORING: F

Project No. \_\_\_\_\_

NOTE: STRATIFICATION LINES REPRESENT THE APPROXIMATE BOUNDARIES BETWEEN SOIL TYPES AND THE TRANSITION MAY BE GRADUAL. GRAPHIC LOG FOR ILLUSTRATION PURPOSES ONLY.

LOG OF BORING: THESIS.GPJ\_GEEES.GDT\_11/5/05

NOTE: STRATIFICATION LINES REPRESENT THE APPROXIMATE BOUNDARIES BETWEEN SOIL TYPES AND THE TRANSITION MAY BE GRADUAL. GRAPHIC LOG FOR ILLUSTRATION PURPOSES ONLY.


Surface Elevation <u>864.6</u>		Completion Date: <u>8/12/04</u>		<b>GRAPHIC LOG</b>		<b>DRY UNIT WEIGHT (pcf) SPT BLOW COUNTS CORE RECOVERY (RQD)</b>		<b>SHEAR STRENGTH, tsf</b>	
Datum <u>NVGD</u>								Δ - UU/2    ○ - QU/2    □ - SV 0,5   1,0   1,5   2,0   2,5	
<b>DEPTH IN FEET</b>	<b>DESCRIPTION OF MATERIAL</b>			<b>GRAPHIC LOG</b>	<b>DRY UNIT WEIGHT (pcf) SPT BLOW COUNTS CORE RECOVERY (RQD)</b>	<b>SAMPLES</b>	<b>STANDARD PENETRATION RESISTANCE</b>		
	CLAY, soft to medium stiff, sandy and silty, low plasticity, light brown to tan - CL						(ASTM D 1586)		
5	Boring terminated at 3.9 feet			92	ST1	<b>WATER CONTENT, %</b>			
10						PLI    10    20    30    40    50    ILL			
15									
20									
25									
30									
35									
<b>GROUNDWATER DATA</b>				<b>DRILLING DATA</b>				 <b>Lateral Load Research</b> <b>Wyandotte County, Kansas</b>  <b>LOG OF BORING: G</b>  Project No.	
ENCOUNTERED AT ___ FEET				___ AUGER <u>3 3/4"</u> HOLLOW STEM					
AT ___ FEET AFTER ___ HOURS				WASHBORING FROM ___ FEET					
AT ___ FEET AFTER ___ HOURS				<u>DE</u> DRILLER <u>RF</u> LOGGER					
<input checked="" type="checkbox"/> FREE WATER NOT ENCOUNTERED DURING DRILLING				<u>CME-45</u> DRILL RIG					
<b>REMARKS:</b>				HAMMER TYPE <u>Auto</u>					

LOG OF BORING: THESIS.GPJ GEES.GDT 11/5/05

NOTE: STRATIFICATION LINES REPRESENT THE APPROXIMATE BOUNDARIES BETWEEN SOIL TYPES AND THE TRANSITION MAY BE GRADUAL. GRAPHIC LOG FOR ILLUSTRATION PURPOSES ONLY.

Surface Elevation <b>864.55</b>		Completion Date: <u>8/12/04</u>		GRAPHIC LOG	DRY UNIT WEIGHT (PCF) SPT BLOW COUNTS CORE RECOVERY/RQD	SAMPLES	SHEAR STRENGTH, tsf			
Datum <b>NVGD</b>		Δ - UU/2    ○ - QU/2    □ - SV 0,5    1,0    1,5    2,0    2,5								
DEPTH IN FEET	DESCRIPTION OF MATERIAL				STANDARD PENETRATION RESISTANCE (ASTM D 1586)					
	CLAY, soft to medium stiff, sandy and silty, low plasticity, light brown to tan - CL  Boring terminated at 4.5 feet.				▲ N-VALUE (BLOWS PER FOOT)					
					WATER CONTENT, %					
								PL   10    20    30    40    50   LL		
5								99	ST2	
10										
15										
20										
25										
30										
35										
<b>GROUNDWATER DATA</b>  ENCOUNTERED AT ___ FEET AT ___ FEET AFTER ___ HOURS AT ___ FEET AFTER ___ HOURS <input checked="" type="checkbox"/> FREE WATER NOT ENCOUNTERED DURING DRILLING		<b>DRILLING DATA</b>  ___ AUGER <u>3 3/4"</u> HOLLOW STEM WASHBORING FROM ___ FEET <u>DE</u> DRILLER <u>RF</u> LOGGER <u>CME-45</u> DRILL RIG HAMMER TYPE <u>Auto</u>								
<b>REMARKS:</b>  		<b>Lateral Load Research</b> <b>Wyandotte County, Kansas</b>								
		<b>LOG OF BORING: H</b>								
		Project No.								

NOTE: STRATIFICATION LINES REPRESENT THE APPROXIMATE BOUNDARIES BETWEEN SOIL TYPES AND THE TRANSITION MAY BE GRADUAL. GRAPHIC LOG FOR ILLUSTRATION PURPOSES ONLY.

Surface Elevation <b>864.4</b>		Completion Date: <b>8/12/04</b>		SHEAR STRENGTH, tsf Δ - UU/2    ○ - QU/2    □ - SV 0,5   1,0   1,5   2,0   2,5	
Datum <b>NVGD</b>					
DEPTH IN FEET	DESCRIPTION OF MATERIAL			GRAPHIC LOG	DRY UNIT WEIGHT (PCF) SPT BLOW COUNTS CORE RECOVERY/RQD
	CLAY, soft to medium stiff, sandy and silty, low plasticity, light brown to tan - CL				
5	Boring terminated at 4.8 feet.				
10					
15					
20					
25					
30					
35					
<b>GROUNDWATER DATA</b>  ENCOUNTERED AT ___ FEET AT ___ FEET AFTER ___ HOURS AT ___ FEET AFTER ___ HOURS <input checked="" type="checkbox"/> FREE WATER NOT ENCOUNTERED DURING DRILLING  <b>REMARKS:</b>		<b>DRILLING DATA</b>  ___ AUGER <u>3 3/4"</u> HOLLOW STEM WASHBORING FROM ___ FEET <u>DE</u> DRILLER <u>RF</u> LOGGER <u>CME-45</u> DRILL RIG HAMMER TYPE <u>Auto</u>		 <b>Lateral Load Research Wyandotte County, Kansas</b>  <b>LOG OF BORING: I</b>  Project No.	

NOTE: STRATIFICATION LINES REPRESENT THE APPROXIMATE BOUNDARIES BETWEEN SOIL TYPES AND THE TRANSITION MAY BE GRADUAL. GRAPHIC LOG FOR ILLUSTRATION PURPOSES ONLY.

Surface Elevation _____ Datum <b>NVGD</b>		Completion Date: <u>6/9/04</u>		GRAPHIC LOG	DRY UNIT WEIGHT (PCF) SPT BLOW COUNTS CORE RECOVERY(ROD)	SAMPLES	<b>SHEAR STRENGTH, tsf</b> Δ - UU/2    ○ - QU/2    □ - SV 0,5    1,0    1,5    2,0    2,5		
DEPTH IN FEET	DESCRIPTION OF MATERIAL	<b>STANDARD PENETRATION RESISTANCE</b> (ASTM D 1586) ▲ N-VALUE (BLOWS PER FOOT)							
		<b>WATER CONTENT, %</b> PL _____ LL _____							
5	CLAY, soft to medium stiff, sandy and silty, low plasticity, light brown to tan - CL	91	ST1	▲ ● □					
10		86	ST2	▲ ● □					
15	SILT, medium stiff, clayey, moist, low plasticity, light brown to tan - ML	91	ST3	▲ ● □					
20		91	ST4	▲ ● □					
25	Boring terminated at 26.8 feet.								
30									
35									


**GROUNDWATER DATA**

ENCOUNTERED AT \_\_\_ FEET  
 AT \_\_\_ FEET AFTER \_\_\_ HOURS  
 AT \_\_\_ FEET AFTER \_\_\_ HOURS  
 FREE WATER NOT ENCOUNTERED DURING DRILLING

**REMARKS:**

**DRILLING DATA**

\_\_\_ AUGER    3 3/4" HOLLOW STEM  
 WASHBORING FROM \_\_\_ FEET  
CH DRILLER    LM LOGGER  
CME-45 DRILL RIG  
 HAMMER TYPE Auto




**Lateral Load Research  
Wyandotte County, Kansas**

**LOG OF BORING: J**

Project No. \_\_\_\_\_



Surface Elevation <b>865.9</b>		Completion Date: <u>6/14/04</u>		
Datum <b>NVGD</b>		GRAPHIC LOG		
DEPTH IN FEET	<b>DESCRIPTION OF MATERIAL</b>	DRY UNIT WEIGHT (PCF) SPT BLOW COUNTS CORE RECOVERY/RGD	SAMPLES	<b>SHEAR STRENGTH, tsf</b> ▲ - UU/2    ○ - QU/2    □ - SV 0,5   1,0   1,5   2,0   2,5
			<b>STANDARD PENETRATION RESISTANCE</b> (ASTM D 1586) ▲ N-VALUE (BLOWS PER FOOT) <b>WATER CONTENT, %</b> PL  -----  LL 10   20   30   40   50	
0	CLAY, soft, silty, moist, low plasticity, light brown to tan - CL	[Hatched Pattern]	CS MDS1 GB RDS1	[Graphical Data]
5			CS MDS2 GB RDS2	[Graphical Data]
10			CS MDS3 GB RDS3	[Graphical Data]
15	SILT, stiff, clayey, dry, low plasticity, light brown to tan - ML	[Vertical Lines]	CS MDS4 GB RDS4	[Graphical Data]
20			CS MDS5 GB RDS5	[Graphical Data]
25			CS MDS6 GB RDS6	[Graphical Data]
30	CLAY, soft, silty, moist, low plasticity, light brown to tan - CL	[Hatched Pattern]	CS MDS7 GB RDS7	[Graphical Data]
35			GB RDS8 GB MDS8	[Graphical Data]
37.7	Boring terminated at 32.7 feet.			
<b>GROUNDWATER DATA</b> ENCOUNTERED AT ___ FEET    ___ AUGER    ___ HOLLOW STEM AT ___ FEET AFTER ___ HOURS    WASHBORING FROM ___ FEET AT ___ FEET AFTER ___ HOURS    ___ ED DRILLER    ___ ED LOGGER <input checked="" type="checkbox"/> FREE WATER NOT ENCOUNTERED DURING DRILLING <input type="checkbox"/> AD Bull DRILL RIG HAMMER TYPE <u>Auto</u>				 <b>Lateral Load Research</b> <b>Wyandotte County, Kansas</b>
REMARKS:				<b>LOG OF BORING: K</b>
Project No. _____				

NOTE: STRATIFICATION LINES REPRESENT THE APPROXIMATE BOUNDARIES BETWEEN SOIL TYPES AND THE TRANSITION MAY BE GRADUAL. GRAPHIC LOG FOR ILLUSTRATION PURPOSES ONLY.

LOG OF BORING: THESIS.GPJ, GEES.GDT 11/5/05

Surface Elevation _____ Datum <u>NVGD</u>		Completion Date: <u>6/9/05</u>		GRAPHIC LOG	DRY UNIT WEIGHT (PCF) SPT BLOW COUNTS CORE RECOVERY/RQD	SAMPLES	SHEAR STRENGTH, tsf		
DEPTH IN FEET	DESCRIPTION OF MATERIAL	$\Delta$ - UU/2 $\circ$ - QU/2 $\square$ - SV 0,5   1,0   1,5   2,0   2,5							
		STANDARD PENETRATION RESISTANCE (ASTM D 1586) $\blacktriangle$ N-VALUE (BLOWS PER FOOT)							
		WATER CONTENT, %							
		PLI							
		10   20   30   40   50   ILL							
	CLAY, medium stiff, silty, moist, low plasticity, medium brown to tan - CL								
	SILT, medium stiff, clayey, moist, low plasticity, medium brown to tan - ML				GB1				
5					GB2				
					GB3				
					GB4				
					GB5				
10					GB6				
					GB7				
					GB8				
					GB9				
15					GB10				
					GB11				
					GB12				
20					GB13				
	Boring terminated at 26.3 feet.								
25									
30									
35									

NOTE: STRATIFICATION LINES REPRESENT THE APPROXIMATE BOUNDARIES BETWEEN SOIL TYPES AND THE TRANSITION MAY BE GRADUAL. GRAPHIC LOG FOR ILLUSTRATION PURPOSES ONLY.

LOG OF BORING: THESIS.GPJ GEES.GDT 11/5/05

**GROUNDWATER DATA**

ENCOUNTERED AT \_\_\_ FEET  
AT \_\_\_ FEET AFTER \_\_\_ HOURS  
AT \_\_\_ FEET AFTER \_\_\_ HOURS  
X FREE WATER NOT  
ENCOUNTERED DURING DRILLING

**REMARKS:**

**2004**

**DRILLING DATA**

\_\_\_ AUGER    \_\_\_ HOLLOW STEM  
WASHBORING FROM \_\_\_ FEET  
DRE DRILLER    JW LOGGER  
AD Bull DRILL RIG  
HAMMER TYPE Auto



**Lateral Load Research  
Wyandotte County, Kansas**

**LOG OF BORING: L**

Project No.

Surface Elevation _____		Completion Date: <u>6/8/05</u>		GRAPHIC LOG	DRY UNIT WEIGHT (PCF) SPT BLOW COUNTS CORE RECOVERY/RQD	<b>SHEAR STRENGTH, tsf</b>																																							
Datum <u>NVGD</u>		$\Delta$ - UU/2 $\circ$ - QU/2 $\square$ - SV 0,5    1,0    1,5    2,0    2,5																																											
<b>DEPTH IN FEET</b>		<b>STANDARD PENETRATION RESISTANCE</b>																																											
		(ASTM D 1586) $\blacktriangle$ N-VALUE (BLOWS PER FOOT) <b>WATER CONTENT, %</b> PL  -----  LL 10    20    30    40    50																																											
<b>DESCRIPTION OF MATERIAL</b>		SAMPLES			<table border="1" style="width: 100%; border-collapse: collapse;"> <tr> <td style="width: 20px;">GB1 CS1</td> <td style="width: 20px;">GB2</td> <td style="width: 20px;">GB3 CS2</td> <td style="width: 20px;">GB4</td> <td style="width: 20px;">GB5 CS3</td> <td style="width: 20px;">GB6</td> <td style="width: 20px;">GB7 CS4</td> <td style="width: 20px;">GB8</td> <td style="width: 20px;">GB9 CS5</td> <td style="width: 20px;">GB 10</td> <td style="width: 20px;">GB 11</td> <td style="width: 20px;">CS6</td> <td style="width: 20px;">GB 12</td> <td style="width: 20px;">GB 13</td> <td style="width: 20px;">CS7</td> <td style="width: 20px;">GB 14</td> <td style="width: 20px;">GB 15</td> <td style="width: 20px;">CS8</td> <td style="width: 20px;">GB 16</td> </tr> <tr> <td colspan="19" style="text-align: center;">           NOTE: STRATIFICATION LINES REPRESENT THE APPROXIMATE BOUNDARIES BETWEEN SOIL TYPES            AND THE TRANSITION MAY BE GRADUAL. GRAPHIC LOG FOR ILLUSTRATION PURPOSES ONLY.         </td> </tr> </table>			GB1 CS1	GB2	GB3 CS2	GB4	GB5 CS3	GB6	GB7 CS4	GB8	GB9 CS5	GB 10	GB 11	CS6	GB 12	GB 13	CS7	GB 14	GB 15	CS8	GB 16	NOTE: STRATIFICATION LINES REPRESENT THE APPROXIMATE BOUNDARIES BETWEEN SOIL TYPES AND THE TRANSITION MAY BE GRADUAL. GRAPHIC LOG FOR ILLUSTRATION PURPOSES ONLY.																		
GB1 CS1	GB2	GB3 CS2	GB4	GB5 CS3				GB6	GB7 CS4	GB8	GB9 CS5	GB 10	GB 11	CS6	GB 12	GB 13	CS7	GB 14	GB 15	CS8	GB 16																								
NOTE: STRATIFICATION LINES REPRESENT THE APPROXIMATE BOUNDARIES BETWEEN SOIL TYPES AND THE TRANSITION MAY BE GRADUAL. GRAPHIC LOG FOR ILLUSTRATION PURPOSES ONLY.																																													
CLAY, medium stiff, silty, moist, low plasticity, medium brown to tan - CL		Boring terminated at 33.8 feet.						<table border="1" style="width: 100%; border-collapse: collapse;"> <tr> <td style="width: 20px;">GB1 CS1</td> <td style="width: 20px;">GB2</td> <td style="width: 20px;">GB3 CS2</td> <td style="width: 20px;">GB4</td> <td style="width: 20px;">GB5 CS3</td> <td style="width: 20px;">GB6</td> <td style="width: 20px;">GB7 CS4</td> <td style="width: 20px;">GB8</td> <td style="width: 20px;">GB9 CS5</td> <td style="width: 20px;">GB 10</td> <td style="width: 20px;">GB 11</td> <td style="width: 20px;">CS6</td> <td style="width: 20px;">GB 12</td> <td style="width: 20px;">GB 13</td> <td style="width: 20px;">CS7</td> <td style="width: 20px;">GB 14</td> <td style="width: 20px;">GB 15</td> <td style="width: 20px;">CS8</td> <td style="width: 20px;">GB 16</td> </tr> </table>			GB1 CS1	GB2	GB3 CS2	GB4	GB5 CS3	GB6	GB7 CS4	GB8	GB9 CS5	GB 10	GB 11	CS6	GB 12	GB 13	CS7	GB 14	GB 15	CS8	GB 16																
GB1 CS1	GB2										GB3 CS2	GB4	GB5 CS3	GB6	GB7 CS4	GB8	GB9 CS5	GB 10	GB 11	CS6	GB 12	GB 13	CS7	GB 14	GB 15	CS8	GB 16																		
SILT, medium stiff, clayey, moist, low plasticity, medium brown to tan - ML																																													
Boring terminated at 33.8 feet.																																													

<b>GROUNDWATER DATA</b>  ENCOUNTERED AT ___ FEET AT ___ FEET AFTER ___ HOURS AT ___ FEET AFTER ___ HOURS <input checked="" type="checkbox"/> FREE WATER NOT ENCOUNTERED DURING DRILLING  <b>REMARKS:</b>  <div style="text-align: center; font-weight: bold; font-size: 1.2em;">2005</div>	<b>DRILLING DATA</b>  ___ AUGER    ___ HOLLOW STEM WASHBORING FROM ___ FEET DRE DRILLER    JW LOGGER AD Bull. DRILL RIG HAMMER TYPE <u>Auto</u>
--	---

**The University of  
KANSAS**

Lateral Load Research  
Wyandotte County, Kansas

---

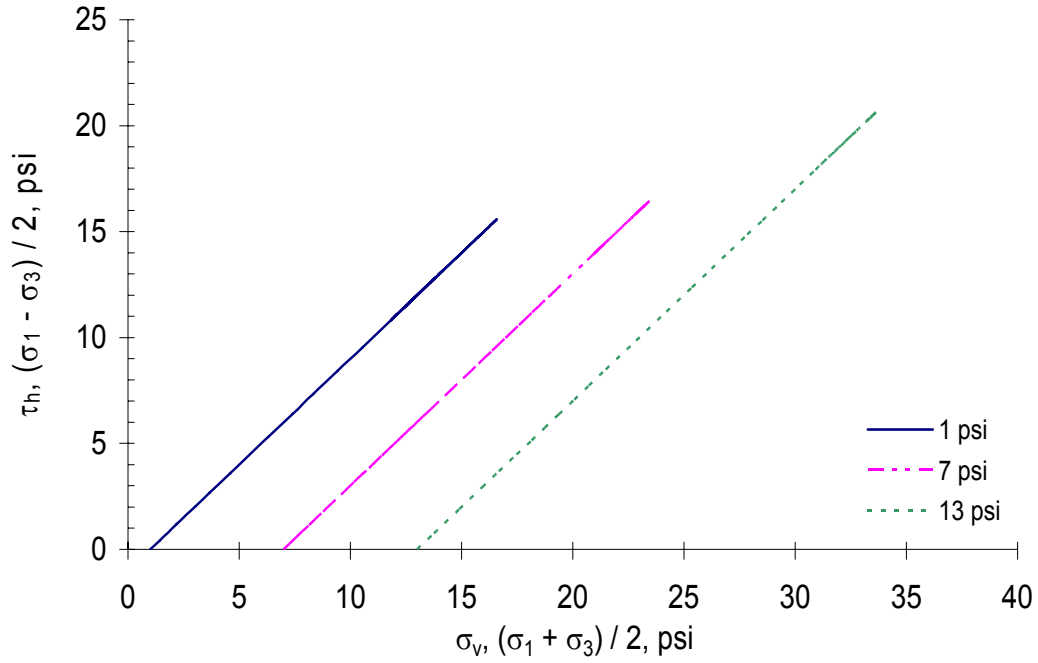
LOG OF BORING: M

---

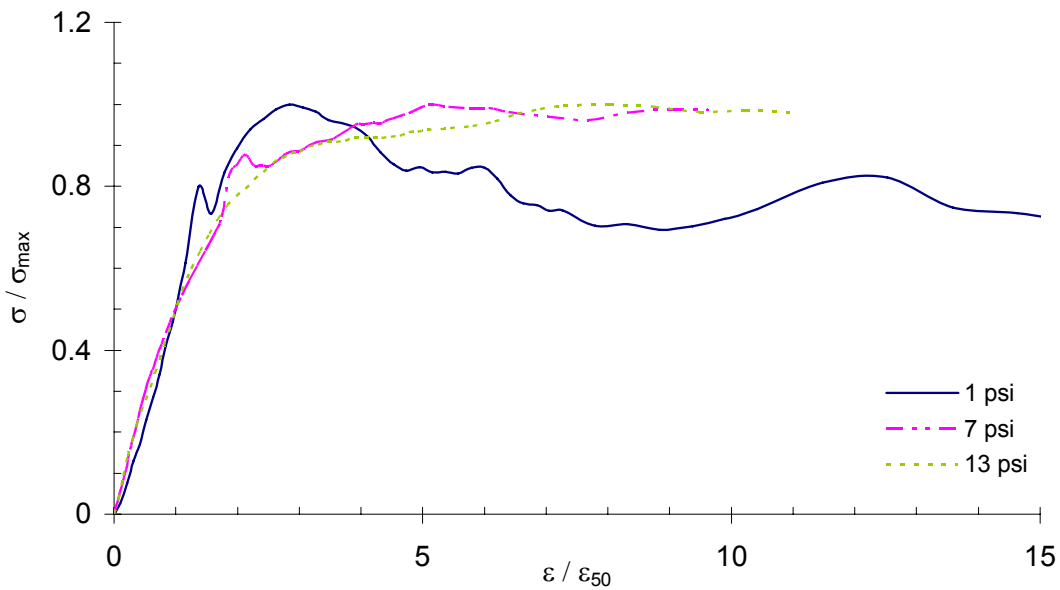
Project No.

# Appendix C

## Laboratory Testing

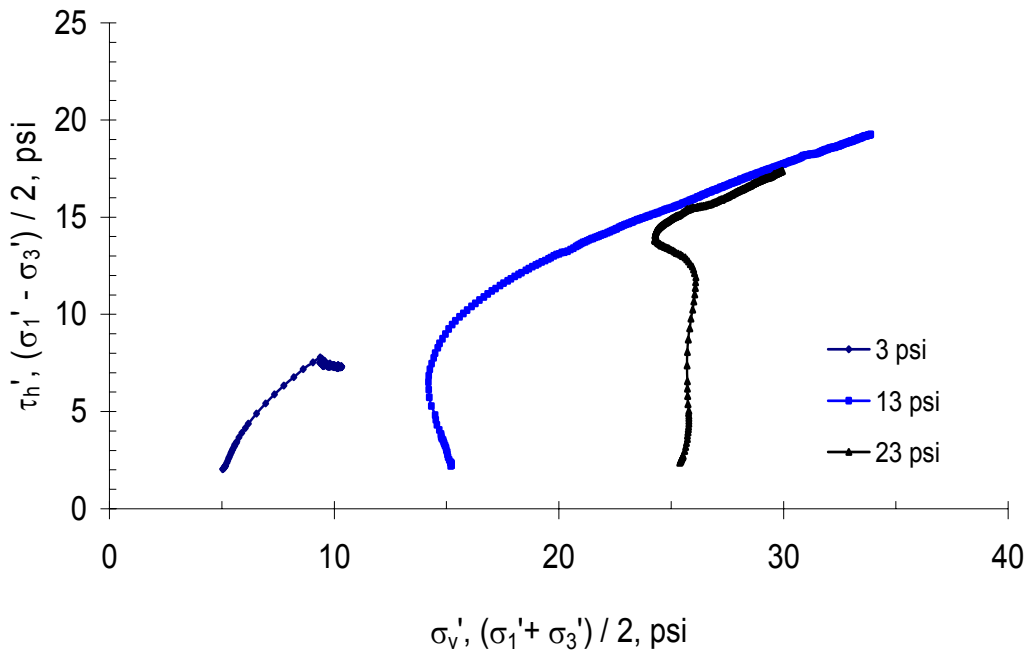


[a] p-q curve

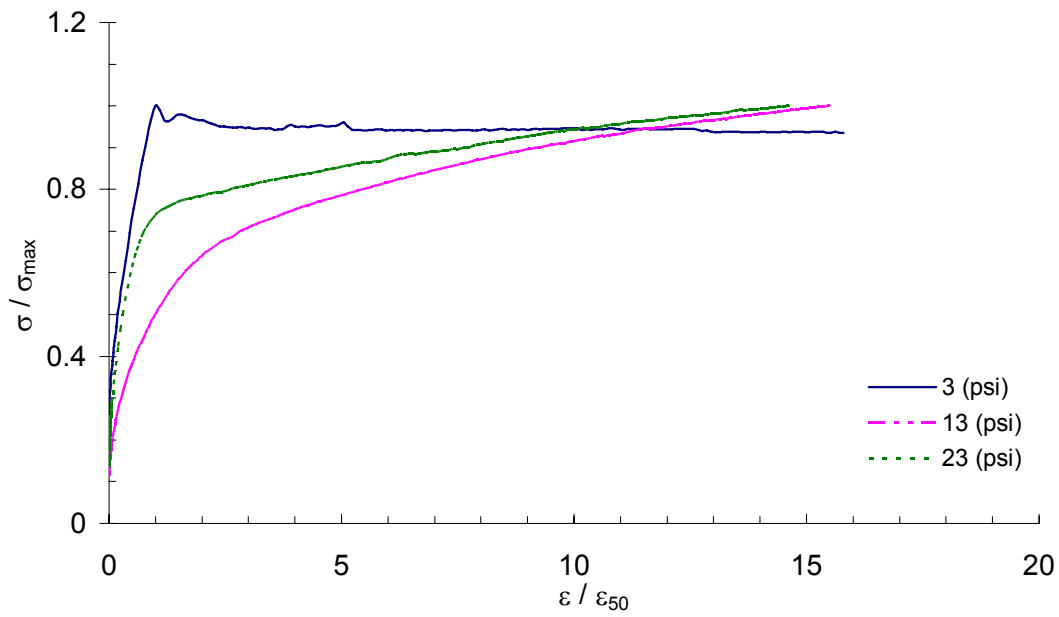


[b] Normalized stress-strain curve

Figure C1.1: UU triaxial compression, 1 foot depth, horizontal shear, 2004

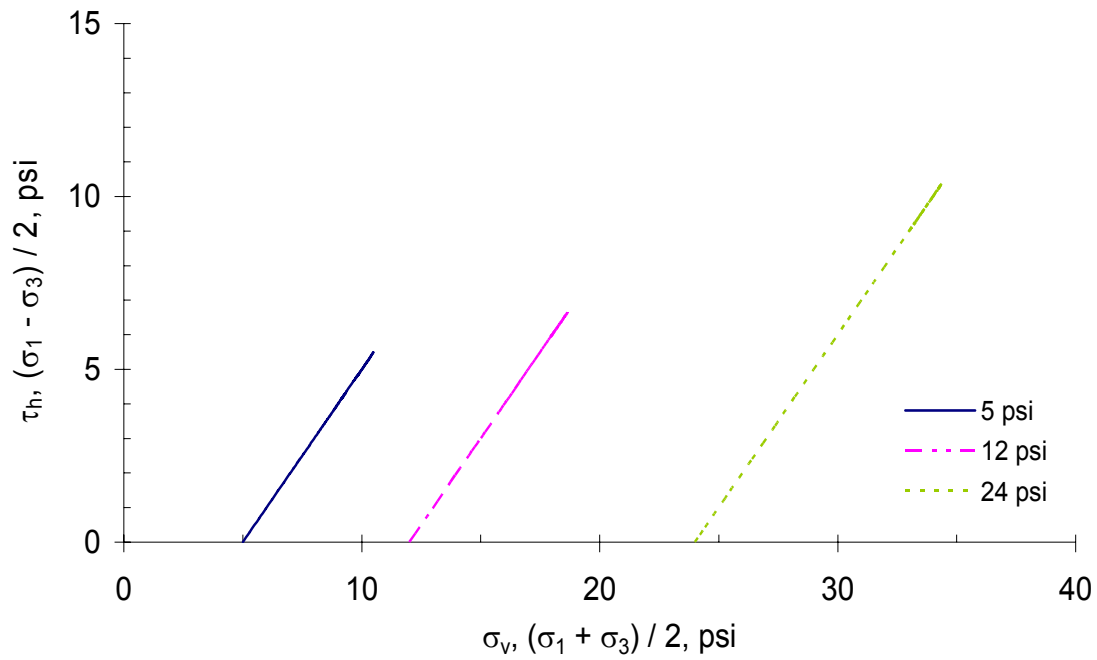


[a] p' – q' curve

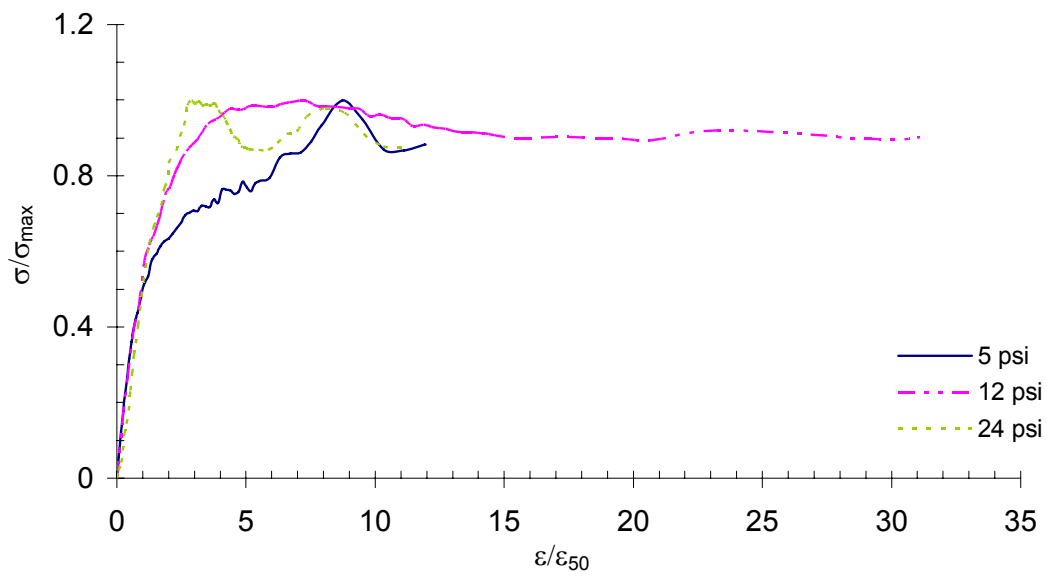


[b] Normalized stress-strain curve

Figure C1.2: CU triaxial compression, 3 foot depth, horizontal shear, 2004

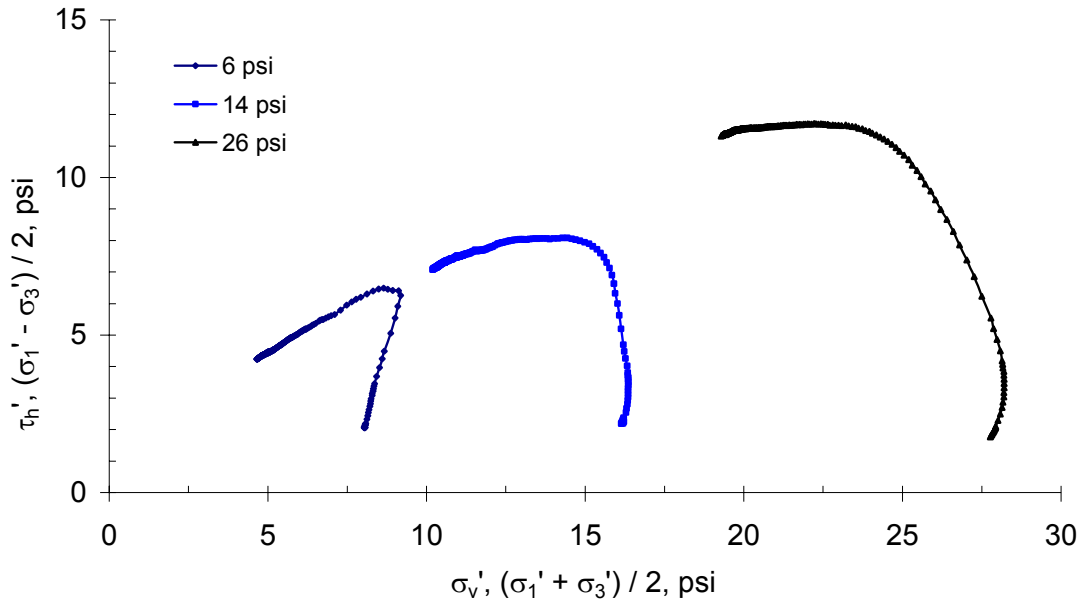


[a] p-q curve

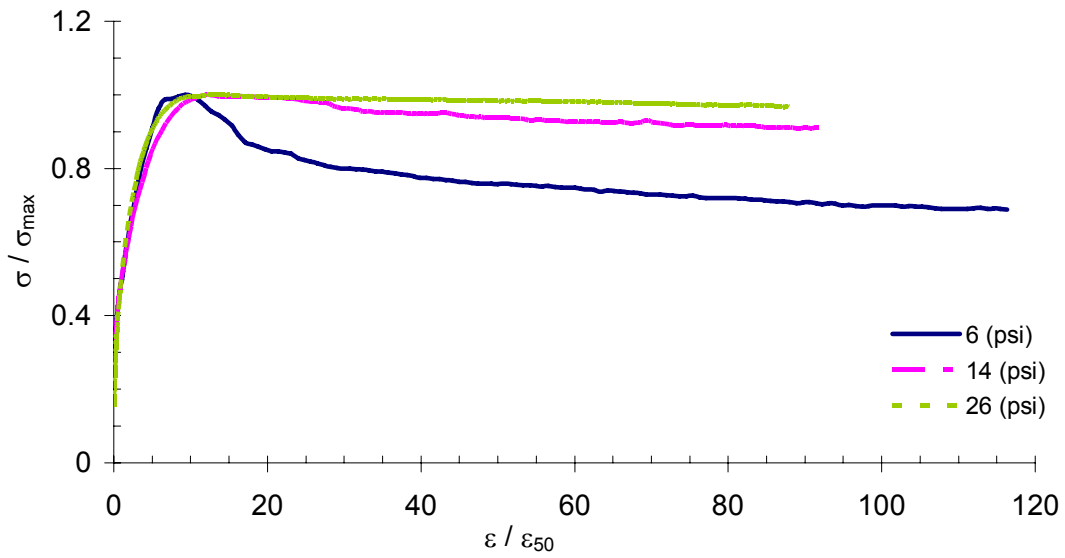


[b] Normalized stress-strain curve

Figure C1.3: UU triaxial compression, 5 foot depth, horizontal shear, 2004

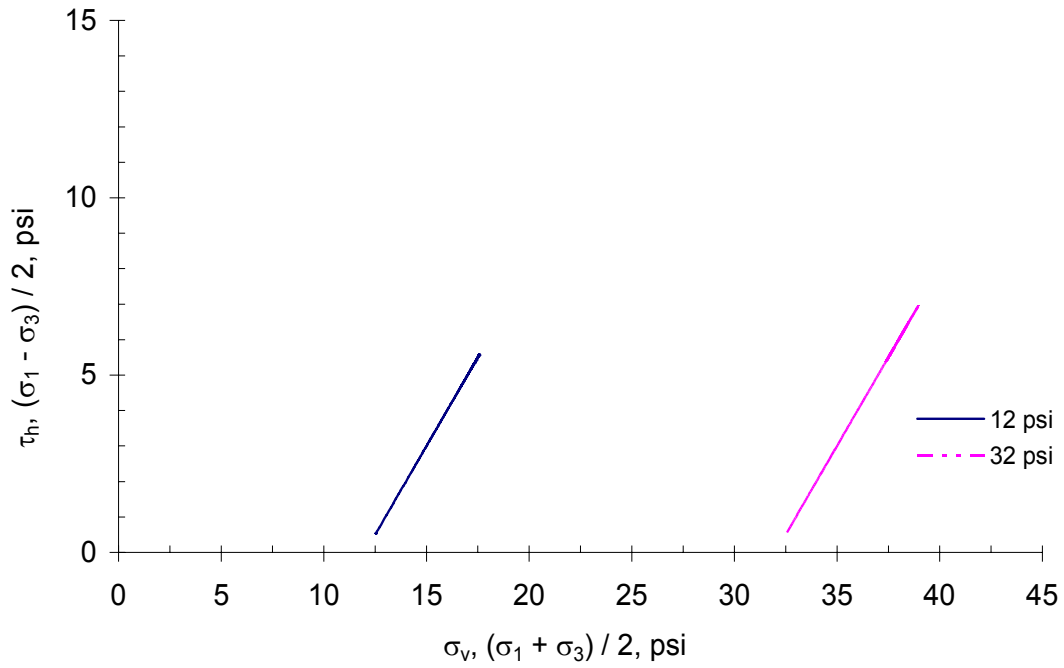


[a] p' - q' curve

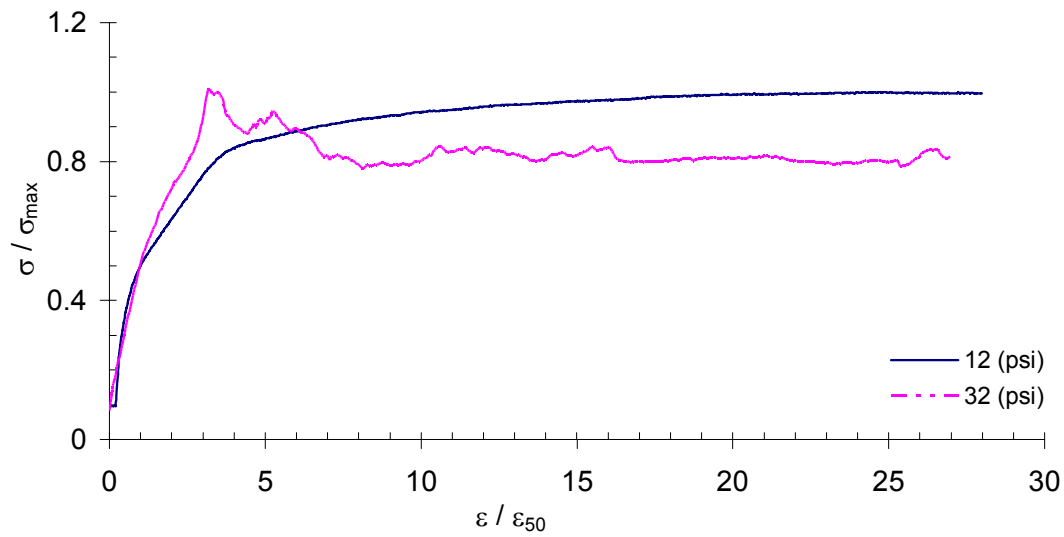


[b] Normalized stress - strain curve

Figure C1.4: CU triaxial compression, 7 foot depth, horizontal shear, 2004



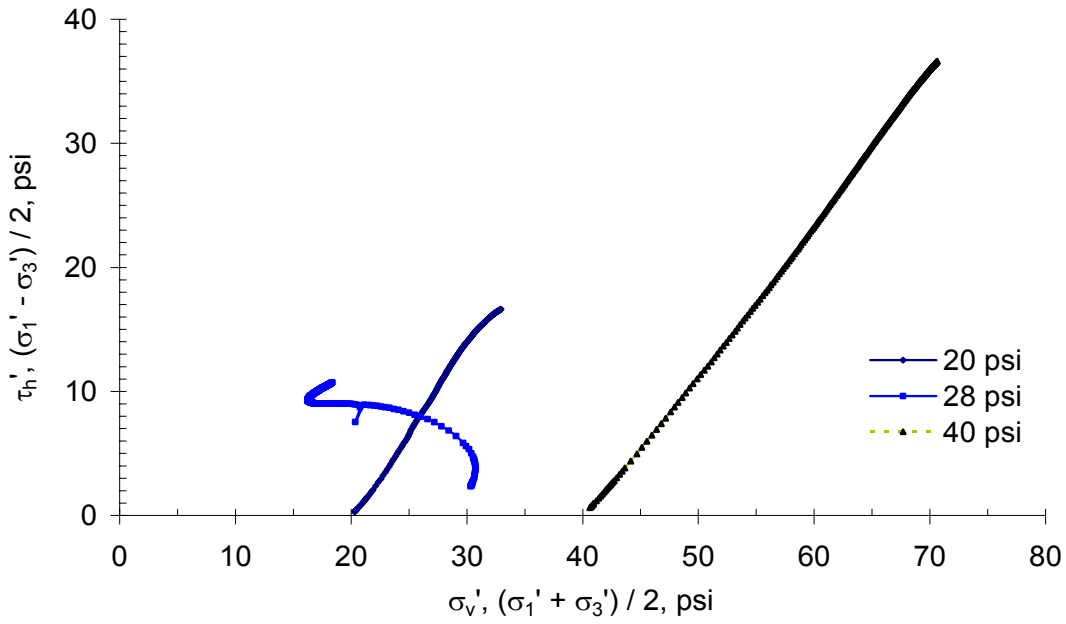
[a] p - q curve



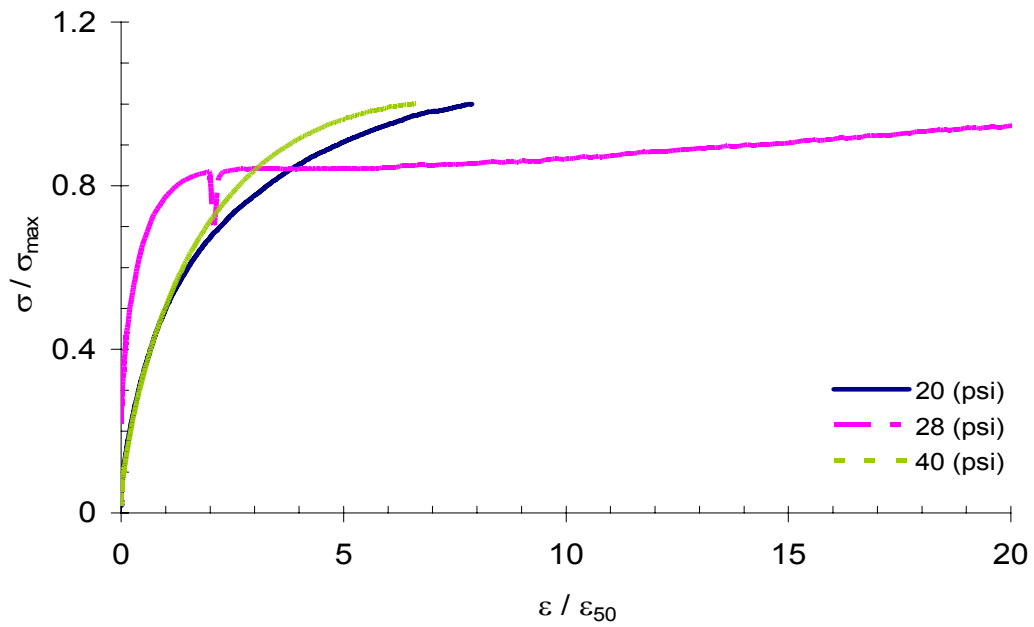
[b] Normalized stress - strain curve

Figure C1.5: UU triaxial compression, 15 foot depth, horizontal shear, 2004



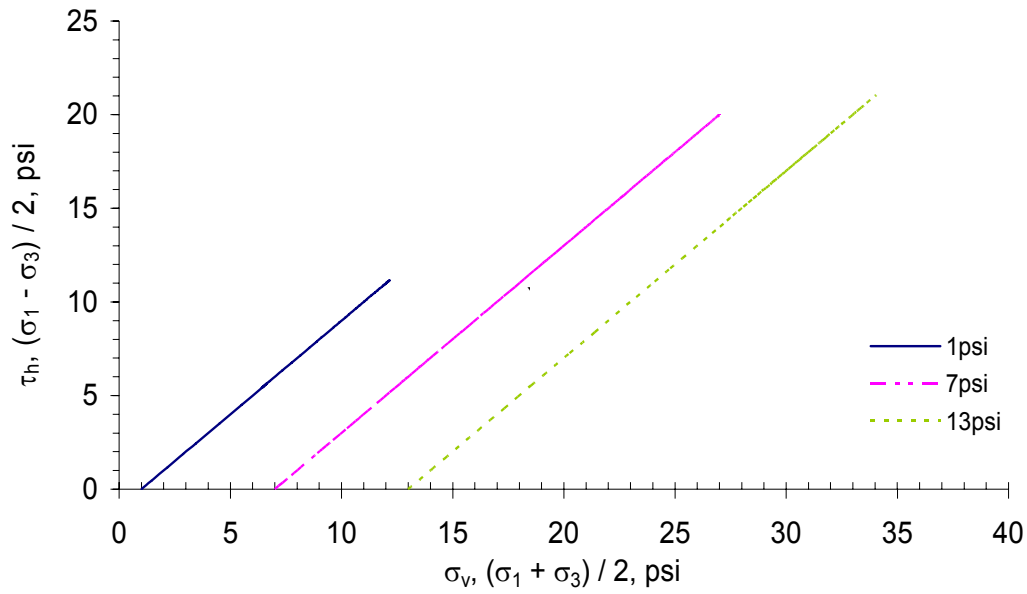


[a] p'-q' curve

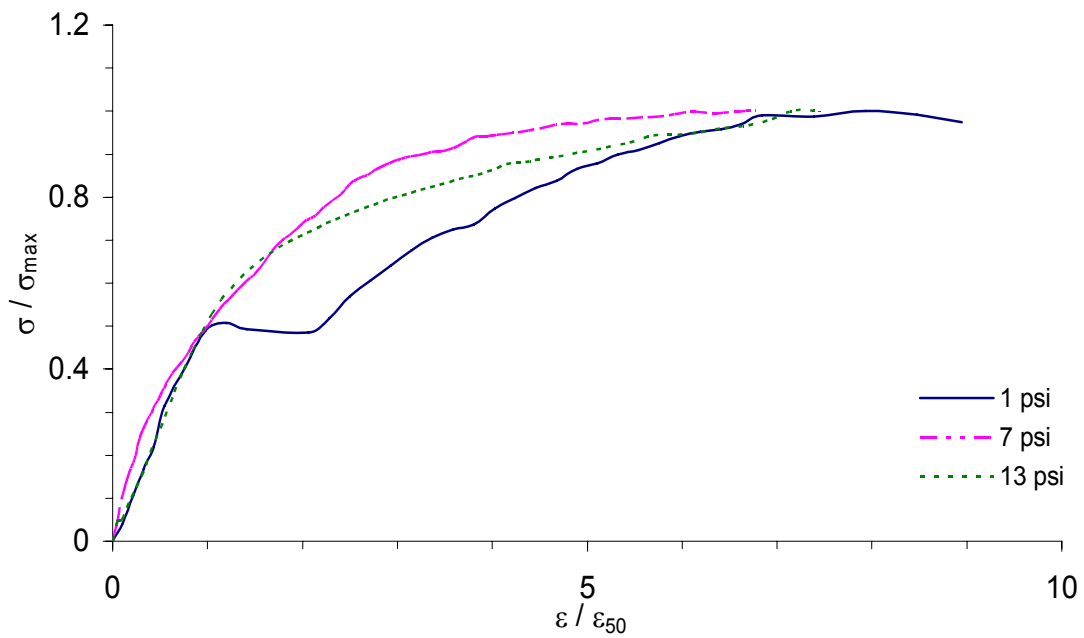


[b] Normalized stress-strain curve

Figure C1.6: CU triaxial compression, 25 foot depth, horizontal shear, 2004

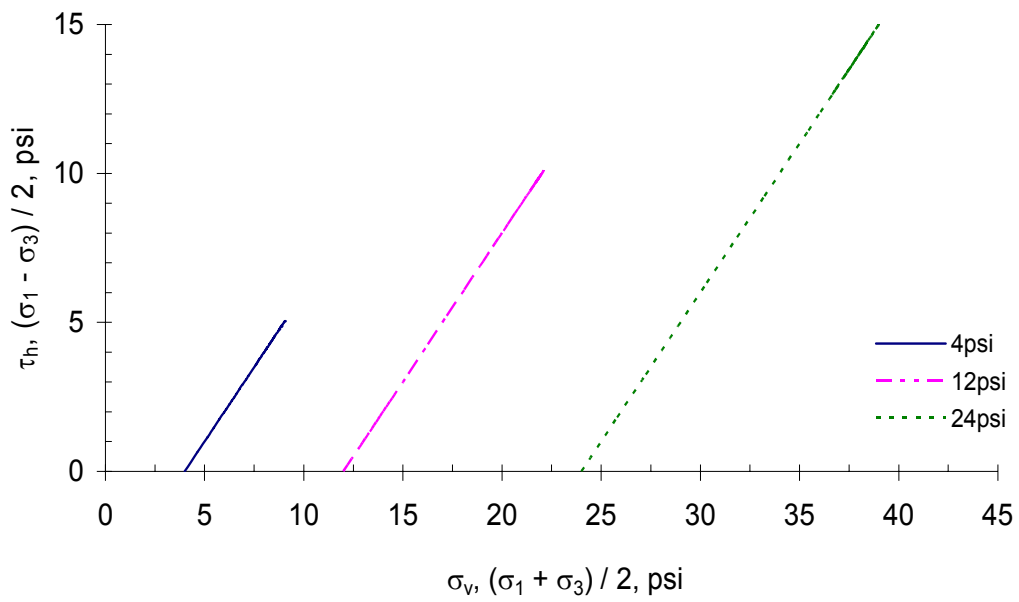


[a] p – q curve

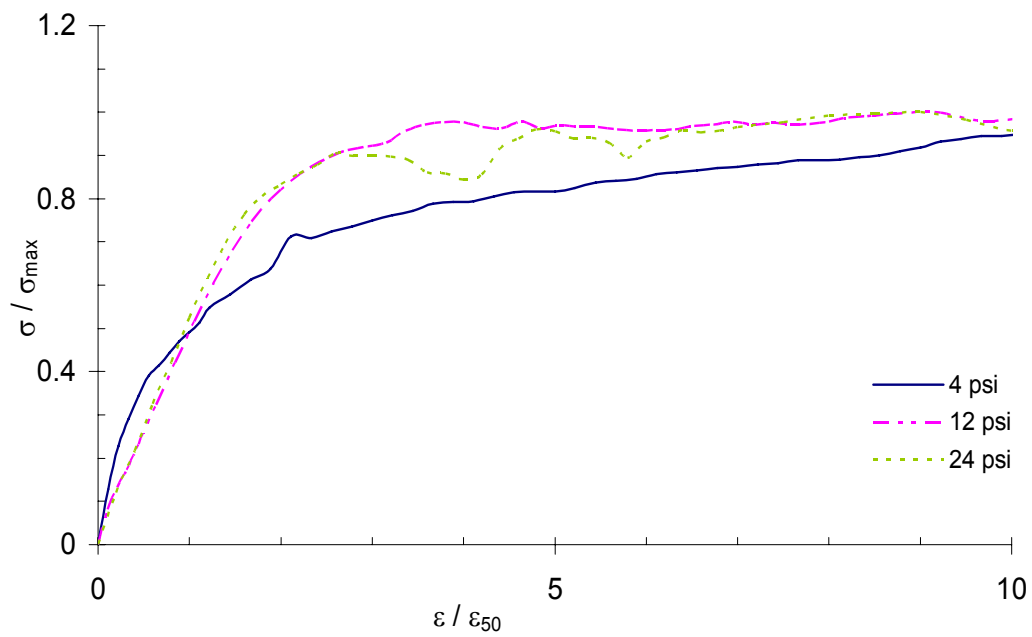


[b] Normalized stress – strain curve

Figure C1.7: UU triaxial compression, 1 foot depth, horizontal shear, 2005

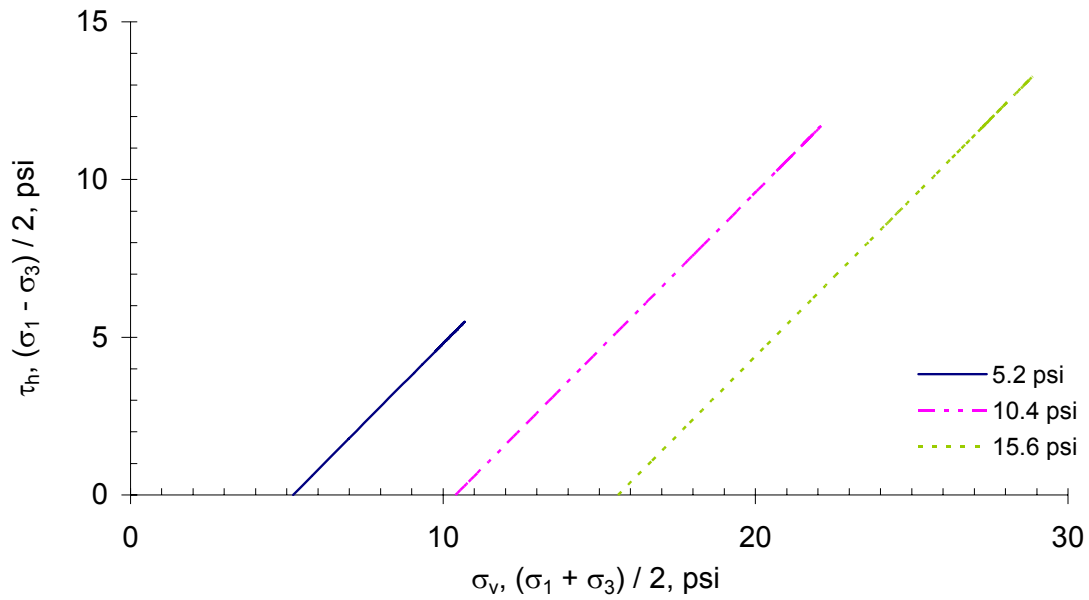


[a] p - q curve

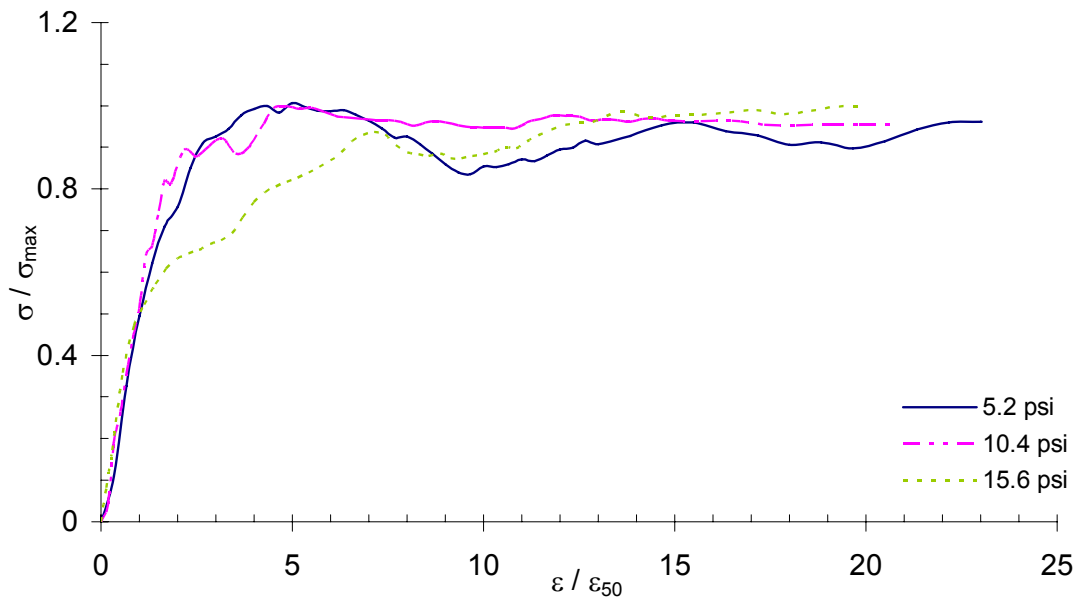


[b] Normalized stress - strain curve

Figure C1.8: UU triaxial compression, 5 foot depth, horizontal shear, 2005

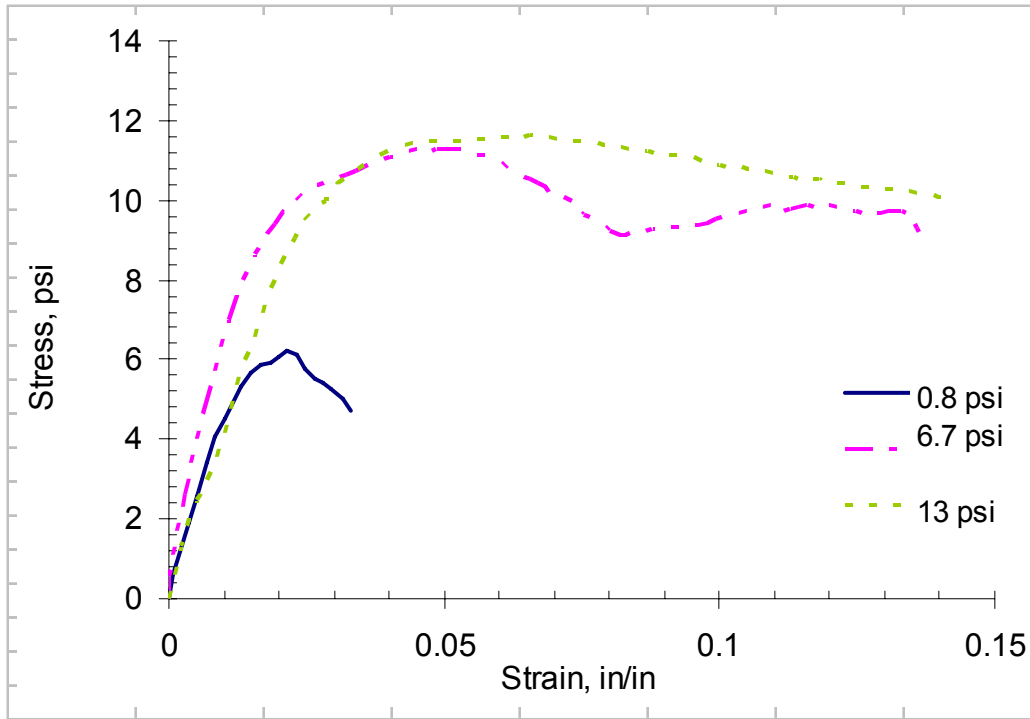


[a] p – q curve

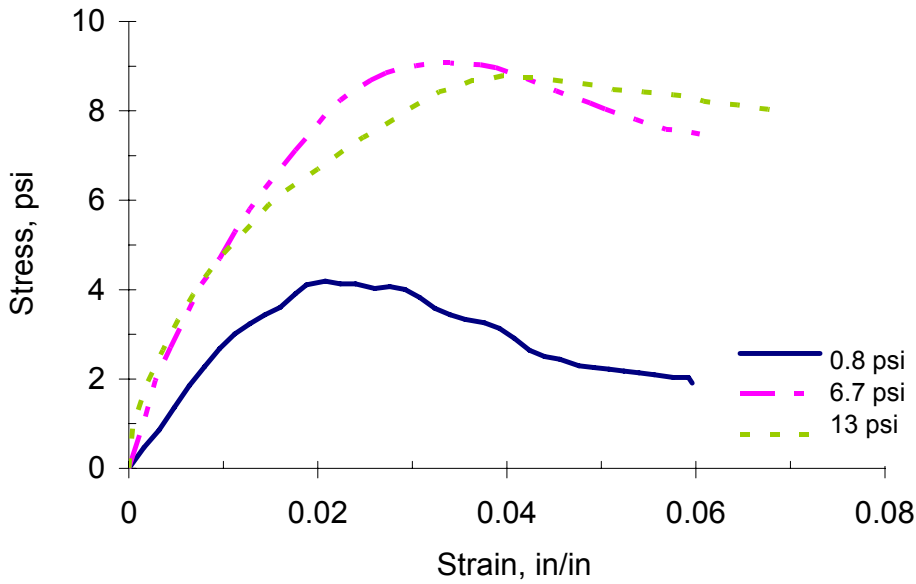


[b] Normalized stress – strain curve

Figure C1.9: UU triaxial compression, 15 foot depth, horizontal shear, 2005

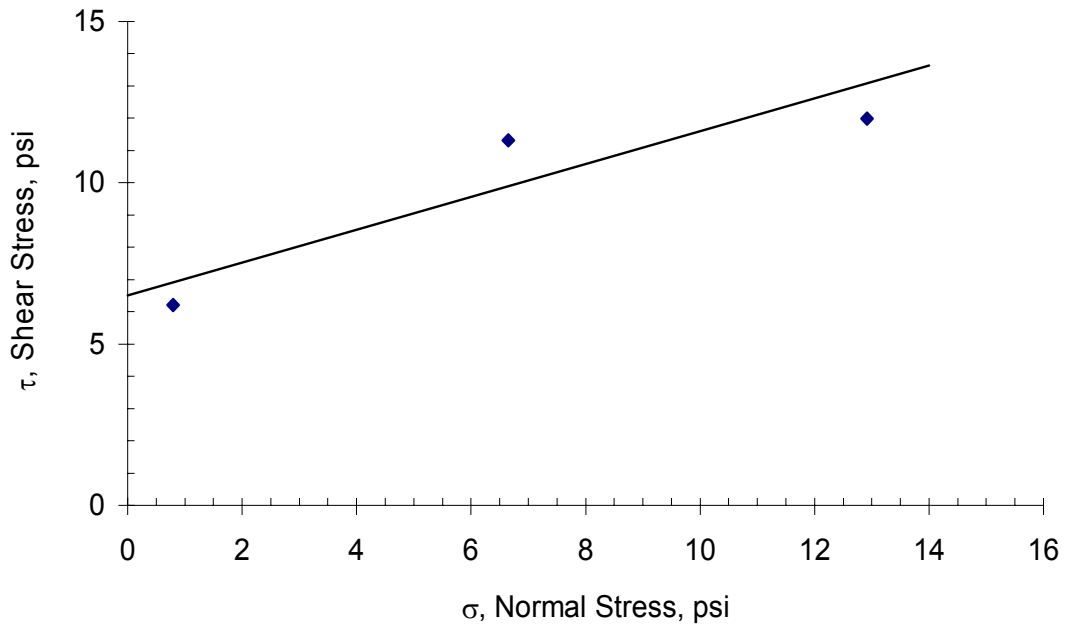


[a] Vertical Shear

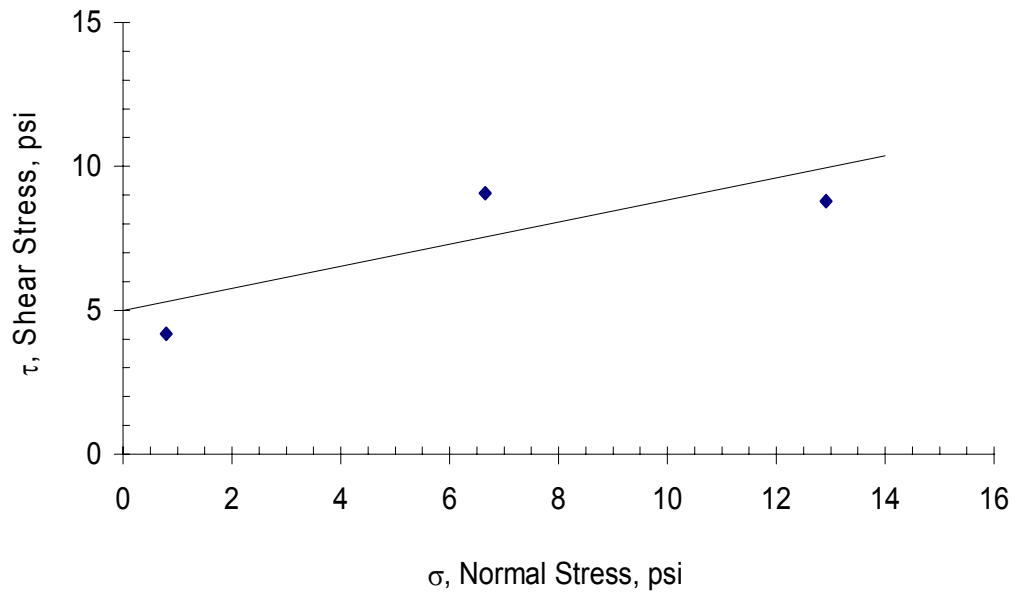


[b] Horizontal Shear

Figure C2.1: Direct Shear, 1 foot depth, 2004

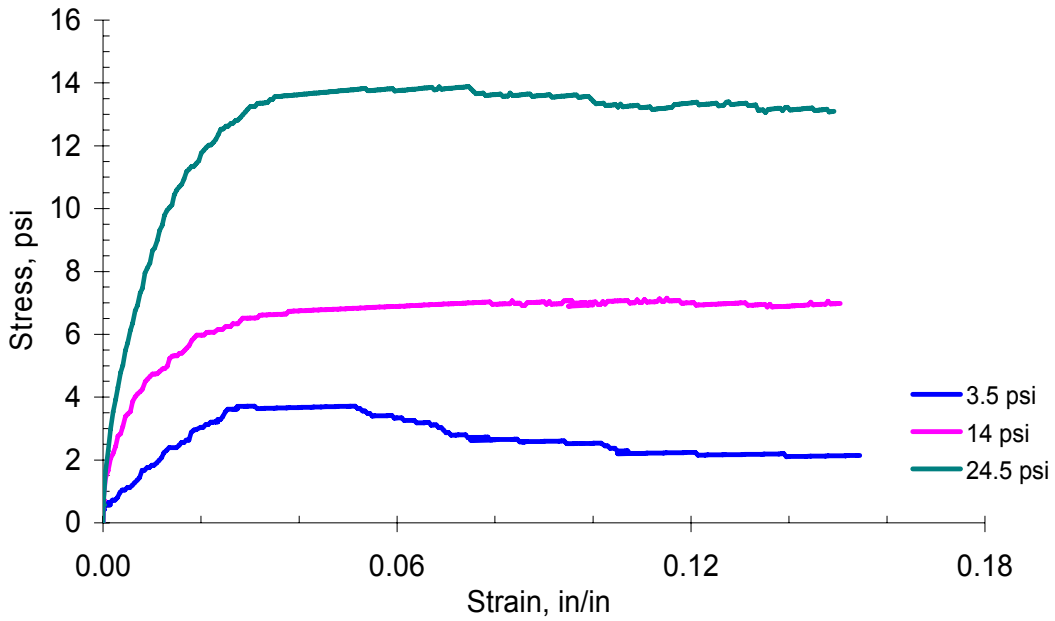


**[a] Vertical Shear**

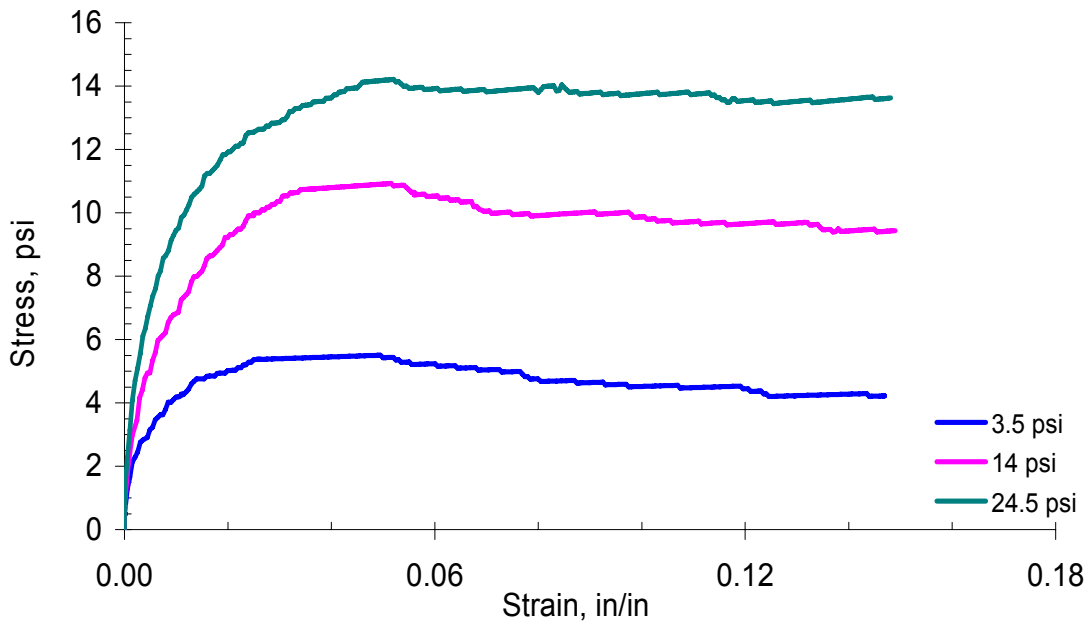


**[b] Horizontal Shear**

**Figure C2.2: Direct Shear, 1 foot depth, 2004**

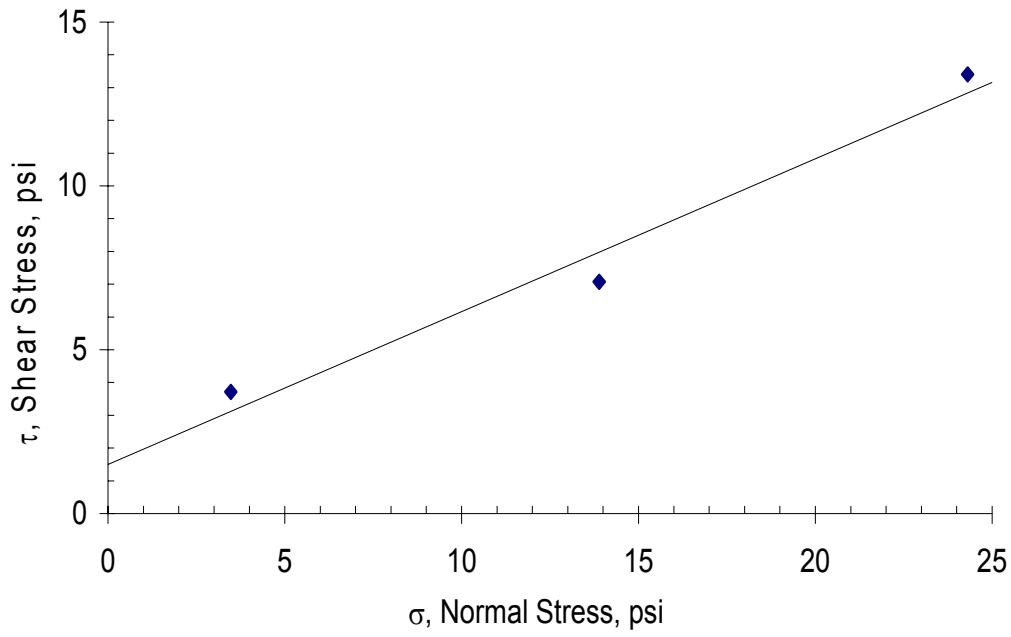


[a] Vertical Shear

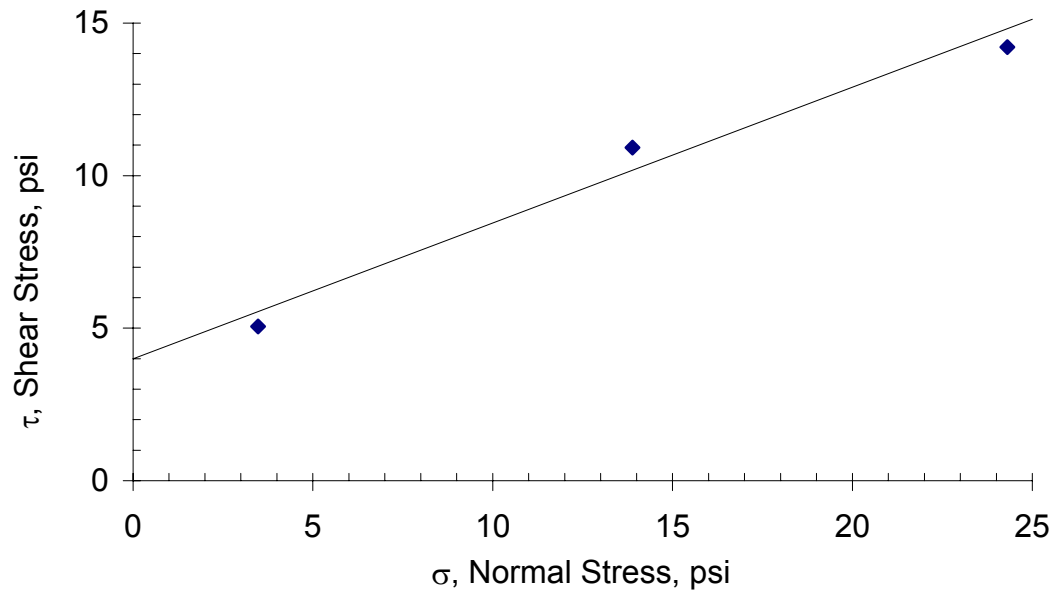


[b] Horizontal Shear

Figure C2.3: Direct Shear, 3 foot depth, 2004



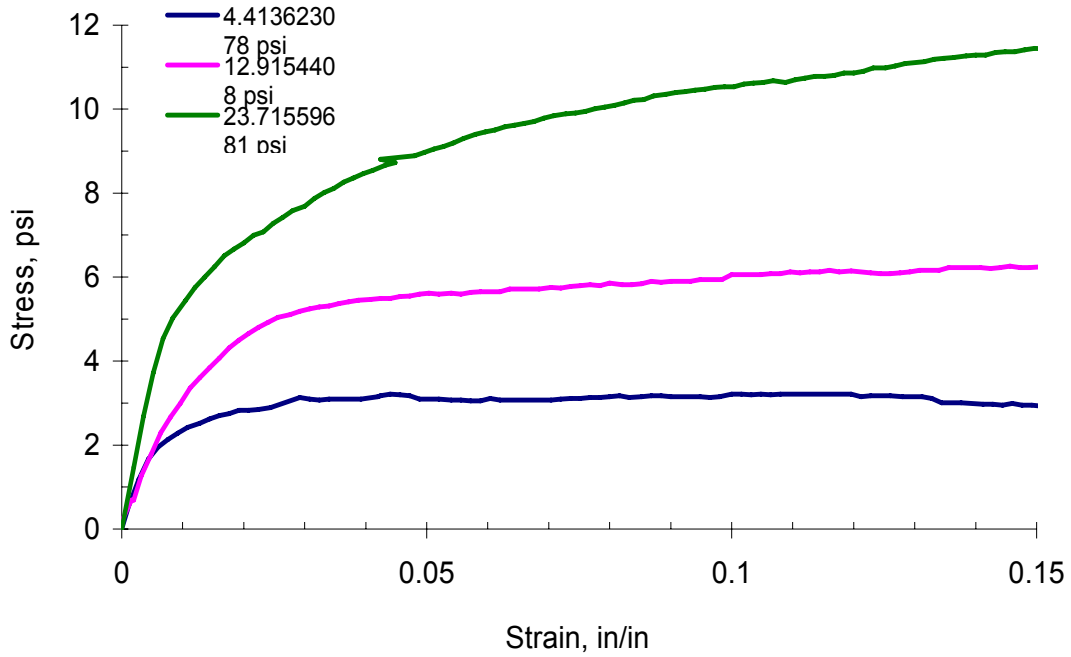
**[a] Vertical Shear**



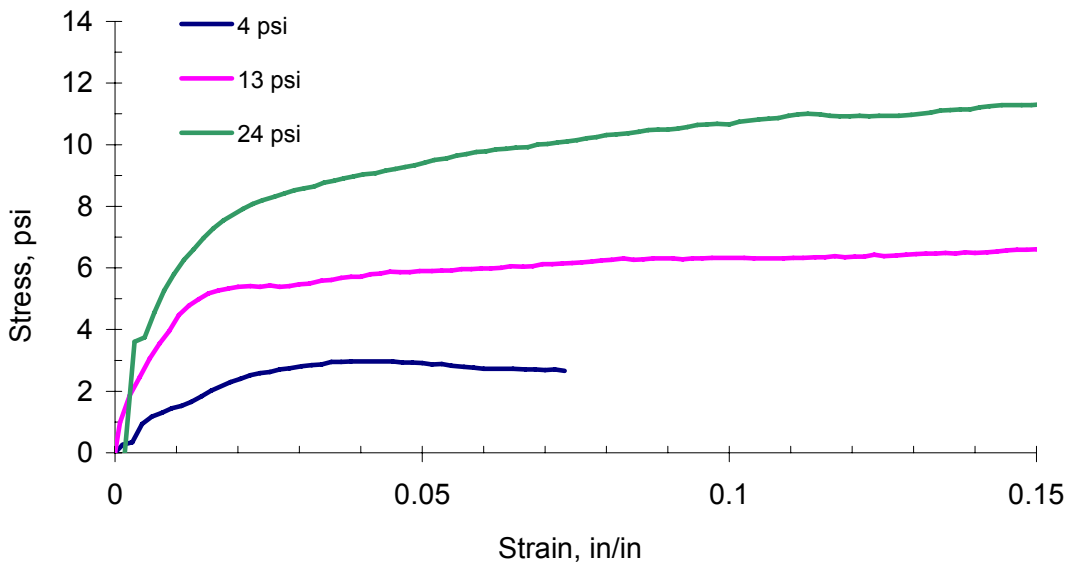
**[b] Horizontal Shear**

**Figure C2.4: Direct Shear, 3 foot depth, 2004**



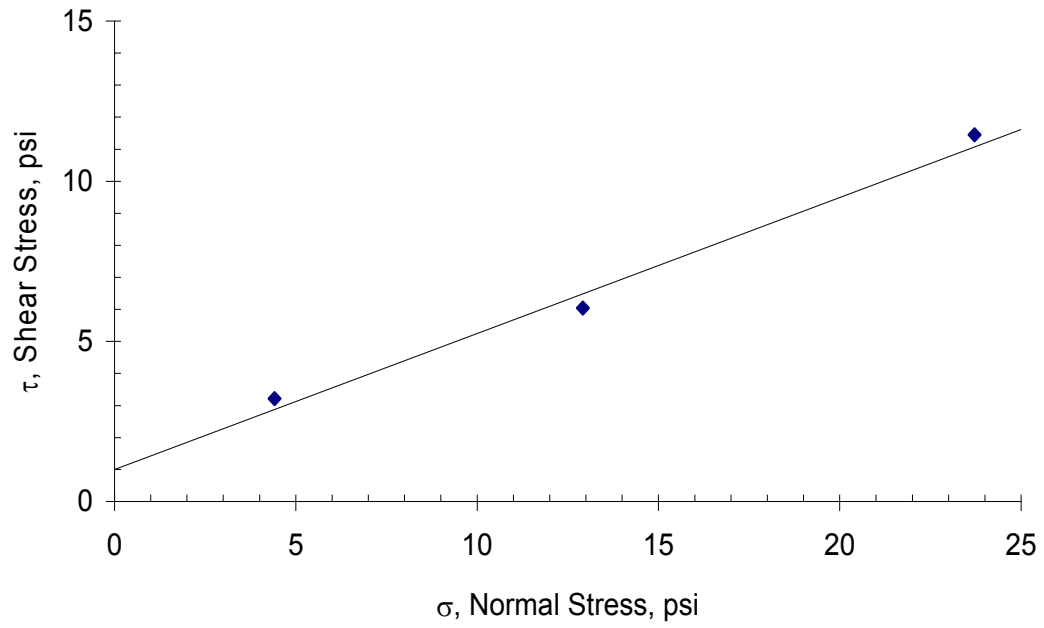


**[a] Vertical Shear**

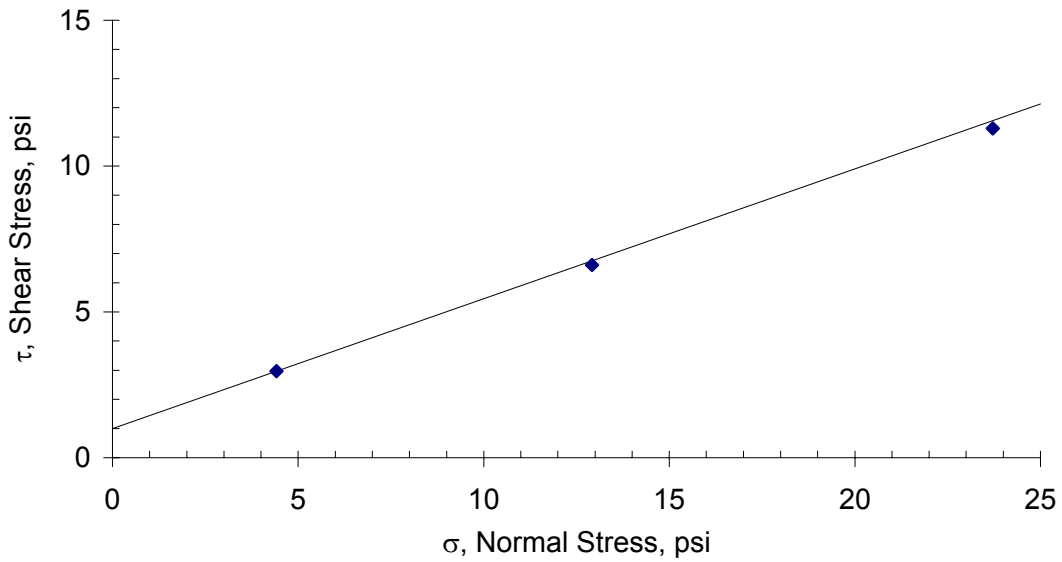


**[b] Horizontal Shear**

**Figure C2.5: Direct Shear, 5 foot depth, 2004**

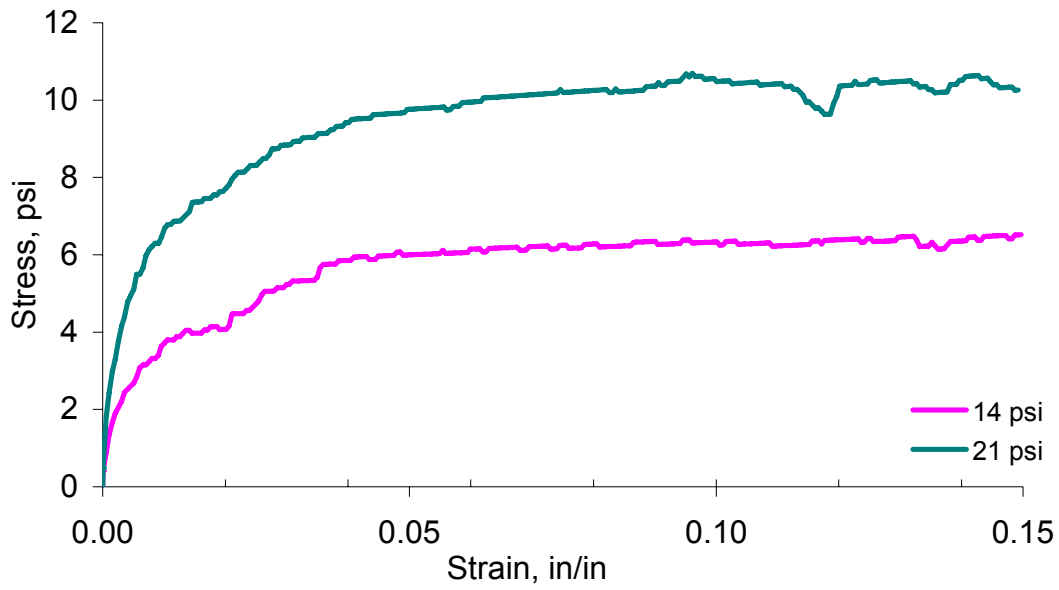


**[a] Vertical Shear**

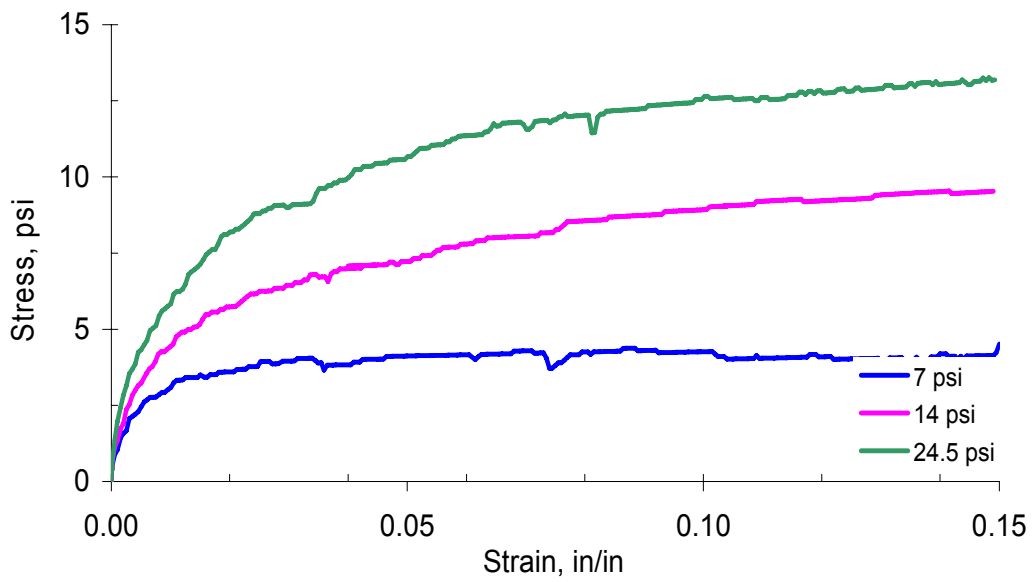


**[b] Horizontal Shear**

**Figure C2.6: Direct Shear, 5 foot depth, 2004**

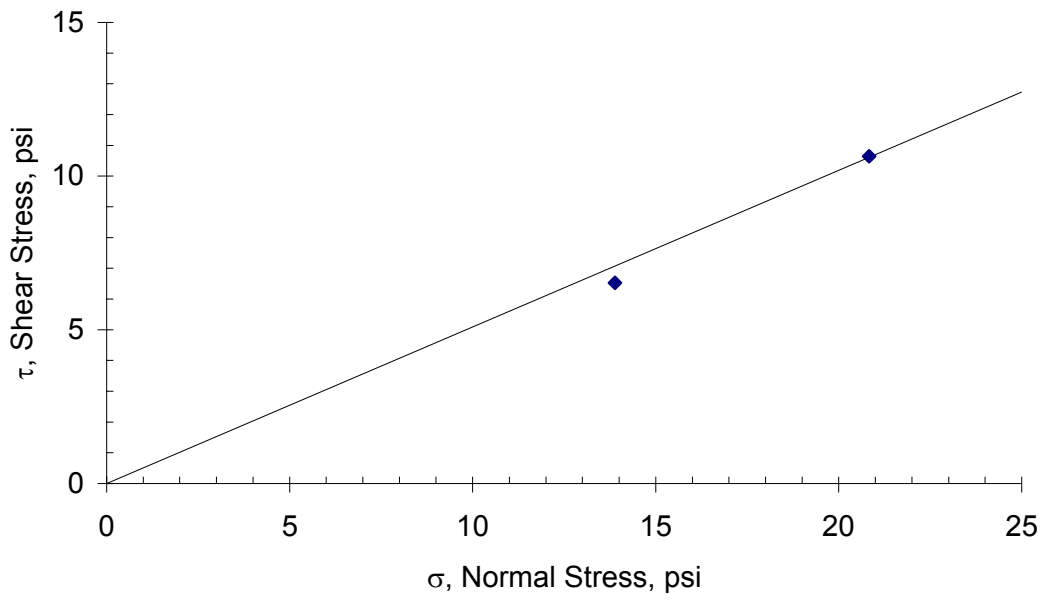


[a] Vertical Shear

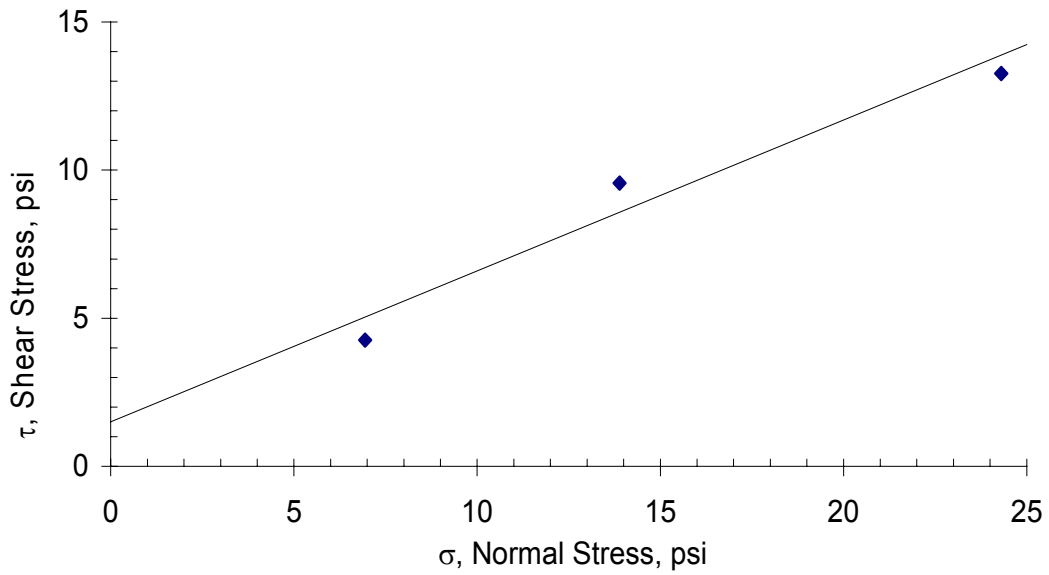


[b] Horizontal Shear

Figure C2.7: Direct Shear, 7 foot depth, 2004

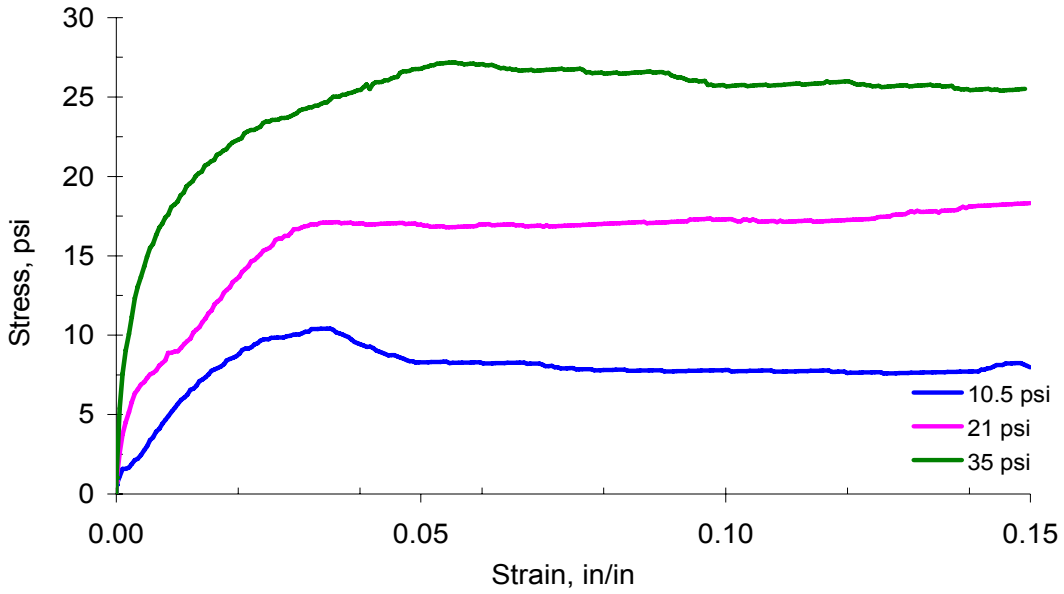


**[a] Vertical Shear**

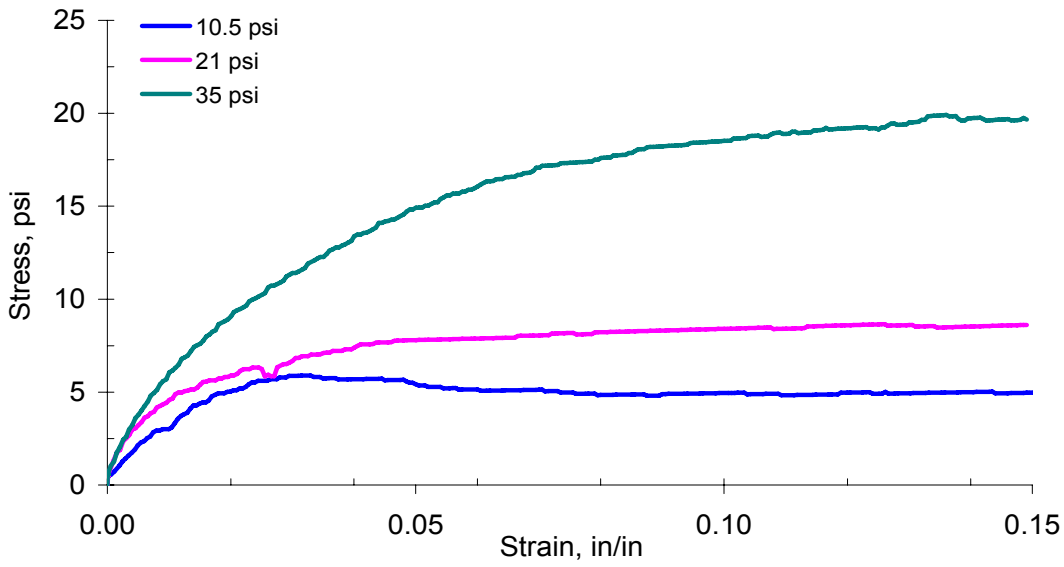


**[b] Horizontal Shear**

**Figure C2.8: Direct Shear, 7 foot depth, 2004**

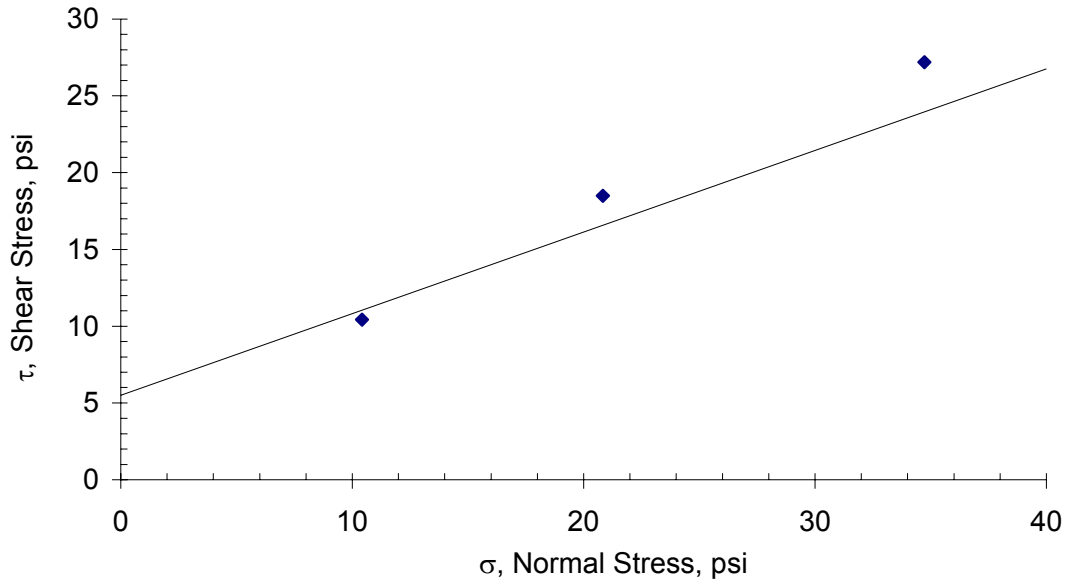


**[a] Vertical Shear**

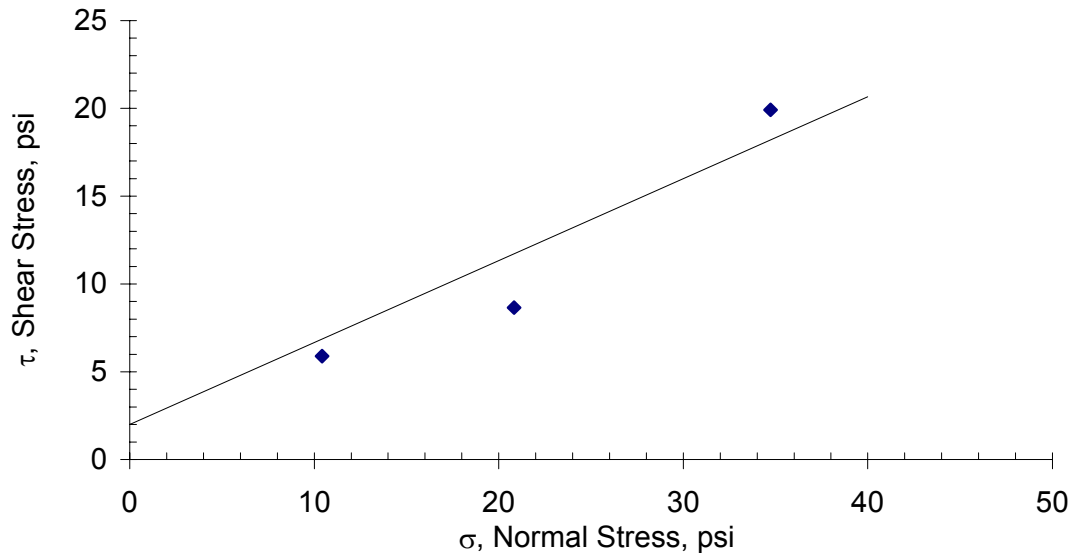


**[b] Horizontal Shear**

**Figure C2.9: Direct Shear, 15 foot depth, 2004**

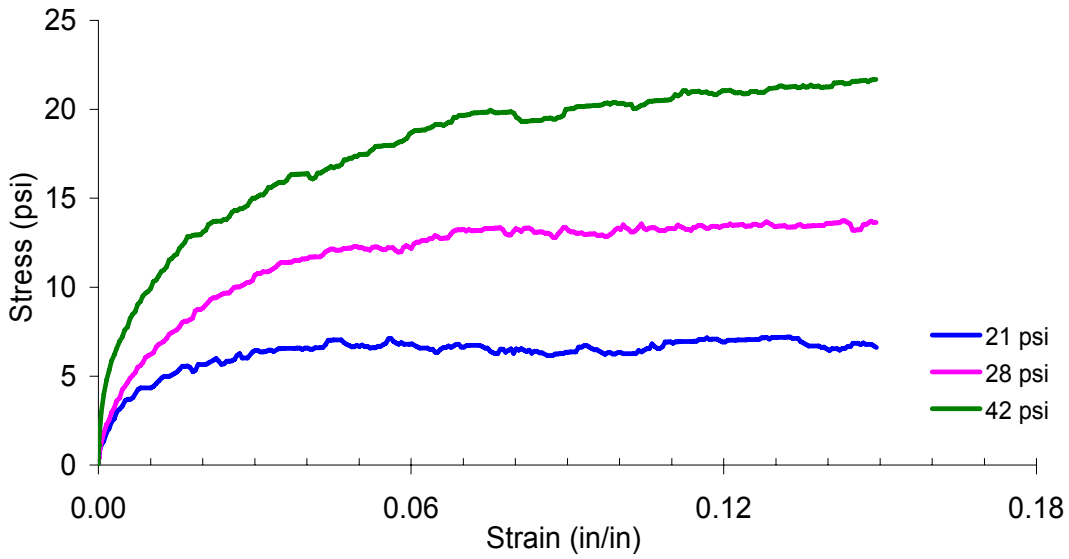


**[a] Vertical Shear**

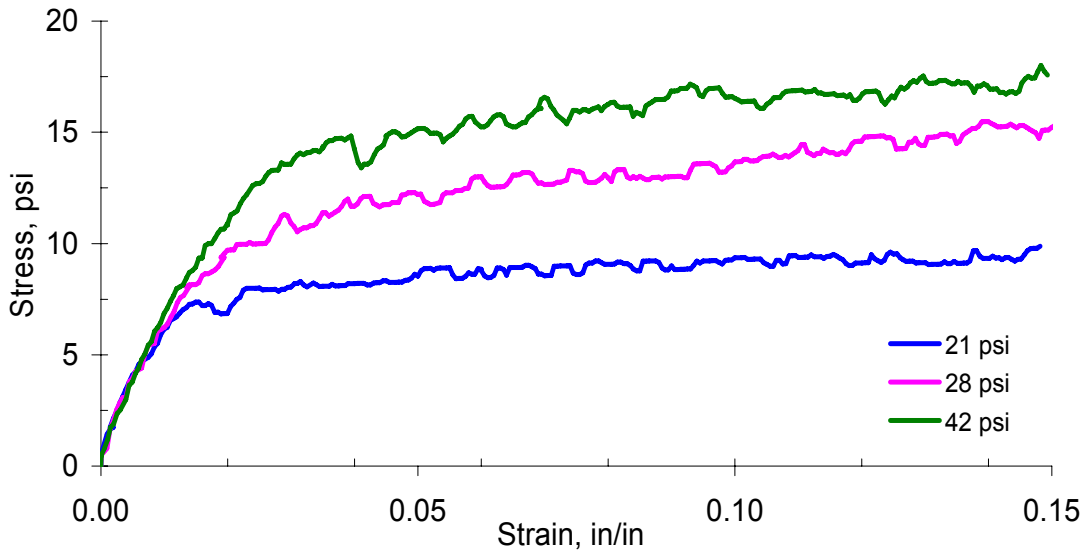


**[b] Horizontal Shear**

**Figure C2.10: Direct Shear, 15 foot depth, 2004**

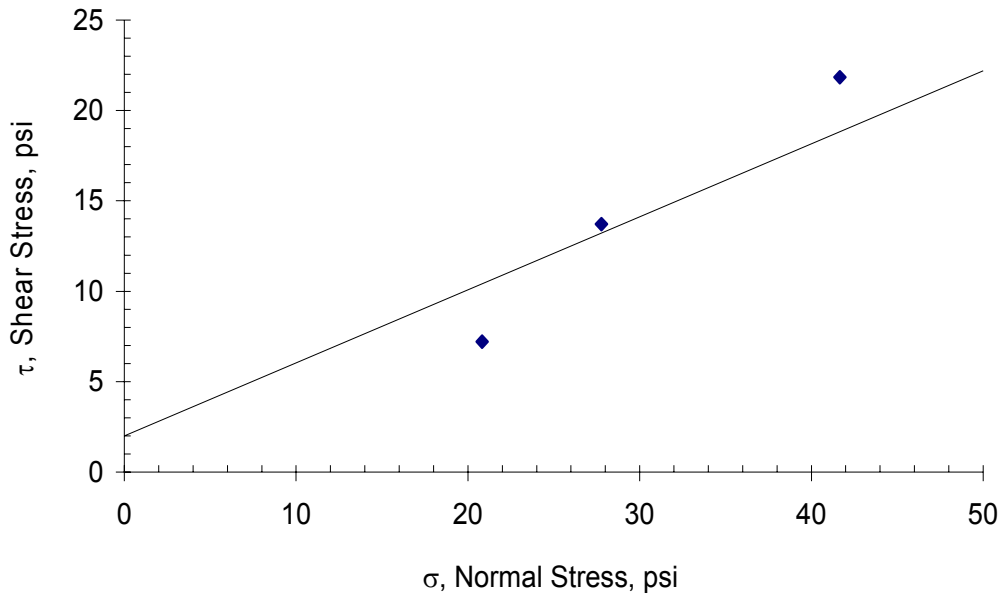


[a] Vertical Shear

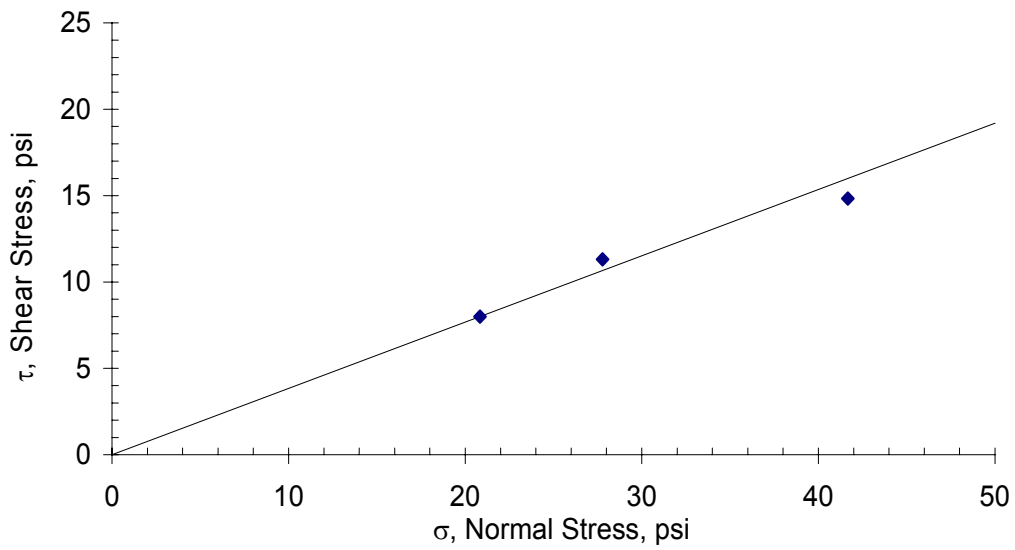


[b] Horizontal Shear

Figure C2.11: Direct Shear, 25 foot depth, 2004



**[a] Vertical Shear**



**[b] Horizontal Shear**

**Figure C2.12: Direct Shear, 25 foot depth, 2004**



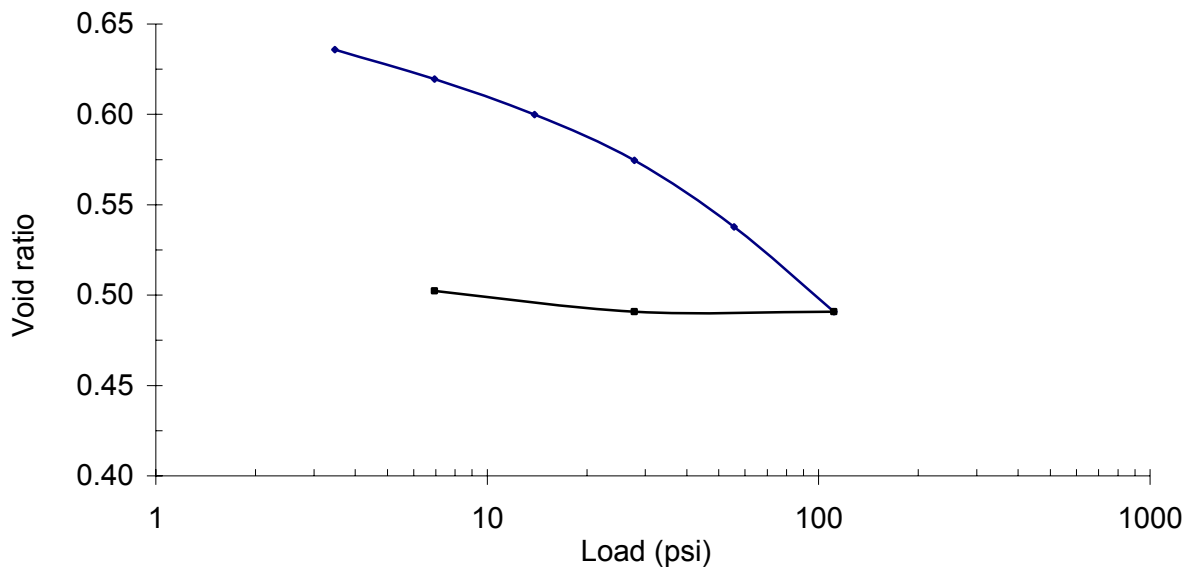


**Figure C3.1: Consolidation, 7 foot depth, 2004**

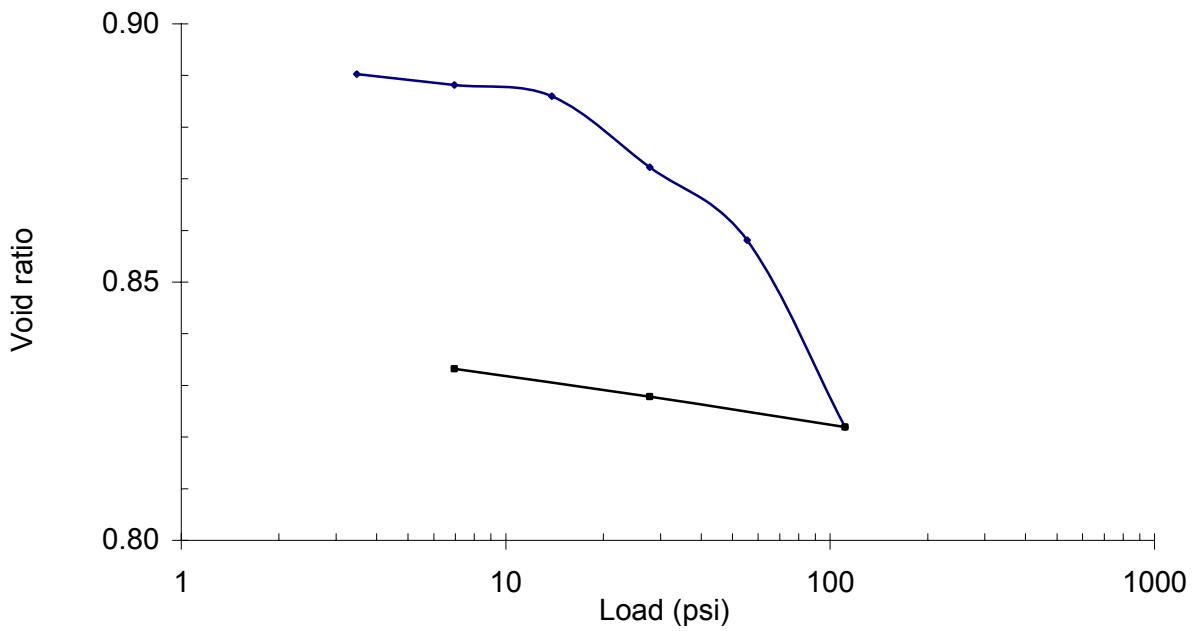


**Figure C3.2: Consolidation, 15 foot depth, 2004**

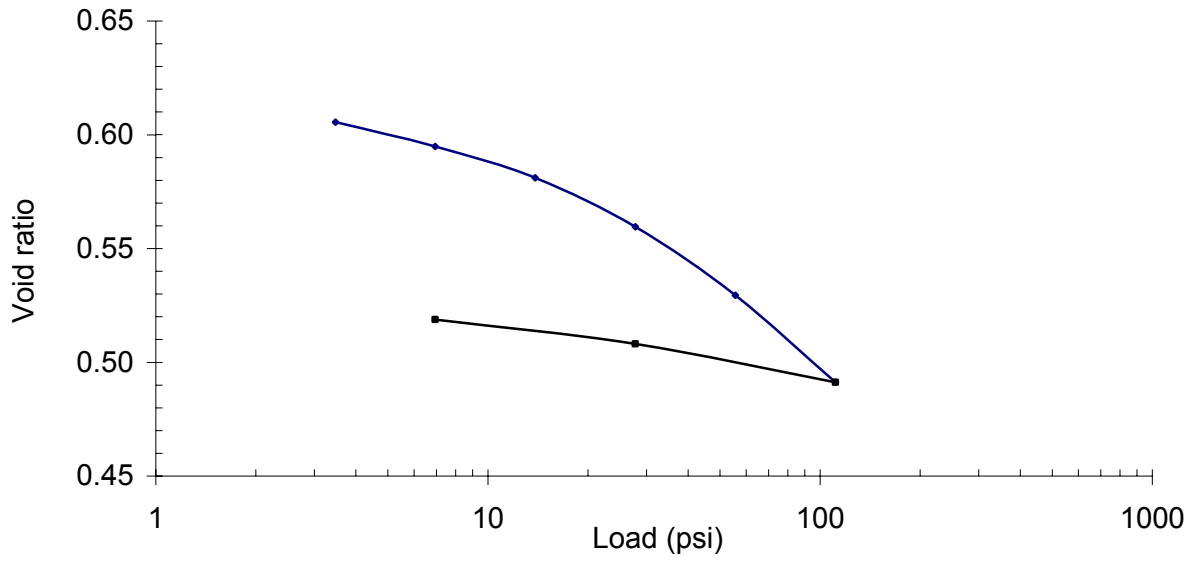
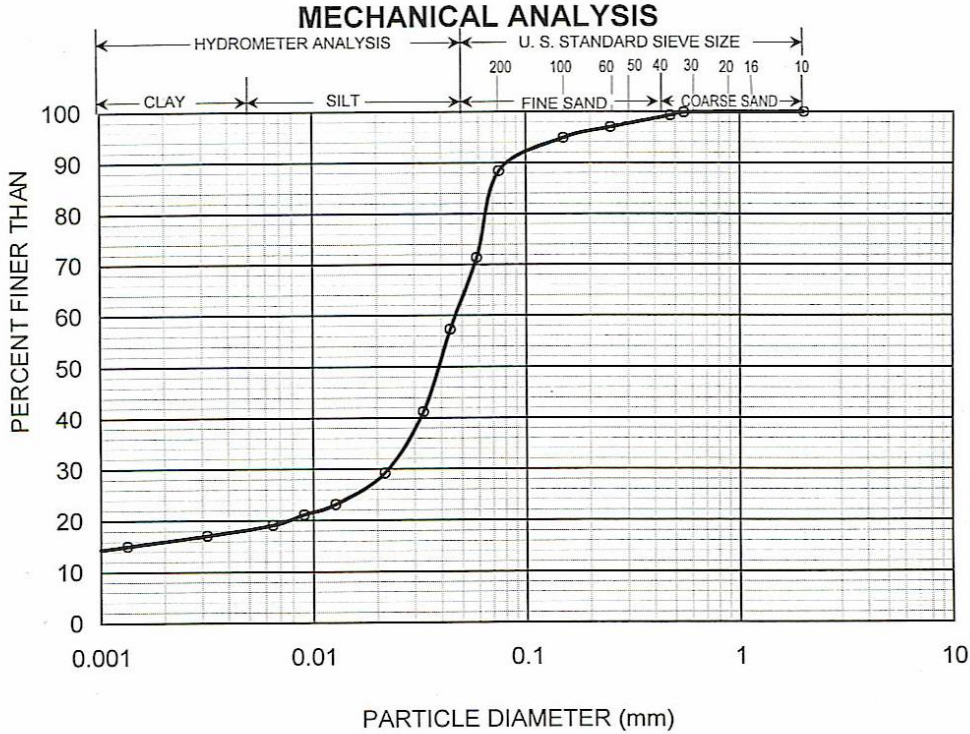


**Figure C3.3: Consolidation, 25 foot depth, 2004**

**KANSAS DEPARTMENT OF TRANSPORTATION  
REPORT OF SOIL TESTS**

SUBMITTED BY Luke Metheny ADDRESS 2300 Van Buren LAB. NO. 04-2218  
 PROJECT EN 2374-05 COUNTY Wyandotte DATE 7/2/2004



**PHYSICAL PROPERTIES**

SAMPLE NUMBER	STATION	DIST. $\phi$	DEPTH	L.L.	P.L.	P.I.	% Ret ON NO. 10	SPEC. GRAV. (PASS NO. 10)	CLASS KS/UNIF.
			ft						
RDS1			0.0-4.0	31	18	13	0	2.63	L-CL

Test Method: ASTM D422 (Iowa Air Dispersion)

REMARKS \_\_\_\_\_  
 \_\_\_\_\_  
 \_\_\_\_\_

L. S. Ingram, P.E.  
 Chief of Bureau of Materials and Research

By Robert A. Fuller, P.E.  
 Soils Engineer

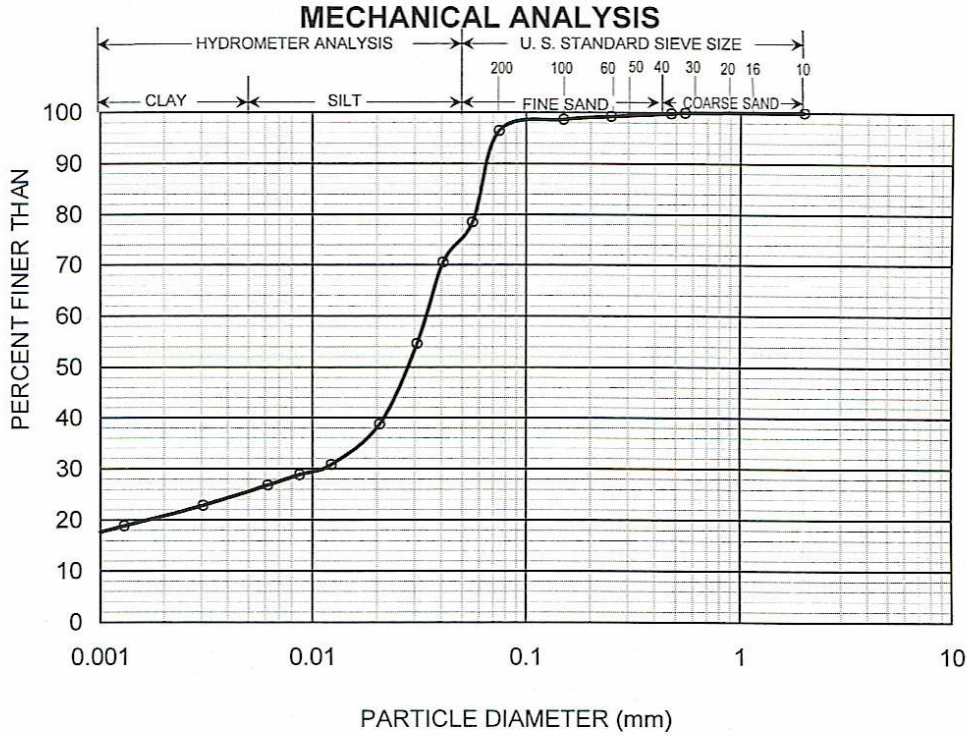
Rev. 3-99

D.O.T. NO. 635

**Figure C4.1: Grain-Size Distribution and Index Properties, 0.0 – 4.0 feet**

**KANSAS DEPARTMENT OF TRANSPORTATION  
REPORT OF SOIL TESTS**

SUBMITTED BY Luke Metheny ADDRESS 2300 Van Buren LAB. NO. 04-2218  
 PROJECT EN 2374-05 COUNTY Wyandotte DATE 7/2/2004



**PHYSICAL PROPERTIES**

SAMPLE NUMBER	STATION	DIST. $\zeta$	DEPTH	L.L.	P.L.	P.I.	% Ret ON NO. 10	SPEC. GRAV. (PASS NO. 10)	CLASS KS/UNIF.
			ft						
RDS2			4.0-8.0	36	17	19	0	2.68	CL-CL

Test Method: ASTM D422 (Iowa Air Dispersion)

REMARKS \_\_\_\_\_  
 \_\_\_\_\_  
 \_\_\_\_\_

L. S. Ingram, P.E.  
 Chief of Bureau of Materials and Research

By \_\_\_\_\_  
Robert A. Fuller, P.E.  
 Soils Engineer

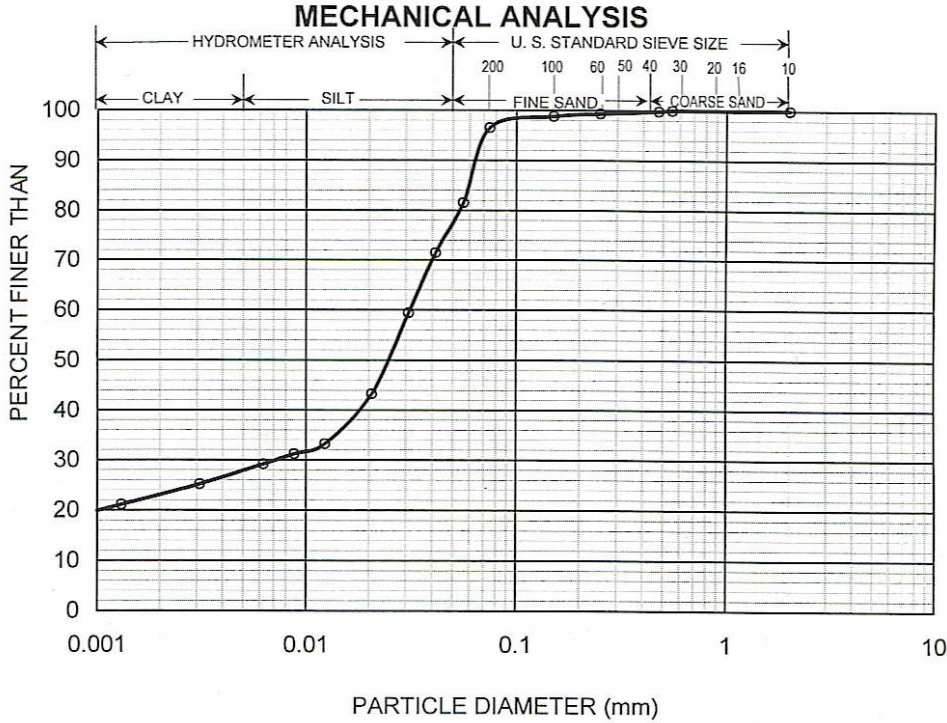
Rev. 3-99

D.O.T. NO. 635

**Figure C4.2: Grain-Size Distribution and Index Properties, 4.0 – 8.0 feet**

**KANSAS DEPARTMENT OF TRANSPORTATION  
REPORT OF SOIL TESTS**

SUBMITTED BY Luke Metheny ADDRESS 2300 Van Buren LAB. NO. 04-2218  
 PROJECT EN 2374-05 COUNTY Wyandotte DATE 7/2/2004



**PHYSICAL PROPERTIES**

SAMPLE NUMBER	STATION	DIST. $\phi$	DEPTH ft	L.L.	P.L.	P.I.	% Ret	SPEC. GRAV.	CLASS
							ON NO. 10	(PASS NO. 10)	KS/UNIF.
RDS3			8.0-12.0	38	16	22	0	2.62	L-CL

Test Method: ASTM D422 (Iowa Air Dispersion)

REMARKS \_\_\_\_\_  
 \_\_\_\_\_  
 \_\_\_\_\_

L. S. Ingram, P.E.  
 Chief of Bureau of Materials and Research

By Robert A. Fuller, P.E.  
 Soils Engineer

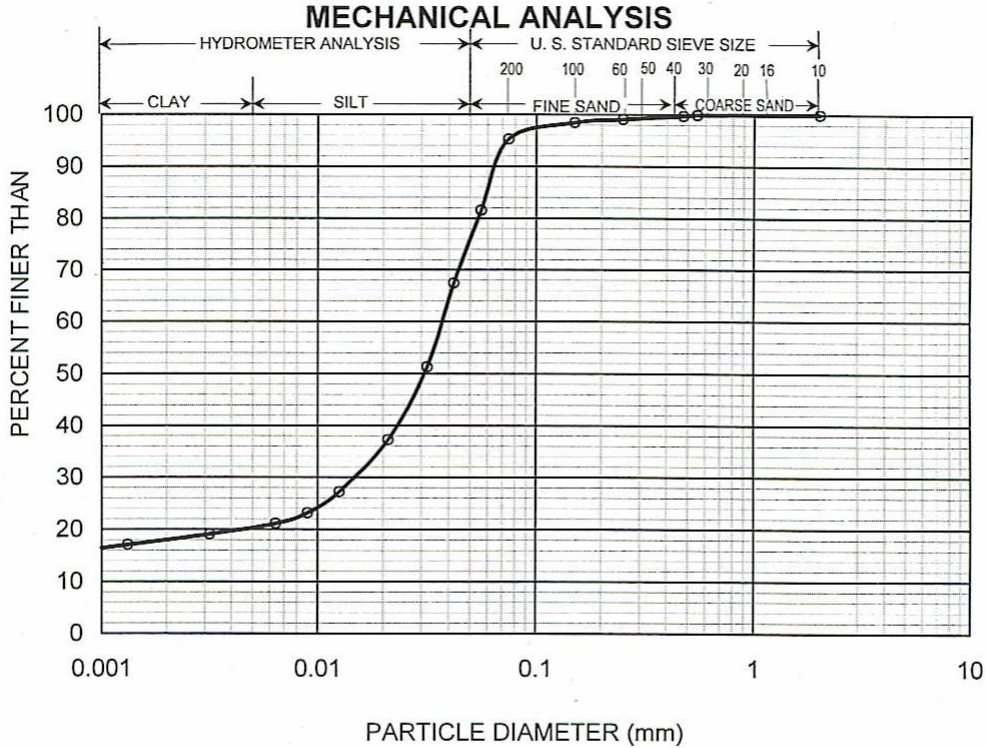
Rev. 3-99

D.O.T. NO. 635

**Figure C4.3: Grain-Size Distribution and Index Properties, 8.0 – 12.0 feet**

**KANSAS DEPARTMENT OF TRANSPORTATION  
REPORT OF SOIL TESTS**

SUBMITTED BY Luke Metheny ADDRESS 2300 Van Buren LAB. NO. 04-2218  
 PROJECT EN 2374-05 COUNTY Wyandotte DATE 7/2/2004



**PHYSICAL PROPERTIES**

SAMPLE NUMBER	STATION	DIST. &lt;	DEPTH	L.L.	P.L.	P.I.	% Ret	SPEC. GRAV.	CLASS
			ft				ON NO. 10	(PASS NO. 10)	KS/UNIF.
RDS4			12.0-16.0	33	18	15	0	2.62	L-CL

Test Method: ASTM D422 (Iowa Air Dispersion)

REMARKS \_\_\_\_\_  
 \_\_\_\_\_  
 \_\_\_\_\_

L. S. Ingram, P.E.  
 Chief of Bureau of Materials and Research

By Robert A. Fuller, P.E.  
 Soils Engineer

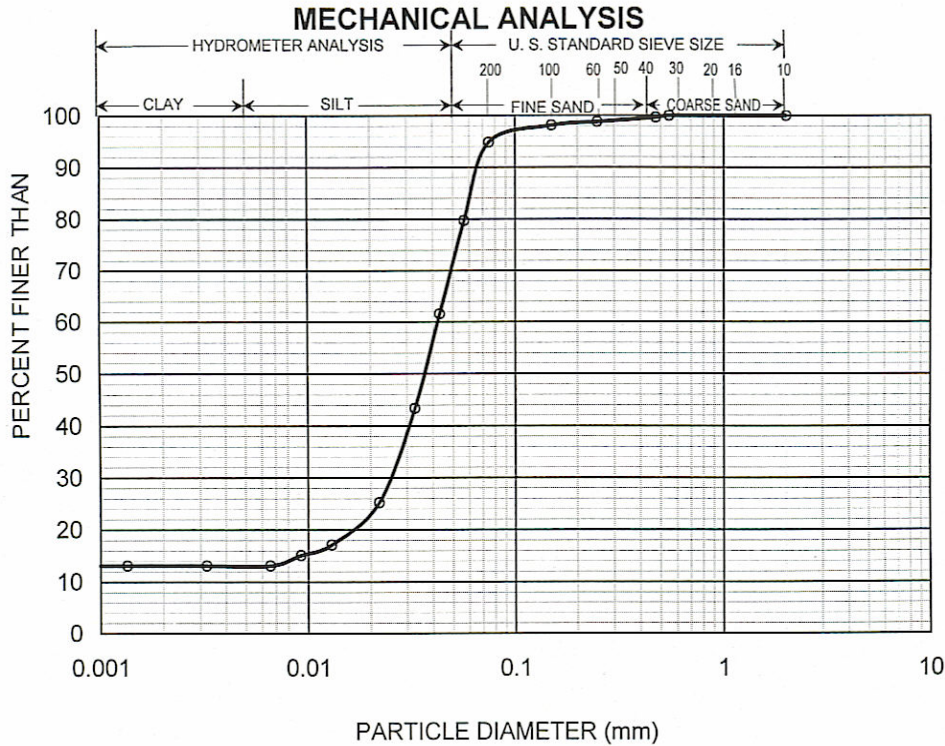
Rev. 3-99

D.O.T. NO. 635

**Figure C4.4: Grain-Size Distribution and Index Properties, 12.0 – 16.0 feet**

**KANSAS DEPARTMENT OF TRANSPORTATION  
REPORT OF SOIL TESTS**

SUBMITTED BY Luke Metheny ADDRESS 2300 Van Buren LAB. NO. 04-2218  
 PROJECT EN 2374-05 COUNTY Wyandotte DATE 7/2/2004



**PHYSICAL PROPERTIES**

SAMPLE NUMBER	STATION	DIST. ☐	DEPTH	L.L.	P.L.	P.I.	% Ret	SPEC. GRAV.	CLASS
			ft				ON NO. 10	(PASS NO. 10)	
RDS5			16.0-20.0			NP	0	2.61	SL/ML

Test Method: ASTM D422 (Iowa Air Dispersion)

REMARKS \_\_\_\_\_  
 \_\_\_\_\_  
 \_\_\_\_\_

L. S. Ingram, P.E.  
 Chief of Bureau of Materials and Research

By \_\_\_\_\_  
 Robert A. Fuller, P.E.  
 Soils Engineer

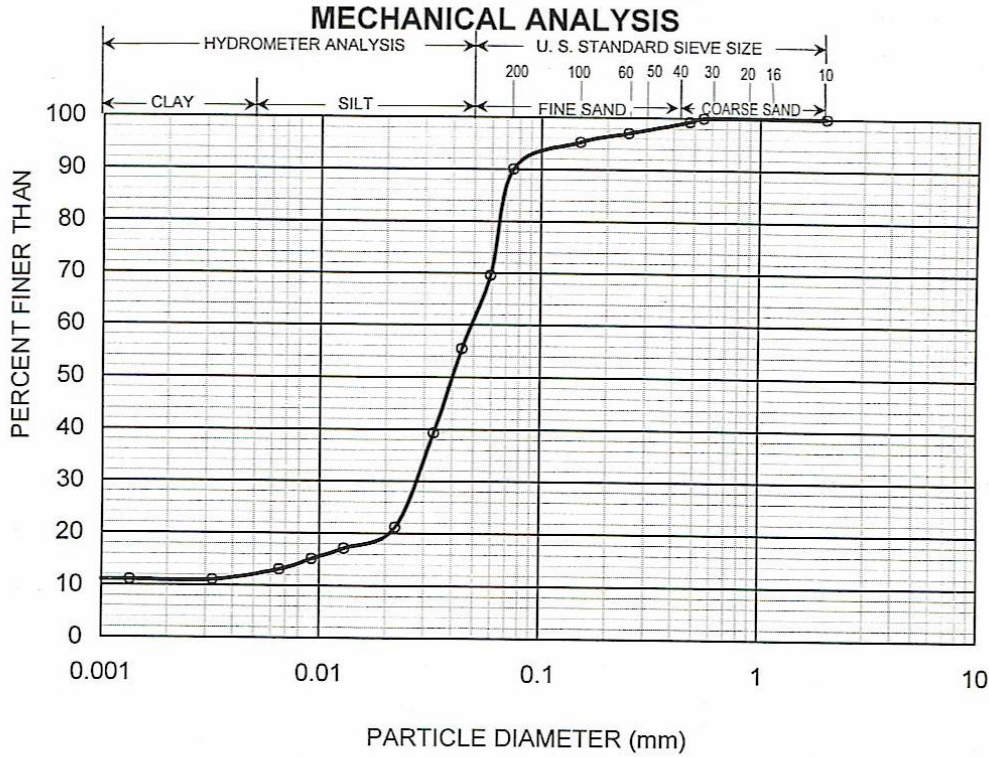
Rev. 3-99

D.O.T. NO. 635

**Figure C4.5: Grain-Size Distribution and Index Properties, 16.0 – 20.0 feet**

**KANSAS DEPARTMENT OF TRANSPORTATION  
REPORT OF SOIL TESTS**

SUBMITTED BY Luke Metheny ADDRESS 2300 Van Buren LAB. NO. 04-2218  
 PROJECT EN 2374-05 COUNTY Wyandotte DATE 7/2/2004



**PHYSICAL PROPERTIES**

SAMPLE NUMBER	STATION	DIST. $\zeta$	DEPTH ft	L.L.	P.L.	P.I.	% Ret	SPEC. GRAV.	CLASS
							ON NO. 10	(PASS NO. 10)	KS/UNIF.
RDS6			20.0-24.0			NP	0	2.61	L/ML

Test Method: ASTM D422 (Iowa Air Dispersion)

REMARKS \_\_\_\_\_  
 \_\_\_\_\_  
 \_\_\_\_\_

L. S. Ingram, P.E.  
 Chief of Bureau of Materials and Research

By Robert A. Fuller, P.E.  
 Soils Engineer

Rev. 3-99

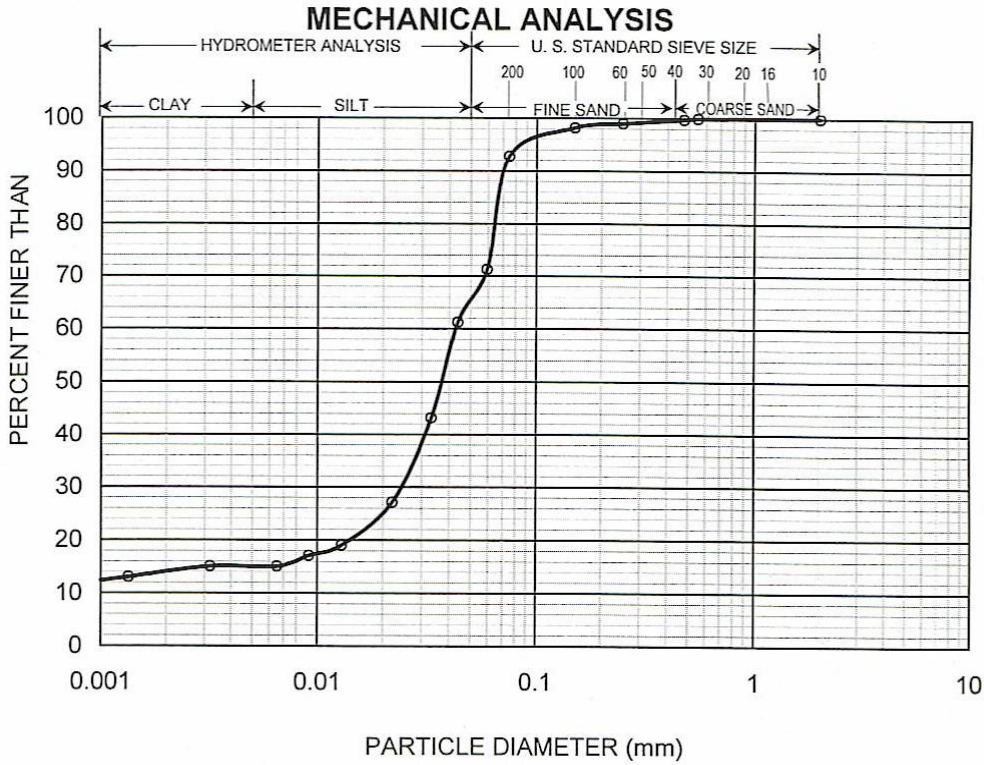
D.O.T. NO. 635

**Figure C4.6: Grain-Size Distribution and Index Properties, 20.0-24.0 feet**



**KANSAS DEPARTMENT OF TRANSPORTATION  
REPORT OF SOIL TESTS**

SUBMITTED BY Luke Metheny ADDRESS 2300 Van Buren LAB. NO. 04-2218  
 PROJECT EN 2374-05 COUNTY Wyandotte DATE 7/2/2004



**PHYSICAL PROPERTIES**

SAMPLE NUMBER	STATION	DIST. &	DEPTH	L.L.	P.L.	P.I.	% Ret	SPEC. GRAV.	CLASS
			ft				ON NO. 10	(PASS NO. 10)	KS/UNIF.
RDS7			24.0-28.0			NP	0	2.63	L/ML

Test Method: ASTM D422 (Iowa Air Dispersion)

REMARKS \_\_\_\_\_  
 \_\_\_\_\_  
 \_\_\_\_\_

L. S. Ingram, P.E.  
 Chief of Bureau of Materials and Research

By \_\_\_\_\_  
 Robert A. Fuller, P.E.  
 Soils Engineer

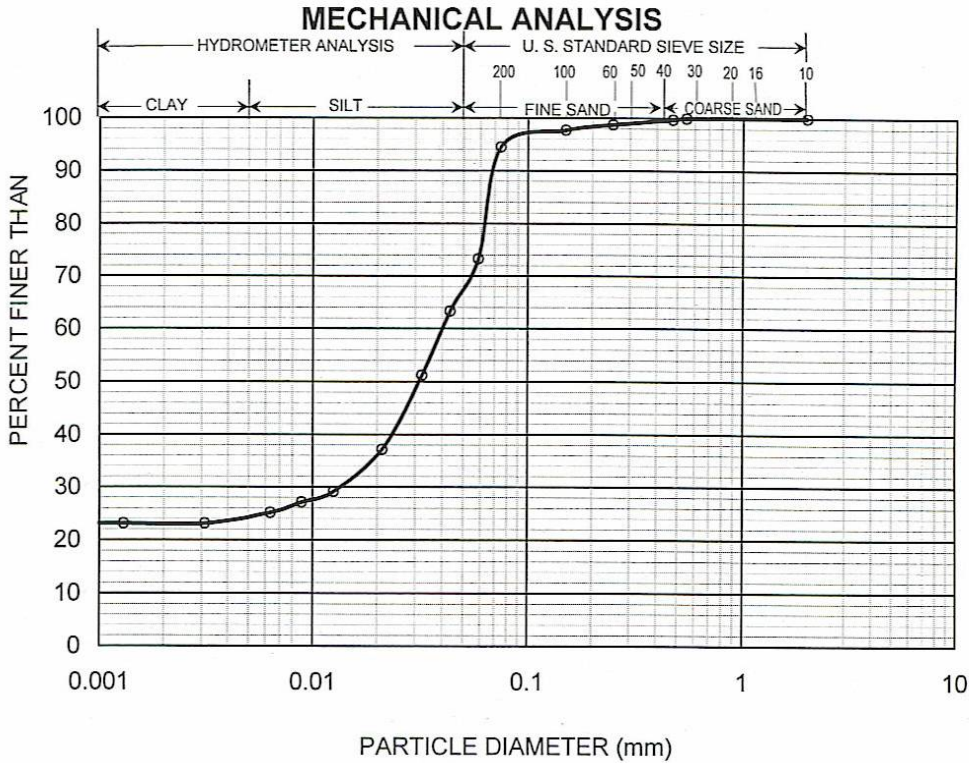
Rev. 3-99

D.O.T. NO. 635

**Figure C4.7: Grain-Size Distribution and Index Properties, 24.0 – 28.0 feet**

**KANSAS DEPARTMENT OF TRANSPORTATION  
REPORT OF SOIL TESTS**

SUBMITTED BY Luke Metheny ADDRESS 2300 Van Buren LAB. NO. 04-2218  
 PROJECT EN 2374-05 COUNTY Wyandotte DATE 7/2/2004



**PHYSICAL PROPERTIES**

SAMPLE NUMBER	STATION	DIST. $\phi$	DEPTH	L.L.	P.L.	P.I.	% Ret	SPEC. GRAV.	CLASS
			ft				ON NO. 10	(PASS NO. 10)	KS/UNIF.
RDS8			28.0-32.0	38	17	21	0	2.63	L-CL

Test Method: ASTM D422 (Iowa Air Dispersion)

REMARKS \_\_\_\_\_  
 \_\_\_\_\_  
 \_\_\_\_\_

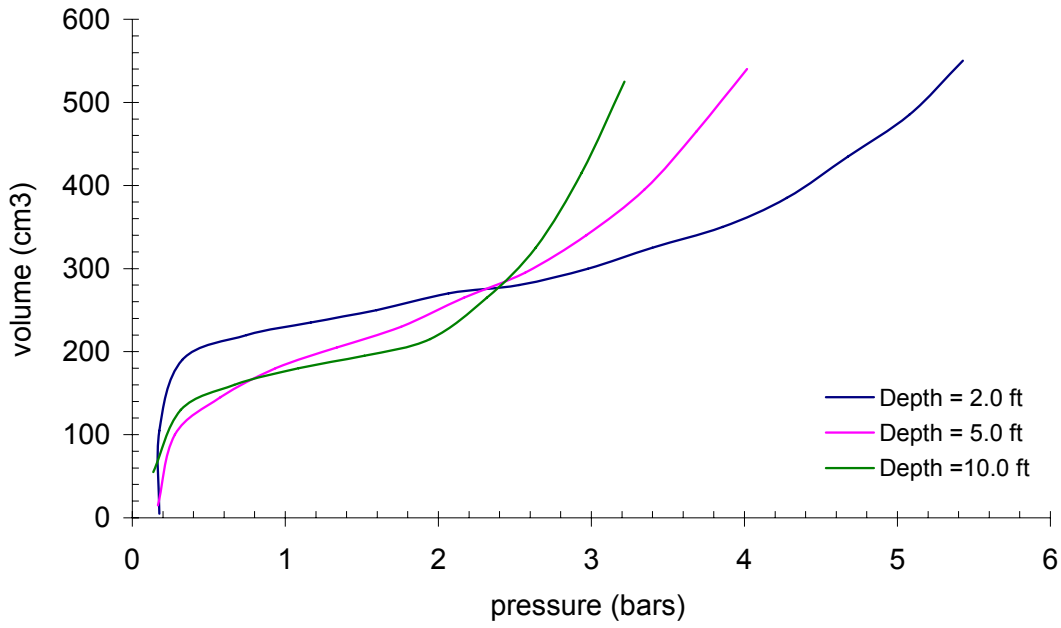
L. S. Ingram, P.E.  
 Chief of Bureau of Materials and Research

By Robert A. Fuller, P.E.  
 Soils Engineer

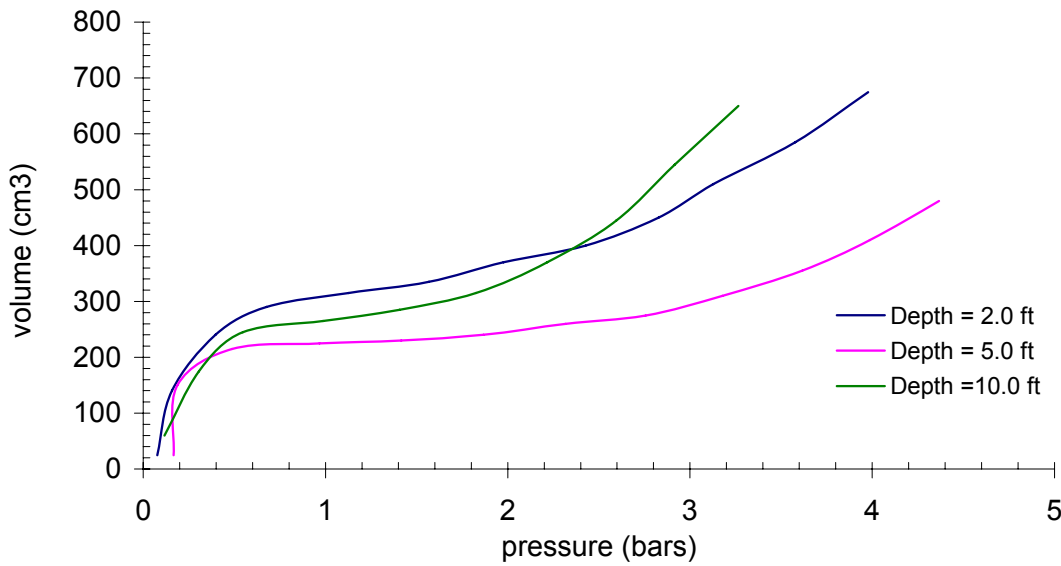
Rev. 3-99

D.O.T. NO. 635

**Figure C4.8: Grain-Size Distribution and Index Properties, 28.0 – 32.0 feet**



[a] 2004



[b] 2005

Figure C5.1: Pressuremeter test

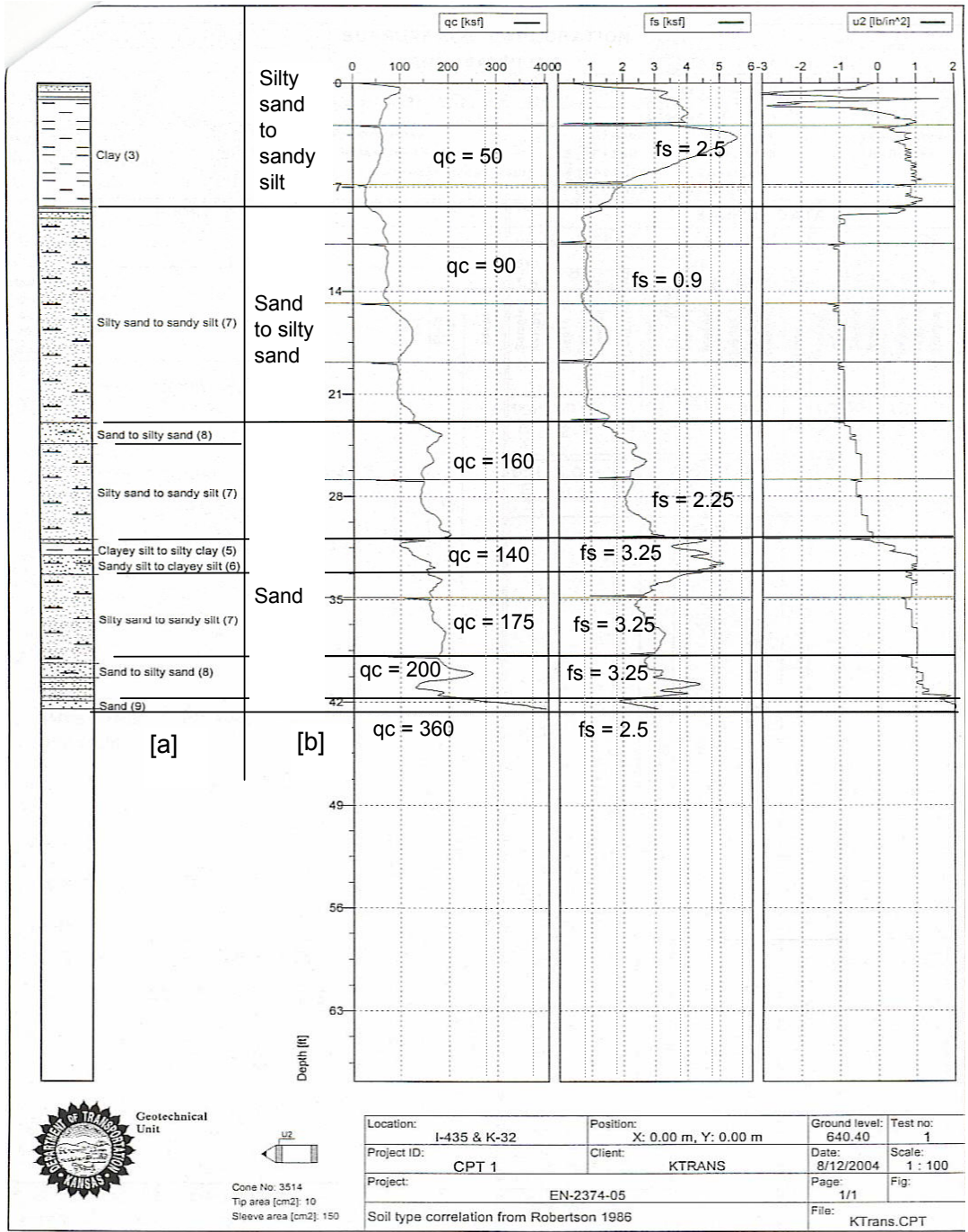
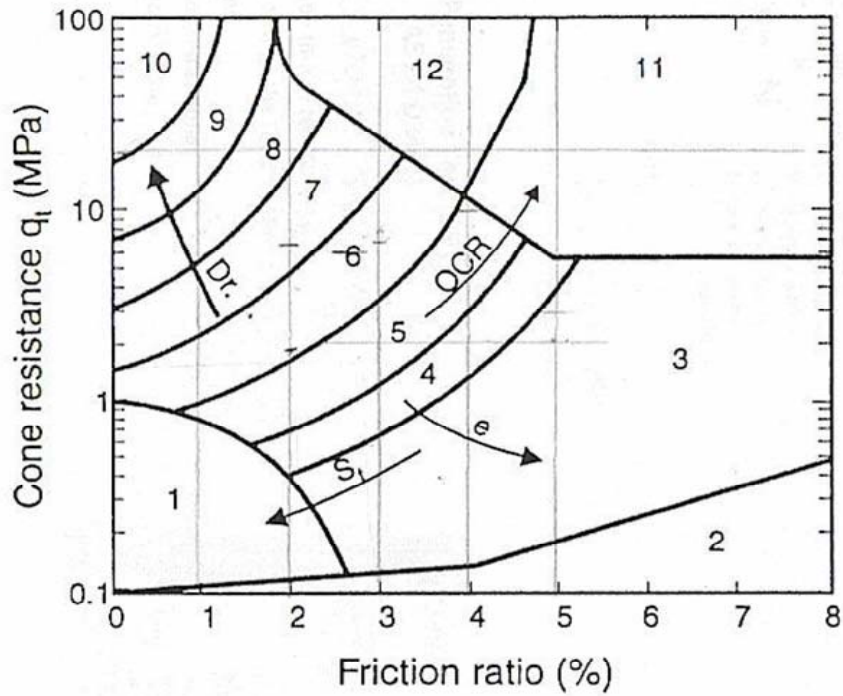


Figure C6.1: CPT, 2004; [a] computer generated profile, [b] KU generated profile



[a]

Soil Behavior Type (Robertson et al., 1986; Robertson & Campanella, 1988)		
1 – Sensitive fine grained	5 – Clayey silt to silty clay	9 – sand
2 – Organic material	6 – Sandy silt to silty sand	10 – Gravelly sand to sand
3 – Clay	7 – Silty sand to sandy silt	11 – Very stiff fine grained*
4 – Silty clay to clay	8 – Sand to silty sand	12 – Sand to clayey sand*

\*Note: Overconsolidated or cemented

[b]

Figure C6.2: Correlation of soil type with CPT data

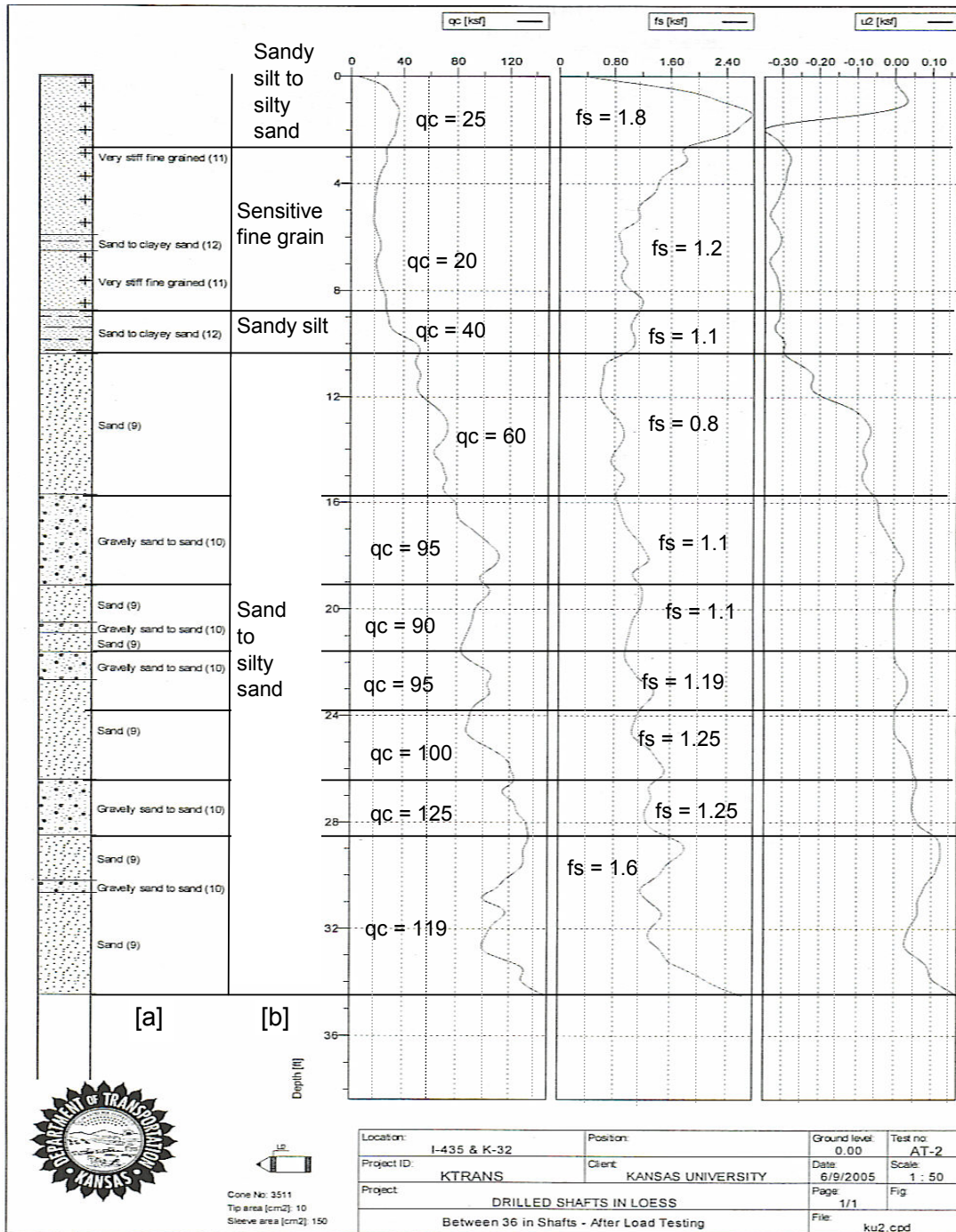


Figure 6.3: CPT 2, 2005; [a] computer generated profile, [b] KU generated profile

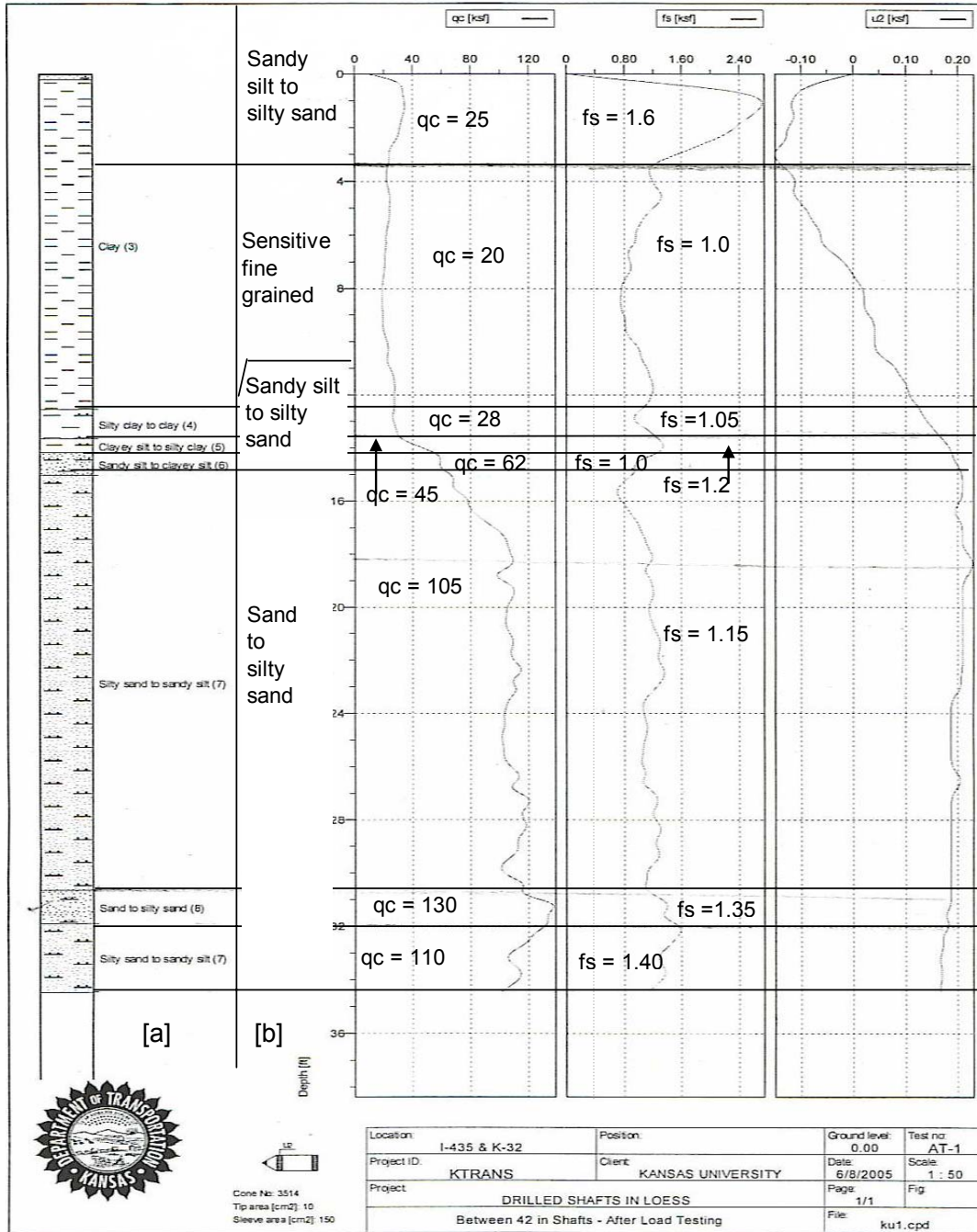


Figure C6.4: CPT 3, 2005; [a] computer generated profile, [b] KU generated profile

**Table C7.1: SPT  $N_{60}$  and  $(N_1)_{60}$  Equations**

Corrected N value	Equation	
$N_{60} =$	$\frac{C_E C_B C_S C_R N}{0.6}$	(See figure C7.4 for $N_{60}$ corrections)
$(N_1)_{60} =$	$N_{60} * (1 \text{ tsf} / \sigma'_z)^{1/2}$	

**Table C7.2: Terzaghi and Peck**

N value	Consistency	$\phi$
0 to 4	Very loose	< 28
4 to 10	Loose	28 to 30
10 to 30	Medium	30 to 36
30 to 50	Dense	36 to 41
> 50	Very dense	> 41



# Corrections to SPT N-value

Effect	Variable	Term	Value
Overburden Stress	$\sigma_{vo}'$	$C_N$	$(P_a/\sigma_{vo}')^{0.5}$ but $\leq 2$
Energy Ratio <sup>1</sup>	Safety Hammer Donut Hammer Automatic Hammer	$C_E$	0.6 to 0.85 0.3 to 0.6 0.85 to 1.0
Borehole Diameter	65 to 115 mm 150 mm 200 mm	$C_B$	1.00 1.05 1.15
Sampling Method	Standard sampler Sampler without liner	$C_S$	1.0 1.1 to 1.3
Rod Length	10 m to 30 m 6 to 10 m 4 to 6 m 3 to 4 m	$C_R$	1.0 0.95 0.85 0.75
Particle Size	Median Grain Size ( $D_{50}$ ) of Sand in mm	$C_P$	$60 + 25 \log D_{50}$
Aging	Time (t) in years since deposition	$C_A$	$1.2 + 0.05 \log (t/100)$
Overconsolidation	OCR	$C_{OCR}$	$OCR^{0.2}$

Figure C7.4: SPT Corrections

<sup>1</sup> Obtain by energy measurement per ASTM D4633

Courtesy of Mayne

**Table C7.5: SPT Field Measurements**

Sample #	Depth (ft)	Depth (m)	Blows	Consistency
SPT1	10	3.0	2,2,3	loose
SPT2	20.5	6.3	2,3,3	loose
SPT3	9.8	3.0	1,2,3	loose
SPT4	19.8	6.0	2,3,3	loose
SPT5	29.8	9.1	4,6,10	medium dense
SPT6	34.8	10.6	4,5,4	loose
SPT7	10	3.0	2,2,3	loose
SPT8	20	6.1	3,3,4	loose
SPT9	30	9.1	4,4,5	loose
SPT10	35	10.7	4,6,8	medium dense
SPT11	10	3.0	2,2,4	loose
SPT12	20	6.1	3,3,4	loose
SPT13	30	9.1	5,8,10	medium dense
SPT14	35	10.7	3,3,3	loose

## Appendix D

### P-Y Model Derived from Lateral Load Testing

#### D.1 Introduction

A new method for generating P-Y curves for use in lateral analyses of drilled shafts in loess soil is formulated, including degradation of the curves with load cycling. The P-Y curves may be used for lateral analyses using any lateral analyses software package that allows for input of user specified P-Y curves.

The strength parameter used in the model is correlated to the cone tip resistance ( $q_c$ ) from CPT testing, and the rate at which the lateral resistance is gained with displacement is presented as a hyperbolic relationship. Recommendations are presented for the model parameters needed, as well as a discussion of their effect, as were obtained from back-fitting of the LPILE analyses to the measured results.

The testing sequence and data reduction methods are presented, along with comparisons of model analyses (LPILE used) to the measured results. A step-by-step procedure is outlined for the use of the model presented to generate user specified P-Y curves for lateral analyses.

#### D.2 Testing Sequence

Shafts were loaded in pairs to provide reaction for each other. Both shafts of a pair were fully instrumented. There was one pair of 30-inch diameter static test shafts, one pair of 42-inch diameter static test shafts, and one pair of 30-inch diameter cyclic test shafts. Loads were maintained near constant at load increments without inclinometer soundings, and the hydraulic pressure was locked off during load increments with

inclinometer soundings to better maintain the deflected pile shape with depth. A more thorough description of the testing set-up and sequence is contained in Chapter 3.

A total of 13 and 15 load increments were used to load the 30-inch and 42 inch diameters pairs of static test piles, respectively, while both sets of static test piles were unloaded in four decrements. A total of six inclinometer soundings were performed for each static test pile, four of which occurred at load increments. Load increments and decrements for the static test shafts were sustained for a duration of approximately 5 minutes, with the exception of the load increments with inclinometer soundings where the duration was approximately 20 minutes (this allowed for approximately 10 minutes for inclinometer measurements for each of the two test shafts in the pair). Lateral loads were applied to the 30-inch and 42-inch diameter static test shafts in approximately 10 kip and 15 kip increments, respectively.

There were a total of four load increments (noted as “A” through “D”) on the 30-inch diameter cyclic test shafts, with ten load cycles (N=1 through 10) performed per load increment. The lateral load for each load cycle were sustained for only a few seconds with the exception of load cycles 1 and 10 which were sustained for approximately 15 to 20 minutes to allow time for the inclinometer soundings to be performed. For load cycles 2 through 9, the duration for each load cycle was approximately 1 minute, 2 minutes, 3.5 minutes, and 6.5 minutes for load increments A through D, respectively, as a greater time was required to reach the larger loads. The load was reversed after each load cycle to return the top of pile to approximately the same location.

### **D.3 Idealized Model Profile from CPT Testing**

A back-fit model of the pile behavior using the variety of soil strength data obtained (both insitu and laboratory) to the measured pile performance led to the conclusion that the CPT testing provided the best correlation. Further, CPT testing is easily performed in the loess soils being modeled, and has become readily available to practicing geotechnical engineers and DOT's. A brief description of CPT testing performed at the site, and the idealization of the tip resistance ( $q_c$ ) with depth profile used subsequently in the model is presented to follow. Complete descriptions of site characterization by means of insitu testing, lab testing, soil classification, etc., is detailed in Chapter 4.

A total of three Cone Penetration Test (CPT) soundings were performed by KDOT at the test site location, and the resulting subsurface profiles are contained in Appendix C. A preliminary sounding was performed on 12 Aug 2004 in the general vicinity of the test shafts (CPT-1). Two CPT soundings were performed subsequent to the lateral load testing. A sounding performed on 8 June 2005 between the 42-inch diameter static test shafts (Shafts 1 and 2) shortly after the completion the load test performed on these shafts that same day. A sounding was performed on 9 June 2005 between the 30-inch diameter static test shafts (Shafts 3 and 4) two days after the completion of the load test performed on these shafts on 7 June 2005. The CPT sounding locations were approximately 5 to 6 feet away from their respective test shafts, and given the nature of the soil condition and the albescence of a ground water table at these elevations it is reasonable to assume that the CPT soundings were unaffected by any pore water pressure effects that may have been induced by the load testing.

An idealized profile of cone tip resistance ( $q_c$ ) with depth interpreted as an average from the CPT soundings performed between the static test shafts (8-9 June 2005) is shown on Figure 1. This profile is considered representative of the subsurface conditions for all the test shaft locations (test shafts 1 – 6). Note that it is most useful to break the idealized soil profile into layers wherein the cone tip resistance ( $q_c$ ) is either constant with depth or linearly varies with depth as these two conditions are easily accommodated by most lateral pile analyses software.

The representative cone tip resistance ( $q_c$ ) is reduced by 50% at the soil surface, and allowed to return to the full value at a depth equal to two pile diameters, as is illustrated in Figure D1. This is done to account for the passive wedge failure mechanism exhibited at the ground surface which reduces the resistance per pile length nearer the ground surface until at some depth (assumed at two diameters) the resistance is considered to be a flow around bearing failure mechanism.

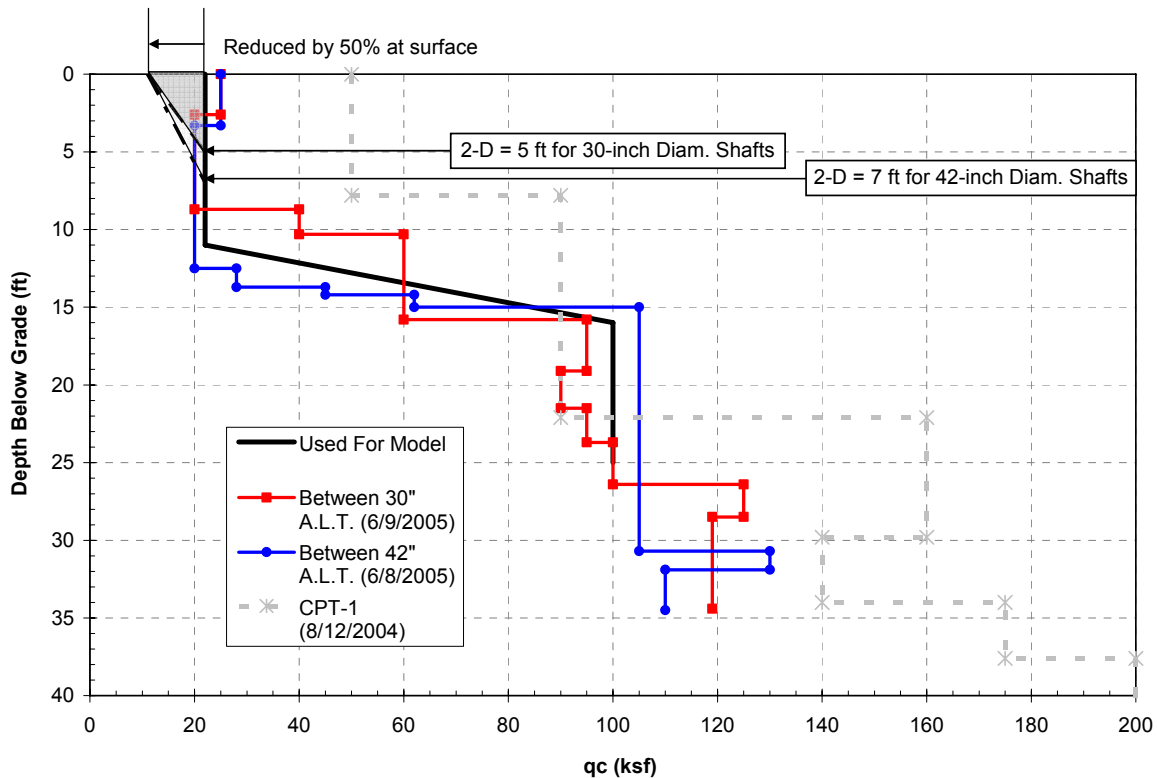


**Figure D1: Idealized Tip Resistance ( $q_c$ ) Profile from CPT Testing Used for Analyses**

The idealized tip resistance ( $q_c$ ) values with depth were correlated to the model parameter of the Ultimate Soil resistance ( $P_{uo}$ ) that can be provided by the soil corresponding depths, as will be detailed in Section D.5 to follow.

#### **D.4 Instrumentation and Test Data Reduction Procedures**

##### **D.4.1 Introduction**

Instrumentation for each shaft consisted of a pair of LVDT's (one above and one below the point of load application) and an inclinometer casing (for inclinometer readings) extending to near pile tip depth. A load cell was inline with the hydraulic actuator that provided the compressive lateral force between the piles. A pressure transducer was located in the high pressure side of the hydraulic supply line to the actuator.

For each pile, the test shaft data of the two LVDT displacements, the load cell, and the pressure transducer were continuously monitored using a Megadac<sup>®</sup> data acquisition system with the sampling rate set at 1 sample every 3 seconds for each channel. At the prescribed load intervals, an inclinometer sounding was performed for each test shaft by KDOT, with data points taken at 2 foot depth intervals.

#### **D.4.2 Load Cell Readings and Hydraulic Pressure Transducer to Provide Load**

A load cell was inline with the hydraulic actuator that provided the compressive lateral force between the piles. A pressure transducer was located in the high pressure side of the hydraulic supply line to the actuator for an indirect back-up to the applied load readings made directly by the load cell. Inspection of the data reveals that the load cell provided reliable direct readings of the applied load.

#### **D.4.3 LVDT Readings to Provide Boundary Condition at Top of Shaft**

Each Test shaft was instrumented with two LVDT's, one approximately 6 inches above and one approximately 6 inches below the point of load application (see Chapter 3 for full details and as-builts of the test shafts). The LVDT's provided a direct measurement of the top of shaft movement for each test shaft.

For the Static test shafts, each LVDT measurement was averaged for the duration of each load increment, which was an approximate 20 minute hold time for load increments with inclinometer soundings (10 minutes each for two shafts).

For Load Cycles 2 through 9 of the Cyclic test shafts (load cycles without inclinometer soundings), each LVDT measurement was averaged for the duration of each load increment (approximate hold times of only several seconds). For Load



Cycles 1 and 10 of the Cyclic test shafts (load cycles with inclinometer soundings), each LVDT measurement was averaged near the onset of the applied load for a duration that corresponded to that of the other load cycles (i.e., the first several seconds of the approximately 20 minutes that it took to run the inclinometer soundings).

In addition to providing top of shaft deflections, the two LVDT data points near the top of each pile were used to provide the pile displacement boundary condition (absolute displacement) corresponding to the uppermost inclinometer data point location. The displacement of the uppermost inclinometer data point was interpolated from the two LVDT data points if it was above the lower LVDT, and extrapolated if below the lower LVDT. This linear interpolation, or extrapolation, is valid due to the close proximity of the first inclinometer data point to the lower LVDT (typically within a few inches), and these data points lying approximately 3 ft above grade.

#### **D.4.4 Inclinometer Readings to Provide Deflected Pile Shape**

For each of the static test shafts, an inclinometer sounding was performed:

- prior to loading to provide a baseline profile to obtain the deflected profiles;
- at four load increments that were chosen to span the range of pile head displacements to the ultimate load (approximately 0.5, 1.0, 2.3, and 4.0 inches);
- at the midpoint of the load decrements; and
- at the end of testing after the load was completely released.

Note that for each of the cyclic test shafts, an inclinometer sounding was performed:

- prior to loading to provide a baseline profile to obtain the deflected profiles;
- at the first and last load cycles (N=1 and N=10) for each of the four load increments (A through D). Note that the four load increments were chosen such that the respective pile head displacements at the first load cycle (N=1) would be at approximately the same as for the static test shafts; and
- at the end of testing after the load was completely released.

See Appendix A for detailed descriptions of load increments and inclinometer soundings.

The inclinometer soundings were fixed at the depth of the first inclinometer sounding data point below the top of each respective shaft by the LVDT readings providing this boundary condition. An off-set correction was then applied to the inclinometer soundings based upon reasonable pile tip displacements. The off-set correction method adjusts displacements proportional to depth (as is the common practice for reduction of inclinometer data). The inclinometer readings provide the deflected pile profile and depth to maximum moment for comparison to that obtained with the LPILE computer simulations.

## **D.5 Formulation of P-Y Model Parameters**

### **D.5.1 Introduction**

The static model parameters were developed upon best fits of full scale load test data from two 30-inch and two 42-inch diameter shafts installed within a loess soil

formation with averaged CPT tip resistance values ranging from 20 to 105 ksf. Caution is warranted when extrapolating the static model to predict results for shaft diameters or soil types and/or strengths outside these limits. Further, the cyclic degradation model parameters are based on sets of ten load cycles ( $N = 1$  to  $10$ ) obtained at four different load increments during the cyclic testing of an additional two 30-inch diameter shafts. Caution is thus also warranted when extrapolating the cyclic model to predict results beyond 10 load cycles ( $N > 10$ ), especially as the magnitude of the load increases.

Recommended procedures and correlation constants are provided to produce a P-Y curve, shown generically in Figure D2, for any given soil layer. The Ultimate Soil Resistance ( $P_{uo}$ ) that can be provided by the soil is simply correlated to the cone tip resistance ( $q_c$ ) at any given elevation. Note that to account for the passive wedge failure mechanism exhibited at the ground surface, the cone tip resistance ( $q_c$ ) is reduced by 50% at the soil surface and allowed to return to the full value at a depth equal to two pile diameters. The Initial modulus ( $E_i$ ) of the P-Y curve is then determined from the Ultimate Soil resistance ( $P_{uo}$ ) expressed on a per unit length of pile basis ( $P_u$ ), and a suggested reference displacement ( $Y_i$ ). A hyperbolic relationship provides the Secant modulus ( $E_s$ ) of the P-Y curve at any given pile displacement ( $Y$ ). The soil resistance is then expressed on a per unit pile length basis ( $P$ ) for any given pile displacement ( $Y$ ) as determined by the Secant modulus ( $E_s$ ) at that displacement. Provisions for the degradation of the P-Y curve based upon the load cycle number ( $N$ ) for cyclic loading are incorporated into the relationship for Ultimate Soil resistance expressed on a per unit length of pile basis ( $P_u$ ).

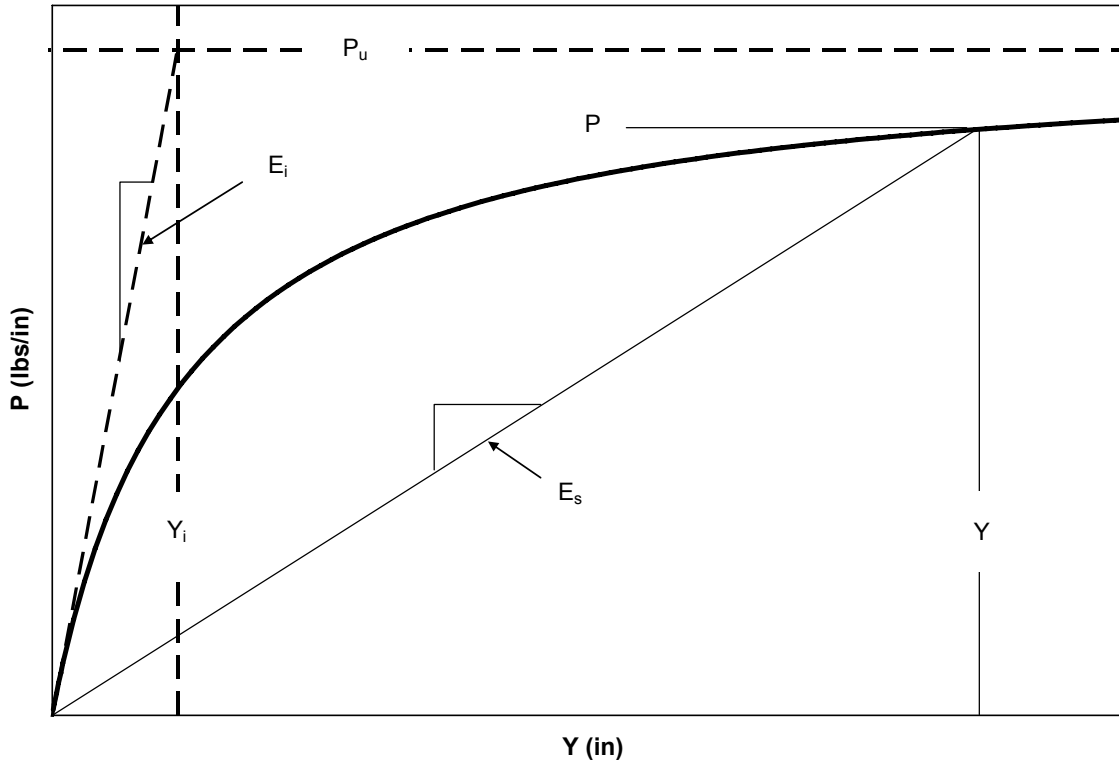


**Figure D2: Generic P-Y curve for Lateral Analyses**

The model presented will generate a P-Y curve that is smooth and continuous. It is believed that this better captures the true behavior of pile-to-soil response. The P-Y curve may easily be generated with a spreadsheet using the functional relationships presented that are expressed without the need for piece-wise continuity. Additionally, this will also help to avoid convergence problems sometimes encountered with lateral analyses software packages, as the iteration solutions often “bounce” around regions of second order discontinuity (the “point” on bilinear curves, for example).

**D.5.2 Ultimate Soil Resistance Parameter ( $P_{uo}$  and  $P_u$ ) from CPT Testing, and Cyclic Degradation with Cycle Number ( $N$ )**

The Ultimate Soil resistance ( $P_{uo}$ ) that can be provided by the soil is proportional to the cone tip resistance ( $q_c$ ) by the CPT strength correlation constant ( $N_{CPT}$ ). Note that the parameter of Ultimate Soil resistance ( $P_{uo}$ ) is dependant only upon soil strength.

$$P_{uo} = N_{CPT} \cdot q_c \quad (\text{Equation D-1})$$

Where:  $N_{CPT}$  is dimensionless, and

$P_{uo}$ , and  $q_c$  are in any consistent units of (force / length<sup>2</sup>)

It was determined that the best fit to the load test data was obtained with the correlation constant presented to follow. It is believed that this correlation constant is relatively insensitive to soil type as this is a ultimate geotechnical strength as determined by insitu testing.

$$N_{CPT} = 0.409$$

The ultimate soil resistance ( $P_{uo}$ ) is made specific to a given pile size ( $P_u$ ) by multiplying by the pile diameter ( $b$ ), and thus may be expressed on a unit length of pile basis. Further, this parameter may be degraded for a given load cycle ( $N$ ) with the correlation constant ( $C_N$ ).

$$P_u = \frac{P_{uo} \cdot b}{1 + C_N \cdot \log(N)} \quad (\text{Equation D-2})$$

Where:  $b$  is in any consistent unit of (length),

$C_N$  and  $N$  are dimensionless, and thus

$P_u$  results in any consistent units of (force / length).

It was determined that the best fit of cyclic degradation to the two 30-inch diameter shaft cyclic load test data was obtained with the following constant:

$$C_N = 0.24$$

The cyclic degradation term (denominator) reduces to 1 for  $N=1$  (initial cycle, or static load). The value of  $C_N$  has a direct effect on the amount of cyclic degradation to the P-Y curve (i.e., a greater value of  $C_N$  will allow greater degradation of the P-Y curve, resulting in a smaller  $P_u$ ). Note that the degradation of the ultimate soil resistance per unit length of shaft ( $P_u$ ) parameter will also have the desired degradation effect built into the computation of the P-Y modulus values ( $E_i$  and  $E_s$ ).

### **D.5.3 Reference Displacement Parameter ( $Y_i$ )**

A parameter is needed to define the rate at which the strength develops towards its ultimate value ( $P_{uo}$ ). The reference displacement ( $Y_i$ ) is defined as the displacement at which the tangent to the P-Y curve at zero displacement ( $E_i$ ) intersects the Ultimate Soil resistance asymptote ( $P_u$ ), as was illustrated in Figure D2. For lateral displacement of the pile-to-soil interface, this reference displacement ( $Y_i$ ) may be considered as analogous to axial quake of a perfectly elastic-plastic bi-linear curve. It was determined that the best fit to the load test data was obtained with the following reference displacement ( $Y_i$ ).

$$Y_i = 0.117 \text{ inches}$$

Where:  $Y_i$  is expressed in any consistent unit of (length).

Note that the suggested value for the reference displacement ( $Y_i$ ) provided the best fit to the piles tested at one test site in a particular loess formation (see Chapter 5 for a full description of soil types). Unlike the ultimate geotechnical resistance ( $P_{uo}$ ), it is

believed that the rate at which the strength develops, represented by the reference displacement ( $Y_i$ ), may be sensitive to soil type. Careful re-evaluation of the reference displacement ( $Y_i$ ) parameter may be warranted when performing lateral analyses for piles within different soil conditions, as this parameter may have substantial effect on the resulting pile deflections and stresses. The effect of the reference displacement ( $Y_i$ ) is direct to pile performance (i.e., a greater value of  $Y_i$  will allow for greater pile head displacements at a given lateral load).

**D.5.4 Initial Modulus Parameter ( $E_i$ ) and Hyperbolic Model of Secant**

**Modulus ( $E_s$ )**

By definition, the initial modulus ( $E_i$ ) is a simple expression of the ultimate soil resistance expressed on a per unit length of pile basis ( $P_u$ ), and the reference displacement ( $Y_i$ ).

$$E_i = \frac{P_u}{Y_i} \quad \text{(Equation D-3)}$$

Where:  $P_u$  is in any consistent units of (force / length).

$Y_i$  is in any consistent units of (length), and thus

$E_s$  results in any consistent units of (force / length<sup>2</sup>).

The secant modulus ( $E_s$ ) may be determined for any given displacement ( $Y$ ) by the following hyperbolic relationship involving the initial modulus expressed on a per unit length of pile basis ( $E_i$ ) and a hyperbolic term ( $Y'_h$ ) which is in turn a function of the given displacement ( $Y$ ), the reference displacement ( $Y_i$ ), and a dimensionless correlation constant ( $a$ ).

$$E_s = \frac{E_i}{1 + Y'_h} \quad \text{and} \quad \text{(Equation D-4)}$$

$$Y'_h = \left( \frac{Y}{Y_i} \right) \cdot \left[ 1 + a \cdot e^{-\left( \frac{Y}{Y_i} \right)} \right] \quad \text{(Equation D-5)}$$

Where:  $E_s$  and  $E_i$  are in any consistent units of (force / length<sup>2</sup>), and  
 $a$  and  $Y'_h$  are dimensionless.

It was determined that the best fit to the load test data was obtained with the correlation constant presented to follow. Note that this value primarily affects the secant modulus ( $E_s$ ) at small displacements (say within approximately 1 inch), and is inversely proportional to the stiffness response of the P-Y curve (i.e., a larger value of  $a$  will curtail early development of soil resistance with displacement).

$$a = 0.10$$

The ratio of Secant Modulus to Initial Modulus ( $E_s/E_i$ ) vs. displacement ( $Y$ ) used for development of the P-Y curves is shown in Figure 3. Note that the modulus ratio ( $E_s/E_i$ ) is only a function of the hyperbolic parameters of the correlation constant ( $a$ ) and the reference displacement ( $Y_i$ ), thus the curve presented is valid for all pile diameters (b) and CPT tip bearing values ( $q_c$ ) tested.



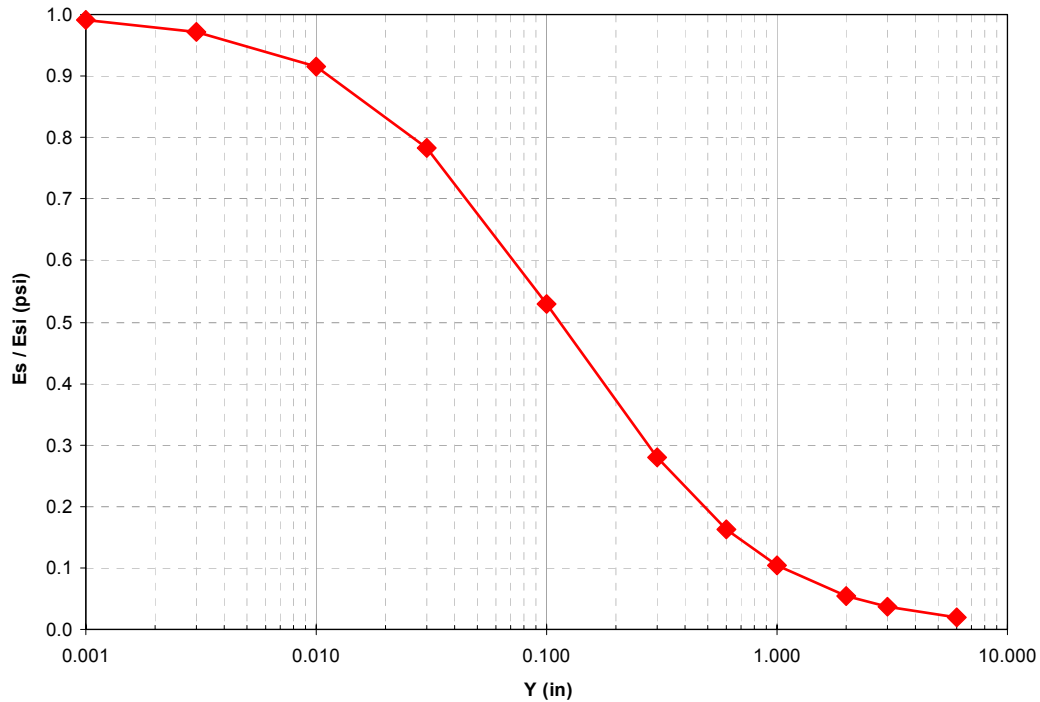


**Figure D3: Ratio of Secant Modulus to Initial Modulus ( $E_s/E_i$ ) with Displacement (Y)**

Both the initial modulus ( $E_i$ ) and the secant modulus ( $E_s$ ) are directly related to the pile diameter ( $b$ ) by way of the ultimate soil resistance ( $P_{u0}$ ) is made specific to a given pile size ( $P_u$ ), as was shown in Equation D2. It follows that the larger the pile diameter ( $b$ ), the stiffer will be the lateral response. While this represents a break from conventional P-Y curve generation methodology, this better matches the observed lateral response behavior, as well as making sense intuitively. For a given soil strength and rate resistance development (expressed on a per unit area basis), a larger pile diameter ( $b$ ) will engage a greater amount of soil per unit length of pile, and thus will generate more load per unit length of pile ( $P$ ) at any given displacement ( $Y$ ).

**D.5.5 Generation of the P-Y Curve from Secant Modulus Relationship with Displacement**

For any given pile displacement (Y), the soil resistance per unit length of pile (P) is thus a simple definitive expression of the pile displacement (Y) and the secant modulus ( $E_s$ ) at that displacement.

$$P = E_s \cdot Y \quad \text{(Equation D-6)}$$

Where:  $E_s$  is in any consistent units of (force / length<sup>2</sup>),  
Y is in units of (length), and thus  
P results in any consistent units of (force / length).

The P-Y curves obtained from the model described previous (with recommended values) is shown in Figure D4 for the 30-inch diameter shafts, and Figure D5 for the 42-inch diameters shafts. Note that there are three sets of curves presented for each shaft diameter which correspond to the CPT tip resistance values of 11 ksf, 22 ksf, and 100 ksf (as was shown in Figure 1). Also presented in the Figures is the relationship of Secant Modulus ( $E_s$ ) with displacement (Y). These P-Y curves were used in the LPILE analyses presented in the section to follow.

The Static P-Y curves shown in Figures D4 and D5 were degraded with Load Cycle Number (N) for use in the Cyclic Load Analyses. Figure D6 presents the Cyclic P-Y curve generated for the analyses of the 30-inch diameter shafts at the CPT tip resistance value ( $q_c$ ) of 22 ksf. Although not shown, note that the remaining static P-Y curves for other CPT tip resistance values ( $q_c$ ) were similarly degraded for the cyclic analyses.

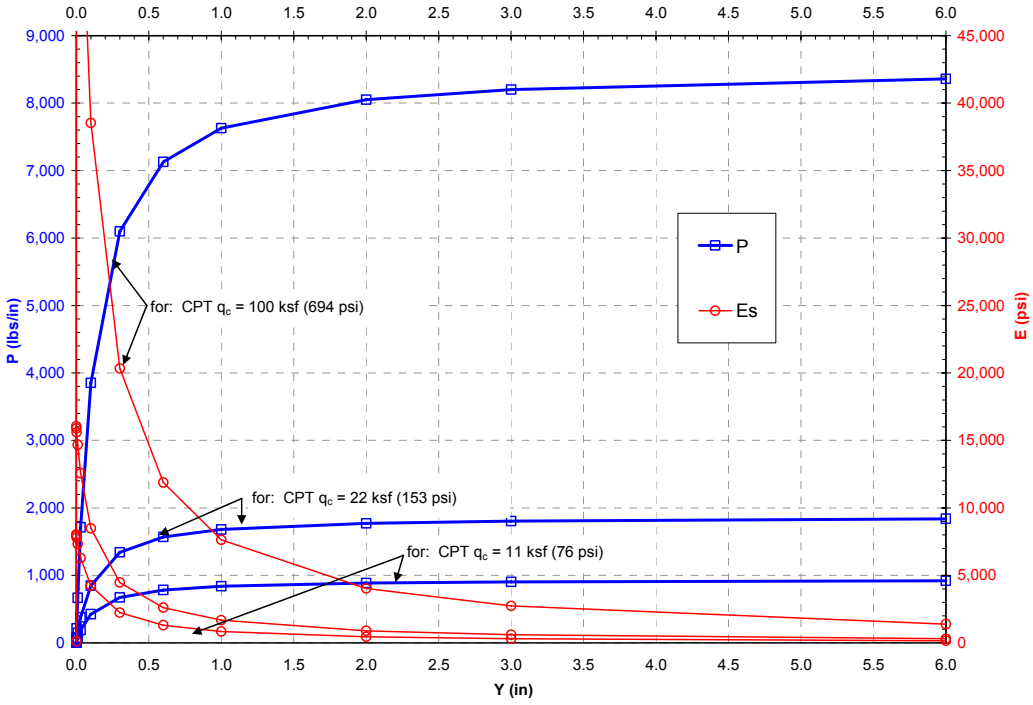


**Figure D4: P-Y Curves and Secant Modulus ( $E_s$ ) for the 30-inch Diameter Shafts**

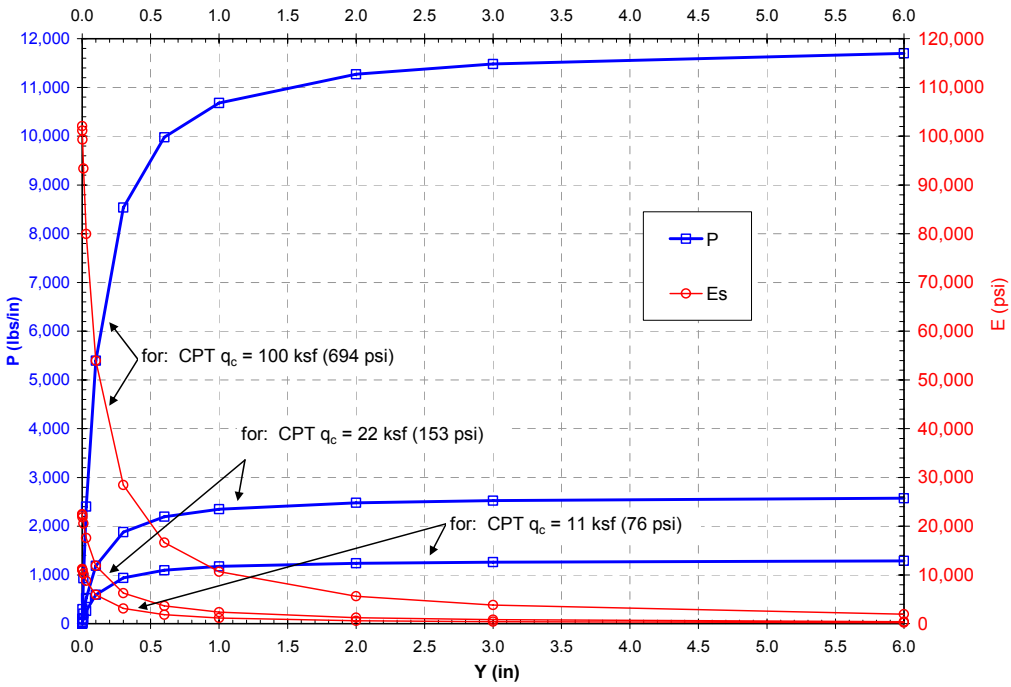


**Figure D5: P-Y Curves and Secant Modulus ( $E_s$ ) for the 42-inch Diameter Shafts**

### **D.5.6 Summary: Step-by-Step Procedure for Generating P-Y Curves**

A step-by-step procedure is listed to follow that may be used to generate P-Y curves in accordance with the model presented. Note that a spreadsheet is an ideal tool for the computationally intensive steps 3 through 9.

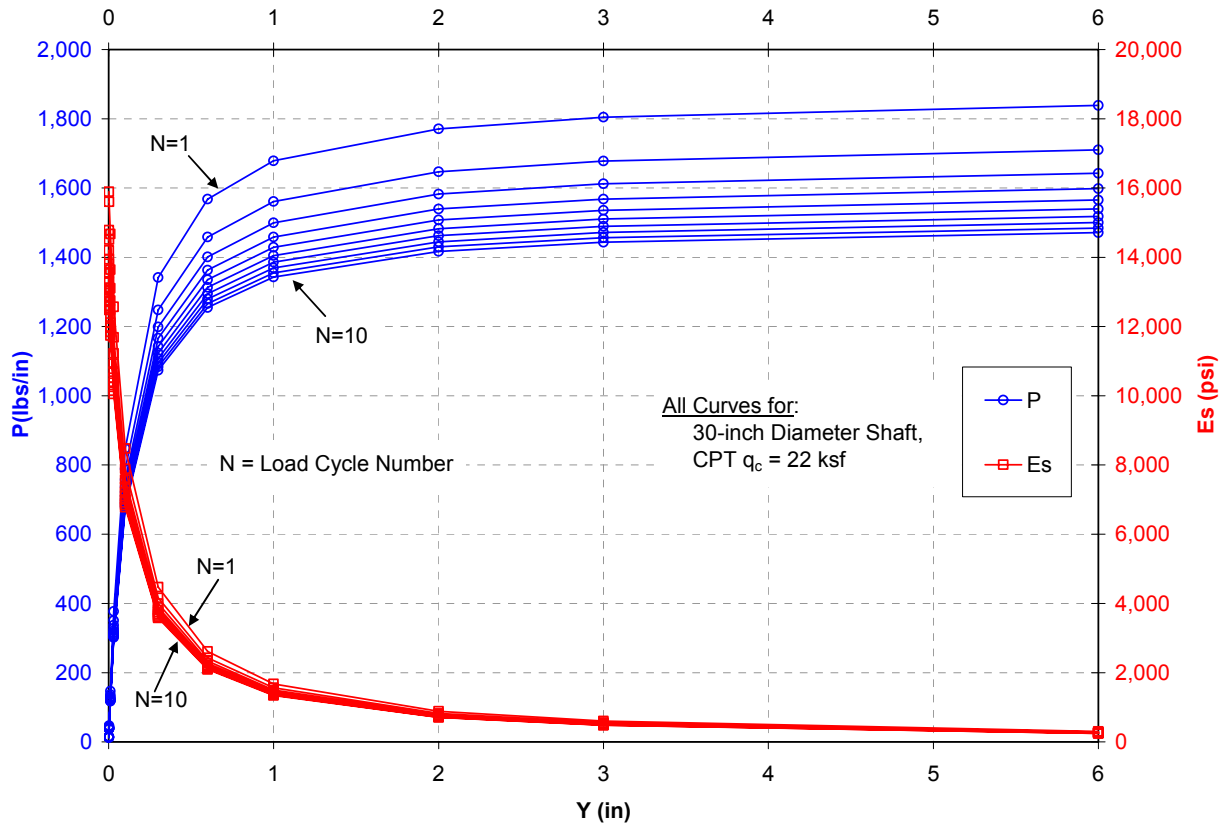


**Figure D6: Cyclic Degradation of P-Y Curves and Secant Modulus ( $E_s$ )**

Step 1: Develop an idealized profile of cone tip resistance ( $q_c$ ) with depth that is representative of the strata at the pile location. Note that it is most useful to break the idealized soil profile into layers wherein the cone tip resistance ( $q_c$ ) is either constant with depth or linearly varies with depth as these two conditions are easily accommodated by most lateral pile analyses software.

- Step 2: For the purposes of lateral pile analyses, reduce the cone tip resistance ( $q_c$ ) by 50% at the soil surface, and allow the value to return to the full measured value at a depth equal to two pile diameters. Linear interpolation may be made between the surface and the depth of two pile diameters.
- Step 3: For each idealized soil layer, determine the ultimate soil resistance ( $P_{uo}$ ) from the cone tip resistance ( $q_c$ ), in accordance with Equation D-1 for both the top and the bottom of each layer.
- Step 4: For the top and bottom of each idealized soil layer, multiply the ultimate soil resistance ( $P_{uo}$ ) by the pile diameter to obtain the ultimate soil resistance per unit length of shaft ( $P_u$ ). For cyclic analyses, this parameter ( $P_u$ ) may be degraded for a given load cycle ( $N$ ) with the correlation constant ( $C_N$ ), in accordance with Equation D-2. Note that when running a lateral pile analyses do NOT select the use of a P-Y multiplier, as the cyclic degradation of the P-Y curve is already taken into account by use of Equation D-2.
- Step 5: For the top and bottom of each idealized soil layer, select a reference displacement ( $Y_i$ ) that will be representative of the rate at which the resistance will develop. Recommendations for values of reference displacement ( $Y_i$ ) are presented in Section D.5.3.
- Step 6: For the top and bottom of each idealized soil layer determine the initial modulus ( $E_i$ ) in accordance with Equation D-3.

- Step 7: For the top and bottom of each idealized soil layer, select a number of pile-to-soil displacements ( $Y$ ) for which a representative P-Y curve is to be generated. Make sure the largest of these values selected will be in excess of the displacements anticipated for that layer, and note that soil layers near the surface will experience much greater displacements than those at greater depths. Concentrate the data points towards the smaller displacements to better define the P-Y curve where the secant modulus values ( $E_s$ ) are changing quickly (for example this study generated P-Y curve data points at displacements of 0, 0.001, 0.003, 0.01, 0.03, 0.1, 0.3, 0.6, 1, 2, 3, and 6 inches).
- Step 8: For the top and bottom of each idealized soil layer, determine the secant modulus ( $E_s$ ) for each of the displacements selected in Step 7 in accordance with Equations D-4 and D-5.
- Step 9: For the top and bottom of each idealized soil layer, determine the soil resistance per unit length of pile ( $P$ ) for each of the displacements selected in Step 7 in accordance with Equations D-6
- Step 10: Run a lateral load analyses using “user specified P-Y” curves. The P-Y curves are generated from the values of soil resistance per unit length of pile ( $P$ ) obtained in Step 9 that correspond to the displacement ( $Y$ ) obtained in Step 7.

## **D.6 Comparisons of Measured Results with LPILE Computer Runs**

### **D.6.1 Introduction**

A free head condition was specified at the pile head, thus an external shear force equal to the lateral load only (without a resisting moment) was applied. Tests shafts #1 and #2 were modeled with a diameter of 42 inches, and Test Shafts #3 through # 6 were modeled with a diameter of 30 inches. Concrete records and visual inspection from the surface during construction (shafts were constructed in the dry) both indicate a very regular shaped cylindrical shaft. Top of shaft, instrument locations, reinforcement, and depth to shaft tip were all input as recorded on the construction records. The soil resistance was modeled with “user specified P-Y curves”. Note that for the LPILE analyses of the cyclic test shafts, a P-Y multiplier was NOT used as the cyclic degradation was already taken into account from the generation of the user specified P-Y curves for these shafts.

The LPILE analyses of the test shafts were complicated by the nonlinear behavior of the reinforced concrete member which tended to crack and change in effective stiffness (EI) as bending occurred. This model included nonlinear EI as a function of bending by selection of LPILE “Analyses Type 3”. Note that the short length of casing, utilized to form the shafts above ground level, had a negligible effect on back-fitted pile performance (LPILE) due to the depth of maximum pile moment occurring several feet below the bottom of the surface casing. As such, the final LPILE runs were performed without the surface casing included.

### **D.6.2 Pile Displacement Profile with Static Lateral Load**

The LPILE predictions of pile displacement with depth (shape) are compared to the four static test shafts at load increments where inclinometer soundings were performed. The measured pile displacement with depth for the pair of cyclic test shafts at load cycles 1 and 10 (the only two load cycles with inclinometer soundings) for all four load increments are also contained in Appendix E.

Summaries of these comparisons to LPILE results using the average of a pair of test shafts is presented in Figures D7 and D8 for the static 30-inch diameter shafts and the static 42-inch diameter shafts, respectively.

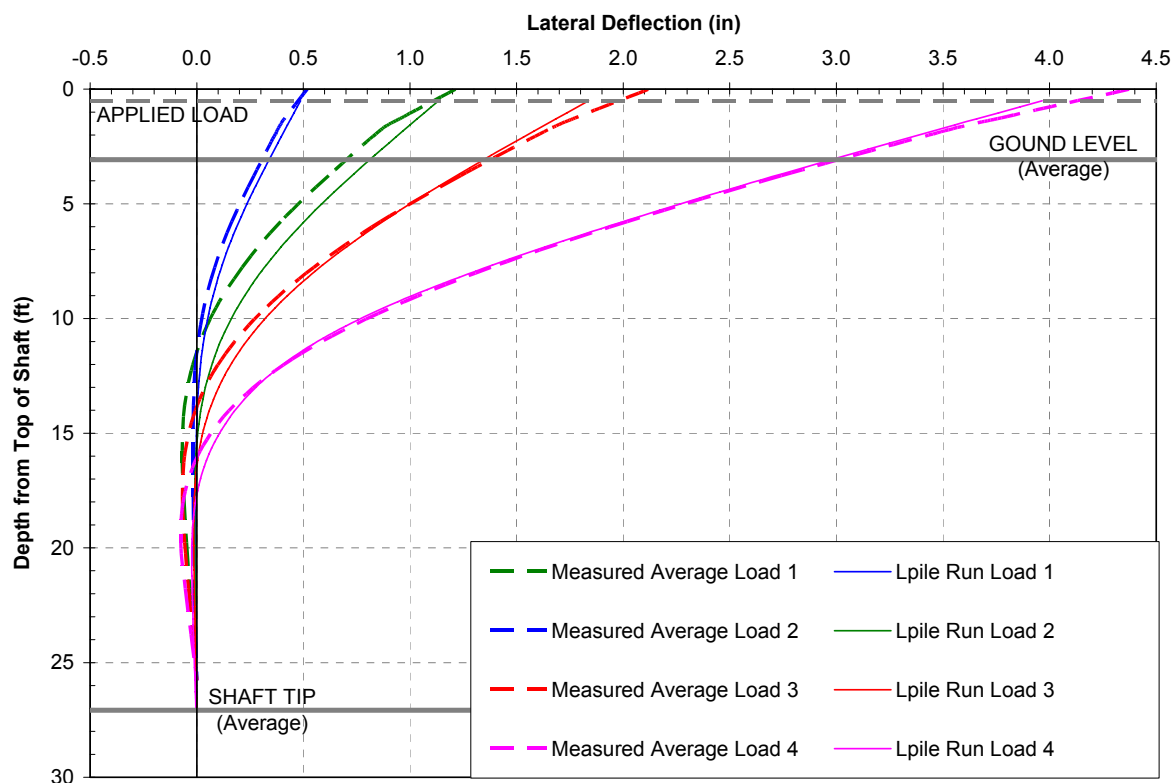


**Figure D7: Average Pile Displacement Profiles for 30-Inch Diameter Static Test Shafts**



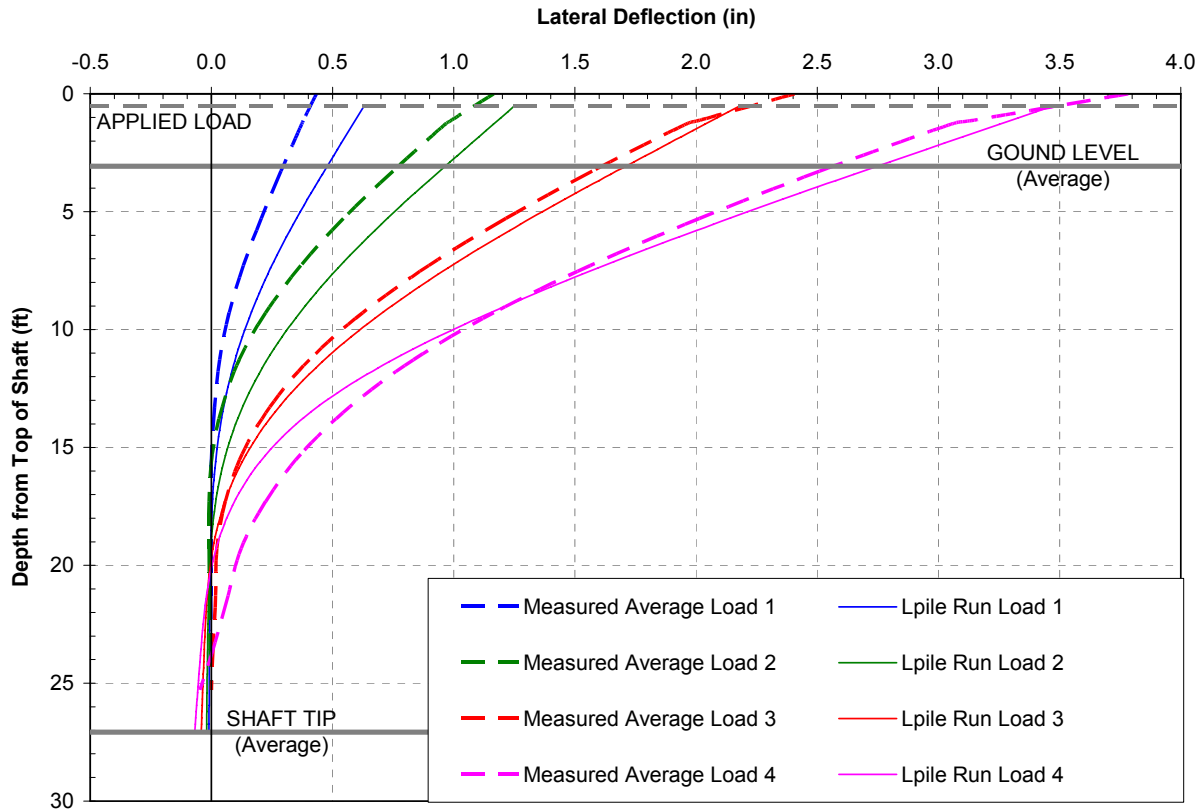


**Figure D8: Average Pile Displacement Profiles for 42-Inch Diameter Static Test Shafts**

For the four static test piles, these comparisons show good general agreement of pile displacement profile with depth over the wide range of lateral loads tested (to geotechnical failure). A summary of the average measured pile displacement with depth for the pair of cyclic test shafts at load cycles 1 and 10 (the only two load cycles with inclinometer soundings) is presented as Figure D9.

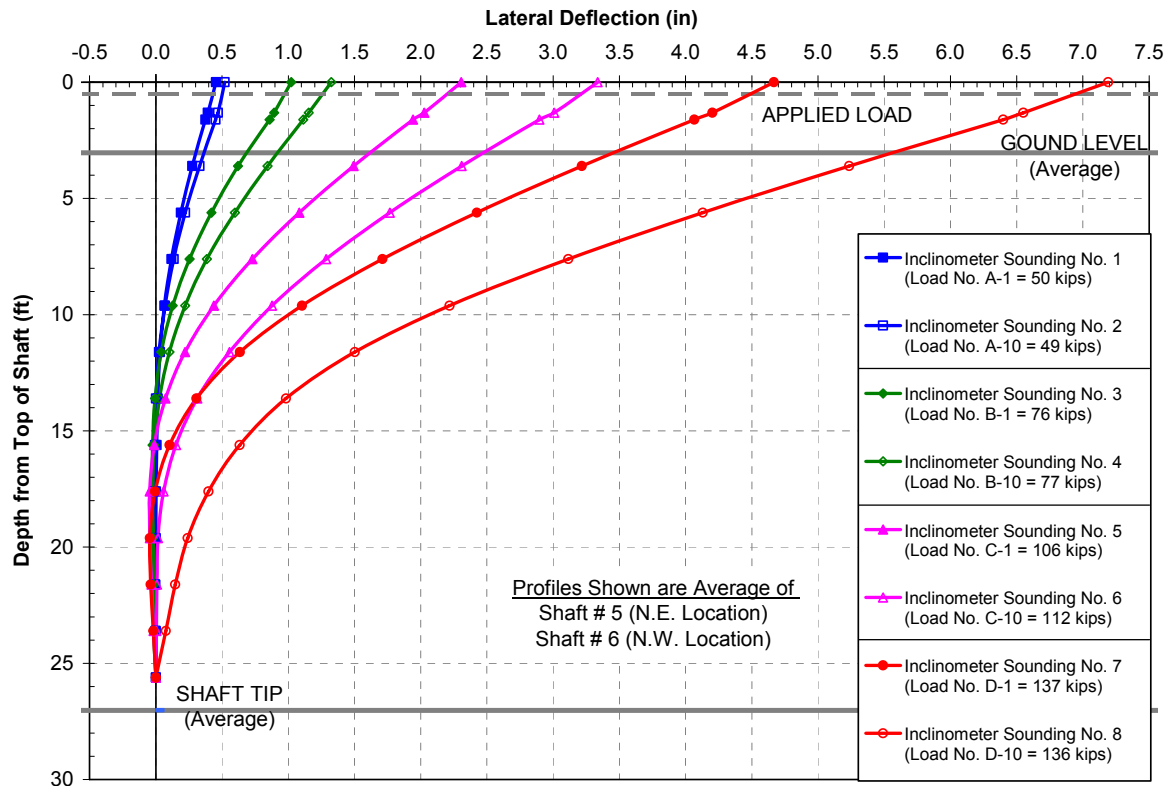


**Figure D9: Average Pile Displacement Profiles for 30-Inch Diameter Cyclic Test Shafts**

**D.6.3 Depth to Maximum Moment in Pile with Static Lateral Load**

The comparison of magnitude and depth to maximum moment within a pile is used for structural design of the pile. Figure D10 presents comparisons of depth to maximum moment in the static test piles, to that obtained from corresponding LPILE runs for the load increments where inclinometer soundings were performed. The depth of maximum curvature of the test piles is determined as the point of maximum curvature (i.e. the maximum change in slope). Although the magnitude of maximum moment was not directly measured, the good agreement of depth to maximum moment between the measured data and the LPILE runs obtained indicated a good agreement in magnitude as well.

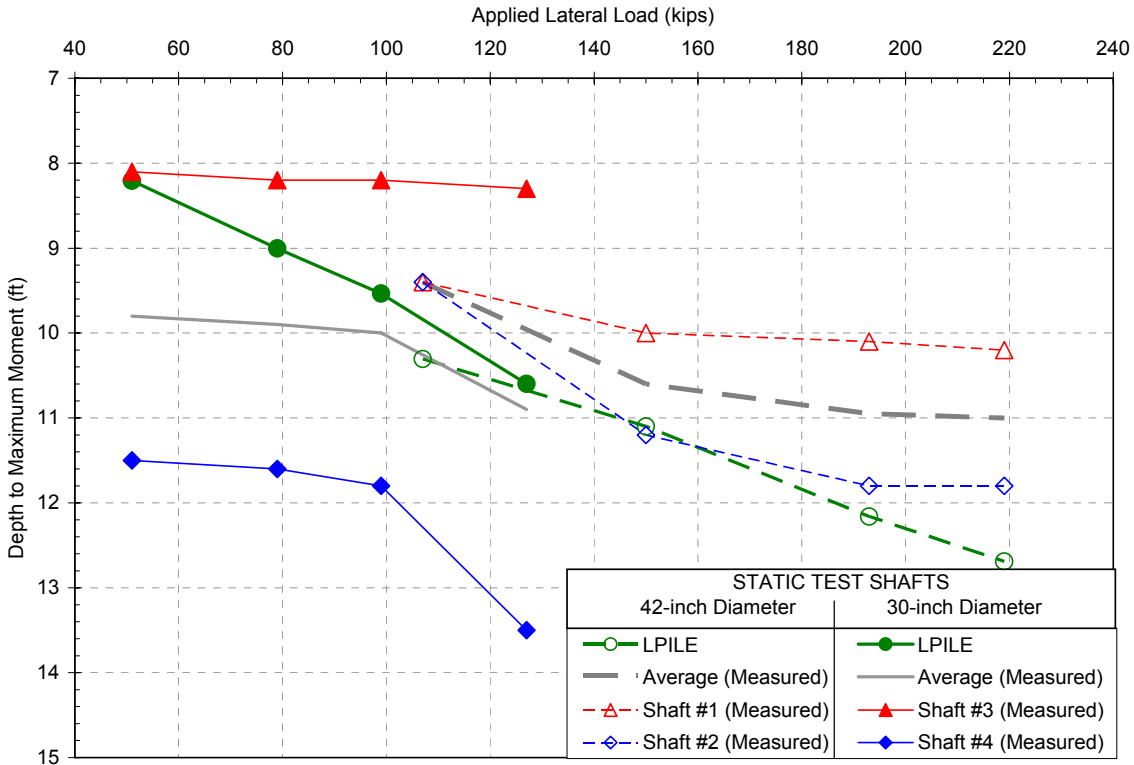


**Figure D10: Depth to Maximum Pile Moments**

**D.6.4 Pile Head Displacement with Static Lateral Load**

The pile head lateral displacements (at the point of load application) are presented in Figure D11 and D12 for the static 30-inch diameter shafts and the static 42-inch diameter shafts, respectively. The Figures illustrate the good overall accuracy of the formulated P-Y response model used for the LPILE runs when compared to the measured static test data. Note that the model appears to be slightly conservative for the larger 42-inch diameter shafts for predictions at pile head deflections under approximately 1 inch.

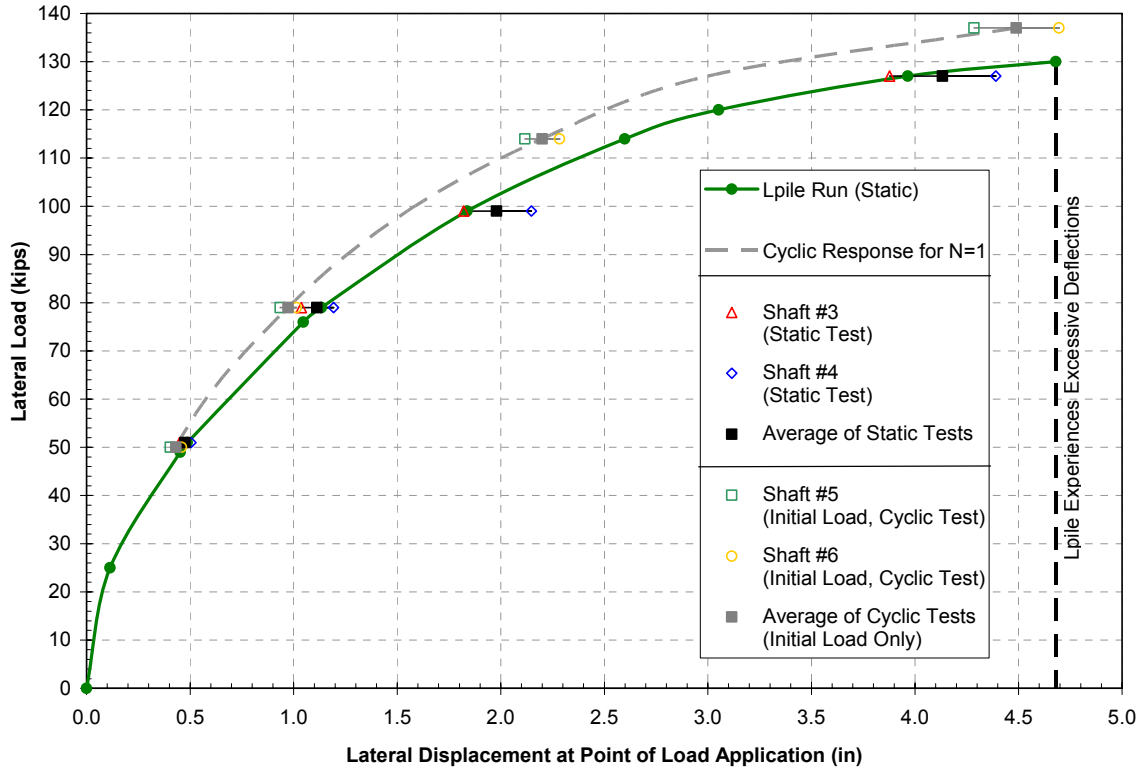


**Figure D11: Top of Shaft Displacement vs. Lateral Load for 30-inch Diameter Shafts**

The pile head displacements of the two 30-inch diameter cyclic test shafts measured at the onset of the initial load cycle (N=1) of each of the four load increments are also included in Figure D11. Note that the pile head displacements for the initial load cycle (N=1) of the cyclic tests shafts become progressively smaller than the pile head displacements for the static load tests shafts with increasing lateral load. The effect of soil creep on pile head displacement was not as fully developed during the initial load cycle of the cyclic tests, as it was on the static test shafts due to the cyclic test shaft measurements reported at a shorter time period after the desired lateral load level was attained. A relationship between the static and the initial load cycle pile head displacements is obtained as the difference between these two curves varying with

lateral load, and is shown as Figure D13. This relationship will be utilized in presentation of the cyclic degradation results to follow in Section D.6.5.

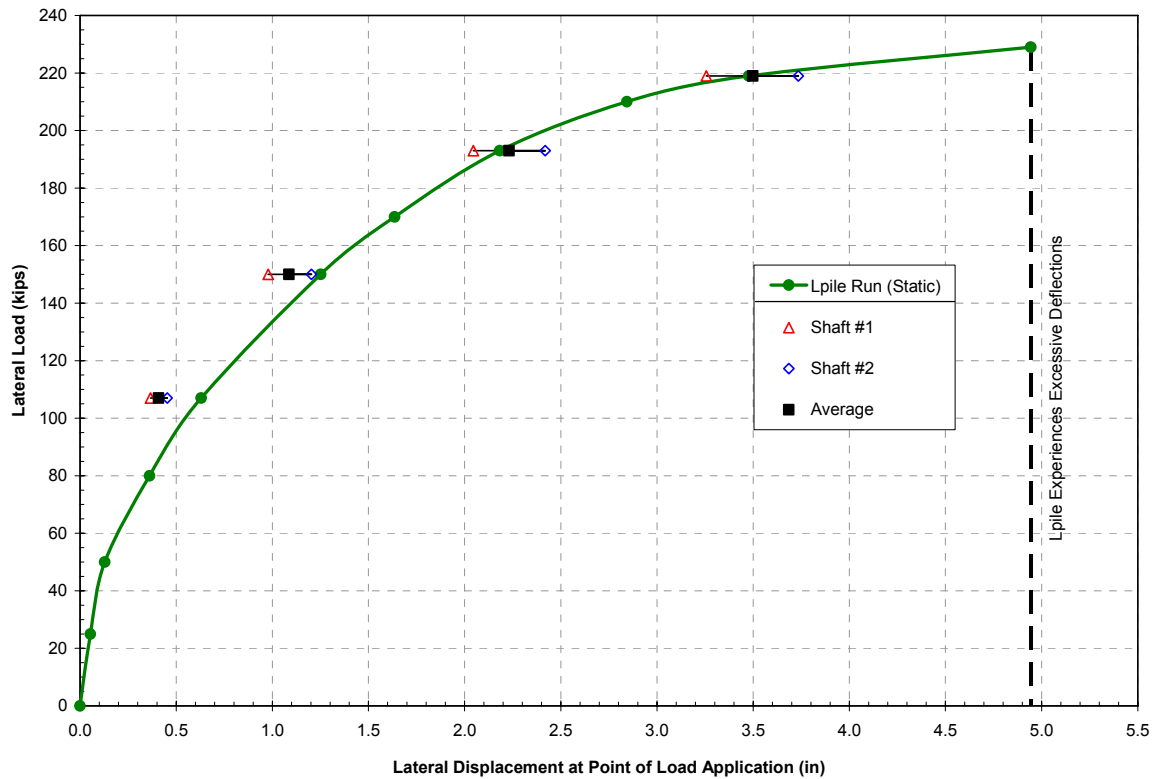


**Figure D12: Top of Shaft Displacement vs. Lateral Load for 42-inch Diameter Shafts**

It is of particular importance to note that the ultimate load attained during the cyclic test would not have been sustainable when tested in a static manner as the static curve appears to asymptote to a static geotechnical limit less than that exhibited by the cyclic tests. This was also observed in the LPILE runs, when a lateral load of 137 tons (ultimate from cyclic testing) resulted in a run time error of excessive displacement when using the static parameters.

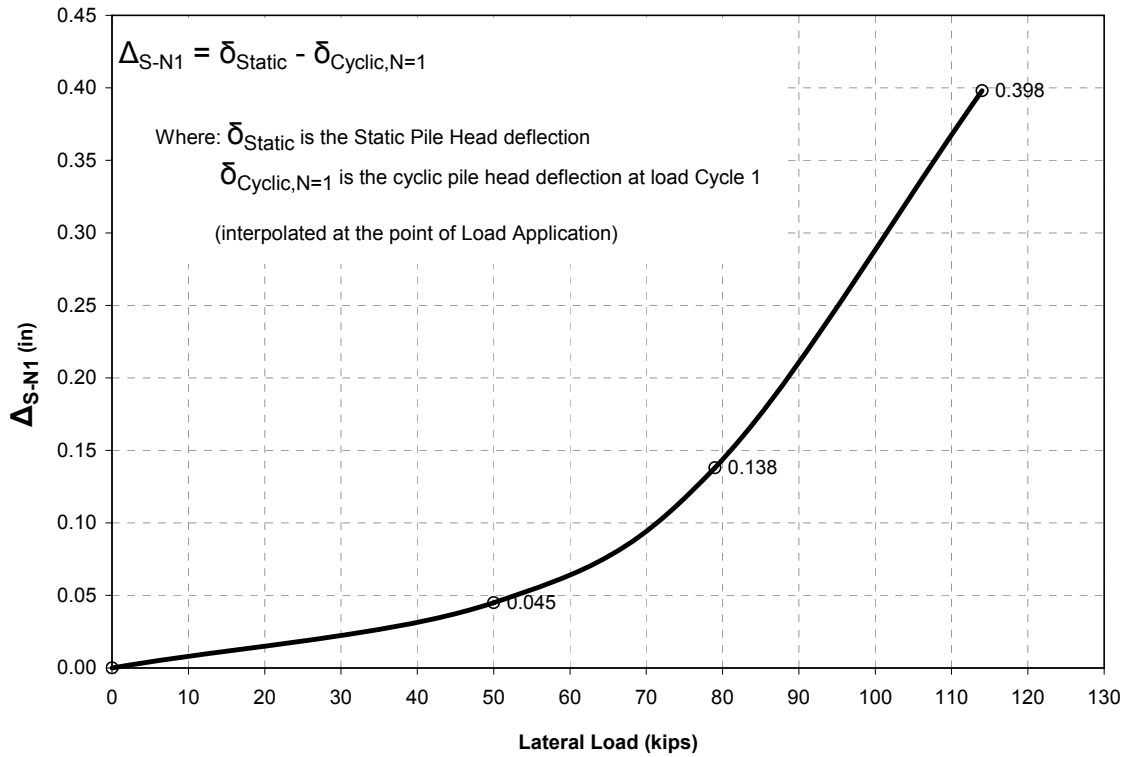


**Figure D13: Creep Relationship Between the Static and the Cyclic Initial Load Cycle (N=1) Pile Head Displacements**

**D.6.5 Cyclic Results**

LPILE Runs were made to compare to pile head displacement measurements (reported at the point of load application) made for all load cycles (N = 1 though 10) within all four load increments (A through D). The Model to generate the P-Y response was degraded by the Load Cycle Number (N) as presented.

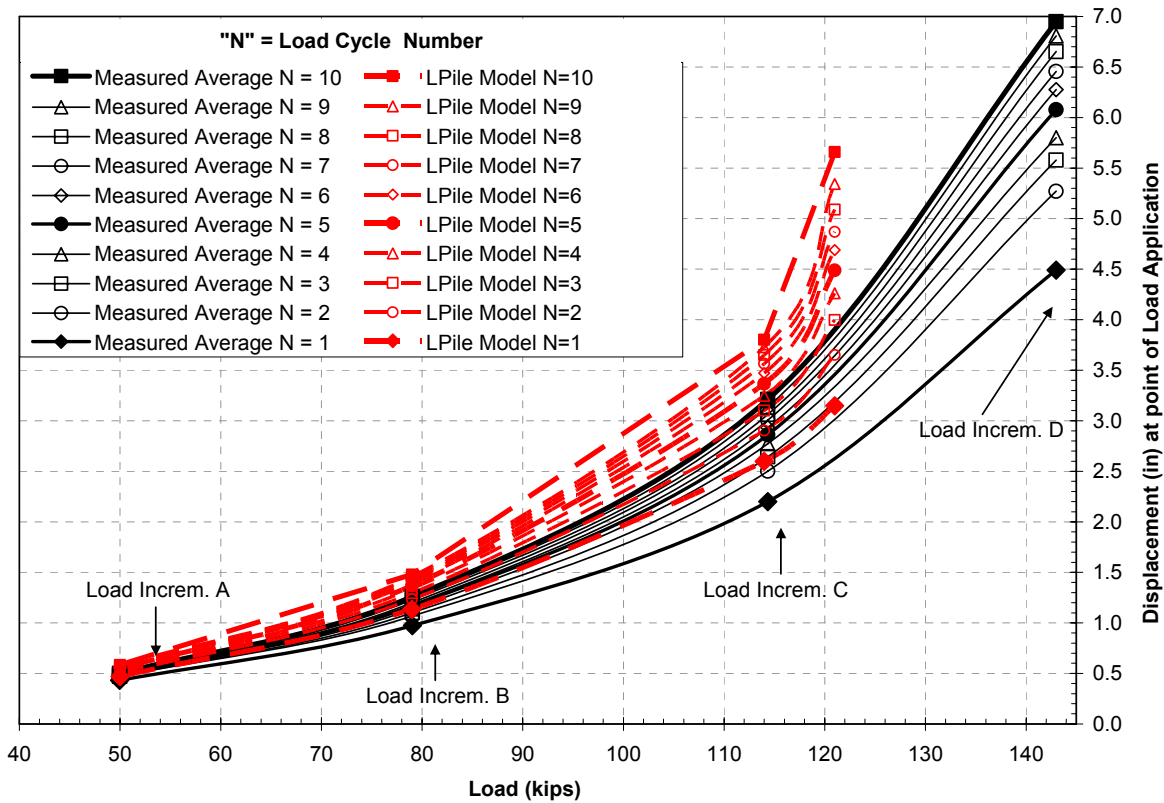


**Figure D14: Pile Head Displacements vs. Lateral Load for 30-inch Diameter Cyclic Test Shafts**

The pile head displacements obtained with LPILE were consistently in excess of that which was measured during the cyclic testing, as shown in Figure D14 where the pile head displacement is plotted vs. the applied lateral load. The reason for this is that the LPILE model developed was based upon the static test shafts with longer hold times than was maintained for Cyclic tests. When the relationship previously shown in Figure D13 was used to account for the differences in soil creep effects between the Static Tests and Cyclic Tests in the measured data, the pile head displacements obtained with LPILE are in good agreement as shown in Figure D15. Alternatively, the ratio of the top of shaft deflection at load cycle N to load Cycle 1 ( $\delta_N / \delta_1$ ) vs. the applied lateral load is

shown in Figures D16 and D17 for the measured deflections and the creep adjusted deflections, respectively.

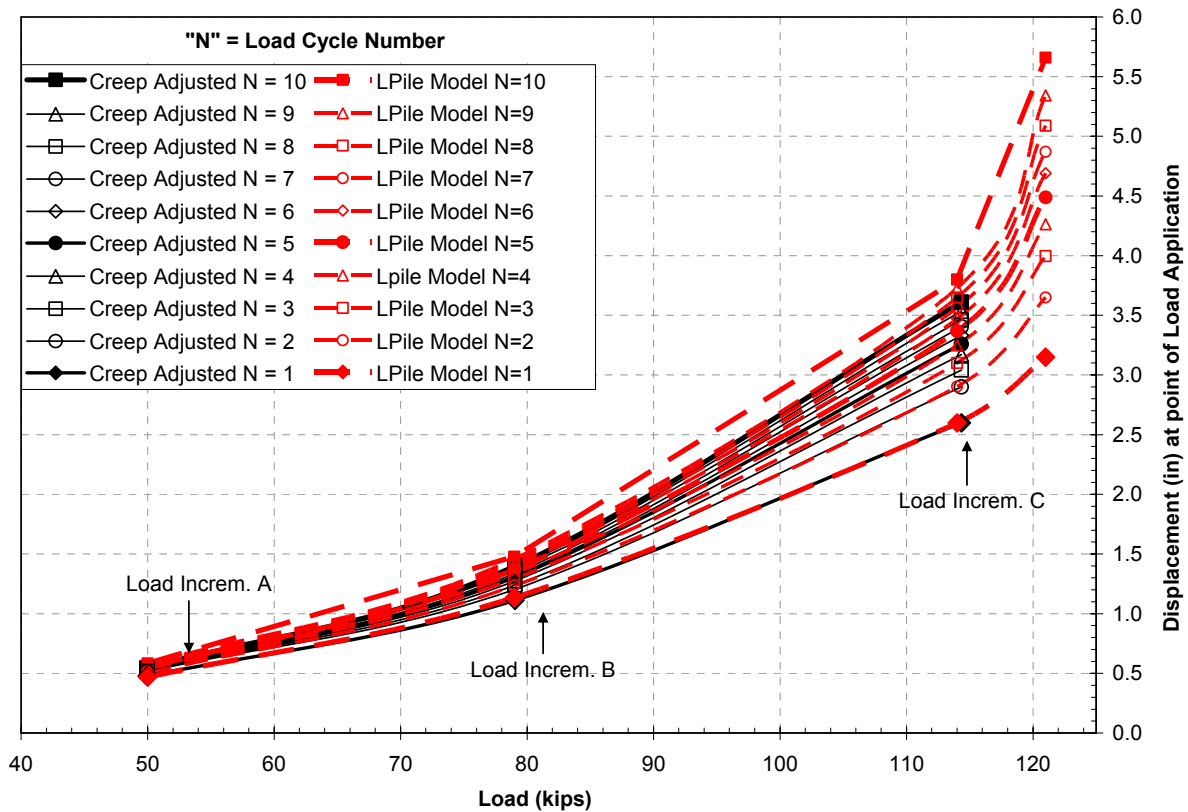


**Figure 15: Creep Adjusted Pile Head Displacements vs. Lateral Load for 30-inch Diameter Cyclic Test Shafts**

Comparisons of the ratio of the top of shaft deflection ratio ( $\bar{\delta}_N / \bar{\delta}_1$ ) are also shown vs. the top of shaft deflection at Load Cycle (N) in Figures D18 and D19 for the measured deflections and the creep adjusted deflections, respectively. Note that when the ordinate has been changed from the lateral load in Figure D17 to the corresponding top of shaft deflections in Figure D19, the line of data points at a given load increment are skewed at an angle to the ordinate rather than at the fixed lateral load. Further, the amount of skew increases with increasing load increments. This demonstrates that the increase in pile head deflection with load Cycle number (N) to have a more pronounced



effect as the load is increased. This is best shown in Figure D20 where the top of shaft deflection ratio ( $\delta_N / \delta_1$ ) is shown vs. the load cycle number (N). Note the increase in angle relative to the ordinate with increasing load increment.

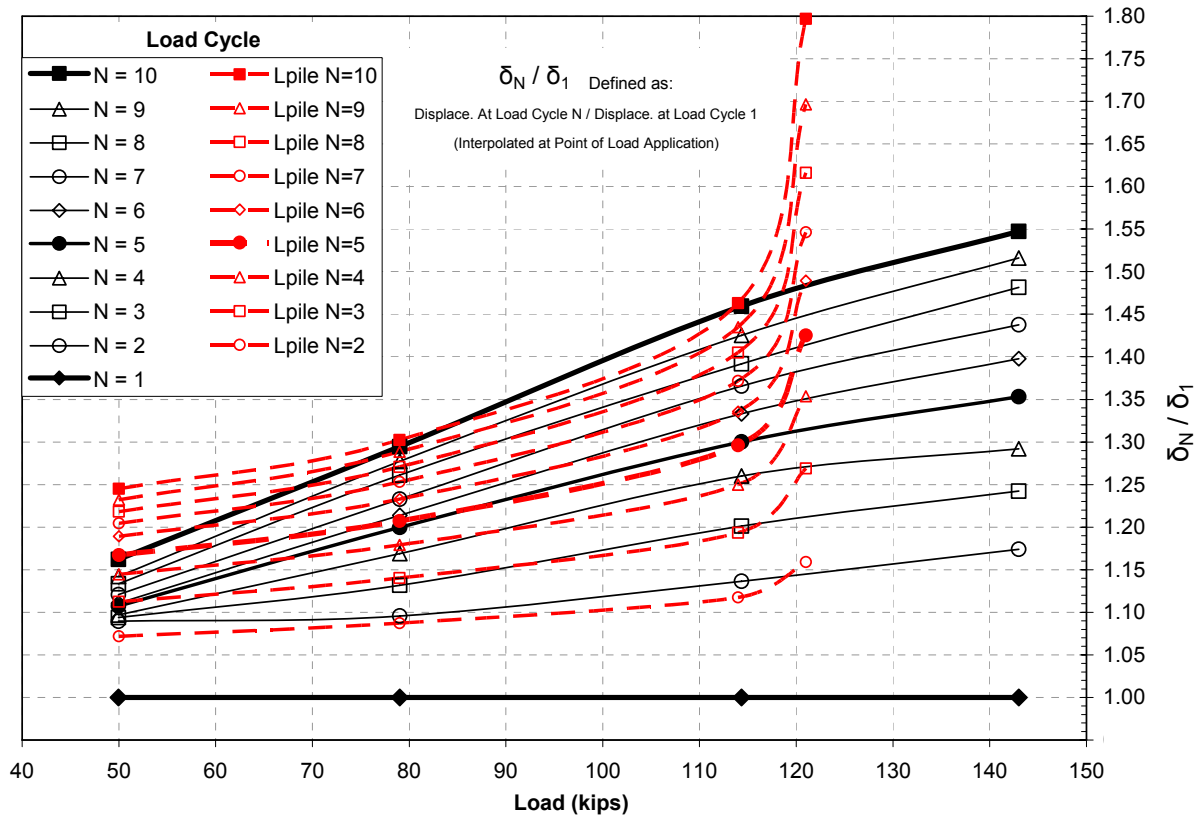


**Figure D16: Pile Head Displacement Ratio ( $\delta_N / \delta_1$ ) vs. Lateral Load for 30-inch Diameter Cyclic Test Shafts**

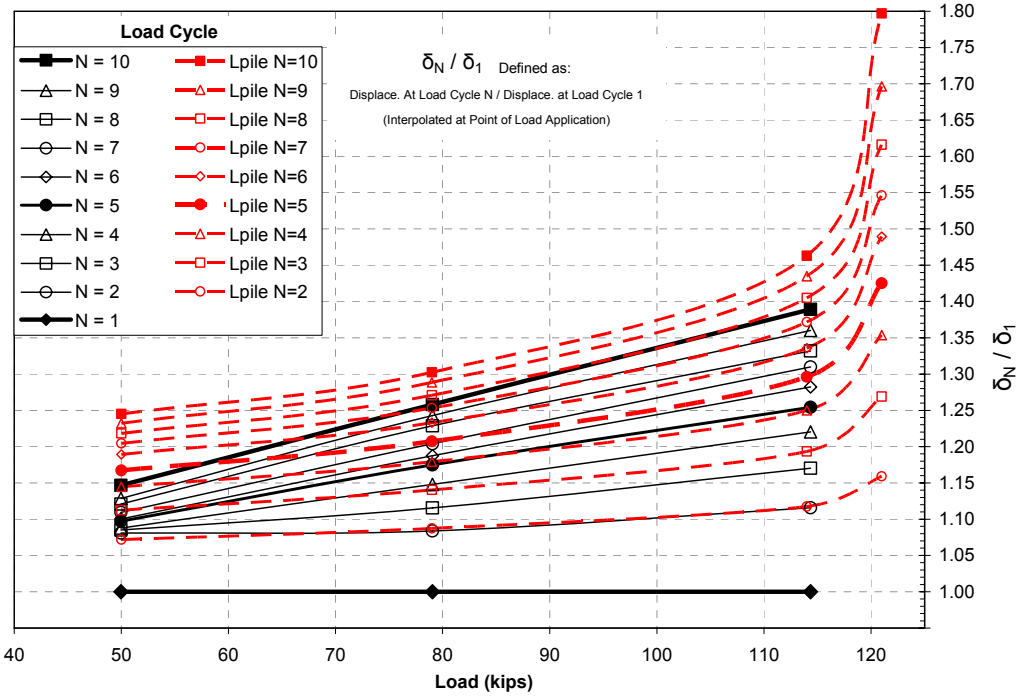


Figure D17: Creep Adjusted Pile Head Displacement Ratio ( $\delta_N / \delta_1$ ) vs. Lateral Load for 30-inch Diameter Cyclic Test Shafts

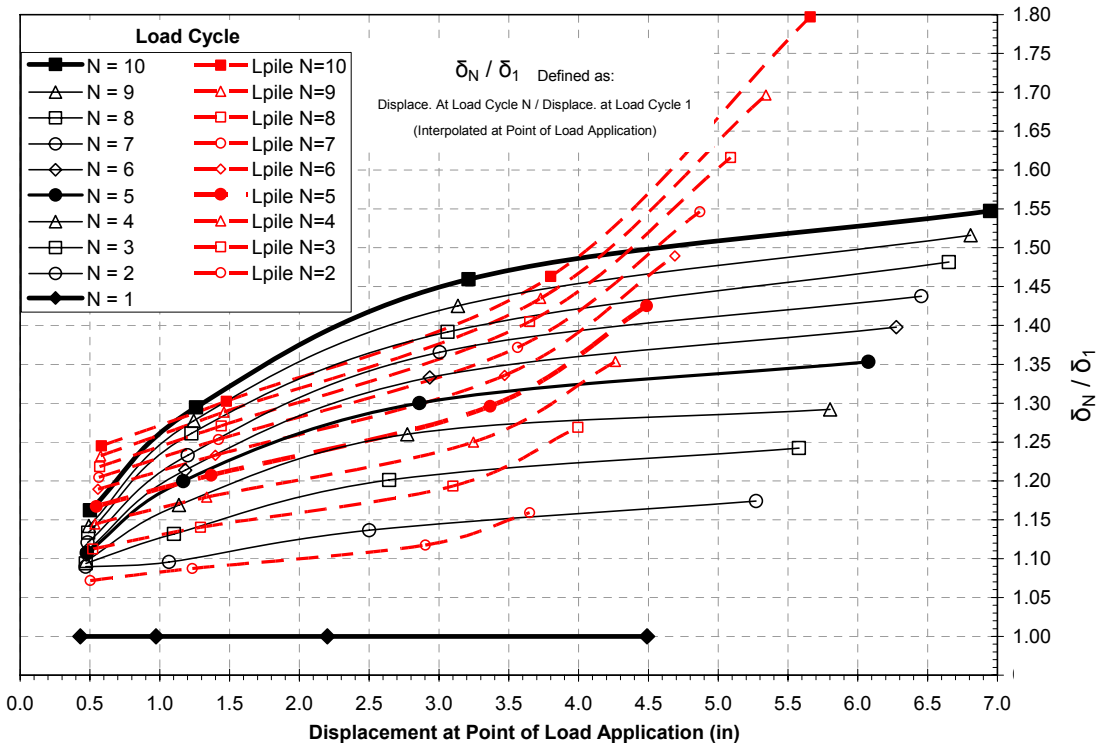
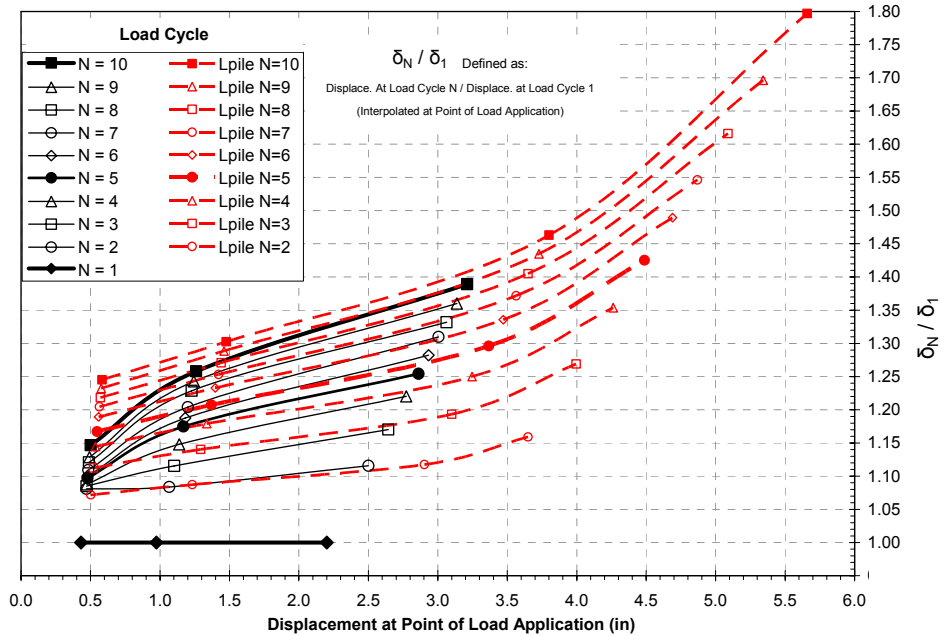
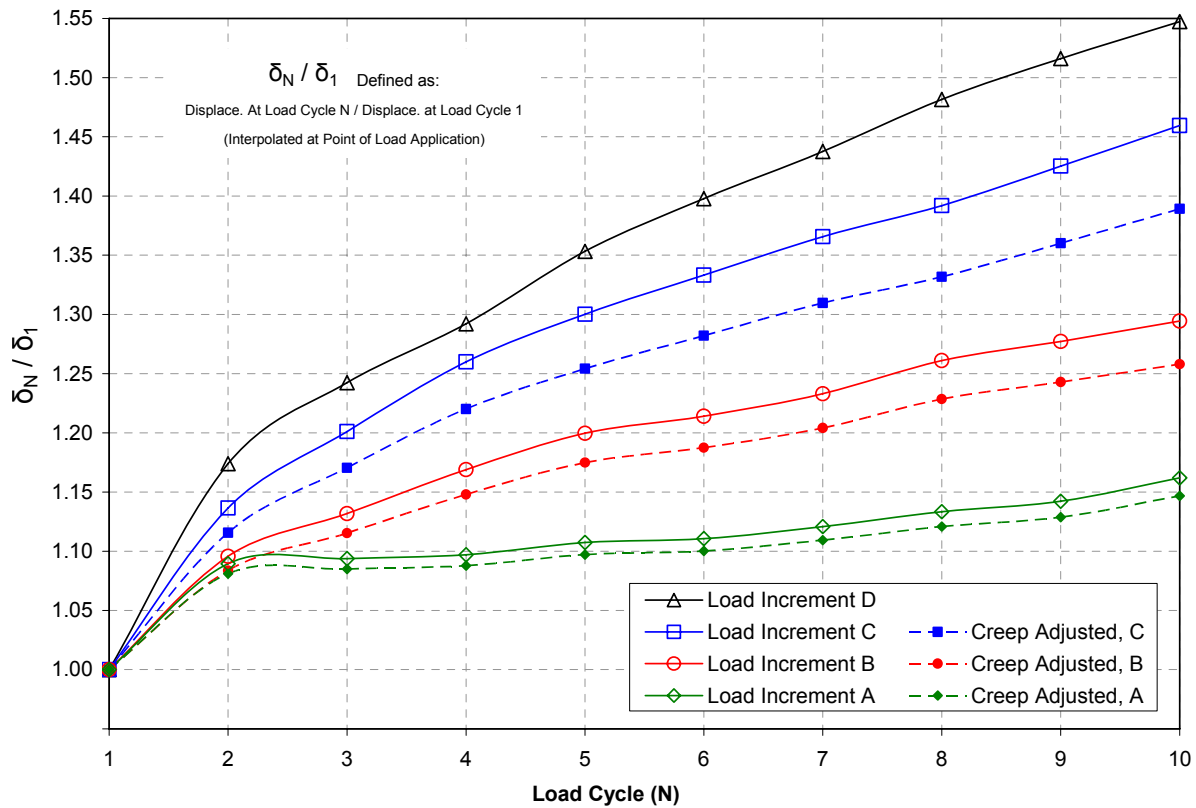


Figure D18: Pile Head Displacement Ratio ( $\delta_N / \delta_1$ ) vs. Top of Shaft Displacement for 30-inch Diameter Cyclic Test Shafts



**Figure D19: Creep Adjusted Pile Head Displacement Ratio ( $\bar{\delta}_N / \bar{\delta}_1$ ) vs. Top of Shaft Displacement for 30-inch Diameter Cyclic Test Shafts**



**Figure D20: Pile Head Displacement Ratio ( $\bar{\delta}_N / \bar{\delta}_1$ ) vs. Load Cycle Number (N) for 30-inch Diameter Cyclic Test Shafts**

## Appendix E

### Inclinometer Data

#### HOLE # 1: SE 42 inch

##### LVDT's 2 & 4

READING # 1		
Depth (ft)	A-axis Disp. (in)	B-axis Disp. (in)
3	0.0000	0.0000
5	0.0420	-0.0264
7	0.1296	-0.0306
9	0.2118	-0.0330
11	0.2880	-0.0360
13	0.3492	-0.0378
15	0.3918	-0.0408
17	0.4128	-0.0450
19	0.4326	-0.0426
21	0.4422	-0.0432
23	0.4500	-0.0444
25	0.4548	-0.0450
27	0.4590	-0.0468
29	0.4644	-0.0504

#### HOLE # 2: SW 42 inch

##### LVDT's 1 & 3

READING # 1		
Depth (ft)	A-axis Disp. (in)	B-axis Disp. (in)
3	0.0000	0.0000
5	0.1038	-0.0360
7	0.2022	-0.0528
9	0.2946	-0.0696
11	0.3786	-0.0876
13	0.4452	-0.0978
15	0.4932	-0.1056
17	0.5250	-0.1140
19	0.5430	-0.1194
21	0.5514	-0.1176
23	0.5574	-0.1194
25	0.5640	-0.1200
27	0.5718	-0.1176
29	0.5760	-0.1098

READING # 2		
Depth (ft)	A-axis Disp. (in)	B-axis Disp. (in)
3	0.0000	0.0000
5	0.1770	-0.0342
7	0.3930	-0.0462
9	0.6012	-0.0546
11	0.7794	-0.0612
13	0.9294	-0.0660
15	1.0404	-0.0684
17	1.1124	-0.0762
19	1.1586	-0.0720
21	1.1796	-0.0708
23	1.1952	-0.0714
25	1.2066	-0.0762
27	1.2168	-0.0744
29	1.2246	-0.0798

READING # 2		
Depth (ft)	A-axis Disp. (in)	B-axis Disp. (in)
3	0.0000	0.0000
5	0.2328	-0.0618
7	0.4746	-0.1044
9	0.7026	-0.1416
11	0.9006	-0.1806
13	1.0698	-0.2082
15	1.2042	-0.2322
17	1.2996	-0.2520
19	1.3620	-0.2652
21	1.3968	-0.2712
23	1.4112	-0.2742
25	1.4250	-0.2754
27	1.4382	-0.2754
29	1.4490	-0.2748

### HOLE # 1: SE 42 inch

READING # 3		
Depth (ft)	A-axis Disp. (in)	B-axis Disp. (in)
3	0.0000	0.0000
5	0.3408	-0.0408
7	0.7308	-0.0600
9	1.0968	-0.0750
11	1.4250	-0.0894
13	1.7082	-0.1044
15	1.9362	-0.1188
17	2.1090	-0.1308
19	2.2374	-0.1374
21	2.3232	-0.1416
23	2.3778	-0.1470
25	2.4102	-0.1512
27	2.4474	-0.1548
29	2.4840	-0.1596

### HOLE # 2: SW 42 inch

READING # 3		
Depth (ft)	A-axis Disp. (in)	B-axis Disp. (in)
3	0.0000	0.0000
5	0.4338	-0.0840
7	0.8838	-0.1626
9	1.2978	-0.2364
11	1.6740	-0.3066
13	2.0052	-0.3684
15	2.2854	-0.4224
17	2.5098	-0.4674
19	2.6802	-0.5010
21	2.8056	-0.5238
23	2.8914	-0.5428
25	2.9448	-0.5508
27	2.9994	-0.5586
29	3.0534	-0.5616

READING # 4		
Depth (ft)	A-axis Disp. (in)	B-axis Disp. (in)
3	0.0000	0.0000
5	0.5010	-0.0534
7	1.0584	-0.0768
9	1.5768	-0.0972
11	2.0484	-0.1194
13	2.4672	-0.1428
15	2.8182	-0.1614
17	3.1014	-0.1800
19	3.3306	-0.1926
21	3.5052	-0.2010
23	3.6414	-0.2118
25	3.7260	-0.2184
27	3.8250	-0.2268
29	3.9352	-0.2364

READING # 4		
Depth (ft)	A-axis Disp. (in)	B-axis Disp. (in)
3	0.0000	0.0000
5	0.6348	-0.1284
7	1.2954	-0.2454
9	1.9032	-0.3492
11	2.4666	-0.4524
13	2.9784	-0.5484
15	3.4260	-0.6324
17	3.8040	-0.7062
19	4.1148	-0.7674
21	4.3686	-0.8148
23	4.5738	-0.8574
25	4.7370	-0.8880
27	4.8864	-0.9150
29	5.0430	-0.9432

### HOLE # 1: SE 42 inch

READING # 5		
Depth (ft)	A-axis Disp. (in)	B-axis Disp. (in)
3	0.0000	0.0000
5	0.1320	-0.0324
7	0.3060	-0.0450
9	0.4674	-0.0540
11	0.6192	-0.0618
13	0.7656	-0.0744
15	0.9006	-0.0876
17	1.0254	-0.0990
19	1.1418	-0.1062
21	1.2534	-0.1164
23	1.3542	-0.1236
25	1.4418	-0.1308
27	1.5384	-0.1380
29	1.6332	-0.1452

### HOLE # 2: SW 42 inch

READING # 5		
Depth (ft)	A-axis Disp. (in)	B-axis Disp. (in)
3	0.0000	0.0000
5	0.2040	-0.0510
7	0.4314	-0.0930
9	0.6432	-0.1344
11	0.8466	-0.1740
13	1.0428	-0.2118
15	1.2306	-0.2490
17	1.4070	-0.2844
19	1.5732	-0.3180
21	1.7304	-0.3498
23	1.8792	-0.3822
25	2.0166	-0.4086
27	2.1510	-0.4362
29	2.2902	-0.4602

**HOLE # 3: CE 30 inch**

READING # 1		
Depth (ft)	A-axis Disp. (in)	B-axis Disp. (in)
3	0.0000	0.0000
5	0.1014	-0.0228
7	0.1962	-0.0444
9	0.2898	-0.0642
11	0.3600	-0.0804
13	0.4104	-0.0918
15	0.4398	-0.0996
17	0.4542	-0.1020
19	0.4590	-0.1020
21	0.4626	-0.1026
23	0.4650	-0.1002
25	0.4656	-0.1002
27	0.4650	-0.0978
29	0.4626	-0.0990

READING # 2		
Depth (ft)	A-axis Disp. (in)	B-axis Disp. (in)
3	0.0000	0.0000
5	0.2256	-0.0498
7	0.4416	-0.1014
9	0.6450	-0.1476
11	0.8076	-0.1878
13	0.9354	-0.2196
15	1.0206	-0.2430
17	1.0686	-0.2544
19	1.0908	-0.2568
21	1.0986	-0.2562
23	1.1028	-0.2550
25	1.1046	-0.2556
27	1.1040	-0.2568
29	1.1022	-0.2562

**HOLE # 4: CW 30 inch**

READING # 1		
Depth (ft)	A-axis Disp. (in)	B-axis Disp. (in)
3	0.0000	0.0000
5	0.1326	0.0336
7	0.2634	0.0594
9	0.3822	0.0858
11	0.4776	0.1068
13	0.5454	0.1236
15	0.5850	0.1278
17	0.6030	0.1320
19	0.6108	0.1302
21	0.6150	0.1314
23	0.6168	0.1320
25	0.6168	0.1338
27	0.6156	0.1362
29	0.6156	0.1380

READING # 2		
Depth (ft)	A-axis Disp. (in)	B-axis Disp. (in)
3	0.0000	0.0000
5	0.2922	0.0720
7	0.5832	0.1344
9	0.8490	0.1938
11	1.0680	0.2430
13	1.2366	0.2808
15	1.3524	0.3042
17	1.4220	0.3192
19	1.4532	0.3234
21	1.4610	0.3246
23	1.4634	0.3252
25	1.4628	0.3258
27	1.4604	0.3282
29	1.4592	0.3288

**HOLE # 3: CE 30 inch**

<b>READING # 3</b>		
<b>Depth (ft)</b>	<b>A-axis Disp. (in)</b>	<b>B-axis Disp. (in)</b>
3	0.0000	0.0000
5	0.3744	-0.0876
7	0.7398	-0.1770
9	1.0824	-0.2568
11	1.3674	-0.3312
13	1.6008	-0.3918
15	1.7736	-0.4362
17	1.8882	-0.4638
19	1.9548	-0.4776
21	1.9848	-0.4842
23	1.9944	-0.4818
25	1.9974	-0.4830
27	1.9980	-0.4770
29	1.9962	-0.4758

**HOLE # 4: CW 30 inch**

<b>READING # 3</b>		
<b>Depth (ft)</b>	<b>A-axis Disp. (in)</b>	<b>B-axis Disp. (in)</b>
3	0.0000	0.0000
5	0.4668	0.1146
7	0.9342	0.2196
9	1.3620	0.3180
11	1.7250	0.4026
13	2.0184	0.4698
15	2.2344	0.5184
17	2.3802	0.5520
19	2.4612	0.5646
21	2.4960	0.5736
23	2.5044	0.5760
25	2.5032	0.5778
27	2.5026	0.5784
29	2.5074	0.5712

<b>READING # 4</b>		
<b>Depth (ft)</b>	<b>A-axis Disp. (in)</b>	<b>B-axis Disp. (in)</b>
3	0.0000	0.0000
5	0.7074	-0.1806
7	1.4118	-0.3576
9	2.0736	-0.5214
11	2.6556	-0.6762
13	3.1584	-0.8136
15	3.5574	-0.9234
17	3.8418	-1.0026
19	4.0302	-1.0542
21	4.1406	-1.0842
23	4.1934	-1.0920
25	4.2138	-1.0980
27	4.2288	-1.0986
29	4.2420	-1.0998

<b>READING # 4</b>		
<b>Depth (ft)</b>	<b>A-axis Disp. (in)</b>	<b>B-axis Disp. (in)</b>
3	0.0000	0.0000
5	0.8784	0.2244
7	1.7700	0.4416
9	2.5896	0.6450
11	3.3144	0.8628
13	3.9186	0.9792
15	4.3788	1.0902
17	4.6950	1.1658
19	4.8930	1.2090
21	5.0052	1.2378
23	5.0598	1.2486
25	5.0748	1.2516
27	5.0850	1.2552
29	5.0952	1.2594



### HOLE # 3: CE 30 inch

READING # 5		
Depth (ft)	A-axis Disp. (in)	B-axis Disp. (in)
3	0.0000	0.0000
5	0.1656	-0.0366
7	0.3294	-0.0750
9	0.4896	-0.1110
11	0.6324	-0.1440
13	0.7656	-0.1734
15	0.8802	-0.1998
17	0.9678	-0.2202
19	1.0344	-0.2340
21	1.0860	-0.2448
23	1.1214	-0.2496
25	1.1436	-0.2544
27	1.1658	-0.2568
29	1.1862	-0.2628

### HOLE # 4: CW 30 inch

READING # 5		
Depth (ft)	A-axis Disp. (in)	B-axis Disp. (in)
3	0.0000	0.0000
5	0.2250	0.0612
7	0.4638	0.1176
9	0.6852	0.1752
11	0.8922	0.2298
13	1.0788	0.2784
15	1.2258	0.3090
17	1.3290	0.3342
19	1.4064	0.3480
21	1.4640	0.3636
23	1.5036	0.3786
25	1.5240	0.3876
27	1.5468	0.3942
29	1.5756	0.3972

**HOLE # 5: NE 30 inch**

READING # 1		
Depth (ft)	A-axis Disp. (in)	B-axis Disp. (in)
3	0.0000	0.0000
5	0.0774	-0.0288
7	0.1338	-0.0570
9	0.1848	-0.0822
11	0.2286	-0.1056
13	0.2640	-0.1242
15	0.2868	-0.1344
17	0.2964	-0.1434
19	0.3036	-0.1488
21	0.3072	-0.1488
23	0.3078	-0.1488
25	0.3078	-0.1488
27	0.3060	-0.1494
29	0.3054	-0.1572

READING # 2		
Depth (ft)	A-axis Disp. (in)	B-axis Disp. (in)
3	0.0000	0.0000
5	0.1164	-0.0444
7	0.2190	-0.0918
9	0.3078	-0.1374
11	0.3804	-0.1764
13	0.4368	-0.2058
15	0.4752	-0.2232
17	0.4944	-0.2436
19	0.5028	-0.2400
21	0.5064	-0.2448
23	0.5058	-0.2466
25	0.5052	-0.2478
27	0.5010	-0.2496
29	0.5004	-0.2538

**HOLE # 6: NW 30 inch**

READING # 1		
Depth (ft)	A-axis Disp. (in)	B-axis Disp. (in)
3	0.0000	0.0000
5	0.1386	-0.0126
7	0.2718	-0.0234
9	0.3900	-0.0336
11	0.4818	-0.0414
13	0.5472	-0.0468
15	0.5892	-0.0516
17	0.6114	-0.0540
19	0.6216	-0.0558
21	0.6276	-0.0552
23	0.6312	-0.0540
25	0.6378	-0.0546
27	0.6324	-0.0546
29	0.6324	-0.0552

READING # 2		
Depth (ft)	A-axis Disp. (in)	B-axis Disp. (in)
3	0.0000	0.0000
5	0.1374	-0.0090
7	0.2730	-0.0192
9	0.3936	-0.0276
11	0.4914	-0.0366
13	0.5646	-0.0432
15	0.6162	-0.0468
17	0.6426	-0.0474
19	0.6552	-0.0492
21	0.6636	-0.0498
23	0.6672	-0.0504
25	0.6672	-0.0516
27	0.6672	-0.0510
29	0.6678	-0.0510

READING # 3		
Depth (ft)	A-axis Disp. (in)	B-axis Disp. (in)
3	0.0000	0.0000
5	0.2016	-0.0894
7	0.3924	-0.1836
9	0.5658	-0.2700
11	0.7080	-0.3426
13	0.8178	-0.4002
15	0.8916	-0.4386
17	0.9342	-0.4614
19	0.9516	-0.4716
21	0.9606	-0.4764
23	0.9630	-0.4788
25	0.9642	-0.4800
27	0.9630	-0.4824
29	0.9624	-0.4878

READING # 3		
Depth (ft)	A-axis Disp. (in)	B-axis Disp. (in)
3	0.0000	0.0000
5	0.2250	-0.0210
7	0.5052	-0.0390
9	0.7320	-0.0552
11	0.9186	-0.0696
13	1.0650	-0.0810
15	1.1694	-0.0888
17	1.2330	-0.0942
19	1.2648	-0.0984
21	1.2774	-0.0996
23	1.2828	-0.1014
25	1.2840	-0.1014
27	1.2840	-0.1014
29	1.2834	-0.1032

READING # 4		
Depth (ft)	A-axis Disp. (in)	B-axis Disp. (in)
3	0.0000	0.0000
5	0.2484	-0.1074
7	0.4788	-0.2214
9	0.6936	-0.3252
11	0.8772	-0.4164
13	1.0242	-0.4926
15	1.1286	-0.5466
17	1.1958	-0.5832
19	1.2336	-0.6048
21	1.2462	-0.6150
23	1.2516	-0.6174
25	1.2540	-0.6198
27	1.2552	-0.5234
29	1.2552	-0.6294

READING # 4		
Depth (ft)	A-axis Disp. (in)	B-axis Disp. (in)
3	0.0000	0.0000
5	0.3036	-0.0228
7	0.6054	-0.0444
9	0.8802	-0.0624
11	1.1188	-0.0804
13	1.2984	-0.0948
15	1.4376	-0.1050
17	1.5312	-0.1110
19	1.5852	-0.1140
21	1.6110	-0.1158
23	1.6212	-0.1176
25	1.6254	-0.1176
27	1.6284	-0.1176
29	1.6314	-0.1176

READING # 5		
Depth (ft)	A-axis Disp. (in)	B-axis Disp. (in)
3	0.0000	0.0000
5	0.4122	-0.1884
7	0.8142	-0.3834
9	1.1832	-0.5622
11	1.5036	-0.7224
13	1.7694	-0.8568
15	1.9698	-0.9588
17	2.1078	-1.0326
19	2.1924	-1.0776
21	2.2314	-1.1034
23	2.2440	-1.1076
25	2.2506	-1.1106
27	2.2530	-1.1142
29	2.2536	-1.1190

READING # 5		
Depth (ft)	A-axis Disp. (in)	B-axis Disp. (in)
3	0.0000	0.0000
5	0.4962	-0.0288
7	0.9852	-0.0600
9	1.4352	-0.0876
11	1.8228	-0.1158
13	2.1444	-0.1404
15	2.3946	-0.1566
17	2.5746	-0.1668
19	2.6868	-0.1728
21	2.7492	-0.1740
23	2.7738	-0.1764
25	2.7804	-0.1776
27	2.7852	-0.1764
29	2.7888	-0.1716

READING # 6		
Depth (ft)	A-axis Disp. (in)	B-axis Disp. (in)
3	0.0000	0.0000
5	0.5184	-0.2412
7	1.0362	-0.4974
9	1.5174	-0.7338
11	1.9446	-0.9540
13	2.3100	-1.1454
15	2.5998	-1.2972
17	2.8170	-1.4136
19	2.9652	-1.4934
21	3.0540	-1.5456
23	3.1014	-1.5702
25	3.1200	-1.5822
27	3.1356	-1.5918
29	3.1494	-1.6032

READING # 6		
Depth (ft)	A-axis Disp. (in)	B-axis Disp. (in)
3	0.0000	0.0000
5	0.6498	-0.0324
7	1.2906	-0.0672
9	1.8840	-0.1008
11	2.4108	-0.1332
13	2.8578	-0.1620
15	3.2220	-0.1818
17	3.5052	-0.1950
19	3.7050	-0.2028
21	3.8352	-0.2064
23	3.9132	-0.2082
25	3.9540	-0.2076
27	3.9906	-0.2046
29	4.0260	-0.2022

READING # 7		
Depth (ft)	A-axis Disp. (in)	B-axis Disp. (in)
3	0.0000	0.0000
5	0.7542	-0.3582
7	1.5132	-0.7314
9	2.2248	-1.0794
11	2.8668	-1.4070
13	3.4254	-1.6962
15	3.8658	-1.9254
17	4.1808	-2.0940
19	4.3890	-2.2056
21	4.5162	-2.2788
23	4.5852	-2.3130
25	4.6170	-2.3310
27	4.6338	-2.3436
29	4.6518	-2.3610

READING # 7		
Depth (ft)	A-axis Disp. (in)	B-axis Disp. (in)
3	0.0000	0.0000
5	0.9780	-0.0492
7	1.9398	-0.0996
9	2.8398	-0.1524
11	3.6516	-0.2046
13	4.3440	-0.2526
15	4.8954	-0.2838
17	5.3022	-0.3024
19	5.5800	-0.3138
21	5.7600	-0.3204
23	5.8716	-0.3258
25	5.9316	-0.3276
27	5.9790	-0.3252
29	6.0270	-0.3216

READING # 8		
Depth (ft)	A-axis Disp. (in)	B-axis Disp. (in)
3	0.0000	0.0000
5	1.0404	-0.5070
7	2.0994	-1.0332
9	3.1074	-1.5378
11	4.0398	-2.0148
13	4.8756	-2.4540
15	5.5572	-2.8116
17	6.0588	-3.0816
19	6.4098	-3.2682
21	6.6570	-3.4074
23	6.8346	-3.5028
25	6.9600	-3.5718
27	7.0572	-3.6312
29	7.1598	-3.6984

READING # 8		
Depth (ft)	A-axis Disp. (in)	B-axis Disp. (in)
3	0.0000	0.0000
5	1.3080	-0.0540
7	2.5920	-0.1092
9	3.8130	-0.1704
11	4.9338	-0.2316
13	5.9196	-0.2844
15	6.7230	-0.3180
17	7.3308	-0.3378
19	7.7724	-0.3498
21	8.1018	-0.3564
23	8.3520	-0.3618
25	8.5380	-0.3588
27	8.7054	-0.3540
29	8.8758	-0.3492

READING # 9		
Depth (ft)	A-axis Disp. (in)	B-axis Disp. (in)
3	0.0000	0.0000
5	0.2328	-0.1140
7	0.4692	0.2394
9	0.6960	-0.3612
11	0.9126	-0.4806
13	1.1184	-0.5964
15	1.2780	-0.6876
17	1.3752	-0.7476
19	1.4304	-0.7836
21	1.4754	-0.8154
23	1.5180	-0.8424
25	1.5576	-0.8700
27	1.5972	-0.8994
29	1.6410	-0.9306

READING # 9		
Depth (ft)	A-axis Disp. (in)	B-axis Disp. (in)
3	0.0000	0.0000
5	0.3300	-0.0072
7	0.6540	-0.0162
9	0.9696	-0.0276
11	1.2732	-0.0408
13	1.5462	-0.0522
15	1.7622	-0.0552
17	1.9098	-0.0510
19	2.0142	-0.0444
21	2.1096	-0.0354
23	2.2038	-0.0270
25	2.2944	-0.0204
27	2.3850	-0.0126
29	2.4774	-0.0060

# K - TRAN

KANSAS TRANSPORTATION RESEARCH  
AND  
NEW - DEVELOPMENTS PROGRAM



A COOPERATIVE TRANSPORTATION RESEARCH PROGRAM BETWEEN:

KANSAS DEPARTMENT OF TRANSPORTATION



THE UNIVERSITY OF KANSAS



KANSAS STATE UNIVERSITY

